IDENTIFICATION OF THE COMPLEMENTARY BINDING DOMAINS OF HISTIDINE-RICH GLYCOPROTEIN AND FACTOR XIIA RESPONSIBLE FOR CONTACT PATHWAY INHIBITION

BY TAMMY K. TRUONG, M.Sc., B.Sc.

A Thesis Submitted to the School of Graduate Studies in Partial Fulfilment of the Requirements for the Degree

DOCTOR OF PHILOSOPHY

DOCTOR OF PHILOSOPHY (2020) McMaster University
Faculty of Health Sciences Hamilton, Ontario
Medical Sciences Graduate Program
Specialization: Blood & Vasculature

TITLE:	Identification of the complementary binding domains of histidine-rich glycoprotein and factor XIIa responsible for contact pathway inhibition
AUTHOR:	Tammy K. Truong M.Sc., Pathology and Molecular Medicine (Queen's University) B.Sc., Honours Life Sciences (McMaster University)
SUPERVISOR:	Jeffrey I. Weitz, M.D. Professor of Medicine, Biochemistry, and Biomedical Sciences, McMaster University Executive Director of the Thrombosis and Atherosclerosis Research Institute (TaARI)
NUMBER OF PAGES:	xix, 271

ABSTRACT

Recent studies suggest that factor (F) XII, which is dispensable for hemostasis, is important for thrombus stabilization and growth. Therefore, FXIIa inhibition may attenuate thrombosis without disrupting hemostasis. FXII activation is stimulated by polyanions such as polyphosphates released from activated platelets, and nucleic acids released by cells. Previously, we showed that histidine-rich glycoprotein (HRG) binds FXIIa with high affinity, inhibits FXII autoactivation and FXIIa-mediated activation of FXI, and attenuates ferric chloride-induced arterial thrombosis in mice. Thus, HRG has the capacity to downregulate the contact pathway *in vitro* and *in vivo*. This thesis aimed to identify the complementary binding domains of HRG and FXIIa, and to further explore the anticoagulants effects of HRG on FXIIa-mediated contact activation. We hypothesized that FXIIa binds to the zinc-binding histidine-rich region (HRR) of HRG and that HRG binds to the non-catalytic heavy chain of FXIIa to exert its anticoagulant activities on FXIIa-mediated contact activation. We have localized the complementary binding sites of HRG and FXIIa to be within the HRR domain of HRG and NH_2-FNII-EGF1 (NFE) domains of FXIIa. Moreover, we show that the HRR binds to short chain polyphosphate with high affinity, suggesting a dynamic complex between HRG, FXIIa, and polyphosphate (polyP) on activated platelets. We provide evidence for two potential mechanisms through which HRG modulates the contact system. These include by 1) inhibiting FXIIa activity and 2) attenuating the procoagulant effect of polyanions, such as polyP on FXIIa-mediated reactions. Indeed, we show that the interaction of HRG with FXIIa and polyphosphate is predominantly mediated by the HRR domain and that HRR analogs have the capacity to

recapitulate the anticoagulant effects of HRG in purified and plasma systems. Therefore, by modulating FXIIa-mediated contact pathway reactions, like HRG, HRR analogs may attenuate thrombosis without disrupting hemostasis.

ACKNOWLEDGEMENTS

To be given the opportunity to complete my Doctor of Philosophy degree at McMaster University has been a great privilege and honour. I am thankful for the incredible opportunities I have been provided as a graduate student in the Medical Sciences Graduate Program, as well as the invaluable skills and knowledge I have acquired, which I will carry with me into my future endeavors. I could not have done this alone and would like to thank those who have helped and supported me along the way.

I would like to express my sincere gratitude to my supervisor, Dr. Jeff Weitz for his mentorship, generosity, and support during graduate school. It has been an honour to have completed my doctoral research training under your supervision. Thank you for always making time for me, believing in my abilities, and challenging me to become the greatest version of myself. It has been inspiring to watch you work relentlessly towards your endeavors and receive many accolades, all while being such a great role model and leader to us at TaARI. I would also like to thank my supervisory committee members, Dr. Patricia Liaw and Dr. Peter Gross for your continued guidance and support.

To my mentor, Dr. Jim Fredenburgh, thank you for always being so patient and supportive, and for all the countless hours of guidance, troubleshooting, editing, and presentation preparations. Thank you for challenging not only me, but everyone in the lab to do better science every day. I would not be the scientist I am today without your guidance and mentorship. It has been an honour to be your student and I am forever grateful. To Alan Stafford, thank you for always taking the time to help me troubleshoot and for all your support in my experiments. Thank you to Rida Malik for all of your amazing support and

work on our research together. I owe much of my success in graduate school to these amazing people and will forever be grateful. I would also like to thank my collaborators, Dr. Colin Kretz, and Hasam Madarati for their countless hours of guidance, support, and generosity. I am so proud of the work we have accomplished together and will always be thankful to everyone in the Kretz Lab.

I would also like to thank my colleagues and friends in the Weitz (Current: Rikki, Hester, Rawaa, Rida, Ji; Past: CJ, Zeyu, Roxanna, Ebenezer, Dorathy, Vishal, Ran, Natalie, Alan, Bev, Sara, Iqbal, Jagman), Gross (Shana, Nima, Crystal), and Kretz (Hasam, Kanwal, Taylor) labs for making graduate school so memorable and for making it enjoyable to come in and work each day. Thank you for being such amazing friends, and for all your kindness and support. I am so grateful to have had the opportunity to meet each and every one of you and wish you all the best in your future endeavors.

Lastly, I would like to thank my friends and family for their unconditional love and support to pursue my education and accomplish my life goals. I could not have gone through this journey without your motivation and encouragement to continue no matter what challenges I was facing. To my brother and sister, thank you for being the greatest support system and for always cheering me on. I would like to dedicate my PhD thesis to my parents for all their love, support, and sacrifices to make this opportunity possible. I owe my success to you both for teaching me the value of hard work, perseverance, and determination. Thank you for always believing in me and for being my constant motivation to accomplish my dreams.

TABLE OF CONTENTS

CHAPTER 7: EFFECT OF SYNTHETIC HRR PEPTIDES ON CONTACT ACTIVATION, PLASMA CLOTTING, AND POLYPHOSPHATE-INDUCED THROMBIN GENERATION

CHAPTER 8: BINDING INTERACTIONS BETWEEN HRG, FACTOR XIIA, AND POLYPHOSPHATE

CHAPTER 9: DISCUSSION

LIST OF FIGURES

CHAPTER 7: EFFECT OF SYNTHETIC HRR PEPTIDES ON CONTACT ACTIVATION, PLASMA CLOTTING, AND POLYPHOSPHATE INDUCED THROMBIN GENERATION

CHAPTER 8: BINDING INTERACTIONS BETWEEN HRG, FACTOR XIIA AND POLYPHOSPHATE

CHAPTER 9: DISCUSSION

LIST OF TABLES

LIST OF ABBREVIATIONS

ACS	acute coronary syndrome
ADP	adenosine diphosphate
APC	activated protein C
aPTT	activated partial thromboplastin time
Arg	arginine
ASO	antisense oligonucleotide
AT	antithrombin
Ca^{2+}	calcium
COOH	C-terminal domain
CTI	corn trypsin inhibitor
Cys	cysteine
C1-INH	C1-inhibitor
Da	Dalton
DNA	deoxyribonucleic acid
DOAC	direct oral anticoagulant
DTI	direct thrombin inhibitor
DTT	dithiothreitol
DVT	deep vein thrombosis
EDTA	ethylenediaminetetraacetic acid
EGF1	epidermal growth factor 1
EGF2	epidermal growth factor 2
EPCR	endothelial protein C receptor
F	factor
FDPs	fibrin degradation products
$FeCl_3$	ferric chloride
FNI	fibronectin type 1
FNII	fibronectin type II
GAGs	glycosaminoglycans
GGCX	γ-glutamylcarboxylase
Gla	γ-carboxyglutamic acid
Glu	glutamic acid
Gly	glycine
GPI	glycosylphosphatidylinositol
HC	heavy chain
HCR	heavy chain remnant
HHPHG	His-His-Pro-His-Gly
HK	high molecular weight kininogen
HPRG	histidine-proline rich glycoprotein
HRG	histidine-rich glycoprotein
HRR	histidine-rich region
HSPG	heparan sulfated proteoglycan

IC_{50}	half maximal inhibitory concentration
IgG	immunoglobulin G
IP_6	inositol hexakisphosphate 6
IPTG	isopropyl β-D-1-thiogalactopyranoside
Ir-CPI	an inhibitor of FXII
K	kringle
Ka	α-kallikrein
K_d	dissociation constant
K_i	inhibition constant
LMWK	low molecular weight heparin
MBP	maltose-binding protein
NETs	neutrophil extracellular traps
NVAF	nonvalvular atrial fibrillation
OPD	o-phenylenediamine dihydrochloride
PAI-1	plasminogen activator inhibitor-1
PAR-1	protease-activated receptor-1
PE	pulmonary embolism
PCPS	phosphatidylcholine-phosphatidylserine vesicles
PCR	polymerase chain reaction
PK	prekallikrein
PolyP	inorganic polyphosphates
PPACK	Phe-Pro-Arg-chloromethylketone
PRR1	proline-rich region-1
PRR2	proline-rich region-2
PS	phosphatidylserine
PT	prothrombin time
RCL	reactive center loop
RNA	ribonucleic acid
RU	response units
SA	streptavidin
SDS	sodium dodecyl sulfate
SE	systemic embolism
SPR	surface plasmon resonance
STI	soybean trypsin inhibitor
TAFI	thrombin activatable fibrinolysis inhibitor
TF	tissue factor
TFPI	tissue factor pathway inhibitor
TM	thrombomodulin
tPA	tissue plasminogen activator
TRAP	thrombin receptor activating peptide
UFH	unfractionated heparin
uPA	urokinase-type plasminogen activator
VKA	vitamin K-antagonist
VKDP	vitamin K-dependent protein

VKOR	vitamin K epoxide reductase
VTE	venous thromboembolism
vWF	von Willebrand factor
Zn^{2+}	zinc
$ZnCl_2$	zinc chloride

DECLARATION OF ACADEMIC ACHIEVEMENT

I, Tammy K. Truong, declare this thesis to be my own work. I am the sole author of this document. No part of this work has been published or submitted for publication or for a higher degree at another institution.

To the best of my knowledge, the content of this document does not infringe on anyone's copyright.

My supervisor, Dr. Jeffrey I. Weitz, and the members of my supervisory committee, Dr. Patricia C. Liaw and Dr. Peter L. Gross, have provided guidance and support at all stages of this project.

Contribution: Tammy K. Truong designed research, contributed vital new reagents, performed research, and analyzed and interpreted data. Alan R. Stafford designed research, contributed vital new reagents, and analyzed and interpreted data. Rida A. Malik designed research, contributed vital new reagents, performed research, and analyzed and interpreted data. Hasam M. Madarati designed and performed research, analyzed and interpreted data. Beverly A. Leslie, Ebenezer Ajewole, Bubacarr G. Kaira, and Jonas Emsley contributed vital new reagents. Dr. Colin A. Kretz, Dr. James C. Fredenburgh, and Dr. Jeffrey I. Weitz designed research, analyzed and interpreted data.

1.0 CHAPTER 1: INTRODUCTION

1.1 OVERVIEW OF HEMOSTASIS

Hemostasis involves a complex network of tightly regulated processes to rapidly respond to vessel injury through formation of fibrin clots, while maintaining blood in a fluid state where the circulation is intact (Colman, 2006; Gailani & Renné, 2007a; Versteeg et al., 2013). This system is required for maintaining the integrity of the circulatory system through a balance between procoagulant, anticoagulant, and fibrinolytic processes (Weitz, 2012). Upon vascular injury, subendothelial components in the vessel wall are exposed to circulating blood, triggering the activation of primary, secondary, and tertiary hemostasis (Colman, 2006; Monroe & Hoffman, 2006).

Primary hemostasis involves the recruitment of platelets by von Willebrand factor (VWF) to the site of injury (Versteeg et al., 2013). Platelets adhere to a VWF/collagen matrix, which triggers platelet activation and aggregation, forming a monolayer (platelet plug) that supports and promotes secondary hemostasis (Weitz, 2012). Once the initial platelet plug is formed, secondary hemostasis occurs through the activation of the coagulation cascade. During coagulation, a series of proteolytic reactions occur, and complexes are formed, which convert zymogens in the blood into active enzymes (Colman, 2006; Mackman, 2004). Through the activation of coagulation factors and cofactors, thrombin is generated and ultimately forms the fibrin mesh that stabilizes the platelet plug to allow wound healing (Grover & Mackman, 2019).

During fibrin clot or “thrombus” formation, circulating red blood cells, white blood cells, and platelets become incorporated into its structure (Gailani & Renné, 2007a). In tertiary hemostasis, fibrinolysis is activated to facilitate healing by fibrin clot degradation through the formation of plasmin (Carpenter & Mathew, 2008; Colman & Schmaier, 1997). The enzymatic breakdown of the fibrin in blood clots is initiated when plasminogen activators released from the vessel wall convert zymogen plasminogen to the active serine protease, plasmin. Proteolysis of fibrin by plasmin degrades the fibrin mesh to dissolve the clot and gives rise to soluble fibrin degradation products (FDPs) (Carpenter & Mathew, 2008). Therefore, hemostasis depends on the dynamic balance and concurrent processes involved in the coagulation and fibrinolysis systems. Fibrin clots that persist can obstruct blood flow, whereas unstable clots that are too rapidly degraded can lead to hemorrhage.

1.2 OVERVIEW OF THROMBOSIS

Dysregulation in the balance between procoagulant, anticoagulant, and fibrinolytic processes can lead to thrombosis or bleeding, which can precipitate life-threatening disorders, such as myocardial infarction, stroke, or venous thromboembolism (VTE) (Gailani & Renné, 2007a). The Global Burden of Disease Study 2010 (GBD 2010) documented that ischemic heart disease and stroke accounted for one in four deaths worldwide, and that thromboembolic conditions are the leading cause of mortality (Raskob et al., 2014; Wendelboe & Raskob, 2016). Thrombosis, which is caused by localized clotting of the blood can occur in the arterial or venous circulation and has a major medical impact. Arterial thrombosis is the most common cause of acute coronary syndrome,

ischemic stroke, and limb gangrene, whereas thrombosis in the deep veins of the legs can lead to pulmonary embolism, which can be fatal or to post-thrombotic syndrome, which decreases quality of life (Badimon et al., 2012; Bentzon et al., 2014).

Most arterial thrombi form on top of disrupted atherosclerotic plaques due to exposure of thrombogenic material in the plaque core to the blood (Bentzon et al., 2014). This material then triggers platelet aggregation and fibrin formation, which results in the generation of platelet-rich thrombus that may temporally or permanently occlude blood flow (Geng & Libby, 2002). Temporary occlusion of blood flow in coronary arteries may trigger unstable angina, whereas persistent obstruction causes myocardial infarction (Badimon et al., 2012). The same processes can occur in the cerebral circulation, where temporary arterial occlusion may manifest as a transient ischemic attack and persistent occlusion can lead to a stroke (Cade, 2008; Laslett et al., 2012). In contrast to arterial thrombi, venous thrombi rarely form at sites of obvious vascular disruption. Although they can develop after surgical trauma to veins or secondary to indwelling venous catheters, they usually originate within the deep veins of the legs, where there is stasis (Stone et al., 2017). Deep vein thrombi can dislodge and travel to the lungs to produce pulmonary embolism (PE), which can be fatal (Beckman et al., 2010). Despite advances in antithrombotic therapy, thrombotic disorders continue to be the leading cause of mortality and disability in Canada and worldwide (Raskob et al., 2014).

1.3 OVERVIEW OF COAGULATION

Coagulation is a rapid response to stem blood loss at the site of vascular injury. The coagulation system is comprised of a tightly controlled network of biochemical reactions that ultimately lead to the cleavage of prothrombin to thrombin and the formation of a fibrin clot (Mackman, 2004). This network includes zymogens, enzymes, co-factors, and inhibitors, which rapidly generate thrombin at the site of injury and efficiently eliminate it in the peripheral area (Rana & Neeves, 2016). The conversion of fibrinogen to fibrin catalyzed by thrombin occurs through two converging cascades: the tissue factor (TF) or extrinsic pathway and the contact or intrinsic pathway (Figure 1) (Colman, 2006). The extrinsic pathway requires TF exposure on sub-endothelial cells following vessel injury or from TF-bearing microparticles and monocytes in circulation (Peterson et al., 1995). In contrast, the initiation of the intrinsic pathway requires only components present in circulation (Renné, 2012). The majority of clotting factors are precursors of proteolytic enzymes known as zymogens that circulate in an inactive form. Coagulation occurs through the action of discrete enzyme complexes, which are composed of an enzyme and a non-enzyme cofactor. Together, these complexes generate a small amount of thrombin, which amplifies its own generation by activating the non-enzyme cofactors and platelets, which then provide an anionic surface on which the complexes assemble. The three predominant enzyme complexes involved in thrombin generation are extrinsic tenase, intrinsic tenase, and prothrombinase. Although extrinsic tenase initiates the system under most circumstances, there is growing evidence that the contact system can also initiate

coagulation independent of the extrinsic pathway (Gailani et al., 2015; Jain et al., 2012; Renné & Gailani, 2007; Weitz, 2016).

1.3.1 Extrinsic Pathway

The extrinsic pathway is initiated when there is TF exposure by sub-endothelial cells after vessel injury, or by either TF-positive monocytes or TF-bearing microparticles in the circulation (Mackman, 2006; Owens & Mackman, 2011). Circulating factor (F) VII binds to its membrane-bound cofactor, TF (Colman, 2006). Once bound to TF, FVII is activated to FVIIa, which may also be present in circulation or activated by autoactivation, as well as by limited proteolysis by FIXa or FXa (Mackman, 2004; Owens & Mackman, 2010; Wildgoose & Kisiel, 1989). The TF-FVIIa complex (extrinsic tenase), in the presence of calcium (Ca^{2+}), then cleaves FX to its activated form, FXa (Mackman et al., 2007). In the presence of Ca^{2+} and phosphatidylserine (PS), FXa is then able to associate with its cofactor, FVa, to form the prothrombinase complex on TF-expressing cells (such as endothelial cells and monocytes) and on the surface of activated platelets (Grover & Mackman, 2018; Versteeg et al., 2013). This in turn converts prothrombin to thrombin, where thrombin can then cleave fibrinogen to fibrin, and thus form the blood clot (Colman, 2006; Mackman, 2006).

1.3.2 Intrinsic Pathway

The intrinsic pathway is triggered when FXII binds to negatively charged surfaces, such as naturally occurring polyanions, including nucleic acids (RNA, DNA) and

polyphosphate, as well as glycosaminoglycans (GAGs) or denatured proteins (Renné et al., 2012; Zhu et al., 2015). Binding to negatively charged surfaces induces a conformational change in FXII resulting in its autoactivation, which is enhanced in the presence of zinc (Zn^{2+}) (Vu et al., 2013). FXII autoactivation occurs by cleavage of the Arg353-Val354 bond, allowing for the conversion of single-chain FXII into its activated, two-chain form (MacQuarrie et al., 2011; Renné et al., 2012). FXIIa activates prekallikrein (PK) to α-kallikrein (Ka) in the presence of high molecular weight kininogen (HK) (Gailani & Renné, 2007a; Renné, 2012). PK activation is then able to provide a second amplification loop as Ka activates FXII (Gailani & Renné, 2007b; Schmaier, 2008). FXIIa initiates coagulation by activating FXI, which circulates in complex with HK (Schmaier, 2016). FXIa then activates FIX, allowing FIXa to be incorporated into the intrinsic tenase complex of FIXa and FVIIIa assembled on anionic phospholipid surfaces in the presence of Ca^{2+} (Gailani & Renné, 2007a). Intrinsic tenase activates FX, which binds to its cofactor, FVa, on an anionic phospholipid surface to form prothrombinase (Chu, 2010). Prothrombinase activates prothrombin to thrombin, which then converts fibrinogen to fibrin (Gailani & Renné, 2007a).

1.3.3 Common Pathway

The common pathway consists of factors I (fibrinogen), II (prothrombin), V, and X. This pathway begins at FX, where both the extrinsic and intrinsic pathways merge in the coagulation cascade (Versteeg et al., 2013). FX is activated to FXa by either the extrinsic or intrinsic tenase complex (Weitz, 2012). The prothrombinase complex is

composed of the protease FXa and its cofactor FVa, which assemble on PS-expressing membranes in the presence of calcium (Amphlett et al., 1981). The prothrombinase complex activates the substrate prothrombin to thrombin. Assembly into prothrombinase complex significantly increases (>100-fold) the catalytic efficiency of FXa to cleave prothrombin to α-thrombin (Fredenburgh & Weitz, 2018). Thrombin goes on to convert fibrinogen into fibrin monomers. Thrombin also goes on to activate other factors in the intrinsic pathway (FXI and FVIII), as well as FV and FXIII (Versteeg et al., 2013). Activated FXIII (FXIIIa) catalyzes the cross-linking of fibrin molecules in the final step of blood coagulation, thereby increasing the mechanical stability of the clot and rendering it resistant to plasmin degradation (Marx et al., 1993; Monroe & Hoffman, 2006).

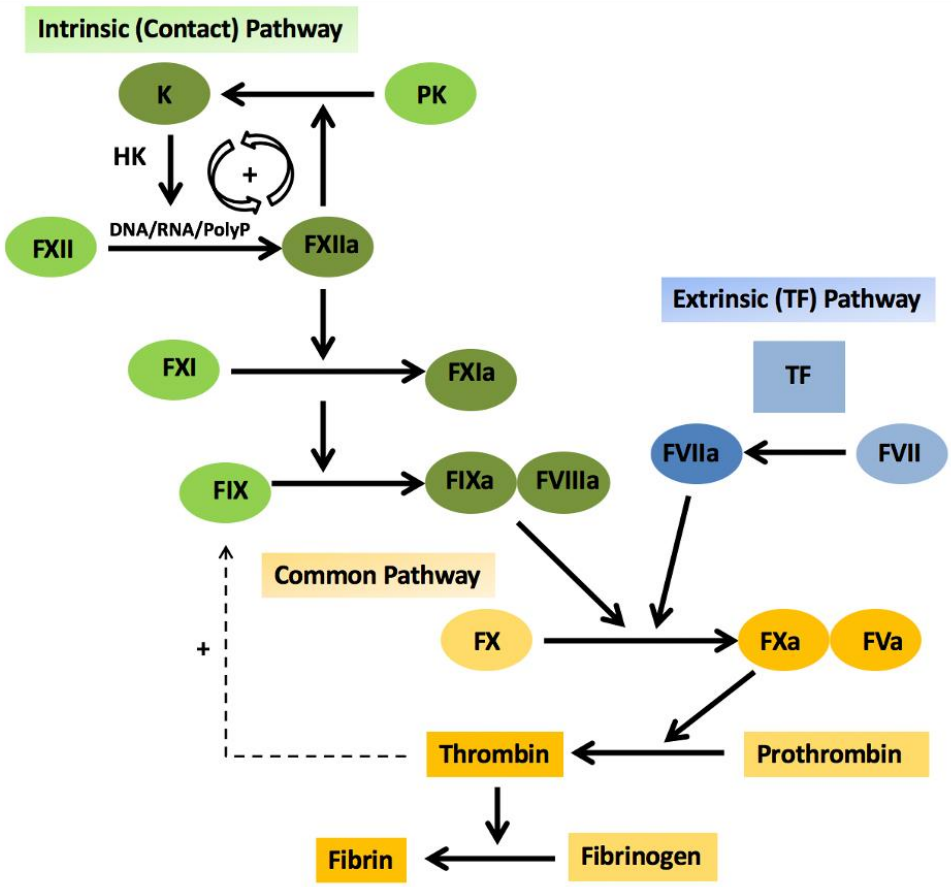
Intrinsic (Contact) Pathway
K
PK
HK
+
FXII
DNA/RNA/PolyP
FXIIa
Extrinsic (TF) Pathway
FXI
FXIa
TF
FVIIa
FVII
FIX
FIXa
FVIIIa
Common Pathway
+
FX
FXa
FVa
Thrombin
Prothrombin
Fibrin
Fibrinogen

Figure 1: Coagulation Cascade

Schematic representation of the components and coagulation factors involved in response to endothelial damage. Tissue factor (TF) is exposed to the bloodstream and binds factor VII. The TF-VIIa complex of the extrinsic pathway enables the subsequent activation of factor X and prothrombin of the common pathway, leading to the initial generation of thrombin. The intrinsic pathway is initiated when factor XII becomes activated upon contact with a negatively charged surface or by polyanions, such as nucleic acids (DNA and RNA) and polyphosphates (PolyP). Activated FXII, FXIIa, then goes on to activate FXI, leading to the subsequent activation and amplification of thrombin, and the formation of the fibrin clot. FXI can be activated by thrombin, independent of FXIIa-mediated activation (+). FXIIa can activate PK upon contact activation of a negatively charged surface, whereby activated kallikrein can back activate further FXII activation, resulting in an autolytic feedback loop (+).

1.3.4 Cell-based model of coagulation

Over recent decades, there has been a paradigm shift from the classic coagulation cascade or "waterfall" model to a more cell-based model of coagulation (Hoffman, 2003; Monroe & Hoffman, 2006). The coagulation cascade model is useful for describing coagulation in closed systems such as clot time assays or thrombin generation assays that are conducted under static conditions in test tubes or well-plates (Rana & Neeves, 2016). In contrast, the cell-based conceptual model of hemostasis proposes that hemostasis occurs in distinct, but overlapping, steps: initiation, amplification, and propagation, which require the participation of two different cell types (TF-bearing cells and platelets) (Figure 2) (Hoffman & Monroe, 2001; Versteeg et al., 2013). The initiation phase, in which low amounts of coagulation factors are activated, is localized to cells that express TF (Hoffman & Monroe, 2001). The coagulation cascade may also be triggered by polyanions, which initiate the intrinsic pathway by inducing FXII autoactivation (Hoffman & Monroe, 2001). It is essential that the initiating and propagation phases are normally sequestered to cell surfaces (ie. TF-bearing cells and platelets) to prevent widespread activation of coagulation (Hoffman & Monroe, 2001). Indeed, localizing FVIIa/TF activity to close proximity to activated platelet surfaces is a critical step in effectively triggering hemostatic coagulation (Hoffman & Monroe, 2001).

During the amplification phase, slow accumulation of thrombin generated on the TF-bearing cell allows for the activation of platelets, exposing receptors and binding sites for activated clotting factors (Hoffman & Monroe, 2001). Small amounts of thrombin also

activate FXI to FXIa on the platelet surface (Hoffman & Monroe, 2001). The thrombin formed during the initiation phase also functions in the activation of the cofactors FV and FVIII on the surface of activated platelets (Hoffman & Monroe, 2001). Collectively, these events set the stage for subsequent large-scale generation of thrombin in the propagation phase (Hoffman, 2003; Monroe & Hoffman, 2006; Versteeg et al., 2013). The activity of FXa formed by the FVIIa/TF complex is restricted to TF-bearing cells due to its rapid inhibition by tissue factor pathway inhibitor (TFPI) or antithrombin (AT) when it dissociates from the cell surface (Hoffman & Monroe, 2007). Moreover, FIXa can disperse to adjacent platelet surfaces as it is not inhibited by TFPI and is eliminated at a slower rate by AT than is FXa (Hoffman & Monroe, 2007). Thus, in order for further thrombin generation to occur, the intrinsic pathway must take over at this point.

In the propagation phase, coagulation factors bind phosphatidyl serine on the surface of activated platelets and fibrin clots are formed (Hoffman, 2003; Versteeg et al., 2013). Activated FXI converts FIX into FIXa, which then associates with thrombin-cleaved FVIIIa (Versteeg et al., 2013). Once intrinsic or platelet tenase is assembled, FX from plasma is activated to FXa on the platelet surface, allowing for assembly of the prothrombinase complex, which supports a burst of thrombin generation of sufficient magnitude to produce a stable fibrin clot (Hoffman, 2003; Hoffman & Monroe, 2007). One key element in propagation is that the intrinsic pathway is more than 10x more efficient at activating FX than the extrinsic pathway (Mann, 1999). Thrombin converts fibrinogen to fibrin, generating soluble fibrin monomers, which spontaneously polymerize into fibrin strands, called protofibrils. As the final step, the thrombin-activated plasma

transglutaminase FXIIIa, covalently cross-links α and γ chains of adjacent fibrin monomers to stabilize the fibrin network to yield an elastic, insoluble fibrin clot (Gross et al., 2012; Versteeg et al., 2013). Thus, the role of the extrinsic pathway in this cell-based model is to act on the TF-bearing cell to generate the small amounts of thrombin involved in initiating coagulation, whereas the role of the intrinsic pathway is to act on the platelet surface to generate the burst of thrombin needed to form a stable fibrin clot (Hoffman & Monroe, 2007).

In order to prevent the generation of thrombin on healthy endothelial cells, there are anticoagulant properties via proteins expressed on their surface, such as heparan sulfated proteoglycans (HSPGs) and TFPI. In addition, the fibrinolytic system helps to localize the formation of thrombin to the immediate area of an injury (Hoffman, 2003). The final effector of the fibrinolytic system is plasmin, which cleaves fibrin into soluble degradation products, resulting in dissolution of the fibrin clot (Hoffman & Monroe, 2007). Other key players of fibrinolysis include, plasminogen, plasminogen activators (tPA, uPA), plasminogen activator inhibitors (PAI-1), TAFI, activated protein C (APC), and thrombomodulin (TM) (Gross et al., 2012; Hoffman, 2003; Hoffman & Monroe, 2001, 2007).

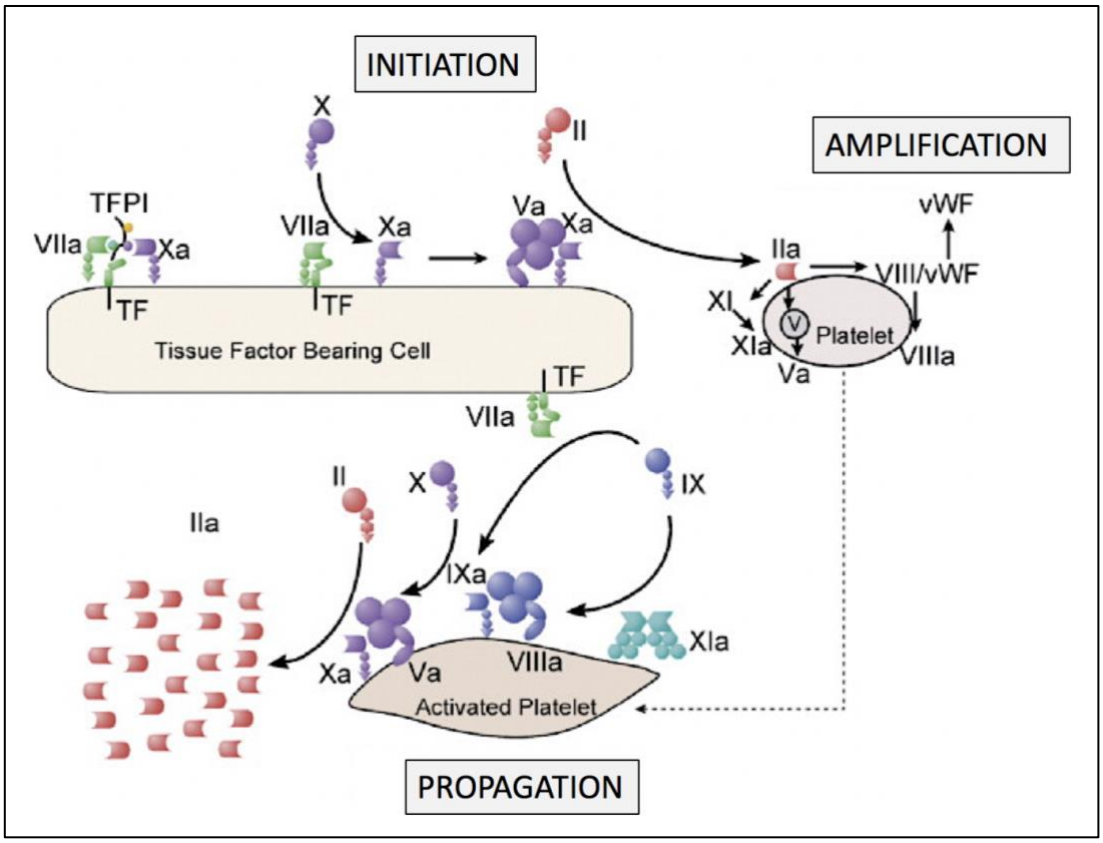
INITIATION
AMPLIFICATION
PROPAGATION
X
II
TFPI
VIIa
Xa
TF
Va
vWF
IIa
VIII/vWF
XI
XIa
Platelet
VIIIa
Va
Tissue Factor Bearing Cell
IX
IXa
VIIIa
Activated Platelet

Figure 2: Cell-based model of coagulation

The cell-based conceptual model of hemostasis proposes that hemostasis occurs in distinct, but overlapping, steps: initiation, amplification, and propagation. The initiation phase, in which low amounts of coagulation factors (FVII) are activated, is localized to cells that express tissue factor. During the amplification phase, slow accumulation of thrombin generated on the TF-bearing cell allows for the activation of platelets. In the propagation phase, coagulant factors bind procoagulant membranes on the surface of activated platelets and fibrin clots are formed. Adapted from Ma, A. D and Key, N. S. *Molecular Pathology: The Molecular Basis of Human Disease.* 2009; 247-264.

1.4 ANTICOAGULANT PATHWAYS OF COAGULATION

There are several anticoagulant pathways positioned to oppose the procoagulant response by inhibiting and redirecting the activity of the proteases. Physiological anticoagulants tightly regulate the activity of the coagulation proteases so as to prevent excessive clotting from occurring. The main anticoagulant pathways include the tissue factor pathway inhibitor (TFPI), antithrombin (AT), and protein C anticoagulant pathways, which function to localize, limit, and control hemostasis (Figure 3).

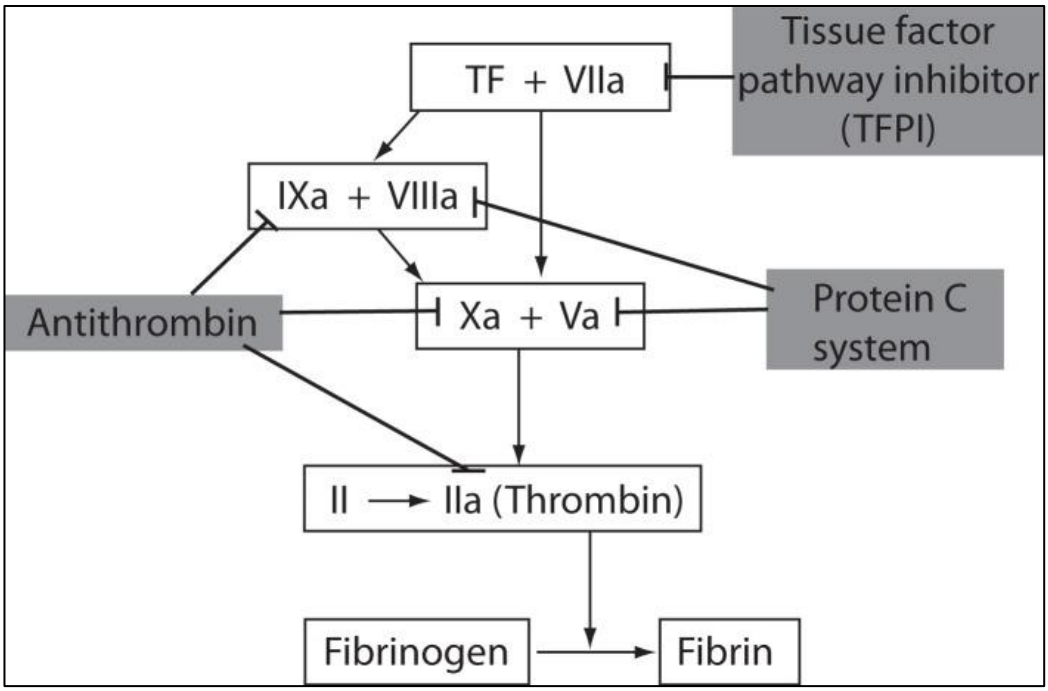
Tissue factor pathway inhibitor (TFPI)
TF + VIIa
IXa + VIIIa
Antithrombin
Xa + Va
Protein C system
II → IIa (Thrombin)
Fibrinogen
Fibrin

Figure 3: Physiological anticoagulant pathways

The three major physiological anticoagulant mechanisms are the antithrombin (AT), protein C (PC) system and tissue factor pathway inhibitor (TFPI) pathways. Antithrombin is the main inhibitor of thrombin, FXa, and FIXa. PC pathway proteolytically cleaves activated coagulation cofactors FVa and FVIIa. TFPI is the main inhibitor of the TF-FVIIa complex. The main function of these coagulation inhibitors is to prevent excessive blood clotting under physiological conditions and to slow down the activated coagulation cascade after vascular injury. Source: Margetic, S. *Biochemia Medica*. 2012; 22(1):49–62.

1.4.1 Tissue Factor Pathway Inhibitor

TFPI, formerly known as extrinsic pathway inhibitor or lipoprotein-associated coagulation, is a Kunitz-type plasma proteinase inhibitor, which circulates in plasma as a heterogenous collection of partially proteolyzed forms (Dickneite & Mescheder, 2000). TFPI forms a quaternary complex with TF, FVIIa, and FXa to prevent production of FXa and FIXa by the TF-FVIIa complex. TFPI is the principal stoichiometric inhibitor of the extrinsic tenase complex (FVIIa-TF) (Dickneite & Mescheder, 2000), as it simultaneously inhibits FXa and TF-FVIIa immediately after FX is activated by TF-FVIIa (Mast, 2016). TFPI also inhibits further thrombin generation by FXa. The majority of TFPI is bound to the endothelium, and a smaller portion is bound to the surface of monocytes and non-specifically to GAGs. Circulating TPFI (20%) is largely found to associate with lipoproteins, primarily low-density lipoprotein (Mast, 2016). TFPI is cleared from the circulation mainly by the liver and has an unusually short half-life of minutes compared with other proteinase inhibitors (Mast, 2016). Two major isoforms of TFPI have been described: TFPIα and TFPIβ, which differ in their affinity for FV/FVa and protein S, their tissue expression (platelet and endothelium, respectively), their mechanism for association with cell surfaces, and their ability to inhibit TF-FVIIa or prothrombinase activity (Wood et al., 2014). TFPIα, the full-length isoform of TFPI, comprises three Kunitz-type inhibitory domains (K1, K2, K3) and a positively charged C terminus domain that contains the binding site for the acidic region in the B-domain of FV (Dahlbäck et al., 2018). TFPIβ, contains the K1 and K2 domains of TFPIα and a unique C terminus that allows for

glycosylphosphatidylinositol (GPI) anchoring for optimal inhibition of TF-FVIIa and FXa on endothelium (Mast, 2016; Wood et al., 2014). TFPI deficiency is embryonic lethal in humans, however murine studies have shown that this lethality can be rescued by heterozygous or homozygous FVII deficiency (Eitzman et al., 2002). This implies that diminishing the level of FVII lessens the need for TFPI-mediated inhibition of the FVIIa-TF coagulation pathway during embryogenesis.

1.4.2 Antithrombin

AT is a serine protease inhibitor (serpin) synthesized in the liver that circulates in the blood as a 58,200 Da single-chain glycoprotein at a concentration of 2.6 ± 0.4 μM (Chandra et al., 1983; Hsu & Moosavi, 2019). AT is the obligatory plasma cofactor for heparin and acts as a suicide substrate for its target enzymes (Chandra et al., 1983; Desai, 2004). AT has a broad spectrum of inhibitory activity with most of its target proteases participating in the coagulation cascade. It is the major inhibitor of the serine proteases thrombin, FXa, FVIIa, and FXIa (Hsu & Moosavi, 2019). AT also inhibits FIXa, FXIIa, and Ka (Abildgaard, 1969; Kurachi et al., 1976).

AT inhibits its target protease by forming a covalent, equimolar, irreversible complex with the protease. This occurs through reaction of the active site of the enzyme with the reactive center loop (RCL) of AT (Hsu & Moosavi, 2019). The target protease binds to the RCL of AT, resulting in the cleavage of the scissile bond P1-P1` in the RCL. This results in the formation of an acyl-enzyme intermediate that undergoes a major rearrangement that disrupts the enzyme's catalytic triad and allows for inhibition of the

protease (Desai, 2004). On the endothelial cell surface, AT binds to heparin-like proteoglycans (heparan sulfate) to accelerate inhibition of its target protease (Shimada et al., 1991). AT acts as cofactor for heparin, a sulfated polysaccharide, catalyzing the inhibitory activity by bridging AT to thrombin together. When AT is complexed with heparin, its rate of inhibition of several coagulation proteases is accelerated by up to 1000-fold (Perry, 1994). Heparin is used for the treatment and prevention of thromboembolic disease and will be further discussed below (Blajchman, 1994; Desai, 2004; Esmon & Esmon, 2011).

1.4.3 Protein C Pathway

The protein C pathway regulates the activity of coagulation cofactors FVIIIa and FVa in the activation of FX and prothrombin, respectively (Esmon, 2000). This anticoagulant pathway plays an important role in stopping the propagation phase of coagulation and limiting further thrombin generation. Thrombin interacts with thrombomodulin on the endothelial cell surface to form a complex (thrombin-TM) (Esmon & Esmon, 2011). PC is activated when thrombin-TM associates in close proximity to PC and endothelial protein C receptor (EPCR) on the endothelium. EPCR enhances the activation of PC by localizing the protein to the cell surface and the thrombin/TM complex (Esmon, 2004). Activated protein C (APC)-mediated cleavage of FVIIIa and FVa occurs on negatively charged phospholipid membranes and involves Ca^{2+} and a protein cofactor, protein S. APC also has anti-inflammatory and anti-apoptotic activities that involve binding of APC to EPCR and cleavage of protease-activated receptor-1 (PAR-1) (Griffin et al.,

2007). In addition, APC plays an indirect profibrinolytic role through its property of limiting thrombin formation and consequently attenuating the subsequent thrombin-catalyzed activation of a fibrinolytic inhibitor, thrombin activatable fibrinolysis inhibitor (TAFI) (Dahlbäck & Villoutreix, 2005). APC enhances fibrinolysis by inactivation of another fibrinolytic inhibitor, plasminogen activator inhibitor-1 (PAI-1). Individuals with protein C deficiency, caused by mutations in the *PROC* gene, are at risk of venous thromboembolism (Dahlbäck & Villoutreix, 2005; Griffin et al., 2007; Manco-Johnson et al., 2016).

1.5 OVERVIEW OF TRADITIONAL ANTICOAGULANTS

Anticoagulants are routinely indicated for the prevention and treatment of venous thromboembolism as venous thrombi consist mainly of fibrin and red blood cells. Strategies to inhibit arterial thrombogenesis focus mainly on blocking platelet function, however, anticoagulants are often indicated to prevent fibrin deposition (Mackman, 2008). Anticoagulant drugs reduce the activity of various coagulation proteases by directly inhibiting them, reducing their post-translational modification or by enhancing the activity of an anticoagulant (Melnikova, 2009). Parenteral anticoagulants that are currently available include heparins (unfractionated heparin, low-molecular-weight heparin, fondaparinux), direct thrombin inhibitors (bivalirudin, argatroban), as well as traditional oral vitamin K antagonists (ie. warfarin) (Stone et al., 2017; Zirlik & Bode, 2017).

1.5.1 Heparin

Heparin, also known as unfractionated heparin (UFH), is a sulfated polysaccharide with a molecular weight range of 3000 - 30,000 Da (mean of 15,000 Da or approximately 45 saccharide units) (Bussey et al., 2004; Hirsh et al., 1995). Heparin exerts its major anticoagulant effects by inactivating thrombin and FXa through an antithrombin (AT)-dependent mechanism. The heparin/AT-complex also inhibits FXIIa, FXIa, and FIXa. To activate AT, heparin binds to lysine sites on AT via a unique high-affinity pentasaccharide sequence, which is present on about a third of heparin molecules (Hirsh & Raschke, 2004; Mulloy et al., 2015). Binding of the pentasaccharide sequence to AT induces an allosteric conformational change in the reactive center loop (RCL) of AT that enhances the rate of inhibition of FXa by greater than 2 orders of magnitude, but not of thrombin (Lindahl et al., 1979; Weitz, 2003). Inhibition of FXa requires only the high affinity pentasaccharide, whereas the inhibition of thrombin requires the formation of a stable covalent ternary complex between heparin, AT, and thrombin (Bussey et al., 2004). Heparin serves as a template that localizes the binding of AT and thrombin; thus, catalyzing the inhibition of thrombin. Moreover, molecules of heparin with at least 18 saccharide units (corresponding to a molecular weight of approximately 5400 Da) are required to bridge thrombin and AT together (Conners & Money, 2002).

1.5.2 Low Molecular Weight Heparin

Like heparin, low molecular weight heparin (LMWH) is an anticoagulant that catalyzes the activity of antithrombin. LMWHs are fragments of commercial grade heparin

that consist of <18 saccharide units, which corresponds to a mean molecular weight of approximately 4500 Da (Conners & Money, 2002). Unlike heparin, at least half of the pentasaccharide-containing chains of LMWH are too short to bridge thrombin to antithrombin but retain their capacity to accelerate FXa inhibition by antithrombin. Consequently, LMWH catalyzes FXa inhibition by antithrombin more than thrombin inhibition. Depending on their unique molecular weight distributions, LMWH preparations have anti-FXa to anti-thrombin ratios ranging from 2:1 to 4:1 (Hirsh, 1998). LMWH can be administered once or twice daily by subcutaneous injection without coagulation monitoring. Compared with heparin, LMWH preparations have more predictable pharmacokinetic and pharmacodynamic properties and have a longer half-life than heparin. LMWHs exhibit less binding to cells and plasma proteins than heparin, and thus are associated with a lower risk of nonhemorrhagic side effects (Hirsh et al., 1995).

1.5.3 Fondaparinux

Fondaparinux is an effective and useful alternative to LMWH for the prevention and initial treatment of VTE, as well as for the treatment of acute coronary syndrome (ACS) (Garcia et al., 2012; Mehta et al., 2008; Reynolds et al., 2004). The synthetic analogue of the antithrombin-binding pentasaccharide sequence binds only to antithrombin and is too short to bridge thrombin to antithrombin (Reynolds et al., 2004). By doing so, fondaparinux selectively catalyzes FXa inhibition by antithrombin and does not enhance the rate of thrombin inhibition. With a plasma half-life of about 17 hours, fondaparinux exhibits

complete bioavailability when administered subcutaneously, is administered once daily, and has a predictable pharmacokinetic profile (Bergqvist, 2006).

1.5.4 Vitamin K Antagonists

Vitamin K is essential for the carboxylation of glutamic acid residues in vitamin K-dependent proteins (VKDP) that are involved in blood coagulation, including prothrombin, and factors VII, IX, and X. More specifically, vitamin K functions as a cofactor for the enzyme γ-glutamylcarboxylase (GGCX) that catalyzes the carboxylation of the amino acid glutamic acid (Glu) to γ-carboxyglutamic acid (Gla) (Tie et al., 2016). The created Gla domains of the VKDP bind to calcium, which is critical for the interaction of the clotting factors with negatively charged phospholipid membranes. All vitamin K-dependent factors possess glutamic acid residues at their N-termini, which is carboxylated by GGCX (Tie & Stafford, 2016). Without these residues carboxylated, the vitamin K-dependent factors are unable to form the appropriate active conformation, thus inhibiting their biological activity. The body recycles vitamin K through a process called the vitamin K-epoxide cycle (De Caterina et al., 2013). Vitamin K hydroquinone (reduced form) is oxidized to vitamin K epoxide (oxidized form). The reaction enables GGCX to carboxylate selective glutamic acid residues on VKDP as mentioned above. To allow for recycling of vitamin K, once vitamin K hydroquinone is oxidized to vitamin K epoxide, the oxidized form is then reduced to vitamin K by the enzyme, vitamin K epoxide reductase (VKOR) (Sinhadri et al., 2017).

Over the past 60 years, vitamin K-antagonists (VKAs), most commonly warfarin, have been widely used as effective oral anticoagulants. VKAs are structurally similar to vitamin K and act as competitive inhibitors of the enzyme, VKOR. By inhibiting VKOR activity, warfarin blocks the γ-carboxylation process, attenuating the recycling of the inactive vitamin K epoxide back to its active reduced form (De Caterina et al., 2013). This results in a functional deficiency of vitamin K and the synthesis of vitamin K-dependent clotting factors that are only partially γ-carboxylated. Warfarin acts as an anticoagulant by generating these partially γ-carboxylated proteins that have reduced or absent biologic activity (Jaffer & Weitz, 2018). Warfarin also reduces the synthesis of the vitamin K-dependent anticoagulant proteins C, S, and Z. The onset of warfarin is delayed until the newly synthesized clotting factors with reduced activity gradually replace their fully active counterparts. Due to its slow onset of action, warfarin must be overlapped with heparin (or another rapidly acting anticoagulant) when treating patients with established thrombosis or who are at high risk for thrombosis (Zirlik & Bode, 2017). Patients on warfarin require frequent blood tests, which is inconvenient for patients and for physicians (Zirlik & Bode, 2017). Warfarin dosing is variable and challenging as its activity is influenced by dietary intake of vitamin K, genetic polymorphisms in enzymes that are involved in its metabolism (Tie et al., 2016), as well as numerous drug-drug interactions that promote or reduce its activity (Zirlik & Bode, 2017). Moreover, vitamin K deficiency increases the risk of excessive bleeding. Thus, despite careful monitoring, the incidence of major bleeding is about 1-3% of warfarin-treated patients per year (Mackman, 2008). Although effective,

warfarin has important limitations that prompted the development of novel anticoagulant therapies.

1.6 OVERVIEW OF ORAL ANTICOAGULANTS

Direct thrombin inhibitors (DTIs) have been used for the prevention and treatment of venous and arterial thromboembolism. DTIs bind directly to thrombin and do not require a cofactor such as antithrombin to exert their effect (Melnikova, 2009). Currently, there are four FDA-approved parenteral DTIs in North America, including bivalirudin, lepirudin, desirudin, and argatroban (Mackman & Becker, 2010). Parenteral DTIs can, however, be difficult to administer and are limited in their indications. In response to the need for oral anticoagulants, direct oral anticoagulants (DOACs) have been developed. In the last 20 years, the DOACs have pioneered a new generation of effective anticoagulants that addresses many of the limitations of the traditional anticoagulant therapies (Bickmann et al., 2017). There was a lot of interest in the introduction of DOACs for the prevention and treatment of venous and arterial thromboembolism with Health Canada approval of rivaroxaban (Xarelto) in 2008, dabigatran (Pradaxa) in 2010, apixaban (Eliquis) in 2012, and edoxaban (Lixiana) in 2016. DOACs selectively target thrombin (e.g. dabigatran) or FXa (e.g. rivaroxaban, apixaban, and edoxaban).

Dabigatran is an oral, direct inhibitor of thrombin that binds to the active site on thrombin, preventing thrombin-mediated activation of coagulation factors (Comin & Kallmes, 2012). Dabigatran is a small molecule (472 Da) that is synthesized as a derivative of a peptide-like, benzamidine-based thrombin inhibitor. After oral administration,

dabigatran etexilate (prodrug of dabigatran) is rapidly converted into dabigatran by means of esterases (Lee & Ansell, 2011). It rapidly and reversibly inhibits both clot-bound and free thrombin in a concentration dependent manner with an inhibition constant (K_i) of 4.5 nmol L^{-1} (Eriksson et al., 2009). Dabigatran is currently licensed in Canada for the prevention of stroke and systemic embolism in patients with non-valvular atrial fibrillation, and for the prevention of deep vein thrombosis (DVT) and pulmonary embolism (PE) after elective hip or knee replacement surgery. In addition, dabigatran is licensed for the treatment of acute DVT and PE in patients who have initially received 5 to 10 days of a parenteral anticoagulant and to prevent recurrent DVT and PE (Jaffer & Weitz, 2018).

Direct factor Xa inhibitors reduce thrombin production by selectively inhibiting factor Xa and prothrombinase activity. As the first marketed oral direct factor Xa inhibitor, rivaroxaban competitively inhibits FXa and does not require cofactors (such as antithrombin) to exert its anticoagulant effect. Rivaroxaban belongs to a new class of oxazaolidinone-based, active site directed, FXa inhibitors. It is a small molecule (435 Da) that binds directly and reversibly to the S1 and S4 pockets of the active site of FXa (Siddiqui et al., 2019). A unique feature of the small molecule is that it lacks a highly basic group in its active site binding region, contributing to its high bioavailability (Eriksson et al., 2009). By binding directly to these active site pockets of FXa, rivaroxaban is more than 10,000-fold more selective for FXa than other related serine proteases (Perzborn et al., 2010). Rivaroxaban reduces the thrombin burst during the propagation phase by inhibiting both free and clot-bound FXa, as well as prothrombinase activity in a concentration-dependent manner (IC_{50} of 0.4 nM) (Perzborn et al., 2009).

As the second oral direct FXa inhibitor to be approved by Health Canada, apixaban inhibits both free and clot bound FXa, as well as prothrombinase activity. It is a small molecule (459 Da) that reversibly binds to the active site of FXa (Eriksson et al., 2009). Apixaban is currently licensed for stroke prevention in atrial fibrillation, for treatment and secondary prevention of venous thromboembolism, and for thromboprophylaxis after hip or knee replacement surgery in many countries (Jaffer & Weitz, 2018). Lastly, the third licensed direct oral FXa inhibitor, edoxaban is a small molecule (548 Da) that binds reversibly to the active site of factor Xa (Siddiqui et al., 2019). Edoxaban is indicated for the prevention of stroke and systemic embolism (SE) in patients with nonvalvular atrial fibrillation (NVAF) and for the treatment of DVT and PE following 5 to 10 days of initial therapy with a parenteral anticoagulant. Edoxaban inhibits free FXa and FXa incorporated into the prothrombinase complex.

The main objective of anticoagulation therapy is to attenuate thrombosis without affecting hemostasis. With the development of DOACs, we have come much closer to this goal because annual rates of major bleeding with DOACs are lower than those with vitamin K antagonists such as warfarin (0.3% to 0.5% vs 1.9%, respectively) (Mekaj et al., 2015). However, patients with atrial fibrillation on DOACs exhibit annual rates of major bleeding of 2% to 3% (Halvorsen et al., 2017; López-López et al., 2017; Weitz & Chan, 2018). Therefore, there remains room for improvement and a need for alternate anticoagulants that are safer than current DOACs.

1.7 STRATEGIES TO TARGET CONTACT PATHWAY

An emerging frontier of anticoagulant therapy involves the contact pathway, particularly FXII and FXI, as potential targets in the development of safer anticoagulants, given the bleeding risk associated with inhibiting the distal part of the coagulation pathway with traditional anticoagulants or with DOACs (Figure 4). As previously mentioned, DOACs target downstream in the coagulation cascade at FXa and thrombin. As a result, these anticoagulants are associated with a risk of bleeding because they target pathways involved in hemostasis, which is required for normal wound healing (Weitz, 2016). There is emerging data from basic and epidemiological studies suggesting that FXII and FXI are important in thrombosis (Geddings & Mackman, 2014; Maas et al., 2018; Pham et al., 2012; Renné et al., 2006). Targeting these factors would allow for the development of safer anticoagulants as they have little to no role in hemostasis. Further studies are needed to assess whether FXII or FXI would be the more attractive target and to compare the efficacy and safety of these new therapeutic strategies with current standards of care for the prevention and treatment of thrombosis. Current strategies to target FXII and FXI include monoclonal antibodies that block activation or activity, antisense oligonucleotides (ASOs) that reduce hepatic synthesis of the clotting proteins, and small molecules that block the active site or induce allosteric modulation (Deloughery et al., 2019; Fredenburgh et al., 2017; Kenne & Renné, 2014; Weitz & Fredenburgh, 2017a). ASOs, antibodies and aptamers require parenteral administration, whereas active site inhibitors, such as small molecules, have the potential for either parenteral or oral delivery. Strategies also vary in terms of their onset and offset of action. A major limitation of ASO treatment is its slow

onset of action. FXII and FXI ASOs require three to four weeks to lower protein levels into the therapeutic range, limiting their utility for initial treatment of thrombosis or for immediate thromboprophylaxis (Crosby et al., 2013; Yau et al., 2014; Zhang et al., 2010). Moreover, the long half-life of FXI-directed ASOs or antibodies may result in challenges in the face of emergent surgery or severe trauma (Bickmann et al., 2017; Weitz & Fredenburgh, 2017a).

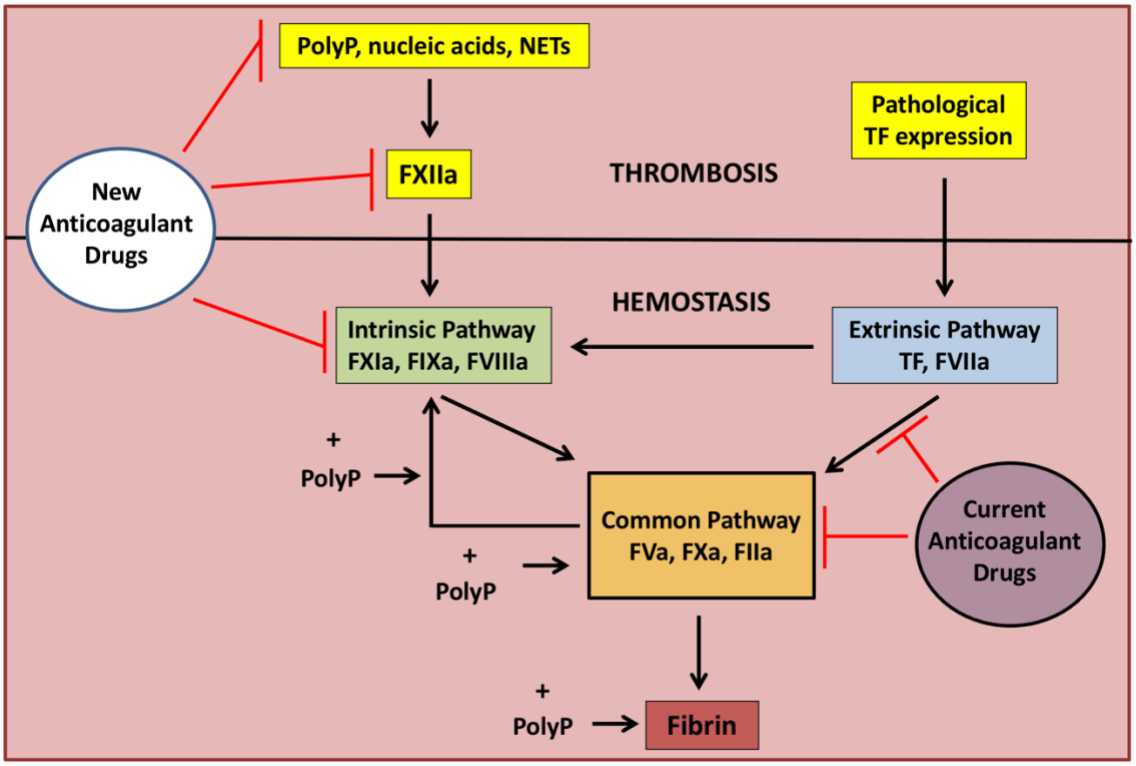
PolyP, nucleic acids, NETs
Pathological TF expression
New Anticoagulant Drugs
FXIIa
THROMBOSIS
HEMOSTASIS
Intrinsic Pathway FXIa, FIXa, FVIIIa
Extrinsic Pathway TF, FVIIa
+ PolyP
Common Pathway FVa, FXa, FIIa
Current Anticoagulant Drugs
+ PolyP
+ PolyP
Fibrin

Figure 4: Novel targets for anticoagulant therapy

Current anticoagulant drugs target the extrinsic and common pathways (i.e direct FXa and thrombin inhibitors), but as a result are associated with a risk of bleeding. Recent studies have identified factors that play an important role in thrombosis, but not in hemostasis (ie. FXII, polyphosphates (polyP), nucleic acids (DNA, RNA), and neutrophil extracellular traps (NETs)). Targeting thrombotic triggers as opposed to targeting pathways involved in hemostasis in the development of novel anticoagulant therapies would allow for the development of novel anticoagulants without the risk of bleeding. Adapted from Geddings, J. E. and Mackman, N. *Thromb Haemost*. 2014; 111(4):570-4.

1.8 CONTACT PATHWAY IN HEMOSTASIS AND THROMBOSIS

Recent studies have shown that the initiator of the intrinsic (contact) pathway FXII is dispensable for normal hemostasis (Gailani & Renné, 2007b; Kleinschnitz, 2006; Renné et al., 2005, 2012). Humans and mice deficient in FXII, PK, or HK have no bleeding complications (Merkulov et al., 2008; Renné et al., 2005, 2012; Revenko et al., 2011). The lack of a bleeding tendency observed in FXII-deficient humans and animals (Maas et al., 2018; Mordillo et al., 2007; Renné et al., 2005) is in sharp contrast to deficiencies of other components of the intrinsic pathways of coagulation cascade such as FVIII or FIX (causing the bleeding disorders hemophilia A and B, respectively) (Mast, 2016). This has led to the reasonable hypothesis that fibrin formation *in vivo* is initiated largely, if not exclusively, through the extrinsic pathway of coagulation. Humans with hereditary deficiencies in FXI, unlike those lacking FXII, suffer from a mild bleeding tendency, suggesting that FXI is required for hemostasis and can be activated independently of FXIIa (Mordillo et al., 2007; Salomon et al., 2003, 2008). Thrombin can cleave and activate FXI, which can then convert FIX to FIXa in the coagulation cascade (Puy et al., 2013). The ability of thrombin to directly activate FXI may provide an explanation as to why FXII is not required for physiological hemostasis. Together, this suggests that the mechanisms regulating these two processes are not identical (Kleinschnitz, 2006; Renné et al., 2005). While the extrinsic pathway is essential for hemostasis, thrombosis may potentially be dependent on the intrinsic pathway, a process initiated by FXII (Renné et al., 2012).

There is growing evidence suggesting that although FXII is dispensable in hemostasis, it may play an important role in thrombosis. Murine studies demonstrate that inhibition of FXIIa attenuates thrombosis, suggesting that FXIIa is a potential target for antithrombotic/anti-inflammatory agents with a low risk of inducing hemorrhage (Colman, 2006; Gailani & Renné, 2007b; Renné et al., 2012). Indeed, thrombosis is attenuated in FXII and FXI knockout mice (Kleinschnitz, 2006; Renné et al., 2005) and intravital microscopy studies have shown that thrombi in these models are small and unstable. Moreover, small molecule inhibitors of FXIIa or FXIa and Ir-CPI, an inhibitor of FXII, FXI and kallikrein, are thromboprotective in mice (Müller, Gailani, & Renné, 2011). In addition, knockdown with ASOs of FXII, FXI or PK reduces arterial and venous thrombosis in mice; and FXI knockdown attenuates thrombosis in primates (Crosby et al., 2013; Matafonov et al., 2014; Revenko et al., 2011; Zhang et al., 2010). These studies support the notion that FXII plays an essential role in fibrin formation during "pathologic" thrombosis, but does not contribute to "physiologic" hemostatic fibrin formation at sites of vessel injury (Geddings & Mackman, 2014; Weitz & Fredenburgh, 2017a). Together, these studies suggest that FXIIa inhibition may attenuate thrombosis without disrupting hemostasis. However, further understanding of how FXII is activated and regulated under pathological conditions such as thrombosis is necessary.

1.9 POLYANIONIC ACTIVATORS OF CONTACT PATHWAY

Apart from exposure of collagen at sites of endothelial injury, the identity of physiologic activators of FXII had remained unclear for decades (Wu, 2015). Recent

studies have demonstrated that naturally occurring polyanions, such as DNA, RNA and inorganic polyphosphates (polyP) are potent activators of FXII (Schmaier, 2016; Vu et al., 2016). Prior to these findings, artificial polyanionic surfaces, such as kaolin, were known to activate FXII *in vitro* and utilized to trigger clotting in the activated partial thromboplastin time (aPTT) assay; a test used to assess the integrity of the intrinsic and common pathways (Gailani et al., 2015). However, the underlying mechanisms through which polyP triggers the contact pathway by activating FXII still remain elusive (Gailani et al., 2015).

1.9.1 Nucleic Acids

Nucleic acids, including DNA and RNA, are released from cells that undergo apoptosis, autophagy or necrosis (Kannemeier et al., 2007; Müller et al., 2009; Vu et al., 2016). Neutrophil extracellular traps (NETs), which contain de-condensed chromatin that is released from activated neutrophils, provide another source of DNA (Brill et al., 2012; von Brühl et al., 2012; Vu et al., 2016). Recent evidence from our laboratory has shown that DNA and RNA promote FXII activation in the presence of PK and HK, and enhance FXI activation by thrombin (Vu et al., 2016) (Figure 5). DNA and RNA bind FXII, HK, FXI, and thrombin, thus serving as a template for these reactions to occur (Vu et al., 2016). The localization of polyanionic activators at sites of vascular injury provides a stimulus for coagulation independent of TF. There is growing evidence suggesting that thrombosis is not simply an imbalance of hemostasis, but rather the result of alternative stimuli that exploit the hemostatic system (Geddings & Mackman, 2014; Jain et al., 2012).

1.9.2 Polyphosphate

PolyP is a naturally occurring, highly anionic linear polymer of phosphate units linked by phosphoanhydride bonds. Expressed in all cells, the polymers vary in length from 30 to 800 phosphate units in mammalian cells, to up to thousands of units in some microorganisms (Morrissey et al., 2012). In the context of hemostasis, short chain polyP is 60-100 phosphate units in length and found in the dense granules of platelets and granules of mast cells and released upon their activation (Fang et al., 2007; Gailani et al., 2015; Moreno-Sanchez et al., 2012) (Figure 5). Long chain polyP (>1000 phosphate units in length) occurs in microbes and some mammalian cells, such prostate cancer cells and has the ability to aggregate into particles, potentially contributing to its propensity to accelerate clotting. Microorganisms store long chain polyphosphate in subcellular organelles called acidocalcisomes (Morrissey et al., 2012). Circulating polyP has a half-life of 90 minutes and is cleared by phosphatases (Smith et al., 2010). Activation of normal circulating levels of platelets is sufficient to generate polyphosphate concentrations of around 1-3 μM in whole blood. However, in the local microenvironment of a thrombus, polyP concentration is likely to be several orders of magnitude higher due to the substantial accumulation of platelets (Morrissey et al., 2012). PolyP is both pro-inflammatory and procoagulant *in vivo* and modulates hemostasis at a number of points in the cascade, including binding fibrin(ogen) and altering the structure of the resulting clot. Studies have shown that inhibition of polyP inhibits thrombin generation as well as fibrin formation *in vitro*, and polyphosphate inhibitors have been proposed as novel antithrombotic agents (Baker et al., 2018; Smith et al., 2012).

PolyP triggers the contact pathway by providing a surface that binds FXII and HK and induces FXII autoactivation and promotes K activation of FXII (Smith et al., 2006, 2010; van der Vaart & Pretorius, 2008). The potential importance of polyP in clotting is demonstrated through observations that humans with dense granule defects have a bleeding diathesis (Masliah-Planchon et al., 2013). Aside from promoting FXII activation (Puy et al., 2013), polyP has also been shown to accelerate FXI and FV activation by thrombin and to increase fibrin clot stability, thereby rendering it less susceptible to degradation (Choi et al., 2011; Smith et al., 2006, 2010). Further, polyP was shown to enhance the activity of TAFI and inhibit TFPI. Recent studies suggest that the role of polyP in coagulation is dependent on the polymer length (Smith et al., 2010). Long chain polyP (>250–500 phosphate units) has been shown to be a strong activator of FXII and to affect fibrin clot structure, whereas shorter polymers (<100 phosphate units) increase FV activation and inhibit TFPI. PolyP in both size categories serves as a cofactor for thrombin activation of FXI (Smith et al., 2010; Weitz & Fredenburgh, 2017b).

Recent murine studies have demonstrated that human platelet polyP induces pulmonary embolism and increases vascular permeability in a FXII-dependent manner. Renne *et al.* suggest that polyP provides a link between platelet plug formation and fibrin generation, i.e., between primary and secondary hemostasis (Renné, 2012). The potential role of platelet polyP in hemostasis was addressed in a recent study by Ghosh *et al.* that showed that mice deficient in inositol hexakisphosphate 6 (IP_6) kinase, the enzyme required for the synthesis of platelet polyP, exhibited reduced platelet aggregation, prolonged clotting times, and altered fibrin structure (Ghosh et al., 2013). Furthermore, the

knockout mice had prolonged tail bleeding times and were protected from pulmonary thromboembolism. These studies have prompted the development of novel anticoagulant drugs targeting polyphosphate. Sullenger *et al*. screened a variety of nucleic acid binding polymers and identified a cationic poly (amido amine) dendrimer called PAMAM-G3 that prevented thrombosis after carotid artery injury and pulmonary thromboembolism without increasing tail bleeding in mice (Jain et al., 2012). Moreover, cationic compounds, such as 1.0 dendrimer and polymyxin B (Smith et al., 2012), have been shown to reduce venous and arterial thrombosis in mice (Kalaska et al., 2012).

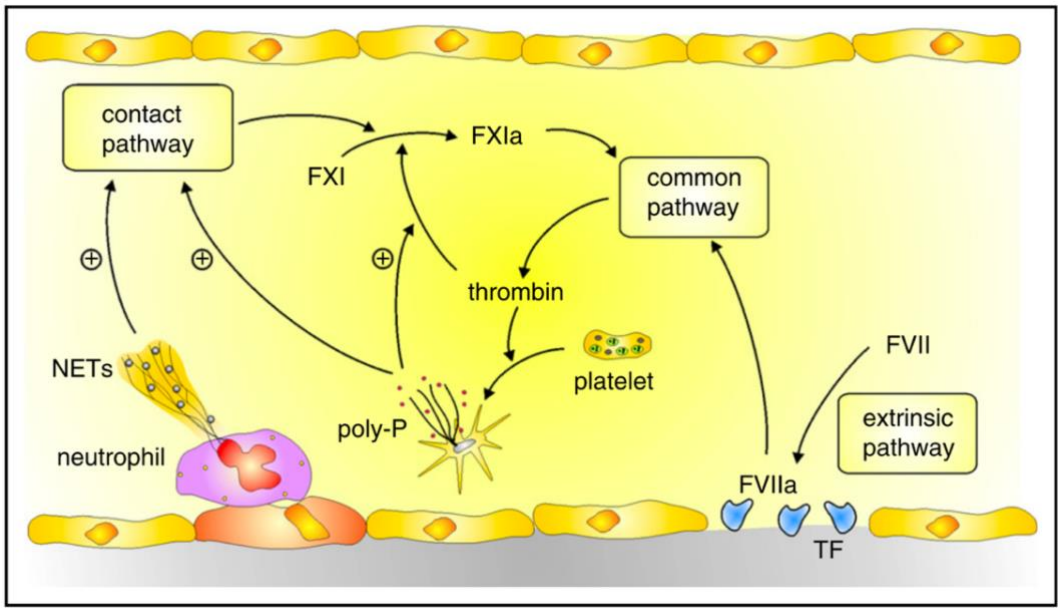
contact pathway
FXI
FXIa
common pathway
thrombin
platelet
FVII
extrinsic pathway
FVIIa
TF
NETs
neutrophil
poly-P

Figure 5: Initiation of coagulation by release of negatively charged polyanions

At the site of vascular injury, coagulation is initiated by the extrinsic pathway when tissue factor (TF) binds and activates FVII, forming extrinsic tenase (TF-FVIIa). Extrinsic tenase activates FX in the common pathway, allowing for thrombin generation and the subsequent formation of the fibrin clot. Activation of coagulation may also occur when 1) thrombin-activated platelets release polyP and 2) activated neutrophils release neutrophil extracellular traps (NETs). PolyP, a linear polymer of inorganic phosphate, are found in the dense granules of platelets and are released upon activation. Activation of the contact pathway by polyP or nucleic acids yield FXIa, which leads to further thrombin generation. PolyP also amplifies coagulation by promoting thrombin-mediated activation of FXI, independent of FXIIa-mediated contact activation. Source: Fredenburgh J. C., Gross P., Weitz J. I. *Blood*. 2017; 129(2):147–154.

1.10 FACTOR XII STRUCTURE, ACTIVATION, INHIBITION

1.10.1 FXII structure

FXII or Hageman factor is a single-chain, 80 kDa glycoprotein that is synthesized in the liver. Upon contact with a negatively charged surface, the zymogen FXII undergoes autoactivation by cleavage at its activation site (Arg343-Val354). With this cleavage, FXII is converted to its activated two-chain polypeptide form, α-FXIIa, consisting of a 50 kDa heavy chain (six non-catalytic domains) and a 28 kDa light chain (catalytic domain) that is bound together by the Cys340-Cys367 disulfide bond (Renné et al., 2012) (Figure 6). The heavy chain of FXIIa consists of the following domains: fibronectin type II (FNII), epidermal growth factor 1 (EGF1), fibronectin type 1 (FNI), epidermal growth factor 2 (EGF2), and kringle (K) domain, as well as a proline-rich region (PR) (Pathak et al., 2015). The EGF domains are responsible for regulating cell growth and proliferation (Stavrou & Schmaier, 2010). Maas and colleagues recently reported that the EGF1 domain mediates surface binding as it contains the binding site for kaolin and polyanions, whereas the FNII domain serves as a critical negative regulator of FXII activation by shielding the activation loop (Hofman et al., 2020). This provides valuable insight into the mechanism of FXII activation and function because the FNII domain contains the binding site for FXI. The light chain contains the catalytic domain with the prototypical serine protease catalytic triad (Asp442, His393, and Ser554). Kallikrein and FXIIa cleave FXII at the Arg343-Val354 peptide bond within the catalytic domain, thereby generating the protease, α-FXIIa. Subsequent cleavage of α-FXIIa by kallikrein generates β-FXIIa, consisting of a two-chain

polypeptide with a 2 kDa heavy chain remnant of the PR domain and a 28 kDa catalytic domain covalently bound together by the same disulfide bond (Figure 6). β-FXIIa loses its capacity to bind polyanions and to activate FXI. Thus, the capacity of kallikrein to cleave FXIIa at multiple sites is important for converting the protease into different forms, which direct its activity. Whereas α-FXIIa triggers coagulation, zymogen FXII and β-FXIIa are proposed to have important roles in inflammation. More recently, it has been hypothesized that the conformation of FXII determines its function. It is believed that when FXII is in solution, the zymogen is protected from activating cleavage by PK because the protease domain is shielded by the heavy chain. In this closed conformation, the FXI-binding site is encrypted (de Maat & Maas, 2016). However, upon contact by a negatively charged surface, the heavy chain is extended, exposing the protease domain for FXII activation. In this procoagulant state, the FXI-binding site is 'decrypted' as a result of full extension of the protein structure, which requires involvement of the N-terminal binding site (de Maat & Maas, 2016).

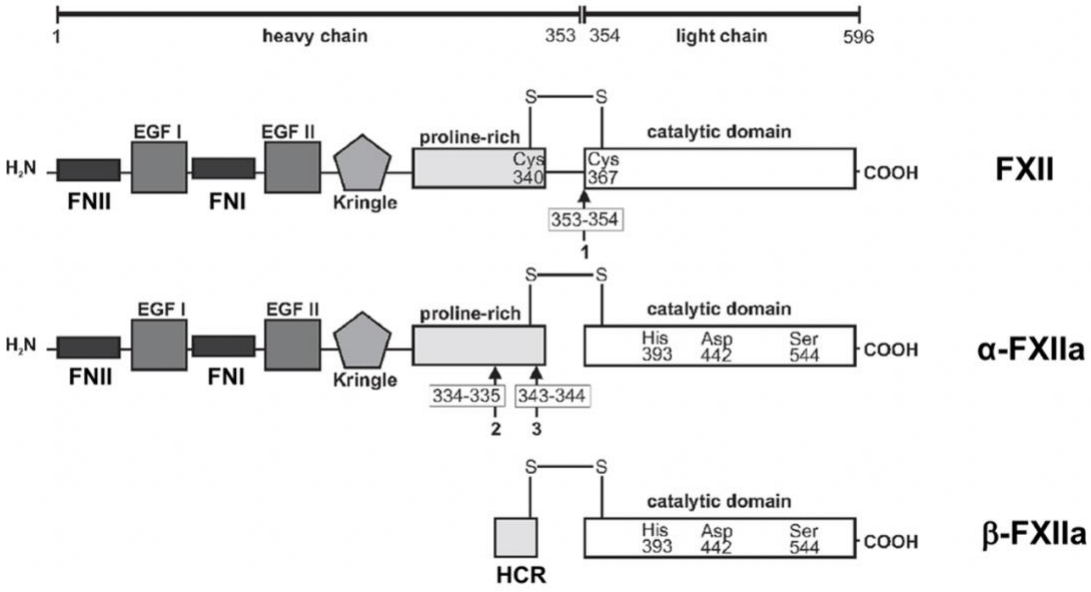
1
heavy chain
353
354
light chain
596
S
S
EGF I
EGF II
proline-rich
catalytic domain
H2N
Cys 340
Cys 367
COOH
FXII
FNII
FNI
Kringle
353-354
1
His 393
Asp 442
Ser 544
α-FXIIa
334-335
343-344
2
3
β-FXIIa
HCR

Figure 6: Domain structure of FXII and FXIIa

The zymogen FXII is an 80 kDa single chain polypeptide zymogen consisting of a heavy chain (non-catalytic domain) and light chain (catalytic protease domain). The non-catalytic domains include fibronectin type II (FNII), epidermal growth factor-like (EGFI/II), fibronectin type I (FNI), kringle, and proline-rich (PR) domains. The light chain contains the catalytic domain and the cleavage site for kallikrein and FXIIa (Arg343-Val354 peptide bond). The cleavage of FXII by autoactivation, kallikrein, or FXIIa converts zymogen FXII into a proteolytically active two-chain FXII (α-FXIIa). The catalytic triad residues His393, Asp442 and Ser544 are indicated. Further proteolysis of the peptide bonds Arg343-Leu344 and Arg334-Asn335 by plasma kallikrein, results in activated FXII-fragment (β-FXIIa). β-FXIIa consists of the catalytic light chain and the heavy chain remnant (HCR; 9 amino acid residues) resulting from autoproteolysis of FXII. Adapted from Björkqvist et al. *Thromb Haemost*. 2014; 112:868–875.

1.10.2 FXII activation

Binding to negatively charged surfaces induces a conformational change in FXII, resulting in its autocatalysis (autoactivation), which is enhanced in the presence of Zn^{2+} (Vu et al., 2013). FXII autoactivation occurs by cleavage of the Arg353-Val354 peptide bond within the catalytic domain, allowing for the conversion of single-chain FXII into its activated, two-chain form α-FXIIa (MacQuarrie et al., 2011; Renné et al., 2012) (Figure 6). FXIIa levels are further amplified through feedback loops, converting more FXII to FXIIa and allowing for PK to be converted to kallikrein in the presence of HK (Gailani & Renné, 2007a; Renné, 2012) (Figure 7). PK activation is then able to provide a second amplification loop as kallikrein activates FXII (Gailani & Renné, 2007b). FXIIa initiates coagulation by activating FXI, which circulates in complex with HK (Schmaier, 2016). The precise mechanism promoting FXIIa generation is unclear. It is hypothesized that the binding of FXII to polyanions induces a conformational change in the zymogen FXII, which primes it for autoactivation. FXII binding to zinc increases the rate of FXII autoactivation by 10-fold. Zn^{2+} binds to FXII through the histidine residues within the FNII-EGF1 and EGF2 domains of FXII (Røjkaer & Schousboe, 1997; Stavrou & Schmaier, 2010). It is still unknown whether autoactivation occurs by a) basal amounts of FXIIa activating FXII bound to polyanions or b) through "self-cleavage" of the zymogen upon induction of a conformational change in FXII by its interaction with polyanions (ie. intra or inter-molecular). Due to this ambiguity, this thesis will refer to the term FXII autoactivation as the process whereby FXII activates its own zymogen, regardless of the mechanism involved.

1.10.3 Inhibitors of FXIIa

There are a number of natural inhibitors of FXIIa in human plasma including C1-inhibitor (C1-INH), antithrombin (AT), α_2-macroglobulin, and histidine-rich glycoprotein (Kenne & Renné, 2014; Kolyadko et al., 2014). Both C1-INH and AT belong to the same family of protease inhibitors and inhibit FXIIa via a common mechanism for serpins (Kolyadko et al., 2014). The N-terminal loop of C1-INH enters the active site of the protease, disrupting the catalytic site of the protease and irreversibly inhibiting FXIIa (Kolyadko et al., 2014). AT inhibits FXIIa in the presence of its cofactor heparin, binding to the antithrombin-binding pentasaccharide sequence on heparin (Kolyadko et al., 2014). Until recently, C1-INH was considered to be the primary physiological plasma inhibitor of FXIIa (Figure 7), although the second-order rate constant suggests that inhibition is slow (Cugno et al., 1997; Wagenaar-Bos & Hack, 2006). However, FXIIa-C1-INH complexes were shown to be produced largely in plasma after surface-mediated activation (ie. glass, kaolin, polyP), whereas in the case of FXIIa activation by activated platelets (TRAP, collagen, or ADP-induced), the FXIIa-antithrombin complexes were predominant (Bäck et al., 2009; Kolyadko et al., 2014). Moreover, FXIIa is protected from inactivation by C1-INH when it binds to endothelial cells (Schousboe, 2003). Thus, the primary regulator of the contact pathway may not be C1-INH when there is physiological activation of FXIIa (Kolyadko et al., 2014). These results lead to the question as to whether there are other regulators of FXIIa.

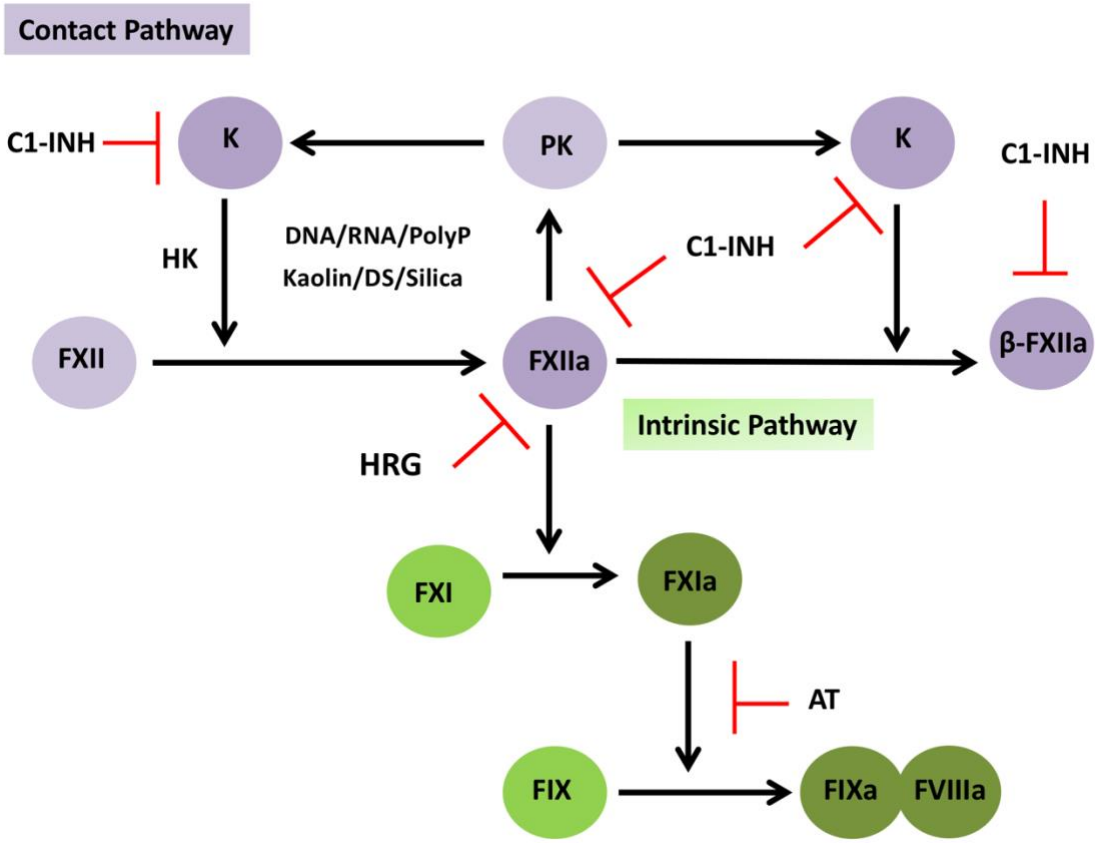
Contact Pathway
C1-INH
K
PK
K
C1-INH
HK
DNA/RNA/PolyP
Kaolin/DS/Silica
C1-INH
FXII
FXIIa
β-FXIIa
Intrinsic Pathway
HRG
FXI
FXIa
AT
FIX
FIXa
FVIIIa

Figure 7: Regulation of FXII in the contact pathway of coagulation

FXII is activated by contact with a negatively charged surface which induces a conformational change in zymogen FXII, activating it to FXIIa. Activators of FXII include non-physiological/synthetic activators (e.g., kaolin, dextran sulfate (DS), silica) and physiological activators (DNA, RNA, and polyphosphate). FXIIa then converts prekallikrein (PK) to kallikrein (K), which in turn reciprocally activates FXII, amplifying its activation. FXIIa can be further cleaved by K to generate β-FXIIa. C1-esterase inhibitor (C1-INH) binds and irreversibly inhibits FXIIa, β-FXIIa, and K. Antithrombin (AT) inhibits FXIa (FXIIa to a lesser extent) in the presence of its cofactor heparin. Histidine-rich glycoprotein (HRG) is a potent inhibitor of FXIIa. HRG binds to an exosite on FXIIa inhibiting FXII autoactivation, as well as FXIIa-mediated contact activation reactions.

Specific antibodies against FXIIa exhibit a high degree of selectivity (Kolyadko et al., 2014). These include antibodies that bind to individual domains of the factor and selectively block some of its functions (Gailani et al., 2015; Gruber, 2014; Kenne & Renné, 2014; Larsson et al., 2014; Zhu et al., 2015). However, the need for intravenous infusions, special requirements for their storage, and possible immune response may limit their potential as a safe drug for thrombosis treatment (Kolyadko et al., 2014). Other FXIIa inhibitors, such as corn trypsin inhibitor (CTI) and infestin 4 have inhibition constants of 2.5 nM and 78 pM, respectively, but are non-specific and also inhibit FXIa, FXa, FIXa, and thrombin (Gailani et al., 2015; Kenne & Renné, 2014; Kolyadko et al., 2014). CTI is a 12 kDa Kunitz-type inhibitor that reversibly binds to the active site of FXII and cleaves the Arg34-Leu35 bond, thereby inhibiting FXII autoactivation and FXIIa chromogenic activity (K_i of 24 nM) (Yau et al., 2012).

1.11 OVERVIEW OF HISTIDINE-RICH GLYCOPROTEIN

1.11.1 Protein synthesis and plasma levels

Histidine-rich glycoprotein (HRG) is an abundant and well-characterized α_2-plasma glycoprotein (Jones et al., 2005). HRG has been referred to as the “Swiss Army knife” of mammalian plasma (Poon et al., 2011), as it has been implicated in diverse processes including coagulation, fibrinolysis, angiogenesis, and immune function in vertebrates (Jones et al., 2005; Kassaar et al., 2014). Second to AT, HRG is one of the most abundant heparin-binding proteins in human plasma (Poon et al., 2011). Human HRG has an approximate mass of 75 kDa and circulates in plasma at a relatively high concentration of

~1-3 μM with a half-life of approximately 3 days (Jones et al., 2005; Kassaar et al., 2014). HRG is synthesized in liver parenchymal cells (Jones et al., 2005), however studies have shown that it may also be found in the α-granules of platelets and in megakaryocytes (Leung et al., 1983). Studies have found HRG on the surface of leukocytes such as macrophages and monocytes, but it is unclear whether these cells synthesize HRG or actively take it up from the blood (Jones et al., 2005; Poon et al., 2011; Sabbatini et al., 2011). Plasma levels of HRG are low in the neonatal stage and gradually increase with age, with some evidence suggesting that levels vary with blood type (Drasin & Sahud, 1996). HRG is a negative acute phase protein, such that HRG plasma levels are markedly reduced during the acute response to injury, advanced liver cirrhosis, sepsis, or with chronic inflammation (Jones et al., 2005; Saigo et al., 1990). HRG levels fall during pregnancy or with use of oral contraceptives (Jespersen et al., 1990). The decrease in HRG levels during pregnancy has been associated with an increased risk of preeclampsia (Bolin et al., 2011).

Evidence for extracellular uptake of HRG comes from studies with muscle and T-cells, where HRG was shown to bind to cellular receptors such as GAGs (ie. heparan sulfate), facilitating the uptake into these cells (Sabbatini et al., 2011). HRG localizes in the vicinity of platelet-rich thrombi where the local concentration of HRG may be increased because of its release from activated platelets (MacQuarrie et al., 2011). This suggests that the manner in which HRG regulates cellular processes such as coagulation may depend on local conditions.

1.11.2 Domain structure and proteolytic cleavage

HRG was first isolated from human serum and characterized by Heimburger et al (Heimburger et al., 1972) and was subsequently isolated from human plasma and platelets (Jones et al., 2005). The human HRG gene has been mapped to position q28-q29 on chromosome 3 and is predicted to encode a 507 amino acid multidomain polypeptide consisting of 2 cystatin-like N-terminal domains (N1 and N2), a central histidine-rich region (HRR) flanked by 2 proline-rich regions (PRR1 and PPR2), and a C-terminal domain (COOH) (Jones et al., 2005; Kassaar et al., 2014) (Figure 8). HRG contains four intra-domain and two interdomain disulfide bridges that link the COOH domain and the HRR to the N1N2 domain, as well as 6 predicted N-linked glycosylation sites (Poon et al., 2009, 2011). The histidine- and proline-rich regions are predicted to be intrinsically disordered but N1, N2, and the COOH domains are likely to have ordered structures (Kassaar et al., 2014). The HRR contains 12 tandem repeats of five consensus amino acids between amino acids 330 and 389, where the last five sequences are exact repetitions of the Gly-His-His-Pro-His (GHHPH) consensus sequence (Jones et al., 2005) (Figure 9A). The abundance of His and Pro residues in the HRR and PRR domains, respectively, imparts HRG with a twisted and elongated HRR core structure (Jones et al., 2005) (Figure 9B). The imidazole side chains of the His residues are thought to extend outward, which allows for multiple Zn^{2+}-binding sites on HRG (Jones et al., 2005; Kassaar et al., 2014). The unusually high content of histidine and proline residues, each constituting approximately 13% of total amino acids has resulted in HRG also being termed ‘histidine-proline rich glycoprotein’ (HPRG) (Ronca & Raggi, 2015). HRG has metal and pH-sensing capabilities because

binding of HRG to its ligands such heparin and FXIIa is regulated by changes in hydrogen ion concentration and Zn^{2+} concentrations, respectively (Borza & Morgan, 1998; Priebatsch, Kvansakul, et al., 2017). When Zn^{2+} or hydrogen ions bind to the PRR-HRR region of HRG, they induce local conformational changes that are transmitted throughout the molecule. Such changes are believed to indirectly modulate the binding of the N1N2 and COOH domains to their ligands (Borza et al., 1996; Jones et al., 2005; Priebatsch, Kvansakul, et al., 2017). Activated platelets release Zn^{2+} from their dense granules, providing a pool of Zn^{2+} that can increase local concentrations (Marx et al., 1993; Vu et al., 2013). Indeed, Zn^{2+} binds to HRG with high affinity (K_d of 0.2 μM to 2.85 μM) and promotes the binding of HRG to its ligands (MacQuarrie et al., 2011; Patel et al., 2007; Priebatsch, Kvansakul, et al., 2017; Ranieri-Raggi et al., 2014; Ronca & Raggi, 2015).

HRG function is regulated by proteolytic cleavage, whereby cleaved derivatives of HRG are found in plasma (Poon et al., 2009, 2011). In patients undergoing thrombolytic therapy, HRG-derived bands of 9-67 kDa are observed, suggesting that plasmin modulates HRG activity (Smith et al., 1985). Plasmin cleaves HRG into disulfide-linked HRR-PRR, N1N2 and COOH-terminal fragments. The susceptibility of HRG to degradation is dependent on the zinc concentration and pH because both elevated levels of zinc and hydrogen ions protect HRG from plasmin degradation (Poon et al., 2009). Upon plasmin cleavage, HRG binding to GAGs, such as heparin and heparan sulfate, is attenuated, whereas binding to necrotic cells and plasminogen is enhanced (Poon et al., 2011). Although kallikrein cleaves HRG in a manner distinct from plasmin, the functional

consequence of this has not been determined (Poon et al., 2009). Therefore, protease cleavage of HRG provides an additional level of regulation that directs HRG activity.

1.11.3 HRG ligands in coagulation, fibrinolysis, and inflammation

The multi-domain structure of HRG provides it with the ability to bind multiple ligands. In plasma, HRG binds to and regulates the function of a diverse variety of targets that include fibrinogen, plasminogen, thrombospondin, immunoglobulin G (IgG), complement factors, and heparin, as well as cell-surface molecules such as Fcγ receptors and heparin sulfate (Jones et al., 2005; Kassaar et al., 2014) (Figure 8). HRG binds divalent metal cations (Cu^{2+}, Zn^{2+}, Ni^{2+}, Cd^{2+}, Co^{2+}, Hg^{2+}) within the HRR and undergoes a conformational change, which may influence its biological activity (Jones et al., 2005; Kassaar et al., 2014; Priebatsch, Poon, et al., 2017). In particular, Zn^{2+} is known to bind this region and can modulate HRG activity by altering the protein's affinity for other targets (Kassaar et al., 2014). Binding of heparin to HRG is thought to be mediated through the NH_2-terminal cystatin domain and formation of the HRG-heparin complex is enhanced by Zn^{2+} (Priebatsch, Kvansakul, et al., 2017). In regards to the mechanism by which HRG and FXIIa interact, SPR analysis by MacQuarrie *et al*. demonstrated that Zn^{2+} significantly increases the affinity of FXIIa for HRG by more than 3 orders of magnitude (1000-fold), supporting the notion that the HRR mediates this interaction (MacQuarrie et al., 2011). Given that the binding site for Zn^{2+} on HRG is within the HRR domain, this suggests that binding of Zn^{2+} to the HRR has the capacity to modulate other domains in HRG (Priebatsch, Kvansakul, et al., 2017). Interestingly, the interaction between HRG and FXIIa can be

inhibited by the addition of heparin, suggesting that FXIIa may also bind to the cystatin-like N-terminal domains and that the affinity of this interaction is heightened by Zn^{2+} binding to the HRR (MacQuarrie et al., 2011). HRG does not bind to the zymogen FXII, but to the activated form, FXIIa (MacQuarrie et al., 2011). In the absence of vascular injury, HRG is unlikely to play a role in hemostasis, as free Zn^{2+} levels in plasma are less than 1 µM, far below the range (6-12 µM) that allows for HRG binding to FXIIa (Priebatsch, Kvansakul, et al., 2017; Vu et al., 2013). However, when FXII is activated at sites of injury and local levels of Zn^{2+} are elevated in response to platelet activation, HRG can bind to FXIIa with high affinity (MacQuarrie et al., 2011). Therefore, HRG may serve as an effector of coagulation and be an important regulator of thrombogenesis (MacQuarrie et al., 2011).

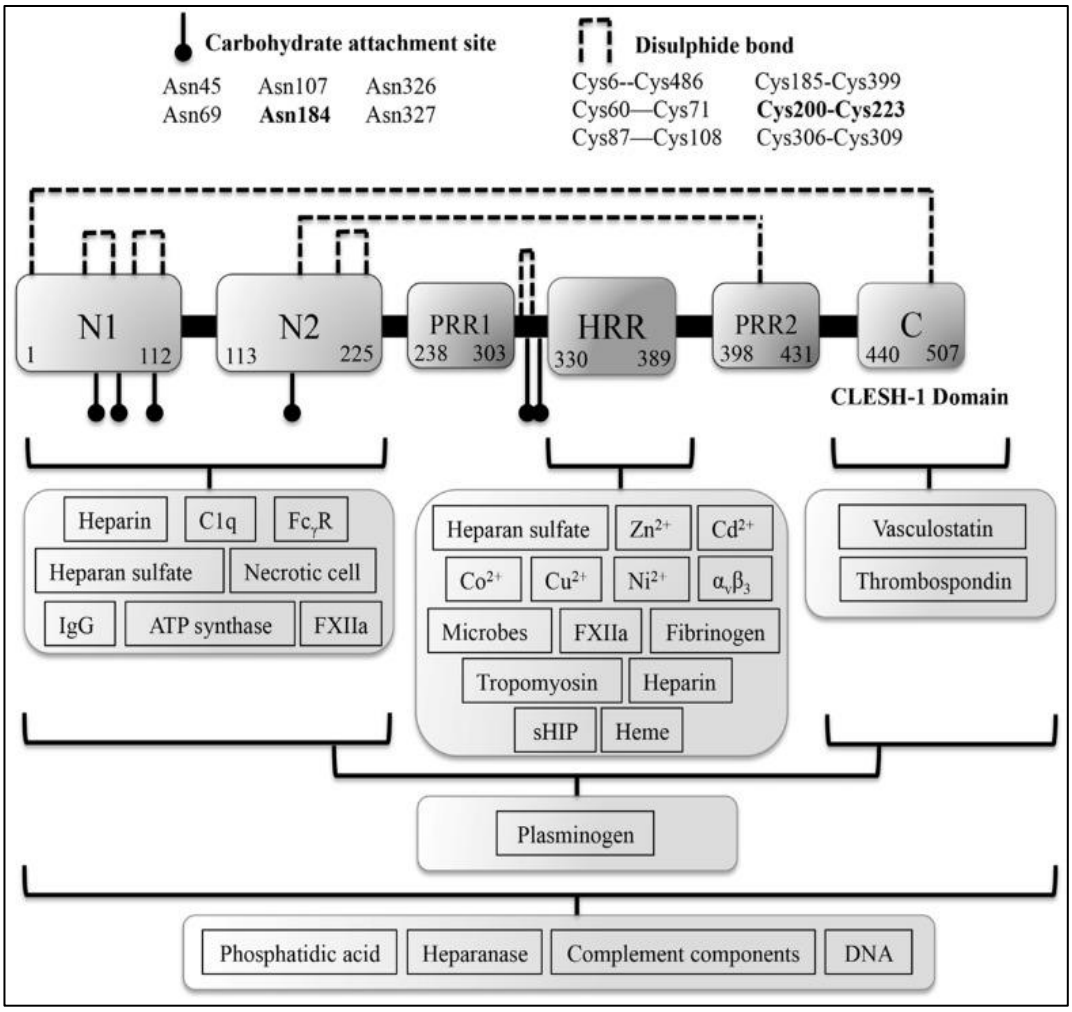
Carbohydrate attachment site
Asn45 Asn107 Asn326
Asn69 Asn184 Asn327
Disulphide bond
Cys6--Cys486 Cys185-Cys399
Cys60—Cys71 Cys200-Cys223
Cys87—Cys108 Cys306-Cys309
N1
1 112
N2
113 225
PRR1
238 303
HRR
330 389
PRR2
398 431
C
440 507
CLESH-1 Domain
Heparin
C1q
FcγR
Heparan sulfate
Necrotic cell
IgG
ATP synthase
FXIIa
Heparan sulfate
Zn2+
Cd2+
Co2+
Cu2+
Ni2+
αvβ3
Microbes
FXIIa
Fibrinogen
Tropomyosin
Heparin
sHIP
Heme
Vasculostatin
Thrombospondin
Plasminogen
Phosphatidic acid
Heparanase
Complement components
DNA

Figure 8: HRG protein domains, post-translational modification, and ligands

HRG is an abundant plasma protein (molecular weight of 75 kDa) composed of two cystatin-like domains N-terminal domains (N1 and N2), a histidine-rich region (HRR) flanked by two proline-rich regions (PRR) and carboxy-terminal domain. HRG contains 6 N-linked glycosylation sites (●), four intra-domain and two inter-domain disulfide bridges (--) linking the C-terminal domain and the HRR to the N1N2 domain. The multidomain structure of HRG allows the glycoprotein to bind multiple ligands, including FXIIa, Zn^{2+}, heparin, plasminogen, fibrinogen, and negatively charged polyanions, such as DNA. The histidine- and proline-rich regions are predicted to be intrinsically disordered but N1, N2, and the C-terminal domains are likely to have ordered structures. Source: Priebatsch et al., *Biomolecules*. 2017; 7(1), 22.

A.

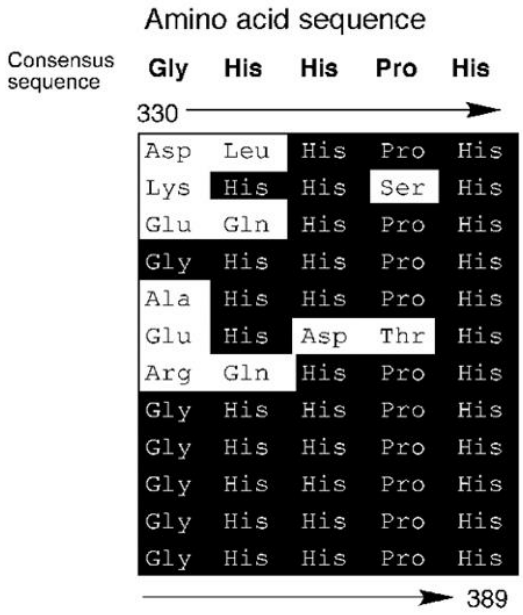
Amino acid sequence
Consensus sequence
Gly His His Pro His
330
Asp Leu His Pro His
Lys His His Ser His
Glu Gln His Pro His
Gly His His Pro His
Ala His His Pro His
Glu His Asp Thr His
Arg Gln His Pro His
Gly His His Pro His
Gly His His Pro His
Gly His His Pro His
Gly His His Pro His
Gly His His Pro His
389

B.

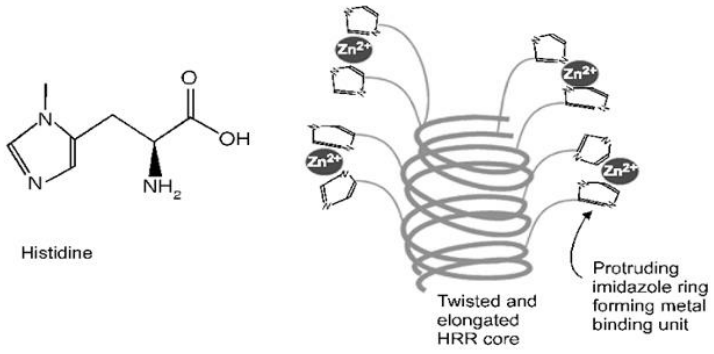
O
OH
N
N
NH2
Histidine
Zn2+
Zn2+
Zn2+
Zn2+
Twisted and elongated HRR core
Protruding imidazole ring forming metal binding unit

Figure 9: Histidine-rich region of histidine-rich glycoprotein

(A) The histidine-rich region (HRR) of histidine-rich glycoprotein (HRG) contains 12 tandem repeats of five consensus amino acids between amino acids 330 and 389, where the last five sequences are exact repetitions of the Gly-His-His-Pro-His (GHHPH) consensus sequence. The amino acid and nucleotide sequence of the HRR is illustrated. (B) Structure of histidine amino acid and HRR of human HRG. The twisted and elongated HRR core has protruding imidazole side chains that form metal binding sites. The HRR has the capacity to modulate other domains in HRG through its metal and pH-sensing capabilities, resulting in local conformational changes that are transmitted throughout the molecule. Such changes are believed to indirectly modulate the binding of the N1N2 and COOH domains to their ligands. HRR plays an important regulatory role in mediating the changes in hydrogen ion concentration and zinc concentrations that are important for HRG binding to heparin and FXIIa, respectively. Source: Adapted from Jones *et al*. *Immunol and Cell Biol*. 2005; 83, 106-118.

1.12 HRG MODULATION OF HEMOSTASIS AND THROMBOSIS

It has been almost 50 years since HRG was first isolated by Heimburger *et al*., but its primary physiological function remains unclear. Clinical studies have shown that families with congenital HRG deficiencies (20-35% of normal plasma levels) have no abnormalities in routine laboratory assays of hemostatic and immunological function. However, cases of familial deficiency of HRG caused by missense mutations suggest HRG plays an antithrombotic role in preventing thrombotic disorders. The reported coagulation disorders in HRG mutation positive patients include cerebral sinus thrombosis (Gly85 to Glu mutation) (Shigekiyo et al., 1998), dual arteriovenous fistula at sites of previous thrombosis (Cys223 to Arg) (Shigekiyo et al., 2000), and early-onset DVT associated with novel HRG mutation in exon 2 of HRG gene (Luo et al., 2018). Since its discovery, many properties of HRG have been reported, such as the interaction of HRG with various molecules such as divalent metal ions, plasminogen, fibrinogen, and glycosaminoglycans (ie. heparin or heparan sulfate). These interactions have prompted the hypothesis that HRG serves as an adaptor protein, modulating blood coagulation and fibrinolysis. Low amounts of HRG in clots and plasma of patients with thrombotic disorders have been reported, whereby downregulation of HRG levels are associated with an increased risk of thrombosis (Stachowicz et al., 2018). In a genome wide association study, genes for FXII, HK, and HRG were identified to be strongly associated with influencing the aPTT, which is clinically used to interrogate the intrinsic and common pathways of coagulation (Hoffman & Monroe, 2007).

To examine the physiological function of HRG, Tsuchida-Straeten *et al*. were the first to produce an HRG-knockout mouse and analyze their hemostatic factors (Tsuchida-Straeten et al., 2005). These mice were viable and fertile, with no appreciable abnormalities in their hemostatic components except for the absence of HRG in their blood. The levels of fibrinogen and monocyte numbers were higher compared with wild-type mice (135% and 252%, respectively). Bleeding time after tail tip amputation was shorter and the spontaneous fibrinolytic activity in clotted blood was higher in HRG knockout mice than in wildtype mice. Moreover, the prothrombin time was shorter in HRG knockout mice than in HRG heterozygous mice or wildtype mice. Thus, these differences in blood tests may not pose problems in the life of a healthy HRG-deficient mouse but may affect the fate of mice under some abnormal or pathological condition.

To determine whether HRG deficiency results in a prothrombotic phenotype under pathological condition, we compared ferric chloride ($FeCl_3$)-induced arterial thrombosis in wild type mice with that in HRG knockout and HRG heterozygous mice (Vu et al., 2015). We showed that thrombosis is significantly accelerated in HRG knockout mice, an effect that was also observed in HRG heterozygous mice. This was shown by a decrease in blood flow as well as time to occlusion. These findings suggest that HRG deficiency results in a prothombotic phenotype and that even 50% residual HRG is not protective. To localize HRG, thrombi from $FeCl_3$-treated wildtype mice were harvested and subjected to immunohistochemical analysis. Whereas platelets were dispersed throughout the thrombi, fibrin disposition was localized to the vessel wall, most likely at the site of the $FeCl_3$ application. HRG is reported to be stored in the α-granules of platelets and released upon

platelet activation (Leung et al., 1983). Because HRG binds to fibrin, we hypothesized that HRG would localize to platelets and fibrin. We show that HRG in thrombi did indeed localize with platelets and to a lesser extent to fibrin, thus confirming that HRG is found in thrombi formed after $FeCl_3$-induced arterial injury in mice and that HRG may play an important antithrombotic role (Vu et al., 2015).

1.12.1 Anticoagulant properties of HRG

MacQuarrie *et al.* demonstrated that HRG inhibited the capacity for FXII to autoactivate upon contact activation, as well as subsequent FXIIa-mediated FXI activation (MacQuarrie et al., 2011). SPR analysis revealed that HRG binds to FXIIa with high affinity (K_d value of 1.6 nM), where the affinity is increased 1000-fold in the presence of Zn^{2+} (K_d value of 9 pM) (MacQuarrie et al., 2011). HRG has been proposed to regulate coagulation through its interaction with the activated form of FXII (FXIIa), as HRG does not bind to the zymogen FXII, or to FXI or FIX (MacQuarrie et al., 2011). Significantly, the binding interaction between HRG and FXIIa is the highest described affinity for any HRG ligand, higher than its affinity for heparin or fibrinogen (Priebatsch, Kvansakul, et al., 2017). Additionally, HRG has been detected in complexes with FXIIa in contact-activated plasma (MacQuarrie et al., 2011). The anticoagulant properties of HRG were further supported when a shorter aPTT was observed in HRG-depleted plasma, where similar results were reported in HRG-deficient mice (MacQuarrie et al., 2011; Vu et al., 2015). Conversely, HRG supplementation of HRG-deficient plasma prolonged this clotting time (MacQuarrie et al., 2011).

The presence of DNA and RNA from apoptotic and necrotic cells, or the release of polyP from activated platelets, serve as potent activators of the intrinsic pathway through FXIIa activation (Priebatsch, Kvansakul, et al., 2017). HRG binds to nucleic acids with high affinity (K_d values of 1 nM) most likely through the phosphate head group of phosphatidic acid of DNA and RNA and attenuates their procoagulant activity by competing with contact factors, such as FXII and FXI, for binding to nucleic acids (Priebatsch, Kvansakul, et al., 2017; Vu et al., 2016). Vu *et al*. demonstrated that nucleic acids are potent activators of the contact pathway and provided evidence that HRG is a dynamic regulator of this pathway (Vu et al., 2016). In support of this concept, HRG attenuates RNA- and DNA-induced thrombin generation and clot formation in HRG knockout mice plasma (Vu et al., 2015, 2016). In addition, HRG competes with thrombin for binding to the carboxy-terminus of the γ'-chain of γA/ γ'-fibrinogen (Vu et al., 2013). HRG has been demonstrated to avidly compete for fibrin binding with both thrombin and FXIIa (Priebatsch, Kvansakul, et al., 2017). Current thinking suggests that once the fibrin matrix assembles, HRG is able to displace either thrombin or FXIIa from fibrin to elicit its antithrombotic, as well as profibrinolytic properties (Priebatsch, Kvansakul, et al., 2017). Together, by inhibiting FXII autoactivation, binding to nucleic acids, and displacing thrombin from fibrin, HRG has the capacity to exert anticoagulant, profibrinolytic, and antithrombotic effects (MacQuarrie et al., 2011; Priebatsch, Kvansakul, et al., 2017; Vu et al., 2013, 2016).

1.12.2 Procoagulant properties of HRG

HRG has both pro- and anticoagulant activities by its interaction with its inorganic cofactor Zn^{2+} (Vu et al., 2013). Transition metals, such as Zn^{2+}, Ni^{2+}, and Cu^{2+}, are regulated by the imidazole side chains of the distinctive histidine-rich region of HRG (Fu & Horn, 2002). Binding of Zn^{2+} to the HRR induces a conformational change in the molecule, increasing the affinity of HRG for a number of molecules, including heparin, fibrinogen, and FXIIa (Kassaar et al., 2015; Vu et al., 2013). HRG binds to the anticoagulant, heparin, with high affinity (K_d value of 2 nM) in the presence of Zn^{2+} and inhibits the formation of heparin-AT complex (Barnett et al., 2013; MacQuarrie et al., 2011). Zn^{2+}, serving as a cofactor, interacts with HRG to stimulate HRG-heparin complex formation (Kassaar et al., 2015). The NH_2-terminal cystatin domains of HRG and not its HRR domain mediate the Zn^{2+}-dependent interaction of heparan sulfate. This suggests that binding of Zn^{2+} to the HRR domain has the capacity to modulate other domains in HRG. Binding of HRG to heparin neutralizes its anticoagulant activity in both purified and plasma systems, therefore the HRG-heparin interaction has a procoagulant effect (Barnett et al., 2013; Fu & Horn, 2002). Neutralization of heparin by HRG attenuates the anticoagulant activity of antithrombin and subsequently promotes thrombosis (Kassaar et al., 2015). Thus, HRG serves as a procoagulant molecule through its ability to bind and neutralize the natural anticoagulant heparin and antithrombin interaction (Kassaar et al., 2015; Priebatsch, Kvansakul, et al., 2017).

1.12.3 Mechanisms of HRG inhibition of FXIIa

HRG has been shown to suppress contact activation via blocking FXII autoactivation, and subsequent FXIIa activation of FXI (MacQuarrie et al., 2011; Vu et al., 2016). In the presence of Zn^{2+}, the affinity of FXIIa for HRG increases by 1000-fold (K_d value of 9 pM) (MacQuarrie et al., 2011; Priebatsch, Kvansakul, et al., 2017). Indeed, HRG will bind to FXIIa more avidly at sites of vascular injury where there is a localized increased of Zn^{2+} due to platelet activation and release of Zn^{2+} from dense granules (MacQuarrie et al., 2011; Renné, 2012). However, this interaction is not Zn^{2+}-dependent, because HRG can still bind FXIIa and modulate clotting even in the absence of Zn^{2+} (K_d value of 1.6 nM at physiological pH) (MacQuarrie et al., 2011; Priebatsch, Kvansakul, et al., 2017; Priebatsch, Poon, et al., 2017). Notably, the affinity of HRG for FXIIa is the highest described for any HRG ligand, more so than for heparin, heme, fibrinogen, or plasminogen (Poon et al., 2011; Priebatsch, Kvansakul, et al., 2017). The HRG-FXIIa interaction would serve to limit the procoagulant stimulus by inhibiting FXIIa-mediated activation of the contact pathway (MacQuarrie et al., 2011). In this setting, Zn^{2+} may serve as an additional control element or cofactor for HRG to locally regulate FXIIa activation at the fibrin clot or the removal of FXIIa from the thrombus site (Priebatsch, Kvansakul, et al., 2017; Ranieri-Raggi et al., 2014; Vu et al., 2013). Given the abundance of HRG in plasma and high affinity of HRG for FXIIa, HRG is more likely than C1-INH to bind FXIIa (Jones et al., 2005; Poon et al., 2011). It is believed that through binding to an exosite of activated FXIIa (α-FXIIa), HRG prevents interactions with FXII and FXI (MacQuarrie et al., 2011). Therefore, the specific and high affinity of HRG for FXIIa, as well as the inhibitory effects of HRG on FXIIa-

mediated contact activation imply a potentially significant physiological, anticoagulant role for this interaction. However, the mechanism of HRG inhibition of FXIIa is not fully understood and necessitates further investigation.

1.12.4 Binding of HRG to FXIIa

Previous studies by our laboratory have shown that HRG binds to the activated form of FXII, but not the zymogen FXII (MacQuarrie et al., 2011). HRG does not bind to the catalytic domain of FXIIa, as HRG does not bind to β-FXIIa, which consists of the catalytic light chain, as well as 9 amino acid residues of the proline-rich domain (heavy chain remnant; Asn335-Arg343) (Fujikawa & McMullen, 1983; MacQuarrie et al., 2011). Therefore, the binding site of HRG must be localized within the heavy chain of FXIIa. In particular, the FN2 domain of FXIIa may be a potential binding site as it mediates Zn^{2+} binding, as well as binding to negatively charged surfaces (Pathak et al., 2015). The surface-independent conformational change (Bernardo et al., 1993) induced by Zn^{2+} in FXII zymogen is insufficient to allow for HRG binding. Therefore, the binding site of HRG on FXII must be cryptic and only exposed when it is converted to its activated form, FXIIa upon contact activation with a negatively charged surface (MacQuarrie et al., 2011). This notion is supported by the interaction with fibronectin, as well as a monoclonal antibody against the kringle domain of FXII, with FXIIa, as these proteins do not bind to the zymogen FXII (MacQuarrie et al., 2011). Moreover, chromogenic assays demonstrating that HRG has no effect on active site-directed inhibition of FXIIa by either CTI or C1-INH (MacQuarrie et al., 2011). These findings suggest that HRG likely binds to an exosite on

the heavy chain of FXIIa that mediates binding to macromolecular substrates. The sites of interaction between HRG and FXIIa, however, remain elusive. Therefore, this project aims to identify the complementary binding domains of HRG and FXIIa to further understand the role of HRG as a novel regulator of coagulation.

2.0 CHAPTER 2: OVERVIEW, HYPOTHESIS & OBJECTIVES

2.1 Thesis Overview: The overall objective of this Ph.D. thesis is to explore the role of HRG in coagulation as a means of further understanding hemostasis and identifying new strategies for prevention and treatment of thrombosis.

2.2 Rationale: Recent studies suggest that coagulation FXII, which is dispensable for hemostasis, is important for thrombus stabilization and growth (Gailani & Renné, 2007b; Grover & Mackman, 2019; Renné et al., 2005, 2012). Thus, compared with wild-type mice, thrombosis at sites of arterial or venous injury is attenuated in FXII- or FXI-deficient mice (Kleinschnitz, 2006; Renné et al., 2005; Wang et al., 2006). Moreover, knockdown of FXII or FXI with ASOs or inhibition of FXIIa or FXIa with antibodies or inhibitors reduces thrombosis in animal models without compromising hemostasis (Crosby et al., 2013; Larsson et al., 2014; Revenko et al., 2011; Younis et al., 2012; Zhang et al., 2010). These findings identify FXII and FXI as promising targets for development of potentially safer anticoagulants (Fredenburgh et al., 2017; Gailani et al., 2015; Müller, Gailani, & Renne, 2011; Weitz, 2016; Weitz & Fredenburgh, 2017a).

With FXII and FXI emerging as therapeutic targets, a better understanding of the regulation of the contact pathway is required. When bound to a negatively charged surface, single chain FXII zymogen undergoes autoactivation to form two-chain α-FXIIa (MacQuarrie et al., 2011; Renné et al., 2012). In the presence of HK, FXIIa activates prekallikrein to α-kallikrein (Gailani & Renné, 2007a; Renné, 2012; Renné & Gailani, 2007), which then activates additional FXII in a reciprocal manner. FXII activation is

enhanced by polyanions, such as polyphosphate released from activated platelets and nucleic acids derived from neutrophil extracellular traps or necrotic or apoptotic cells (Baker et al., 2018; Jain et al., 2012; Schmaier, 2016; Vu et al., 2016). FXIIa propagates coagulation by activating FXI, which circulates in complex with HK, and culminates in thrombin generation and fibrin formation (Schmaier, 2016). C1-INH is considered the major inhibitor of FXIIa with antithrombin and α2-macroglobulin playing lesser roles (Kenne & Renné, 2014; Kolyadko et al., 2014). However, C1-INH is not specific for FXIIa and the second order rate constant suggests that inhibition is slow (Cugno et al., 1997; de Agostini et al., 1984; Olson & Gettins, 2011; Wagenaar-Bos & Hack, 2006). Moreover, FXIIa bound to endothelial cells or nucleic acids is protected from inhibition by C1-INH (Kolyadko et al., 2014; Pixley et al., 1985, 1987; Schousboe, 2003; Wagenaar-Bos & Hack, 2006). Therefore, there are likely to be additional regulators of FXIIa.

HRG is an abundant plasma protein of uncertain function. Often referred to as the Swiss army knife of mammalian plasma, HRG has been implicated in diverse processes, including coagulation, immunity, fibrinolysis, and angiogenesis (Jones et al., 2005; Poon et al., 2011; Priebatsch, Kvansakul, et al., 2017; Ronca & Raggi, 2015). Previously, we showed that HRG binds FXIIa with high affinity, inhibits FXII autoactivation and FXIIa-mediated activation of FXI, and attenuates ferric chloride-induced arterial thrombosis in mice (MacQuarrie et al., 2011; Vu et al., 2015). HRG binds to nucleic acids with high affinity (K_d values of 1 nM) most likely through the phosphate head group of phosphatidic acid of DNA and RNA and attenuates their procoagulant activity by competing with contact factors, such as FXII and FXI, for binding to nucleic acids (Priebatsch, Kvansakul, et al.,

2017; Vu et al., 2016). Vu *et al*. demonstrated that nucleic acids are potent activators of the contact pathway and provided evidence that HRG is a dynamic regulator of this pathway (Vu et al., 2016). HRG has a modular structure consisting of two NH_2-terminal cystatin-like domains, a central histidine-rich region (HRR) flanked by two proline-rich regions (PRR), and a COOH-terminal domain (Jones et al., 2005; Poon et al., 2011). We demonstrated that the affinity of HRG for FXIIa increases 1000-fold in the presence of Zn^{2+} and that the HRG-FXIIa interaction is abrogated with imidazole, a histidine analogue (MacQuarrie et al., 2011). These findings suggested that the HRG-FXIIa interaction is mediated by the HRR domain of HRG, which is its Zn^{2+}-binding domain.

Previous studies by our laboratory have shown that HRG binds to the activated form of FXIIa, not the zymogen FXII (MacQuarrie et al., 2011). HRG does not bind to the catalytic domain of FXIIa, as HRG has been demonstrated to not bind to β-FXIIa, which consists of the catalytic light chain, as well as 9 amino acid residues of the PRR (Asn335-Arg343) (Fujikawa & McMullen, 1983; MacQuarrie et al., 2011). Therefore, the binding site of HRG must be localized within the heavy chain of FXIIa. In particular, the FN2 domain of FXIIa may be a potential binding site as it mediates Zn^{2+} binding, as well as negatively charged surfaces (Pathak et al., 2015). The surface-independent conformational change (Bernardo et al., 1993) by Zn^{2+} in FXII zymogen is insufficient to allow for HRG binding. Therefore, the binding site of HRG on FXII must be cryptic and only exposed when it is converted to its activated form, FXIIa upon contact activation with a negatively charged surface (MacQuarrie et al., 2011). This notion is supported by the interaction with fibronectin, as well as a monoclonal antibody against the kringle domain of FXII, as these

proteins do not bind to FXII, but only to FXIIa (MacQuarrie et al., 2011). Moreover, HRG has no effect on active site-directed inhibition of FXIIa by either CTI or C1-INH (MacQuarrie et al., 2011). Together, these findings suggest that HRG likely binds to an exosite on the heavy chain of FXIIa that mediates binding to macromolecular substrates. The interaction between HRG and FXIIa, however, remains elusive and necessitates further studies.

2.3 Hypothesis: Based on these observations, we hypothesize that (1) FXIIa binds to the Zn^{2+}-binding histidine-rich region (HRR) of HRG and that (2) HRG binds to the non-catalytic heavy chain of FXIIa to exert its anticoagulant activities on FXIIa-mediated contact activation.

2.4 Overall Objective: To address this hypothesis, 4 main objectives were proposed. The overall objective was to identify the complementary binding domains of HRG and FXIIa to further understand the role of HRG as a novel regulator of coagulation.

2.4.1 Objective 1: Characterization of the effect of HRG fragments obtained by limited proteolysis on FXIIa-mediated contact activation

2.4.2 Objective 2: Characterization of recombinant HRG domain constructs in plasma clotting and FXIIa-mediated contact activation

2.4.3 Objective 3: Characterization of synthetic HRR peptides in FXIIa-mediated contact activation, plasma clotting, and polyphosphate-induced thrombin generation

2.4.4 Objective 4: Characterization of binding interactions between HRG, FXIIa, and polyphosphate

3.0 CHAPTER 3: MATERIALS

3.1 Common Reagents

Zinc chloride ($ZnCl_2$), silicon dioxide (silica; 5-15 nm), EDTA, streptavidin-agarose, and human leukocyte elastase were purchased from Sigma Aldrich (St. Louis, MO, USA). Trypsin- sequencing grade was purchased from Roche (Mississauga, ON, CA). Short chain polyP (70-100 phosphate units) was provided by Dr Thomas Stoffel (BK Giulini GmbH, Ladenburg, Germany), whereas long chain polyP (>1000 phosphate units) was generously provided by Dr. James Morrissey (University of Michigan, MI). Dextran sulfate (500 kDa) and PD-10 column were purchased from GE Healthcare (Pittsburgh, PA, USA). APTT-SP and RecombiPlasTin 2G were purchased from Instrumentation Laboratory Company (Bedford, MA). Phosphatidylcholine-phosphatidylserine (3:1) vesicles (PCPS) were prepared as described (Kretz et al., 2010). Glu-plasminogen was isolated from human plasma as previously described (MacQuarrie et al., 2011). Chromogenic substrates (S2484, S2222, S2366, S2302) and thrombin chromogenic substrates were obtained from Hyphen BioMed (Zac Neuville Université, Neuville sur Oise, France).

3.2 Enzymes and Inhibitors

Human factor (F) XII, FXIIa, FXI, prekallikrein (PK), high molecular weight kininogen (HK), and corn trypsin inhibitor (CTI) were purchased from Enzyme Research Laboratories (South Bend, IN, USA). The following enzyme inhibitors were purchased

from Sigma-Aldrich, Inc.: MeOSu-AAPV-AFC (94-AFC), α_1-antitrypsin from human plasma, soybean trypsin inhibitor (STI). Phe-Pro-Arg-chloromethylketone (PPACK) was purchased from Cedarlane Laboratories (Burlington, ON, CA). Human alpha-2 plasmin inhibitor, plasmin, biotinylated Phe-Pro-Arg-chloromethyl ketone (b-FPRCK), fluorescein Phe-Pro-Arg-chloromethyl ketone (F-PPACK) were purchased from Haematologic Technologies Inc. (Essex Junction, VT). Plasmin inhibitor D-Val-Phe-Lys chloromethyl ketone (VFK-CMK) was purchased from Calbiochem-Novabiochem Corporation (La Jolla, CA, USA).

3.3 Protein Purification Reagents

HRG was isolated from human plasma using a Ni-NTA agarose column as previously described (MacQuarrie et al., 2011). HRG-depleted human plasma was prepared by repeated (3x) chromatography over the affinity purified anti-HRG column as previously described (MacQuarrie et al., 2011). HRG antibody column was prepared using CNBr Activated Sepharose 4B (GE Healthcare). As a control, a second sample of human plasma was subjected to chromatography on unmodified Sepharose. Removal of HRG from human plasma was verified by Western blot analysis using the same affinity purified antibody (MacQuarrie et al., 2011). Mini-PROTEAN TGX precast gels (4-15%), SYPRO Ruby protein gel stain, and Coomassie Brilliant Blue R-250 staining solution were purchased from Bio-Rad Laboratories (Mississauga, ON, CA). SOC Outgrowth Medium, amylose resin, and enterokinase light chain were purchased from New England Biolabs Ltd.

(Whitby, ON, Canada). Millipore Sigma™ Amicon™ Ultra Centrifugal Filter Units was purchased from Thermo Fisher Scientific (Burlington, ON, Canada).

3.4 Antibodies

Sheep polyclonal antibody against human HRG and unconjugated monoclonal goat anti-human FXII antibody were purchased from Affinity Biologicals (Ancaster, ON, Canada), HRG antibody was affinity purified as previously described (Vu et al., 2015). HRG-directed IgG-horseradish peroxidase (HRP) conjugate was prepared as specified by the manufacturer using a Lightning-Link HRP conjugation kit (Cedarlane, Burlington, ON). Rabbit polyclonal anti-human IgG-maltose-binding protein (MBP) antibody was purchased from Thermo Fisher Scientific (Burlington, ON, Canada).

3.5 Surface Plasmon Resonance Reagents

Biacore sensor chips (CM4, CM5), an amine coupling kit, and acetate 5.0 buffer were purchased from Cytiva (formerly GE Healthcare Life Sciences, Burlington, ON, Canada). Biotinylated short chain polyphosphate (70-100 phosphate units) and biotinylated long chain polyphosphate (700-1000 phosphate units) were purchased from Kerafast, Inc. (Boston, MA, and supplied by Dr. James Morrissey, University of Michigan).

3.6 Molecular Cloning Reagents

PCR Master Mix (2x) was purchased from Thermo Fisher Scientific Inc. (Mississauga, ON, Canada). Oligonucleotide primers were ordered from MOBIX

(McMaster University, Hamilton, ON) and described in Table 1. QIAprep Spin Miniprep Kit, QIAquick PCR Purification Kit, QIAquick Gel Extraction Kit, and CompactPrep Plasmid Maxi Kit were purchased from QIAGEN Inc. (Mississauga, ON, Canada). HRG (NM_000412) Human Tagged ORF Clone (cDNA) was purchased from OriGene Global (Rockville, MD, USA). Expression vector, pMAL-c5e and BL21-Gold (DE3) *E. coli* were a gift from Dr. Colin Kretz (McMaster University, purchased from New England Biolabs). Restriction enzymes (BamH1-HF, Not1, Ava1, Nde1) were purchased from New England Biolabs Ltd. (Whitby, ON).

Oligonucleotide	**Primer Sequence**
N1- Sense	5'-CATATGTCCATGG*GCGGCCGC***GTGAGTCCCACTGACTGCAGT**-3'
N1- Antisense	5'-GCAGGGAATTC*GGATCC*GTCA**AGAACTTGTGGTGCAGTTAAAGTC**-3'
N2- Sense	5'-GATGACAAGGTACCG*CATATG***GTCTCTTCAGCACTGGCCAAT**-3'
N2- Antisense	5'-GCAGGGAATTC*GGATCC*GTCA**GACTTCACAGTTTATGACAAGGTTTT**-3'
N1N2- Sense	5'-CATATGTCCATGG*GCGGCCGC***GTGAGTCCCACTGACTGCAGT**-3'
N2N2- Antisense	5'-GCAGGGAATTC*GGATCC*GTCA**GACTTCACAGTTTATGACAAGGTTTT**-3'
PRR1- Sense	5'-GATGACAAGGTACCG*CATATG***CCGCCTCATTTGGGACATCC**-3'
PRR1- Antisense	5'-GCAGGGAATTC*GGATCC*GTCA**GGGCAATAGTGGAGGAGGG**-3'
HRR- Sense	5'-GATGACAAGGTACCG*CATATG***GACCTCCATCCCCATAAGCAT**-3'
HRR- Antisense	5'-GCAGGGAATTC*GGATCC*GTCA**GTGGGGATGGTGTCCATGG**-3'
PRR2- Sense	5'-CAATAACAACAAC*CTCGGG***CCTTGTGACCCACCACC**-3'
PRR2- Antisense	5'-GCAGGGAATTC*GGATCC*GTCA**GGGACGGGGTCCTTTACCTG**-3'
COOH- Sense	5'-CATATGTCCATGG*GCGGCCGC***GTGTACCGACTCCCTCCTCTA**-3'
COOH- Antisense	5'-CAGGGAATTC*GGATCC*GTCAT**TTTGGAAATGTATGTGTAAAAAACATGG**-3'
HRG- Sense	5'-CATATGTCCATGG*GCGGCCGC***GTGAGTCCCACTGACTGCAGT**-3'
HRG- Antisense	5'-CAGGGAATTC*GGATCC*GTCAT**TTTGGAAATGTATGTGTAAAAAACATGG**-3'
Sequencing- Sense	5'-**TACTGCGGTGATCAACGC**-3'
Sequencing- Antisense	5'-**AACGTTCAAATCCGCTCCC**-3'

Table 1: Oligonucleotide Sequence of HRG Domain Fragments Primers

Primers were designed to PCR-amplify individual domains of human HRG and fragments containing multiple domains (source of sequence: UniProtKB- P04196, HRG_Human). **Bold – annealing to template,** non-bolded – overhang containing restriction sites. Restriction sites are italicized; BamH1 (5'-*GGATCC*-3'), Not1 (5'-*GCGGCCGC*-3'), Ava1 (5'-*CTCGGG*-3'), Nde1 (5'-*CATATG*-3').

3.7 Synthetic HRR Peptides

Peptide analogs of the histidine-rich region (HRR) of HRG containing 1 to 4 repeats of the His-His-Pro-His-Gly $(HHPHG)_{1-4}$ consensus sequence (Doñate et al., 2004), a scrambled peptide, $Scr(HAHG)_5H$ containing five repeats of HAHG, and poly-His peptides consisting of 6 or 12 residues (H-6 and H-12) were synthesized by Biomatik (Cambridge, ON) (Table 2).

Synthetic Peptide	Sequence	Consensus Sequence Repeats	No. of His Residues
$(HHPHG)_1$	HHPHG	1	3
$(HHPHG)_2$	HHPHGHHPHG	2	6
$(HHPHG)_3$	HHPHGHHPHGHHPHG	3	9
$(HHPHG)_4$	HHPHGHHPHGHHPHGHHPHG	4	12
$Scr(HAHG)_5H$	HAHGHAHGHAHGHAHGHAHGH	0	11
H-6	HHHHHH	0	6
H-12	HHHHHHHHHHHH	0	12

Table 2: HRR-derived peptide analogs of HRG

Peptide analogs of the histidine-rich region (HRR) of HRG were synthesized based on the His-His-Pro-His-Gly (HHPHG) consensus sequence repeats unique to that domain. A scrambled variant and poly-His peptides served as controls.

4.0 CHAPTER 4: METHODS

4.1 RESTRICTION ENZYME DIGESTION OF HRG

4.1.1 Digestion of HRG with proteolytic enzymes

Proteolytic enzymes were used to generate fragments of human HRG. To determine optimal digestion times, 5 μM human HRG in HEPES-buffered saline consisting of 20 mM HEPES-NaOH, 150 mM NaCl, pH 7.4 (HBS) was incubated with 200 nM trypsin for 180 min at 37°C. At various time points, 10 μl aliquots were removed from the digestion mixture and added to 2.5 μl of SDS gel sample buffer to stop trypsin activity. For HRG fragments used in FXIIa autoactivation assays, trypsin was inhibited with 20 nM STI and residual FXIIa chromogenic activity was determined after digestion to ensure complete inhibition by STI. The effect of STI on FXIIa chromogenic activity was assessed to ensure addition of STI to digestion samples would not influence functional assays. The reaction was initiated by the addition of 0-40 nM STI to 20 nM FXIIa in HBS-Tween20. After 5-min incubation, 200 μM S-2302 substrate was added to each well and absorbance was monitored at 405 nm in a plate reader (Molecular Devices) using SoftMax Pro Version 5.4.1. Optimal proteolytic digestion time was obtained in a similar manner for 200 nM elastase and plasmin treatment (500 nM Glu-plasminogen, 200 nM tPA) of 5 μM HRG, using α_1-antitrypsin and α_2-antiplasmin to stop enzyme activity, respectively.

4.1.2 SDS-PAGE analysis

Samples were denatured by boiling for 3 min and after centrifugation at 10,000 rpm for 30 s, 2 to 3 µg of protein was loaded onto a 4-15% polyacrylamide gradient Mini-PROTEAN TGX pre-cast gel (Bio-Rad Laboratories, Inc.). To run under reducing conditions, 2-mercaptoethanol was added to protein samples. Electrophoresis was performed under denaturing conditions in the presence of 0.01% SDS at 50 volts for 10 min and then at 180 volts for an additional 40 min. Gels were fixed by 15-min incubation in 40% methanol-10% acetic acid solution, followed by a series of three 5-min washes in filtered Milli-Q H_2O. Gels were stained with Bio-Safe Coomassie G-250 blue stain (Bio-Rad Laboratories, Inc.) for 60 min, followed by overnight de-staining in filtered MilliQ H_2O. Other gels were stained with Sypro™ Ruby Protein Gel Stain (Bio-Rad Laboratories, Inc.) over night at room temperature with shaking. Gels were then de-stained in 10% methanol-7% acetic acid solution for 30 min, before a 15-min wash in MilliQ water. Gels were imaged using Image Lab Software (Version 5.2.1.) on the Gel/ChemiDoc MP Imager System (Bio-Rad Laboratories, Inc.).

4.1.3 Reduction and alkylation of trypsin digested HRG

Reduction was initiated with the addition of 5 µM trypsin digested HRG (100 µl) to a mixture of 0.1 M phosphate buffer, 25 mM DTT, and 5 mM EDTA. After 60-min incubation at 4°C, with gentle mixing, 13.2 µl of a 550 mM iodoacetamide solution was added and incubated for 30 min. Reduced and alkylated (RA) trypsin digested HRG samples were dialyzed in HBS buffer at 4°C, changing buffer three times every 2 h, then

once more overnight. After transferring RA samples from dialysis tubing to Eppendorf tube, absorbance was measured at 280 nm and 320 nm to determine the protein concentration (0.1% extinction coefficient= 0.39 mL/mg/cm) (Bloom et al., 1979; Borza et al., 2004). Samples were subjected to SDS-PAGE analysis to compare the trypsin-digested HRG fragments with intact HRG to confirm reduction and alkylation.

4.1.4 Purification of trypsin digested HRG fragment

Dialyzed trypsin digested HRG was loaded onto a Ni-NTA column, which was washed with HBS, and then eluted with 50 mM or 250 mM imidazole. After collection of 1 ml fractions, protein concentrations were determined using A280 spectrometry readings. Protein containing fractions were subjected to SDS-PAGE analysis and gels were stained with Sypro™ Ruby Protein Gel stain (Bio-Rad Laboratories, Inc.).

4.2 STREPTAVIDIN-AGAROSE PULL-DOWN ASSAY

4.2.1 Biotinylation of FXIIa

FXIIa was first incubated with biotin-FPR-CMK (b-FPRCK) and residual FXIIa activity was quantified by monitoring hydrolysis of S-2302. The reaction was initiated by the addition of 200 µl of a 200 µM solution of S-2302 to 1 µl of 6.25 µM FXIIa in a 96 well plate. Absorbance was measured at 405 nm every 6 sec for 5 min at 23°C. Addition of 1 µl of 6.6 mM b-FPRCK to 400 µl of a 6.26 µM FXIIa mix was followed by 15-min incubation at room temperature. FXIIa chromogenic activity (T=15 min) was measured as previously described. If complete inhibition of FXIIa activity was achieved, no further b-FPRCK was

added. Residual free b-FPRCK was removed by passing the sample mixture through an Amicon Ultra-4 Centrifugal Filter Device (Thermo Fisher Scientific, Inc.) equilibrated with HBS. Finally, 400 µl fractions were collected and absorbance was measured at 280 nm and 320 nm to determine the concentration of b-FPRCK-FXIIa (0.1% extinction coefficient= 1.41 mL/mg/cm) (Fujikawa & McMullen, 1983; Konings et al., 2011).

4.2.2 Biotinylated FXIIa-streptavidin agarose binding of HRG

To minimize non-specific binding, streptavidin-agarose (SA) (Sigma-Aldrich) was pre-washed with two consecutive 1 ml buffer washes (1M $NaCl_2$, 0.5 mM EDTA, 0.05% Tween-20 in HBS) prior to incubation with b-FPRCK-FXIIa. Pre-washed SA (100 µl) was then added to 400 µl of b-FPRCK-FXIIa and incubate for 15 min at room temperature with gentle mixing. After centrifugation at 6000 rpm for 30 sec, the supernatant was removed, and absorbance was determined at 280 nm and 320 nm to calculate the protein concentration and determine the yield of b-FPRCK-FXIIa. HRG dilutions were prepared in HBS containing 12.5 µM $ZnCl_2$ and 0.1% P-40 and 3.5 µM (20 µl) SA-b-FPRCK-FXIIa was incubated with 12.6 µM (60 µl) HRG for 30 min at room temperature with gentle mixing. Binding of SA-b-FPRCK-FXIIa was repeated with trypsin-treated HRG fragments after digestion. After incubation, samples were consecutively washed with 1 ml HBS + 12.6 µM $ZnCl_2$ buffer twice before the pellet was re-suspended in sample buffer prior to SDS-PAGE analysis.

4.2.3 Agarose pull-down assay

To detect interactions between biotinylated FXIIa and HRG digestion fragments, biotin-streptavidin agarose pull-down analysis was performed. In the presence of 12.5 µM $ZnCl_2$, 3.5 µM of the biotinylated FXIIa-streptavidin agarose preparation was added to 12.6 µM of trypsin-treated HRG fragments. After 30 min incubation, samples were washed twice with 1 ml aliquots of HBS buffer containing 12.6 µM $ZnCl_2$, and after centrifugation, the pellet was re-suspended in sample buffer and subjected to SDS-PAGE analysis. Controls included the following: streptavidin agarose (SA), SA-b-FPRCK-FXIIa, intact HRG (HRG), HRG + SA and Zn^{2+}, SA-b-FPRCK-FXIIa + HRG + Zn^{2+}, RA trypsin-digested HRG (RA Tryp-HRG), RA Tryp-HRG + SA. Finally, RA Tryp-HRG was incubated with SA-b-FPRCK-FXIIa in the presence of Zn^{2+}.

4.3 MASS SPECTROMETRY AND PROTEIN SEQUENCING

4.3.1 Mass spectrometry analysis of trypsin digested HRG and FXII fragments

Trypsin digested samples of HRG and FXII were prepared for mass spectrometry analysis. Digestion samples were run on 4-15% SDS-PAGE gels and the gels were stained with Coomassie blue stain as previously described. After overnight de-staining in MilliQ H_2O, selected bands were excised using a sterilized razor and submitted to SickKids Proteomics, Analytics, Robotics & Chemical Biology Centre (SPARC BioCentre). Samples for sequencing were subjected to in-gel trypsin digestion, PNGase treatment, and C_{18} cleanup prior to mass spectrometry analysis using the Obri-trap Classic instrument.

Standard database searching and Scaffold4 Proteome Software were used to compare, identify and analyze the trypsin digested HRG and FXII fragments.

4.4 GENERATION OF PCR-AMPLIFIED HRG DOMAIN FRAGMENTS

4.4.1 PCR amplification of HRG domain fragments

Primers were designed to PCR-amplify individual domains of human HRG, as well as fragments containing multiple domains (Table 1). In 200 μl PCR reaction volume, 10 μl of 100 μM oligonucleotide sense primer and 10 μl of 100 μM oligonucleotide antisense primer for each specific domain of HRG was added to 70 μl of DNAase-free H_2O, 10 μl of 30 ng/μL dilution human HRG cDNA (NM_000412) template, and 100 μl of PCR Master Mix (2x). PCR cycling conditions are provided in Table 3. PCR products were analyzed by agarose gel electrophoresis. PCR products were gel extracted and purified using the QIAquick Gel Extraction kit (QIAGEN Inc.).

PCR Step	Temperature °C	Duration
1	95°C	3 min
2	95°C	30 sec
3	60°C	30 sec
4	72°C	1 min 45 sec
5	72°C	5 min for last cycle
6	4°C	0 min to overnight
Repeat steps 2-4		29 cycles

Table 3: PCR cycling parameters for amplification of HRG domain fragments

4.4.2 Agarose gel electrophoresis

To prepare 1% agarose gels, 1.5 g of agarose (Thermo Fischer Scientific) was added to 150 ml of 40 mM Tris-acetate, 1 mM EDTA (TAE buffer). The mixture was heated for 2 min in the microwave and allowed to cool before the addition of 3 μl of ethidium bromide for visualization of DNA bands. Electrophoresis was performed at 80 volts for 30 to 45 min until optimal separation of DNA bands was achieved. Gels were imaged using Image Lab Software (Version 5.2.1.) on the Gel/ChemiDoc MP Imager System (Bio-Rad Laboratories).

4.5 PLASMID CLONING BY RESTRICTION ENZYME DIGESTION

4.5.1 Restriction enzyme digestion of PCR-amplified HRG domain fragments

PCR products encoding individual human HRG domains and restriction enzyme sites were digested with Ava1 or Nde1 and BamH1 overnight at 37°C. The restriction enzymes used to digest each PCR product are provided in Table 4. In 200 μl reactions, 50 μl of PCR amplified, gel purified DNA (3 μg to 10 μg) was added to 20 μl of Cut Smart Buffer, 32 μl of pMAL-C5e vector (311 ng/μl), 2 μl of restriction enzyme 1 (20 units), and 94 μl of DNAase-free H_2O. The expression vector, pMAL-C5e, was digested with either Not1 and BamH1, Nde1 and BamH1, or Ava1 and BamH1. Digested pMAL-C5e vectors were subjected to agarose gel electrophoresis analysis and selected bands were extracted and purified using QIAquick Gel Extraction kit (QIAGEN Inc.).

HRG Domain	Sense Primer Restriction Site	Antisense Primer Restriction Site
N1	Not1	BamH1
N2	Nde1	BamH1
N1N2	Not1	BamH1
PRR1	Nde1	BamH1
HRR	Nde1	BamH1
PRR2	Ava1	BamH1
COOH	Not1	BamH1

Table 4: Digestion of PCR-amplified HRG domain fragments

Restriction enzyme sites corresponding to each sense and antisense primer used to amplify HRG domain fragments.

4.5.2 Ligation of HRG domain fragments into pMAL-C5e vector

Digested PCR products were then ligated into the pMAL-c5e expression vector containing an NH_2-terminal maltose-binding protein (MBP)-tag (generously provided by Dr. Colin Kretz). The constructs are as follows: MBP-N1, MBP-N2, MBP-N1N2, MBP-PRR1, MBP-HRR, MBP-PRR2, and MBP-COOH (Figure 10). In a 300 µl reaction volume, 30 µl of T4 DNA ligase buffer (10x) and 1µl of T4 DNA ligase (3 units) were added in a 3:1 molar ratio of digested pMAL-c5e vector (1 µg) to PCR product (DNA insert) and incubated overnight in a 37°C water bath. To precipitate ligation products, 30 µl ($1/10^{th}$ volume) 3M sodium acetate (pH 2.5) and 300 µl isopropanol was added to 300 µl ligation sample. After freezing samples for 1 h at -80°C followed by centrifugation at 21,130 x g for 30 min at 4°C, supernatants were removed, and the pellets were carefully washed with 200 µl 70% ethanol. After a second centrifugation step under the same conditions, the ethanol was removed, and the pellets were dried at room temperature overnight. The dried DNA pellets were then resuspended in 20 µl of DNAase-free H_2O.

4.5.3 Transformation of plasmid DNA into competent *E. coli*

Transformation of ligation products was performed using BL21-Gold (DE3) chemically competent *E. coli* (New England Biolabs Inc., gift from Dr. Colin Kretz). After *E. coli* were briefly thawed on ice for 20 min, 5 µl of ligated plasmid DNA was added to each sample and samples were maintained on ice for an additional 20 min. Samples were heat shocked at 42°C in a water bath for 45 sec before being quickly returning to ice for 2

min. To obtain maximal transformation efficiency of *E. coli*, 200 µl of SOC outgrowth medium (New England Biolabs) was carefully added to transformed plasmid DNA and incubated while shaking for 1 h at 37°C. Finally, transformed cells in SOC media were plated onto LB agar plates containing 100 µg/ml ampicillin to allow for colony growth of recombinant plasmid DNA. Ampicillin-resistant colonies were screened by PCR using sense and antisense sequencing primers (Table 1), followed by agarose gel electrophoresis analysis. Positive colonies were further expressed in 5 ml LB culture containing 100 µg/ml ampicillin overnight at 37°C. Plasmid DNA was purified from bacteria culture using QIAprep Spin Miniprep Kit (QIAGEN Inc.). All clones were verified by Sanger sequencing using "sense" primer (Table 1) (MOBIX Lab, McMaster University, Hamilton, ON).

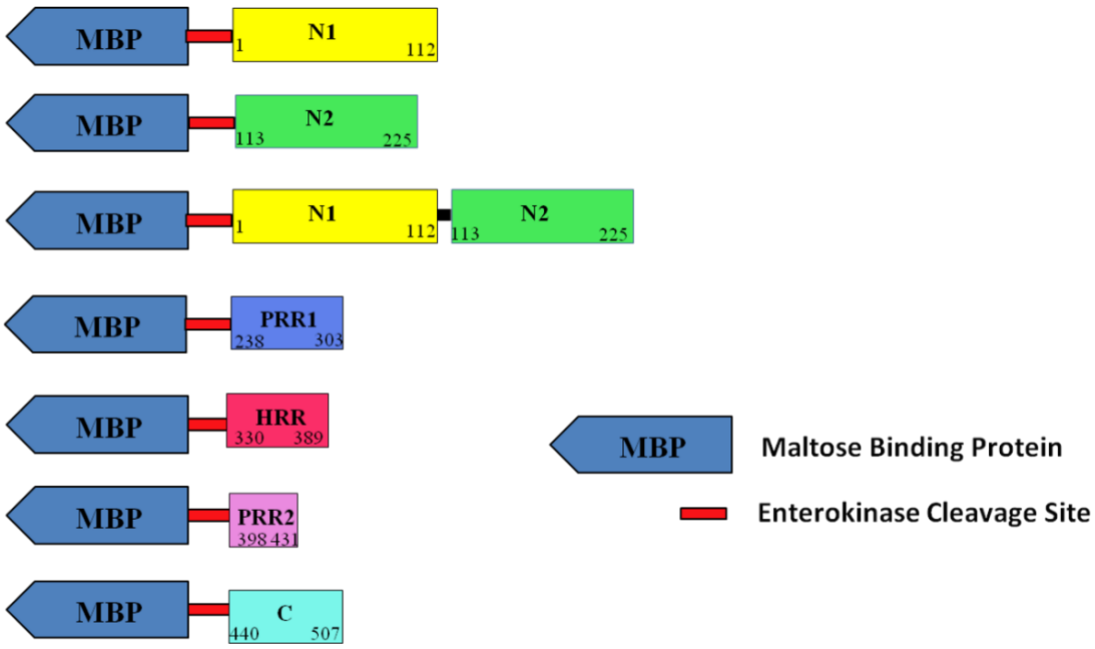
MBP
N1
1
112
MBP
N2
113
225
MBP
N1
1
112
N2
113
225
MBP
PRR1
238
303
MBP
HRR
330
389
MBP
PRR2
398
431
MBP
C
440
507
MBP
Maltose Binding Protein
Enterokinase Cleavage Site

Figure 10: MBP-HRG domain constructs

PCR-amplified HRG domain fragments were ligated into pMAL-c5e expression vector containing an NH_3-terminal maltose-binding protein (MBP)-tag. MBP-HRG domain constructs were transformed into BL21 (DE3) *E. coli* cells. Expressed protein constructs are as followed: MBP-N1, MBP-N2, MBP-N1N2, MBP-PRR1, MBP-HRR, MBP-PRR2, MBP-COOH. MBP, maltose-binding protein; HRG, histidine-rich glycoprotein; N1/2, cystatin-like N1/N2 terminal domain; PRR1/2, proline-rich region; HRR, histidine-rich region; C, carboxyl terminal domain (COOH)

4.6 PROTEIN EXPRESSION OF MBP-HRG DOMAIN CONSTRUCTS

4.6.1 Protein expression in competent *E. coli*

Purified plasmid DNA of MBP-HRG domain constructs were expressed in 5 ml LB starter culture containing 100 μg/ml ampicillin overnight while shaking at 37°C. The starter culture was then transferred to 250 ml LB with 100 μg/ml ampicillin and allowed to grow for 1-2 h at 37°C until reaching mid-log phase (A_{600} of about 0.6). Expression was induced with 1 mM IPTG for an additional 4 h. Cells were harvested by centrifugation at 4000 x g for 20 min and supernatant was discarded. Cell pellets were stored at -80°C overnight. Bacteria were resuspended in 25 ml of column buffer (20 mM Tris-HCl, 200 mM NaCl, 1 mM EDTA, 1 mM azide, pH 7.4) in the presence of cOmplete™ ULTRA protease inhibitor cocktail tablets (Roche). To lyse bacteria, resuspended bacteria were placed in an ice water bath and sonicated in short pulses of 5 sec on/off for 20 min using a FB120 Sonic Dismembrator fitted with a CL-18 probe (Fisher Scientific). Lysed bacteria were subjected to centrifugation at 20,000 x g for 20 min. The crude extract (supernatant) was harvested and diluted 1:6 with column buffer.

4.6.2 Amylose affinity chromatography

Expressed HRG domain constructs were purified by amylose affinity chromatography at 4°C in the cold room. After washing the amylose resin with 5x column volume of buffer (20 mM Tris-HCl, 200 mM NaCl, 1 mM EDTA, 1 mM azide, pH 7.4), diluted crude extract was loaded onto the column and the flow through was collected. The

column was then washed with 12x column volumes of buffer. Finally, protein was eluted with 15 ml of 10 mM maltose in buffer and 1 ml fractions were collected. Absorbance was measured at 280 nm and 320 nm to determine the protein concentrations in the elution fractions. Proteins were buffer exchanged 4 times into HBS and concentrated to a final volume of 50-100 µl using Amicon® Ultra-15 Centrifugal Filter Units (Thermo Fisher Scientific, Inc.) and then stored at -80°C. Purity was assessed by SDS-PAGE analysis and Western blotting. Molecular weight and extinction coefficient (Abs 0.1%) values of each MBP-HRG domain construct were determined using ExPASy Bioinformatics Resource Portal compute pI/Mw tool (UniProtKB- P04196, HRG_Human sequence) (Table 5).

Protein Construct	MW (kDa)	Ext Coeff (mL/mg/cm)
MBP	40.4	1.64
MBP-N1	56.4	1.38
MBP-N2	56.2	1.29
MBP-N1N2	69.5	1.21
MBP-PRR1	50.4	1.43
MBP-HRR	50.7	1.31
MBP-PRR2	45.7	1.46
MBP-COOH	51.3	1.32
*HRG	75.0	0.39

Table 5: Protein characteristics of MBP-HRG domain constructs

Molecular weight and extinction coefficient (Abs 0.1%) values were determined using ExPASy Bioinformatics Resource Portal compute pI/Mw tool using UniProtKB- P04196, HRG_Human sequence). *Human plasma HRG molecular weight and extinction coefficient values are provided.

4.6.3 Western blot analysis

Purified recombinant MBP-HRG domain constructs were subjected to SDS-PAGE analysis on 4-15% polyacrylamide gels (Bio-Rad Laboratories) in the presence of 0.1% sodium dodecyl sulfate (SDS) and 0.14 M β-mercaptoethanol. Separated proteins were transferred onto a nitrocellulose membrane (Bio-Rad Laboratories) overnight at 4°C. The membrane was blocked for non-specific interaction using 1% BSA in TBS containing 50 mM Tris-HCl, 150 mM NaCl, pH 7.4 and 0.005% Tween20 (TBS-Tw). Membranes were probed with affinity-purified polyclonal sheep anti-human IgG-HRG-HRP antibody (0.2 µg/ml) for 2 h or with affinity-purified polyclonal rabbit anti-human IgG-MBP antibody (0.1 µg/ml) overnight at 4°C. Blots were then incubated with HRP-linked secondary antibody (0.2 µg/ml) for 2 h followed by incubation with the detection reagent (Immune-Star HRP kit, Bio-Rad Laboratories) and chemiluminescence determination using Chemi-Doc gel.

4.7 PROTEIN AFFINITY ASSAYS

4.7.1 Surface Plasmon Resonance

The affinities of soluble HRG and HRR-peptides for FXIIa, β-FXIIa, and FXII were determined by surface plasmon resonance (SPR) on a Biacore T200 (GE Healthcare, Mississauga, Canada). Streptavidin (Cedarlane, Burlington, Canada) was attached onto flow cells of a CM4 sensor chip (GE) to 2000-3000 response units (RU) using an amine coupling kit (GE) (MacQuarrie et al., 2011). FXIIa or β-FXIIa, labeled at their active sites

with b-FPRCK, was absorbed to bound SA to ~500 RU at a flow rate of 10 µl/min at 25°C. FXII (500-700 RU) was immobilized directly onto flow cell of a CM4 chip by amine coupling (GE) to 700-800 RU. Binding experiments were performed in HBS- containing 0.005% Tween-20, 2 mM $CaCl_2$, and 13 µM $ZnCl_2$ at a flow rate of 50 µl/min at 25°C. Increasing concentrations of analyte, either 0-500 nM HRG or 0-1000 nM HRR-derived peptides, were injected into all four flow cells for 300 sec, followed by running buffer alone for 900 sec. Flow cells were regenerated with 250 mM NaCl 62.5 mM imidazole and 5 mM EDTA for 60 sec. The affinities of soluble HRG and HRR-peptides for polyphosphate (70-100 phosphate units) (Kerafast Inc.) were also determined using SPR. Biotinylated polyphosphate was absorbed to bound SA to ~100-180 RU at a flow rate of 10 µl/min at 25°C. Binding experiments were performed like those described above. Sensorgrams were analyzed with BIAcore T200 evaluation software Version 1.0 (BIAcore). RU values were obtained from the instrument software. Dissociation constant (K_d) values were determined from equilibrium values or calculated from rate constants using 1:1 Langmuir analysis by the instrument software, and χ^2 values were calculated to assess closeness of fit.

4.7.2 Enzyme-linked immunosorbent assays (ELISA)

To coat 96 well plates (Corning® EIA/RIA Clear Flat Bottom Polystyrene High Bind Microplate) with streptavidin, 100 µl of 10 µg/ml streptavidin (prepared in 50 mM carbonate-bicarbonate, pH 9.6, coating buffer) was added and incubated overnight at 4°C. Wells were blocked with phosphate buffered saline (137 mM NaCl, 2.7 mM KCl, 10 mM phosphate buffer, pH 7.4 (PBS) containing 2% BSA and 0.05% Tw20) blocking buffer for

90 min. After washing the wells three times with PBS containing 0.1% Tw20, the wells were incubated with 100 µl biotinylated polyphosphate in sample diluent buffer (10 mM HEPES, 100 mM NaCl, 1% BSA, 0.1% Tw20, pH 7.2) overnight at 4°C and then washed again three times. Increasing concentrations of HRG or HRG domain constructs prepared in sample diluent buffer were then added (0-500 nM) to the wells. After incubation for 2 h at 22°C and washing three times, the primary polyclonal rabbit anti-MBP antibody (0.1 µg/ml) in conjugate buffer (PBS, 1% BSA, 0.1% Tw20) was added and incubated overnight at 4°C. After washing the wells three times, the secondary goat anti-rabbit HRP-conjugated antibody (0.2 µg/ml) in conjugate buffer was added and incubated for 2 h at 22°C. After three washes, OPD was added. To prepare OPD (o-phenylenediamine dihydrochloride) substrate buffer, a 5 mg OPD tablet was dissolved in 12 ml substrate buffer (citrate-phosphate containing 0.027 M citric acid, 0.097 M Na_2HPO_4, pH 5.0) containing 12 µl of30% H_2O_2. To start the reaction, 100 µl of freshly prepared OPD substrate buffer was added to each well. The plate was covered with tin foil to minimize light exposure and colour was developed for 5 min at 22°C. Reactions were stopped by the addition of 50 µl of sulphuric acid stopping buffer (2.5M H_2SO_4) to each well. Absorbance was measured at 490 nm using SpectraMax® M3 Microplate Reader and non-linear regression analysis using TableCurve 2D (Version 4, Jandel Scientific Software, SPSS Inc., Chicago, IL) was used to determine dissociation constant (Kd) values.

4.8 PLASMA ASSAYS

4.8.1 Thrombin generation

Thrombin generation was quantified using the previously described (Vu et al., 2015) calibrated automated thrombogram assay with some modifications. In a 50 µl sample, HRG-depleted human plasma in the presence or absence of HRG or HRR-derived peptides were added to wells of a black, 96-well plate (Costar, Lowell, MA). To assess the contact pathway, plasma was incubated with 40 µg/mL short chain polyphosphate (70 phosphate units) and 15 µM PCPS for 10 min at 37°C. Clotting was initiated with 15 mM $CaCl_2$ and thrombin generation was monitored by measuring the hydrolysis of 1 mM Z-Gly-Gly-Arg AMC substrate (Bachen, Bubendorf, Switzerland) at 360 nm (excitation) and 460 nm (emission) for 90 min at 37°C using a SpectraMax M5e pate reader (Molecular Devices). Thrombin generation profiles and data were analyzed using Technothrombin TGA software (Technoclone, Vienna, Austria) (Vu et al., 2015).

4.8.2 Plasma clotting assays

In wells of a 96-well plate, 90 µl aliquots of control or HRG-depleted human plasma in the presence of 0-5 µM HRG or HRR-derived peptides were incubated for 10 min at 37^{o}C with either 10 µl of 1:10 aPTT-SP or 10 µl of 1:100 RecombiPlasTin reagent and clotting was initiated by addition of 10 µl of 260 mM $CaCl_2$ (final concentration 26 mM). Absorbance was monitored at 405 nm for 1 h at 37^{o}C and the time to reach half-maximal absorbance as determined by instrument software was used as the clot time. Additional clotting experiments

were performed in the presence or absence of 0-8 μM MBP-HRG domain constructs in HRG-depleted human plasma in a similar manner. Experiments were done in duplicate at least three times for each construct.

4.9 CHROMOGENIC ACTIVITY ASSAYS

4.9.1 FXIIa chromogenic activity

The effect of increasing concentrations of HRG on FXIIa chromogenic activity was assessed. Reaction were initiated by the addition of 20 nM FXIIa to a mixture of 12.5 μM $ZnCl_2$ and 0 to 1 μM HRG in HBS-Tween20. After 5-min incubation at room temperature, 200 μM S-2302 was added and FXIIa activity was monitored by measuring hydrolysis of S-2303 by monitoring absorbance at 405 nm every 10 sec for 30 min. To confirm that FXIIa chromogenic activity inhibition is achievable, the effect of HRG on the inhibition of FXIIa by C1-INH was assessed. Reaction were initiated by the addition of 500 nM C1-INH to a mixture of 50 nM FXIIa, 12.5 μM $ZnCl_2$, ± 200 nM HRG in HBS-Tween20. After incubation at room temperature for 0-60 min, 200 μM S-2302 was added at the same time to each sample and absorbance was monitored at 405 nm every 6 sec for 10 min at 37°C. Rates of FXIIa activity (mOD/sec) were determined using the linear portion of the slope of plots of OD vs s^2.

4.9.2 FXII autoactivation by various activators

To initiate FXII autoactivation, non-physiological activators (dextran sulfate or silica dioxide) or physiological activators (short or long chain chain polyP) were used. In a 100 μl

reaction volume, dextran sulfate (1 μg/mL), silica dioxide (40 μg/mL), or short chain or long chain polyP (8 μg/mL, monomer phosphate concentration) was added to wells of a 96-well plate containing 6 μM $ZnCl_2$ and 100 nM FXII in HBS buffer containing 0.005% Tween-20 (HBS-Tw20) in the absence or presence of 0-5000 nM HRG or HRR-derived peptides. After 15 min incubation at 37°C, 200 μM S-2302 substrate was added to each well and absorbance was monitored at 405 nm. FXIIa generation was quantified by comparison with a standard curve of FXIIa activity. The slopes (OD/s^2) of the linear portion were converted to activation rate values, nM/second, by dividing slopes by the specific activity of 100 nM FXIIa (OD/s/nM). The concentration of FXIIa generated was plotted against the concentration of HRG or HRR-derived peptide and the data were analyzed using TableCurve 2D (Version 4, Jandel Scientific Software, SPSS Inc., Chicago, IL) to determine the concentration required for 50% inhibition of FXII activation (IC_{50}) using rectangular hyperbola, non-linear regression analysis. Similar experiments were performed to determine the effect of 0-8 μM MBP-HRG domain constructs on FXII autoactivation induced by short chain polyphosphate.

4.9.3 FXIIa activation of FXI

In 100 μl reaction volumes, increasing concentrations of HRG or HRR-derived peptides (0-5000 nM) were added to wells containing 12.5 μM $ZnCl_2$, 10 nM FXIIa, 100 nM FXI, 100 nM HK, and 0.2 μg/ml dextran sulfate in HBS-Tw20 containing 2 mM $CaCl_2$ and 0.005% Tween-20. After 30-min incubation at 37°C, 30 nM CTI was added to inhibit FXIIa and the reaction was incubated for an additional 5 min prior to addition of, 200 μM S-2366. Absorbance was monitored at 405 nm as described above to monitor FXIa generation. FXIa

generated was quantified by comparison with a standard curve of FXIa activity. Rates of FXI activation were normalized relative to that obtained in the absence of HRG or HRR-derived peptides and plotted against HRG or peptide concentration. IC_{50} values were determined as described above.

4.9.4 Prekallikrein activation by FXIIa

In 100 µl reactions, increasing concentrations of HRG or HRR-derived peptides (0-5000 nM) were added to wells containing 120 nM PK, 6 µM $ZnCl_2$, 5 µg/ml SC-polyP, and 2 mM $CaCl_2$ in TBS-Tw20. To initiate the reactions, 2 nM FXIIa was added and the mixture was incubated for 10 min at 37°C prior to addition of 1 µM CTI to inhibit FXIIa. After a 5-min incubation period, 200 µM S-2302 and 3 mM EDTA were added and absorbance was measured at 405 nm for 60 min as described above. Kallikrein generation was quantified by comparison with a standard curve of kallikrein activity. Rates of prekallikrein activation were normalized relative to that obtained in the absence of HRG or HRR-derived peptides and plotted against HRG or peptide concentration. IC_{50} values were determined as described above.

5.0 CHAPTER 5: CHARACTERIZATION OF HRG FRAGMENTS GENERATED BY LIMITED PROTEOLYSIS IN CONTACT ACTIVATION PATHWAY

5.1 Effect of HRG on FXII autoactivation induced by dextran sulfate

To evaluate the inhibitory effects of HRG and HRG fragments in contact activation, the effect of HRG on FXII autoactivation was first investigated using a non-physiological activator, dextran sulfate. FXII (100 nM) autoactivation was induced with 2 μg/ml dextran sulfate in the presence or absence of HRG. FXII activation was monitored by measuring the hydrolysis of the FXIIa-directed chromogenic substrate S-2302 (Figure 11). HRG completely inhibits FXII autoactivation with an IC_{50} of ~200 nM. These results are in agreement with previous findings that HRG modulates FXII autoactivation in a dose-dependent and saturable manner (MacQuarrie et al., 2011).

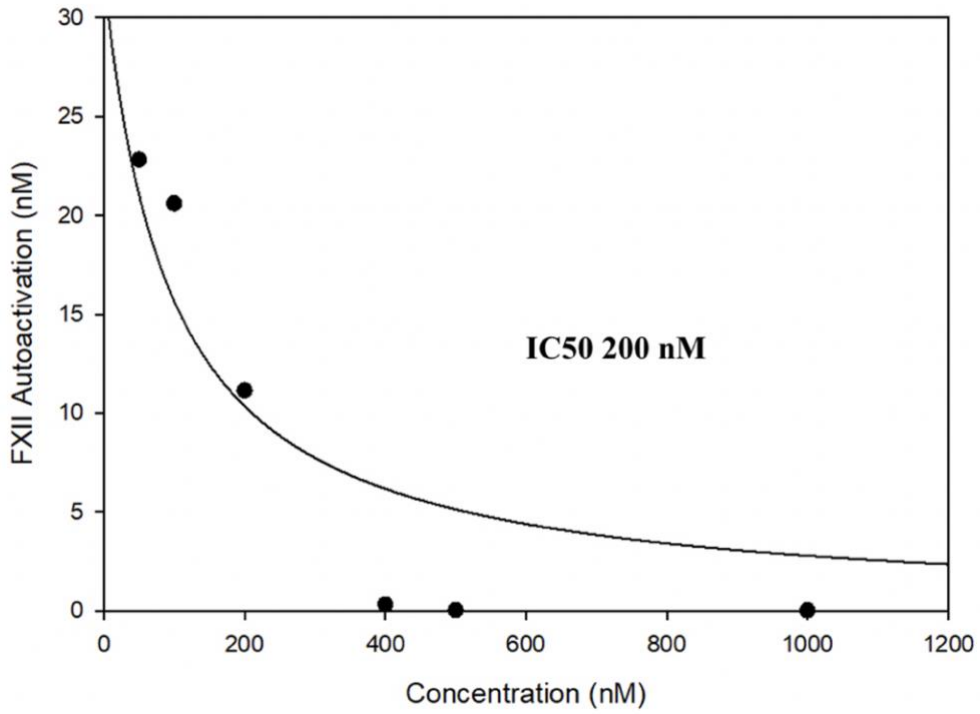
30
25
20
15
10
5
0
FXII Autoactivation (nM)
IC50 200 nM
0
200
400
600
800
1000
1200
Concentration (nM)

Figure 11: Inhibition of FXII autoactivation by HRG

FXII (100 nM) autoactivation was stimulated by 2 μg/ml dextran sulfate in the presence of 12.5 μM ZnCl2 and 0-1000 nM HRG. FXIIa activity was monitored by measuring the hydrolysis of FXIIa-directed chromogenic substrate (S-2302) at A405 in a continuous assay. FXIIa generation was quantified by comparison to a standard curve of FXIIa activity and was plotted against HRG concentration. Non-linear regression analysis was performed to determine IC_{50} value (fitted line) by rectangular hyperbola (non-linear regression) analysis (TableCurve 2D). The data points were representative of two independent experiments (mean).

5.2 Effect of HRG on FXIIa chromogenic activity and C1-INH inhibition

We have previously shown that HRG binds FXIIa, but not FXII or β-FXIIa, suggesting that HRG does not bind the active site of FXIIa (MacQuarrie et al., 2011). To test this hypothesis, control experiments to determine the effect of HRG on FXIIa chromogenic activity were performed using the chromogenic substrate S-2302. We show here that HRG, at concentrations up to 1000 nM, has no effect on the chromogenic activity of FXIIa. This indicates that the effects on activation assays involving HRG are on FXII autoactivation (as previously shown in Figure 11) and do not reflect an alteration in chromogenic substrate hydrolysis (Figure 12). Next, we assessed the effect of HRG on inhibition of FXIIa by C1-INH. The first order rate constant of inhibition (k1) of FXIIa by C1-INH in the presence of 200 nM HRG was similar to that determined in its absence, 0.0492 min^{-1} and 0.0614 min^{-1}, respectively (Figure 13). These results are consistent with previous studies that show that HRG does not exert its inhibitory effect through the active site, but rather on an exosite of FXIIa (MacQuarrie et al., 2011).

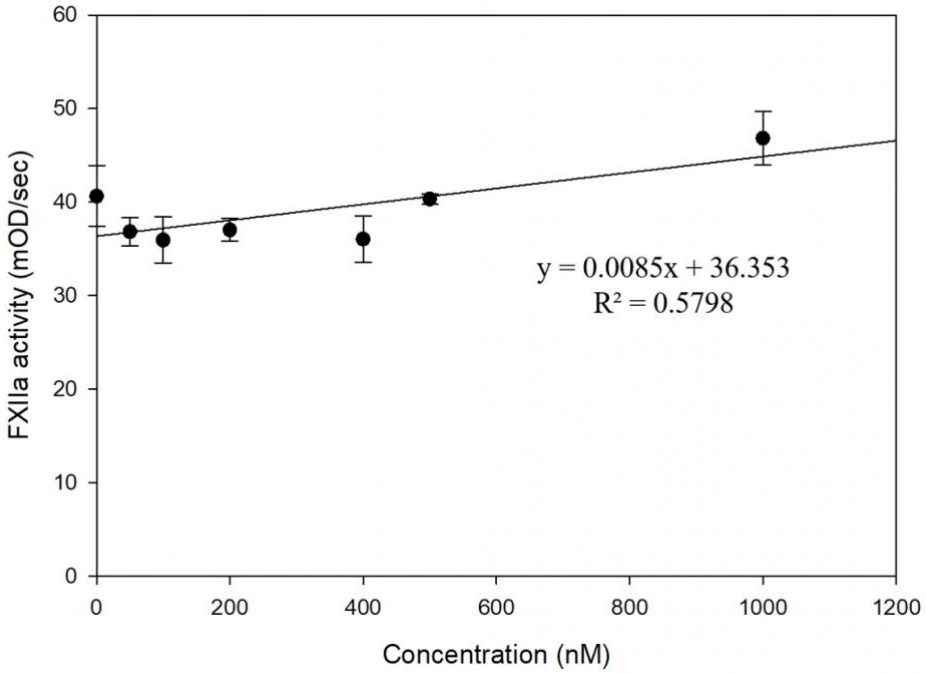
FXIIa activity (mOD/sec)
Concentration (nM)
y = 0.0085x + 36.353
R² = 0.5798
0
10
20
30
40
50
60
0
200
400
600
800
1000
1200

Figure 12: Effect of HRG on FXIIa chromogenic activity

FXIIa chromogenic activity was initiated by the addition of 20 nM FXIIa to a mixture of 12.5 μM $ZnCl_2$ and 0-1000 nM HRG in HBS-Tween20. FXIIa activity was monitored by measuring hydrolysis of S-2303 at 405 nm. Rates of FXIIa activity (mOD/sec) were plotted against HRG concentration (nM). Linear regression analysis was performed to determine the correlation (fitted line). The data points were representative of three independent experiments (mean ± SD).

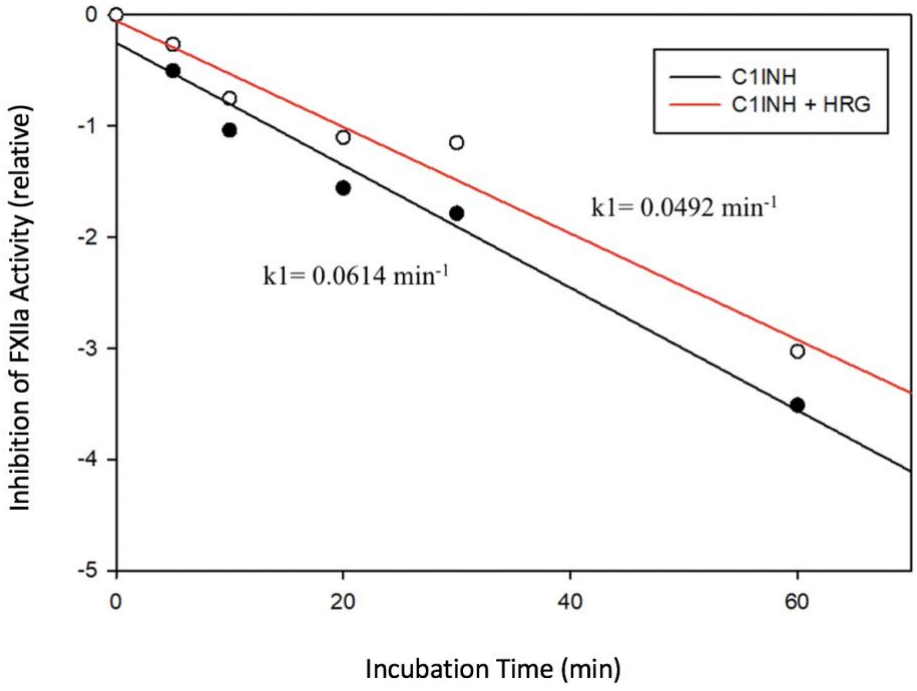
C1INH
C1INH + HRG
k1= 0.0492 min-1
k1= 0.0614 min-1
Inhibition of FXIIa Activity (relative)
Incubation Time (min)
0
-1
-2
-3
-4
-5
0
20
40
60

Figure 13: The effect of HRG on inhibition of FXIIa by C1-INH

The reaction was initiated by the addition of 500 nM C1-INH to a mixture of 50 nM FXIIa, 12.5 μM $ZnCl_2$, ± 200 nM HRG in HBS-Tween20. Mixture was incubated with C1-INH for 0-60 min at room temperature. FXIIa activity was monitored by measuring the hydrolysis of chromogenic substrate (S-2302) in a kinetic assay. The rate constant of inhibition (k1) was calculated by linear regression to determine the slope (fitted lines). FXIIa inhibition was determined by taking the natural logarithm (ln) of the normalised FXII activity and plotted against incubation time (min). The data points were representative of two independent experiments (mean).

5.3 Generation of HRG fragments by limited proteolysis

Limited proteolysis was used to generate fragments that are suitable for identification of the potential inhibitory domain of human HRG. Plasma derived HRG was digested with 200 nM trypsin for 0 to 22 hours at 37°C (Figure 14). The main criterion for the time course was evidence of disappearance of intact HRG on SDS-PAGE analysis. After 1h of trypsin digestion, there was the removal of the intact protein (68 kDa) and the progressive digestion of tryptic fragments with further incubation time (6-22 h). Under non-reduced conditions, trypsin digestion of HRG (1-6 h incubation) produced 4 distinct bands between 37-55 kDa. However, in the presence of a reducing agent, these tryptic HRG fragments were smaller in size (MW of 40, 37, 30 kDa). The differences in molecular masses suggest that there is disulfide linkage within the tryptic fragments of HRG. The multidomain structure of HRG is linked by 6 disulfide bonds, whereby 4 are intradomain and 2 are interdomain (Kassaar et al., 2014). To test whether these tryptic digestion fragments are stable upon further proteolysis, we continued to digest the samples overnight. After 22 h incubation, there was a loss of the 37 kDa band under non-reduced and reduced conditions as shown in Figure 15 (depicted by red arrow). Although there was a loss of the 37 kDa tryptic band, there was an increase in the 30 kDa tryptic band under reduced conditions. There are 47 predicted trypsin cleavage sites according to sequence analysis of human HRG (UniProtKB-P04196) (ExPASy PeptideCutter), however, limited proteolysis resulted in the generation of only a small number of large tryptic fragments. This suggests that there is incomplete digestion of HRG by trypsin, potentially due to poor access of trypsin to its cleavage sites (carboxylic side of amino acids lysine and arginine).

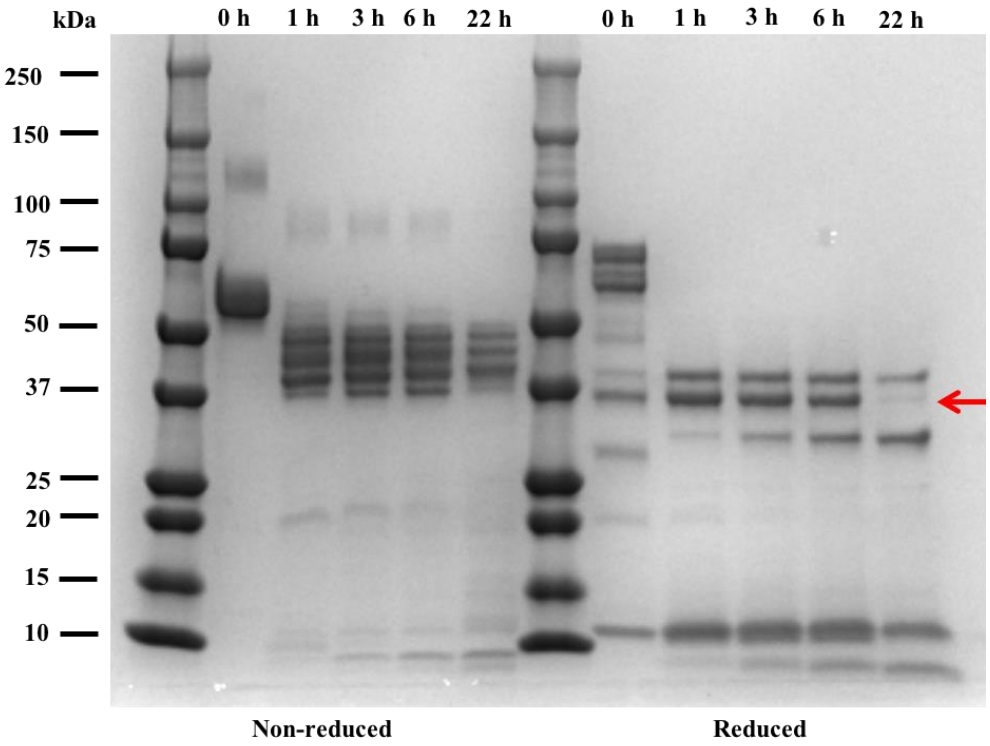
kDa
0 h
1 h
3 h
6 h
22 h
0 h
1 h
3 h
6 h
22 h
250
150
100
75
50
37
25
20
15
10
Non-reduced
Reduced

Figure 14: Limited proteolysis of HRG by trypsin digestion

Digestion of 5 µM HRG was initiated by addition of 200 nM trypsin in HBS-Tween (0.005%) for 0 to 22 hours at 37°C. Sample buffer (2x) was added to stop reaction at each timepoint (hr). SDS-PAGE samples were run under non-reduced and reduced conditions. Red arrow points to 37 kDa band of interest. Approximately, 2.5 µg of protein were loaded onto a 4-15% polyacrylamide gradient gel and electrophoresed in the presence of SDS. Gels were stained with Bio-Safe Coomassie G-250 blue stain and imaged using Image Lab Software on the Gel/ChemiDoc MP Imager System. Molecular weight markers are indicated on the left and middle lane. Red arrow depicts loss of 37 kDa tryptic band after 22h trypsin digestion of HRG.

Next, limited proteolysis with other enzymes was performed to further generate fragments of HRG. Treatment of 5 µM HRG with 200 nM elastase generated several distinct fragments. There are 48 predicted elastase cleavage sites according to sequence analysis of human HRG (UniProtKB-P04196) (ExPASy PeptideCutter). After 1-6 h incubation, 3 bands were observed with molecular masses of approximately 40, 37 and 10 kDa (Figure 15). Removal of intact HRG was not observed until 3 h of incubation with elastase. Further proteolytic cleavage of HRG (24 h) resulted in the partial and complete loss of the 10 kDa and 37 kDa bands, respectively. Differential separation of digested HRG fragments on SDS-PAGE under reduced conditions suggest removal of disulfide linkage between cleaved fragments. It is important to note that the 37 kDa band generated by elastase is most likely different from the band of similar size generated with trypsin digestion. Elastase cleaves the carboxyl side of small, hydrophobic amino acids such as glycine, alanine, and valine. Lastly, treatment of HRG with plasmin (500 nM Glu-plasminogen, 200 nM tPA) for 1-6 h produced several bands ranging between 40-50 kDa in size (Figure 16). In the presence of a reducing agent, disulfide linkage was removed and resulted in two distinct bands with molecular masses of 40 kDa and 37 kDa. Further digestion of HRG (24 h) resulted in little to no loss of the two distinct bands unlike what was observed with trypsin or elastase treatment. Together, these findings show that digestion of human HRG with proteolytic enzymes generates fragments which are stable to limited proteolysis and will allow for further analysis.

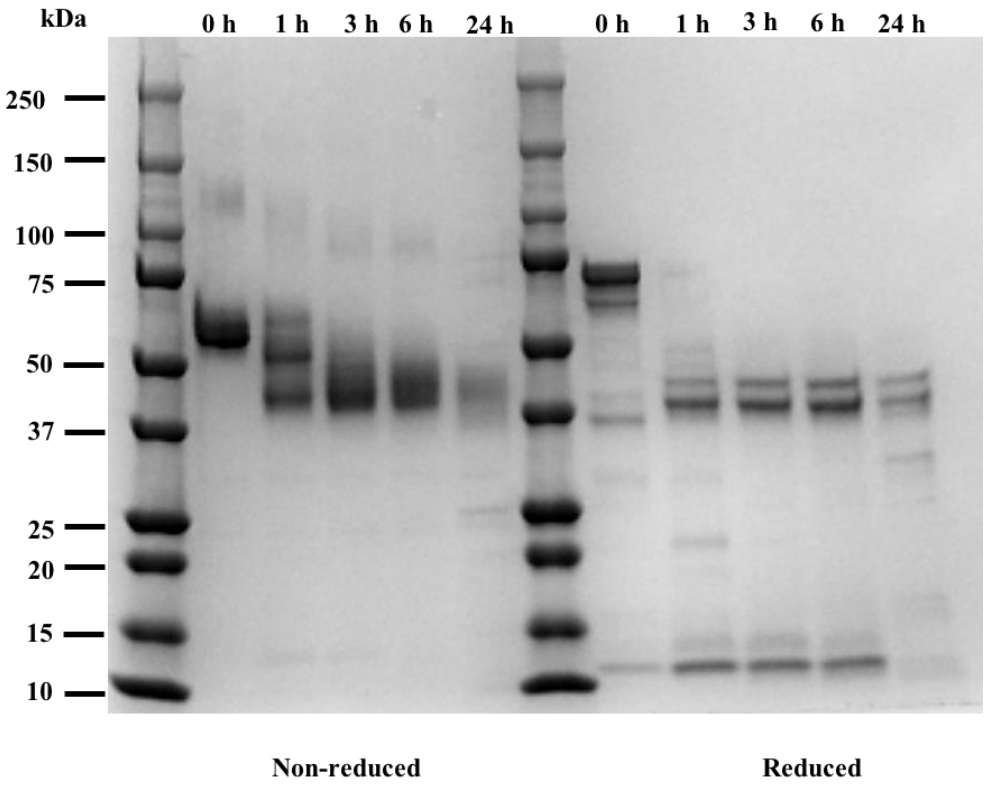
kDa
0 h
1 h
3 h
6 h
24 h
0 h
1 h
3 h
6 h
24 h
250
150
100
75
50
37
25
20
15
10
Non-reduced
Reduced

Figure 15: Limited proteolysis of HRG by elastase

Digestion of 5 μM HRG was initiated by addition of 200 nM elastase in HBS-Tween (0.005%) for 0 to 24 hours at 37°C. Sample buffer (2x) was added to stop reactions at each timepoint. and aliquots (2.5 μg) were subjected to SDS-PAGE analysis on 4-15% gradient gels under non-reduced and reduced conditions. Gels were stained with Bio-Safe Coomassie G-250 blue stain and imaged using Image Lab Software on the Gel/ChemiDoc MP Imager System. Molecular weight markers are indicated on the left and middle lane.

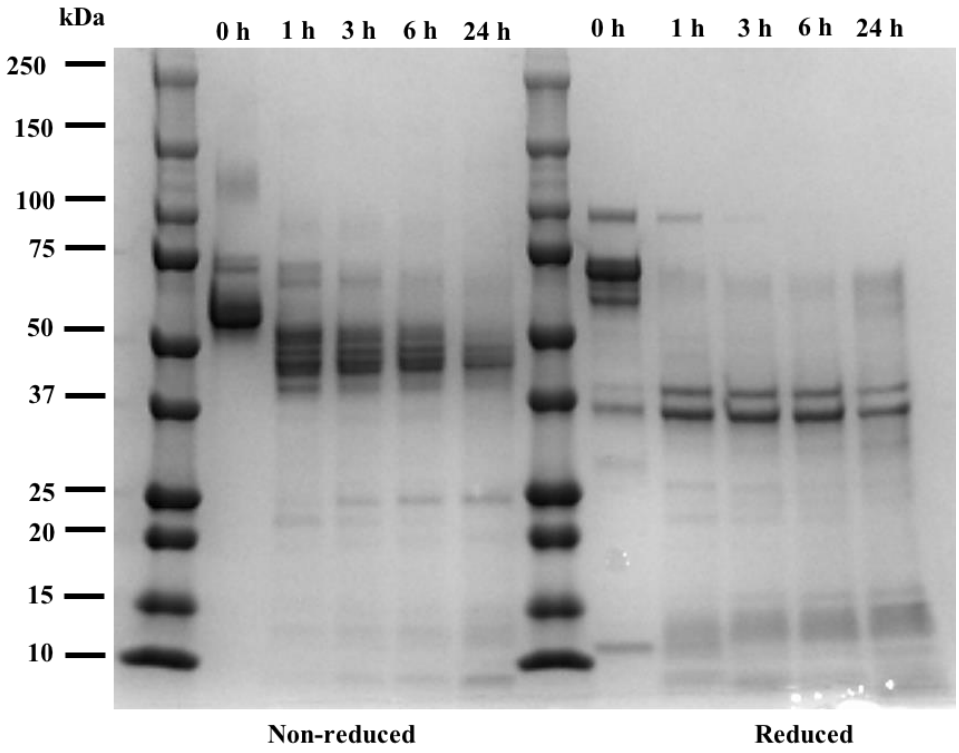
kDa
0 h
1 h
3 h
6 h
24 h
0 h
1 h
3 h
6 h
24 h
250
150
100
75
50
37
25
20
15
10
Non-reduced
Reduced

Figure 16: Limited proteolysis of HRG by plasmin

Digestion of 5 µM HRG by plasmin was initiated by addition of 500 nM Glu-plasminogen and 200 nM tPA in HBS-Tween (0.005%) for 0 to 24 hours at 37°C. Sample buffer (2x) was added to stop reactions at each timepoint. and aliquots (2.5 µg) were subjected to SDS-PAGE analysis on 4-15% gradient gels under non-reduced and reduced conditions. Gels were stained with Bio-Safe Coomassie G-250 blue stain and imaged using Image Lab Software on the Gel/ChemiDoc MP Imager System. Molecular weight markers are indicated on the left and middle lane.

5.4 Inhibitory effect of HRG fragments on FXII autoactivation

The inhibitory effects of HRG fragments were tested in a FXII autoactivation chromogenic assay. FXII autoactivation was initiated by the addition of 100 nM FXII to a mixture of 0.5 µg/ml dextran sulfate, 12.5 µM $ZnCl_2$ in the absence or presence of 200 nM intact HRG (Control, Intact) or HRG fragments. Trypsin activity was stopped using 400 nM soy trypsin inhibitor (STI), which was determined by monitoring STI inhibition of trypsin-directed chromogenic substrate (S-2222) hydrolysis and dose-response assessment (data not shown). Elastase activity was stopped using 2 µM α_1-antitrypsin, which was determined as similarly described using elastase-directed fluorogenic substrate (94-AFC). Plasmin activity was stopped using 400 nM α_2-anti-plasmin, which was determined as similarly described using plasmin-directed chromogenic substrate (S-2251).

Like intact HRG, HRG fragments generated with plasmin, elastase, or trypsin retained significant inhibitory activity (97-99%) (Figure 17). HRG fragments generated retained 92% the inhibitory capacity of intact HRG. Further proteolysis with elastase or trypsin (22-24 h) decreased the inhibitory activity to 55% and 27%, respectively. These data suggest that the domain responsible for HRG interaction with FXIIa may reside within the 37 kDa tryptic fragment generated by proteolytic cleavage. To further investigate the tryptic band of interest, we purified and isolated the 37 kDa band to investigate its interaction with FXIIa.

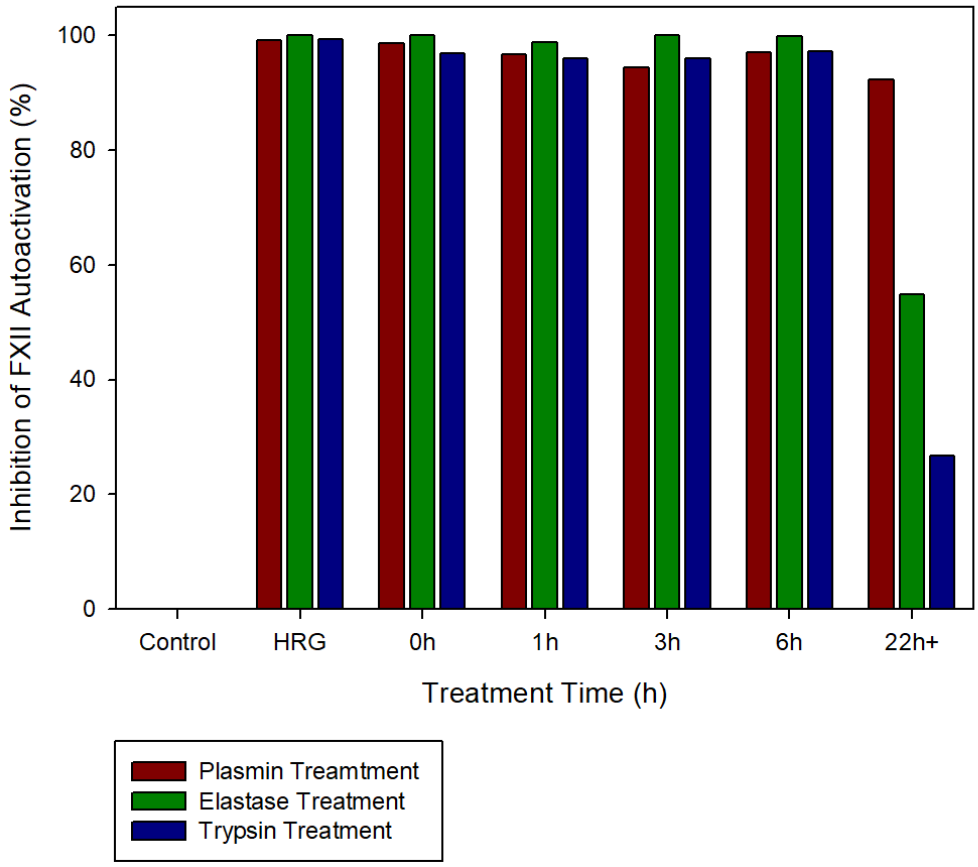
Inhibition of FXII Autoactivation (%)
100
80
60
40
20
0
Control
HRG
0h
1h
3h
6h
22h+
Treatment Time (h)
Plasmin Treamtment
Elastase Treatment
Trypsin Treatment

Figure 17: Effect of HRG fragments on FXII autoactivation

The reaction was initiated by the addition of 100 nM FXII to a mixture of 0.5 μg/mL of dextran sulfate, 12.5 μM $ZnCl_2$, in the absence (control) or presence of 200 nM intact or HRG fragments generated by digestion with plasmin, elastase, or trypsin for the times shown on the x-axis. FXIIa activity was monitored as previously described and the percentage inhibition percentage was calculated by dividing the FXII autoactivation rate difference between intact HRG and digested HRG fragments by the activation rate of intact HRG. The data points were representative of two independent experiments (mean).

5.5 Purification of tryptic HRG fragments by column chromatography

Tryp-HRG fragments were subjected to Ni-NTA affinity chromatography to separate and purify individual fragments of interest. Tryp-HRG (1 mg) was loaded onto a Ni-NTA column, and the column was washed with HBS, and then eluted with 50 mM or 250 mM imidazole. Fractions were collected and analyzed for total protein concentration using A280 spectrometry readings. SDS-PAGE analysis showed that all five distinct HRG fragments remained strongly bound to the Ni-NTA column and were eluted only with 250 mM imidazole (Figure 18). No protein was eluted in the flow through in HBS buffer wash fractions or with the 50 mM imidazole elution buffer. This suggests strong histidine-binding of the tryptic fragments to the nickel column and the presence of the histidine-rich region of HRG.

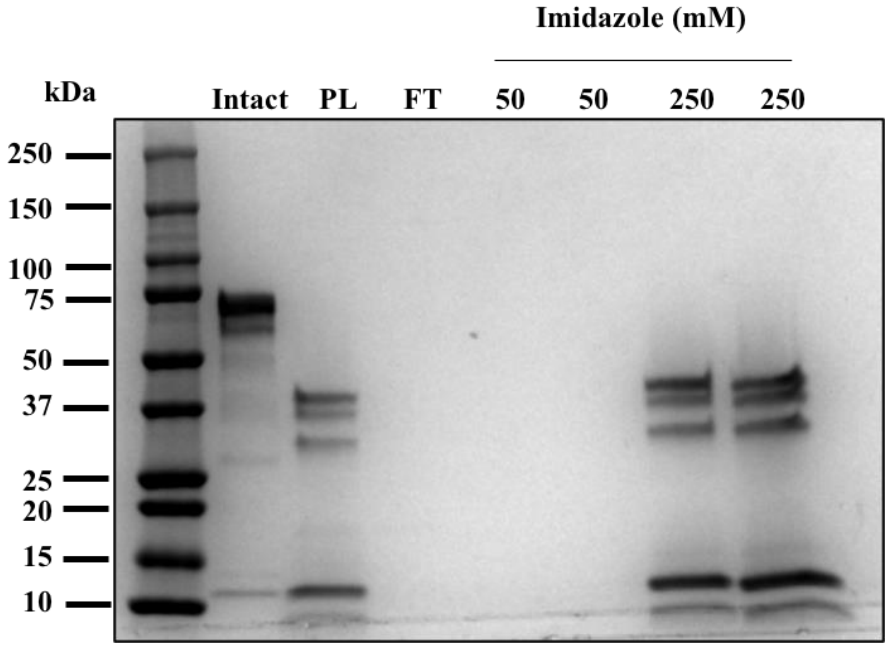
Imidazole (mM)
kDa
Intact
PL
FT
50
50
250
250
250
150
100
75
50
37
25
20
15
10

Figure 18: Purification of tryptic HRG fragments by Ni-NTA affinity chromatography

Tryp-HRG (1 mg) was loaded onto Ni-NTA (nickel-nitrilotriacetic acid) agarose column, washed with HBS, and then eluted with 50 mM or 250 mM imidazole. Approximately 1 ml fractions were collected, and each tube was analyzed for total protein concentration using A280 spectrometry readings. SDS-PAGE analysis included 3.5 µg intact plasma-derived HRG, pre-loaded dialyzed trypsin-digested HRG (PL), flow through from buffer wash (FT), and two individual samples from 50 mM and 250 mM imidazole collected fractions each. Gels were stained with Bio-Safe Coomassie G-250 blue stain and imaged using Image Lab Software on the Gel/ChemiDoc MP Imager System. Molecular weight markers are indicated on the left lane.

5.6 Reduction and alkylation of tryptic HRG fragments

In preparation for streptavidin-agarose pull down analysis, digested samples were first reduced and alkylated to allow for separation of tryptic HRG fragments by removing disulfide bonds and alkylating free cystine residues. Reduction was initiated by the addition of 6 h trypsin digested HRG to a mixture of 0.1 M phosphate buffer (containing 25 mM DTT and 5 mM EDTA). After 60-min incubation, reduced samples were alkylated by the addition of 550 mM iodoacetamide. Reduced and alkylated (RA) trypsin digested HRG samples were subjected to SDS-PAGE gel analysis and compared with control HRG and non-reduced and alkylated trypsin-digested HRG fragments to confirm reduction and alkylation. Under non-reduced conditions, control intact HRG had a molecular weight of approximately 68 kDa as expected (Figure 19). Control tryptic HRG fragments consisted of 4 bands that ran closely together between 37 kDa to 50 kDa in size, as well as a lower molecular weight band at 10 kDa. RA tryptic fragments consisted of 2 distinct bands with molecular masses of 37 kDa and 40 kDa, faint bands at 45 kDa and 30 kDa, and 2 lower bands between 10-15 kDa. Thus, reduction and alkylation of tryptic fragments affected the band pattern by removal of the 50 kDa band and resulted in further separation of the 37 kDa tryptic band of interest.

When the same tryptic HRG digestion samples were subjected to SDS-PAGE analysis under reduced conditions, tryptic HRG fragments (control and RA) separated in a similar manner. Both control and RA tryptic HRG fragments had 3 distinct bands with molecular masses of 40 kDa, 37 kDa, 30 kDa, and two lower bands between 10-15 kDa. These findings suggest that the larger tryptic HRG fragments (>30 kDa in size) likely

consist of multiple domains, as each domain has a molecular mass of 10-15 kDa. Moreover, the lower bands isolated by limited proteolysis appear to coincide with individual domains. Thus, partial reduction and alkylation of tryptic HRG fragments was achieved, allowing for further separation of tryptic bands of interest in preparation for streptavidin-agarose pull down analysis.

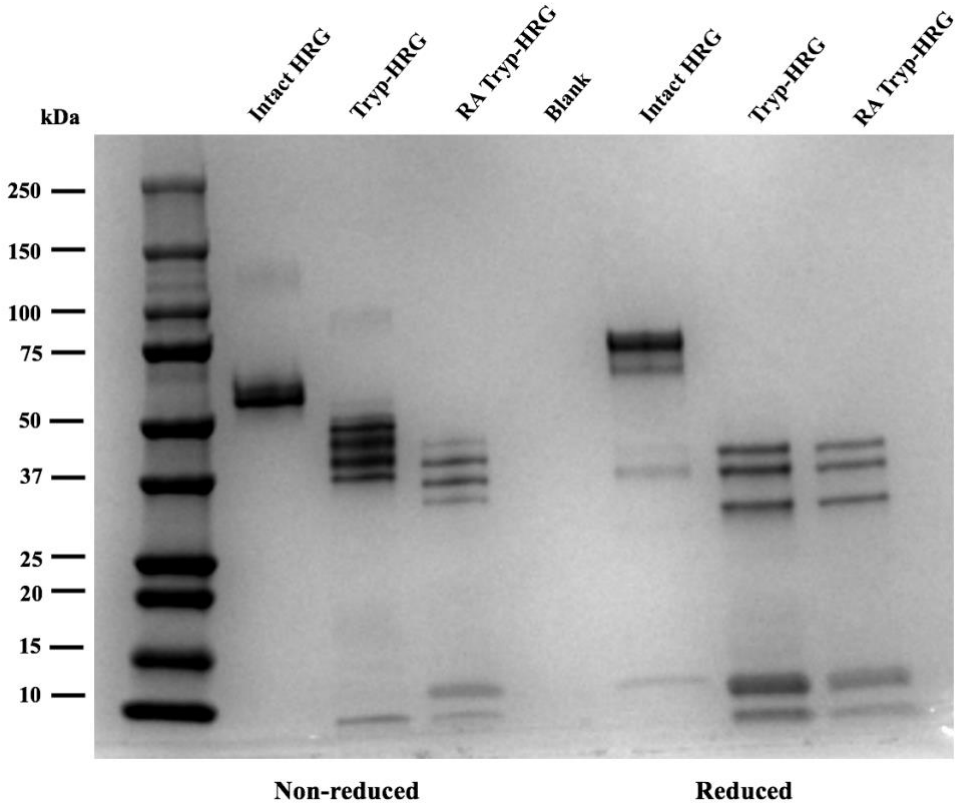
kDa
Intact HRG
Tryp-HRG
RA Tryp-HRG
Blank
Intact HRG
Tryp-HRG
RA Tryp-HRG
250
150
100
75
50
37
25
20
15
10
Non-reduced
Reduced

Figure 19: SDS-PAGE analysis of reduced and alkylated Tryp-HRG

Reduction was initiated by the addition of 5 µM trypsin treated HRG (100 µl of 6 hr digested Tryp-HRG) to a mixture of 0.1 M phosphate buffer, 25 mM DTT, and 5 mM EDTA. After 60-minute incubation at 4°C, 13.2 µl of 550 mM iodoacetamide was added to sample and further incubated for 30 minutes. Reduced and alkylated (RA) Tryp-HRG samples were dialyzed in HBS buffer at 4°C overnight. Protein samples (3.5 µg) were loaded in each well under non-reducing and reducing conditions. Gels were stained with Bio-Safe Coomassie G-250 blue stain and imaged using Image Lab Software on the Gel/ChemiDoc MP Imager System. Molecular weight markers are indicated on the left lane. Intact HRG; plasma-derived HRG, Tryp-HRG; trypsin-digested HRG

5.7 Streptavidin-agarose pull down analysis of FXIIa binding to HRG fragments

The interaction between biotinylated FXIIa and tryptic HRG fragments was investigated by streptavidin agarose (SA) pull down. In the presence of 12.5 µM $ZnCl_2$, 3.6 µM of biotinylated FXIIa-streptavidin agarose preparation was added to 12.6 µM of trypsin-treated (reduced and alkylated) HRG preparation. After incubation, samples were consecutively washed with HBS with and without 12.6 µM $ZnCl_2$. Pellets were re-suspended in sample buffer for SDS-PAGE analysis. SA control exhibited a distinct single band at 13 kDa, which corresponds to molecular weight of each of the four subunits of SA (intact MW is 55 kDa) (Figure 20). In the presence of biotinylated FXIIa (b-FXIIa), there was a single band at 75 kDa and a faint band at 13 kDa, corresponding to FXIIa and SA as expected. Intact HRG was shown to have an expected molecular weight of 68 kDa. There was little to no binding of intact HRG control to SA, as there was only a faint band at 68 kDa and a single band at 13 kDa. SDS-PAGE analysis showed distinct bands at 75 kDa, 68 kDa, 15 kDa, corresponding to b-FXIIa, intact HRG, and SA, respectively. Thus, intact HRG interacts with b-FXIIa in the presence of $ZnCl_2$, which is consistent with our previous findings (MacQuarrie et al., 2011).

Tryp-HRG control exhibited two distinct bands at 37 kDa and 40 kDa, two faint bands at 45 kDa and 30 kDa, and two lower bands between 10-15 kDa (Figure 20). This is consistent with reduced and alkylated Tryp-HRG preparations as shown above (Figure 19). RA Tryp-HRG did not interact with SA, whereby only a single band at 15 kDa was observed. Finally, treated Tryp-HRG was shown to interact with biotinylated FXIIa in the presence of $ZnCl_2$. There was a prominent FXIIa-interaction band at 37 kDa corresponding

to the Tryp-HRG fragment of interest. Additional bands were observed at 30 kDa and 50 kDa, which likely correspond to the light and heavy chains of FXIIa, respectively. Together, these data support the interaction between HRG and FXIIa, and that the FXIIa-binding domain on HRG may be isolated within the 37 kDa tryptic fragment.

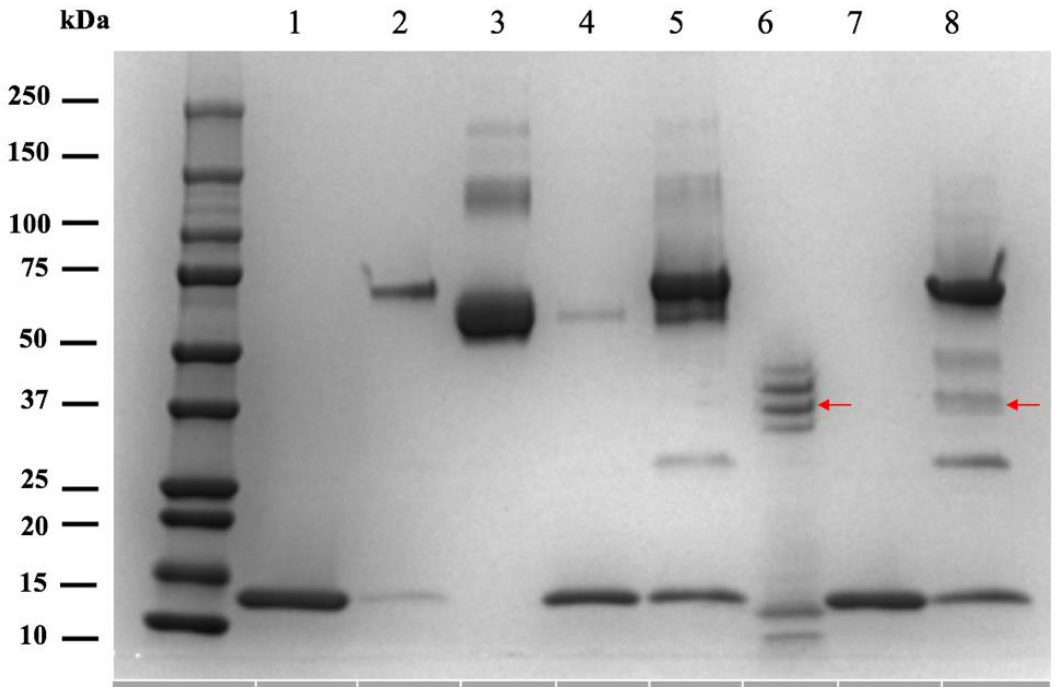

	1	2	3	4	5	6	7	8
SA	+	+		+	+		+	+
b-FXIIa		+			+			+
Intact HRG			+	+	+			
$ZnCl_2$				+	+			+
Tryp-HRG						+	+	+

Figure 20: SDS-PAGE analysis of FXIIa binding to tryptic HRG fragments

In the presence of Zn^{2+}, SA-b-FXIIa was added to Tryp-HRG for 30 minutes. After incubation, samples were consecutively washed in HBS-$ZnCl_2$ buffer, before the pellet was re-suspended in sample buffer for SDS-PAGE analysis. Controls used are shown in wells 1-7 (legend). Tryp-HRG was incubated with SA-b-FXIIa in HBS-$ZnCl_2$ buffer (8). Approximately 2-3 µg protein loaded per sample well. Red arrow denotes band corresponding to 37 kDa tryptic band of interest. Gels were stained with Bio-Safe Coomassie G-250 blue stain and imaged using Image Lab Software on the Gel/ChemiDoc MP Imager System. Molecular weight markers are indicated on the left lane. SA, streptavidin agarose; b-FXIIa, biotinylated FXIIa; Zn, $ZnCl_2$; intact HRG, plasma-derived histidine-rich glycoprotein; Tryp-HRG, partially reduced and alkylated trypsin-digested HRG fragments

5.8 Mass spectrometry analysis of tryptic HRG fragments

Finally, we set out to identify the tryptic fragments that bind to FXIIa and inhibit FXII autoactivation. Mass spectrometry analysis was performed on three individual Tryp-HRG bands for protein identification (40 kDa, 37 kDa, and 30 kDa) (Figure 14). After 6-h digestion, tryptic HRG samples were run on SDS-PAGE under reduced conditions and stained with Coomassie blue stain as previously described above.

LC-MS/MS data for the 40 kDa Tryp-HRG fragment showed sequencing of 147/525 amino acids (28% coverage), which includes 22 exclusive unique peptides, 32 exclusive unique spectra, and 178 total spectra (Figure 21A). MS results show that the 40 kDa tryptic fragment corresponds to the N1 and N2 domains (amino acids 6-217). However, based on the molecular mass, the 40 kDa Tryp-HRG fragment should correspond to ~2/3 of the molecule (364/525 amino acids), which contains the N-terminal, the PRR1 and a portion of the HRR domains (amino acids 6-369) (Figure 22). Thus, LC-MS/MS analysis of the 40 kDa tryptic HRG fragment failed to identify the complete segment.

Although there was incomplete sequencing data, it appears that the other tryptic fragments are subsets of the 40 kDa Tryp-HRG fragments. Data for the 37 kDa Tryp-HRG fragment shows 228/525 amino acids (43% coverage), which includes 38 exclusive unique peptides, 60 exclusive unique spectra, and 361 total spectra (Figure 21B). Results shows that the 37 kDa HRG fragment corresponds to the full-length N1N2 domain and a small portion of the PRR1 domain of HRG (1-252). However, based on the MW, the 37 kDa tryptic HRG fragment should include the N-terminal domains, PRR1, and a small portion

of the HRR domain (amino acids 1-337) (Figure 22). Therefore, approximately 109 amino acids were not represented by LC-MS/MS analysis. Lastly, sequencing data for the 30 kDa Tryp-HRG fragment shows 167/525 amino acids (32% coverage), including 27 exclusive unique peptides, 37 exclusive unique spectra, and 209 total spectra (Figure 21C). Similar to the 40 kDa Tryp-HRG fragments, results show that the 30 kDa Tryp-HRG fragment corresponds to the N1 and N2 domains (amino acids 6-217). However, the expected coverage of the tryptic fragment includes 273/525 amino acids (52% coverage) and corresponds to the N1, N2 and a portion of the PRR1 domain (amino acids 6-278) (Figure 22). Together, these findings suggest that trypsin digestion of HRG results in the cleavage of the HRR and COOH domains, while the N-terminal domains and PRR1 largely remains intact and resistant to further trypsin digestion.

There is a disconnect between the sequenced data and the expected protein coverage of each tryptic HRG fragment. Some potential explanations for the limited data obtained by LC-MS/MS analysis may include inadequate fragmentation of protein samples by the trypsin digestion that was performed to further cleave the protein sample into smaller fragments. Alternative enzymes may have been more effective at digesting the already trypsin digested HRG fragments. However, we have shown that digestion of HRG with elastase or plasmin produced only limited digestion. Moreover, hydrophilic or small peptides derived from tryptic HRG fragments may pass through the reverse phase column with salt and are not analyzed. The large portion of amino acids that were not sequenced based on the expected coverage may be due to the hydrophobic proline-rich regions, which are more likely to create issues with sticking to gels, absorbing to tubes, failing to elute

from the column, or being too large for the mass spectrometry instrument to analyze (University of Virginia Medical School, 2020) In addition, the high content of histidine-residues, as well as some internal lysine and arginine residues may not provide complete fragmentation data. Given the potential limitations and incomplete sequencing data from LC-MS/MS analysis, it is difficult to definitively determine the identity of the domain(s) within the tryptic HRG fragments. Thus, we were unable to identify the FXIIa binding fragment of HRG with this approach due to the challenges of limited proteolysis and lack of information provided by mass spectrometry. Accordingly, we used an alternative approach to identify the domain responsible for inhibition of FXIIa-mediated contact activation.

A.

P04196 (100%), 59,576.6 Da
Histidine-rich glycoprotein OS=Homo sapiens GN=HRG PE=1 SV=1
22 exclusive unique peptides, 32 exclusive unique spectra, 178 total spectra, 147/525 amino acids (28% coverage)

B.

P04196|HRG_HUMAN (100%), 59,576.6 Da
Histidine-rich glycoprotein OS=Homo sapiens GN=HRG PE=1 SV=1
38 exclusive unique peptides, 60 exclusive unique spectra, 361 total spectra, 228/525 amino acids (43% coverage)

C.

P04196 (100%), 59,576.6 Da
Histidine-rich glycoprotein OS=Homo sapiens GN=HRG PE=1 SV=1
27 exclusive unique peptides, 37 exclusive unique spectra, 209 total spectra, 167/525 amino acids (32% coverage)

Figure 21: Protein identification of HRG fragments by mass spectrometry

Mass spectrometry analysis was performed on three individual Tryp-HRG bands for protein identification. Coverage maps for 40 kDa Tryp-HRG (A), 37 kDa Tryp-HRG (B), and 30 kDa Tryp-HRG (C) fragments are provided. Sequencing samples were subjected to in-gel trypsin digestion, PNGase treatment, C_{18} cleanup prior to liquid chromatography with tandem mass spectrometry (LC-MS/MS) analysis using the Obri-trap Classic instrument for protein identification. Standard database searching was performed using UniProtKB-P04196 (HRG_Human), and Scaffold4 Proteome Software was used to compare, identify and analyze sequenced trypsin digested HRG samples. Mapped peptides are identified in yellow, whereas sites of post-translational modification are indicated in green.

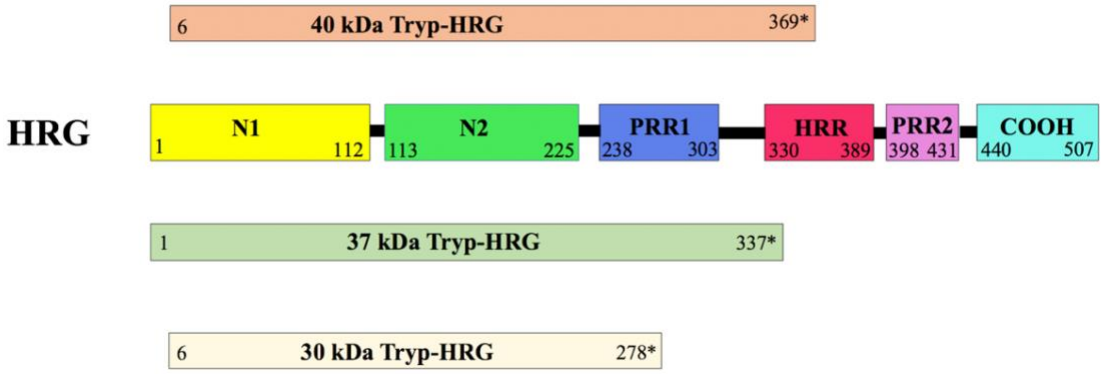
6
40 kDa Tryp-HRG
369*
HRG
N1
1
112
N2
113
225
PRR1
238
303
HRR
330
389
PRR2
398
431
COOH
440
507
1
37 kDa Tryp-HRG
337*
6
30 kDa Tryp-HRG
278*

Figure 22: Schematic representation of tryptic HRG fragments

Predicted protein coverage of sequenced Tryp-HRG fragments based on LC-MS/MS mass spectrometry sequencing data. The 40 kDa Tryp-HRG fragment (light pink) corresponds to the full-length N1N2, PRR1, and a portion of the HRR domain of HRG (amino acids 6-369*). The remaining two tryptic fragments are further cleaved products of the 40 kDa Tryp-HRG fragment. The 37 kDa Tryp-HRG fragment spans the N1N2, PRR1, and a small portion of the HRR (amino acids 1-337*), whereas the HRR domain is predicted to be fully cleaved in the 30 kDa Tryp-HRG fragment (amino acids 6-278*). The asterisks depict predicted amino acid sequence coverage based on mass spectrometry analysis and sequence alignment of UniProtKB sequence database (P04196 (HRG_Human)). Adapted from: Patel *et al., IUBMB.* (2013).

6.0 CHAPTER 6: CHARACTERIZATION OF RECOMBINANT HRG DOMAIN CONSTRUCTS IN CONTACT ACTIVATION AND PLASMA CLOTTING

6.1 Generation and expression of PCR-amplified HRG domain fragments

To further examine the role of the histidine-rich region (HRR), as well as the potential role of other HRG domains in FXII-mediated contact activation, we used recombinant DNA technology to PCR-amplify individual HRG domain fragments (Figure 23). MBP-tagged HRG domain constructs were expressed and purified in *E coli*. Complementing the proteolytic fragmentation approach, generation of MBP-HRG domain constructs will provide greater versatility and precise fragment boundaries rather than random proteolytic cleavages, as well as a more comprehensive examination going forward. The constructs are as followed: MBP-N1, MBP-N2, MBP-N1N2, MBP-PRR1, MBP-HRR, MBP-PRR2, and MBP-COOH (Figure 10). All clones were verified by Sanger sequencing (MOBIX Lab, McMaster University, Hamilton, ON). MBP-HRG fragments were transformed into BL21 (DE3) *E. coli*, and expression was induced with 1 mM IPTG for an additional 4 hours upon reaching mid-log phase (A_{600} reading of 0.5 to 0.6).

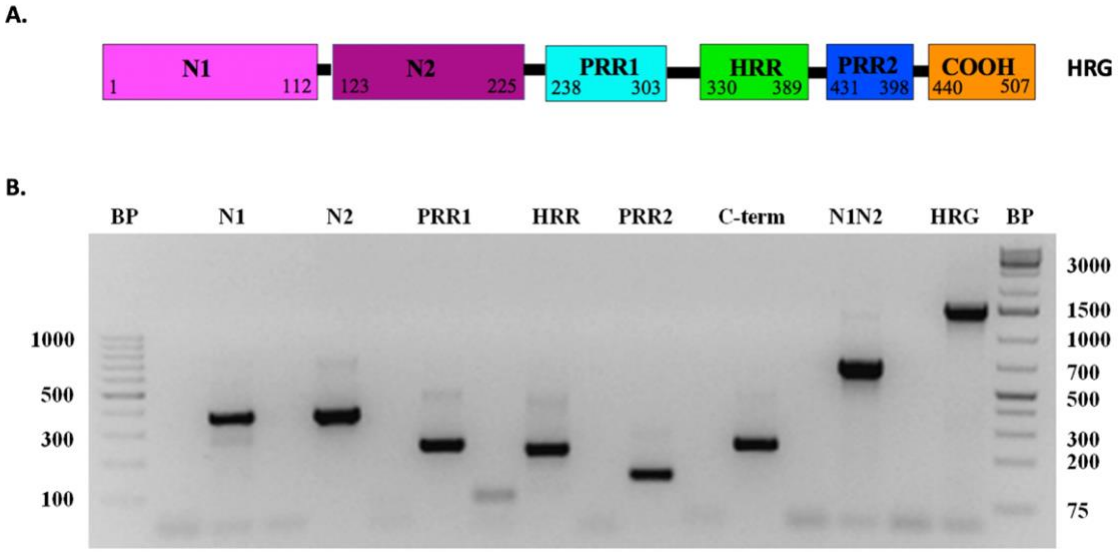
A.
N1
1
112
N2
123
225
PRR1
238
303
HRR
330
389
PRR2
431
398
COOH
440
507
HRG
B.
BP
N1
N2
PRR1
HRR
PRR2
C-term
N1N2
HRG
BP
1000
500
300
100
3000
1500
1000
700
500
300
200
75

Figure 23: PCR-amplified HRG domain fragments

Primers were designed to PCR-amplify each individual domain of HRG, fragments containing multiple domains, and full length HRG (A). Ethidium bromide (0.5 μg/ml) was added before agarose gel (1%) electrophoresis, followed by separation of PCR bands for 1 h at 80V (B). The DNA fragments are as follows: N1, N2, PRR1, HRR, PRR2, COOH, N1N2, and HRG. Wells in between DNA samples represent controls for each PCR reaction, where nuclease-free water was used as a template with respective sense and antisense primer sets. NEB 100 bp DNA ladder (first well), and NEB 1 kb DNA ladder (last well) were used. The agarose gel was imaged under UV light using Image Lab Software on the Gel/ChemiDoc MP Imager System.

6.2 Protein purification of recombinant MBP-HRG domain constructs

Harvested cells from each bacterial culture (250 ml to 500 ml) were sonicated to extract recombinant protein. Lysed bacteria were centrifuged and crude extract (supernatant) was harvested and diluted for purification. Varying yields of expressed MBP-HRG domain constructs (5 to 30 mg) were purified and eluted with 10 mM maltose by amylose affinity chromatography (binding capacity; 6-8 mg/ml of bed volume). Eluted protein fractions were pooled, concentrated, and buffer exchanged into HBS buffer. As outlined in Table 6, MBP-HRG domain constructs were expressed with varying protein yields. The expected protein yield of fusion proteins expressed in *E. coli* is >5 mg per 1 L culture or 0.005 mg/ml (Costa et al., 2014). Control MBP expressed with a yield of 0.112 mg per ml of bacterial culture volume, which shows efficient protein expression of soluble MBP by the empty vector (pMAL-c5e) (22-fold greater than expected). Although the protein yield was lower than control MBP, there was sufficient expression of recombinant MBP-HRG domain constructs. Protein yields of MBP-N2, MBP-HRR, and MBP-COOH constructs ranged from 0.011 mg/ml to 0.017 mg/ml (2.2- to 3.4-fold greater than expected yield). The remaining MBP constructs (-N1, -N1N2, -PRR1, -PRR2) expressed with protein yields of 0.006 mg/ml to 0.008 mg/ml (1.2- to 1.6-fold greater than expected).

The decrease in protein expression between control MBP and MBP-HRG domain constructs is most likely due to differences in protein folding and solubility (Rosano & Ceccarelli, 2014). In particular, lower protein expression levels may be due to the multidomain structure of N1N2 or the intrinsically disordered nature of proline residues which result in an unstable three-dimensional structure. To achieve expected protein

expression yield (0.005 mg/ml) of MBP-HRG domain constructs, we increased the expression culture volume for each construct (multiple batches of 250 ml to 500 ml LB), combined and purified the combined expressed protein yield, and concentrated and pooled the eluted protein fractions. We were able to isolate 28 mg of MBP, 6 mg of MBP-N1, 17 mg of MBP-N2, 13 mg of MBP-N1N2, 7 mg of MBP-PRR1, 22 mg MBP-HRR, 16 mg of MBP-PRR2, and 12 mg of MBP-COOH. Thus, sufficient protein was expressed and purified using amylose affinity chromatography.

MBP-HRG Construct	LB Culture Volume	Combined Protein Yield	Protein Yield (mg/ml)
MBP	250 ml	28 mg	0.112
MBP-N1	1000 ml	6 mg	0.006
MBP-N2	1000 ml	17 mg	0.017
MBP-N1N2	2000 ml	13 mg	0.0065
MBP-PRR1	1000 ml	7 mg	0.007
MBP-HRR	2000 ml	22 mg	0.011
MBP-PRR2	2000 ml	16 mg	0.008
MBP-COOH	1000 ml	12 mg	0.012

Table 6: Protein expression of MBP-HRG domain constructs in *E. coli*

To isolate recombinant MBP-HRG domain constructs, sonicated cell lysates from bacteria culture were diluted in column buffer (20 mM Tris-HCl, 200 mM NaCl, 1 mM EDTA, 1 mM azide, pH 7.4) and passed over an amylose column, which was washed (12x volume), and eluted with 10 mM maltose. Fractions were collected, pooled, and concentrated. Absorbance at 280 nm was measured using a NanoDrop™ spectrophotometer to calculate protein concentrations. MBP, maltose-binding protein; N1/2, N-terminal domains; PRR1/2, proline-rich regions; HRR, histidine-rich region; COOH, carboxyl terminal.

Protein preparations were first subjected to SDS-PAGE analysis to assess protein expression, purity, and construct size for individual MBP-HRG domain constructs: MBP-N1 (Figure 24), MBP-N2 (Figure 24), MBP-N1N2 (Figure 25), MBP-PRR1 (Figure 26), MBP-HRR (Figure 27), MBP-PRR2 (Figure 28), and MBP-COOH (Figure 29). In each preparation, additional, less abundant bands were observed, potentially corresponding to protein degradation or the presence of protein aggregates. We further assessed purity of the protein preparations by western blot analysis using antibodies against MBP or HRG. Western blots of MBP-HRG domain constructs probed with a rabbit polyclonal anti-MBP antibody showed a single band at the expected molecular weight of MBP (40 kDa) and expected bands for each MBP-HRG domain construct (46-70 kDa) (Figure 30). However, additional higher molecular weight bands were still observed. Western blot analysis using an affinity purified sheep antibody against human HRG revealed single bands for each MBP-HRG domain construct with the exception of MBP-N2, and for plasma derived HRG (Figure 31). Thus, these findings confirm that there was effective purification and stable expression of MBP-HRG domain constructs.

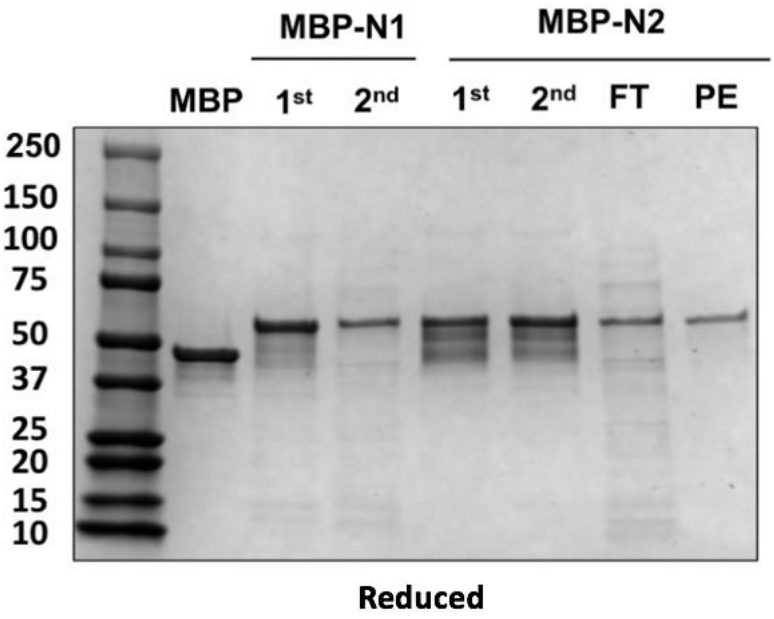

Reduced

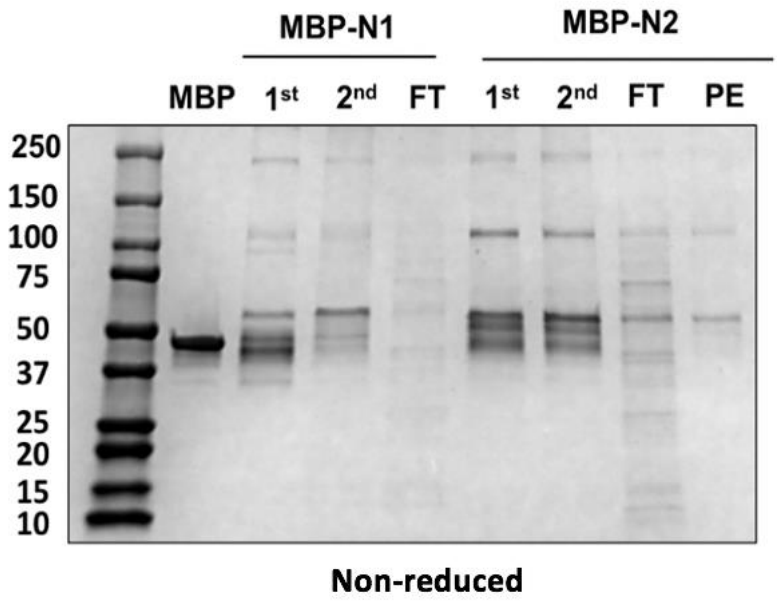

Non-reduced

Figure 24: SDS-PAGE analysis of MBP-N1 and MBP-N2 constructs

To isolate recombinant MBP-N1 (MW 56 kDa) and MBP-N2 (MW 56 kDa) domain constructs, sonicated cell lysates from bacterial cultures were diluted in column buffer and passed over an amylose column, which was then washed (12x volume) and eluted with 10 mM maltose. Fractions were collected, pooled, and concentrated. Absorbance at 280 nm measured using a NanoDrop™ spectrophotometer was used to calculate the protein concentrations of protein. SDS-PAGE gels were stained with Coomassie blue for 1 h and de-stained with MilliQ water overnight. Samples from two individual expression and purification preparations (1^{st} and 2^{nd}) are loaded. MW, molecular weight; MBP, maltose-binding protein; N1/2, N-terminal domains; FT, flow through; PE, post-elution.

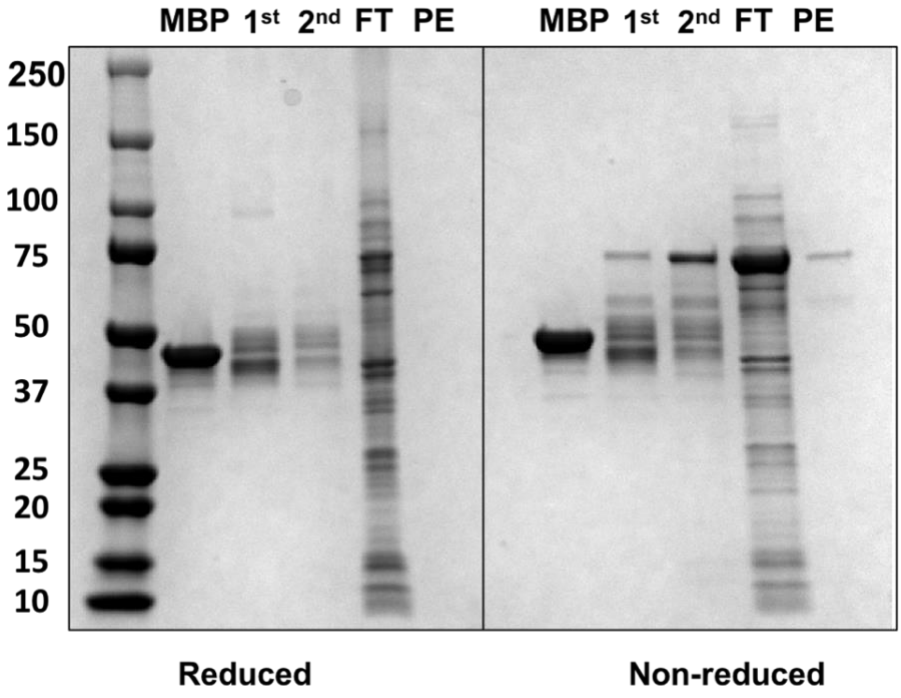
MBP 1st 2nd FT PE
MBP 1st 2nd FT PE
250
150
100
75
50
37
25
20
15
10
Reduced
Non-reduced

Figure 25: SDS-PAGE analysis of MBP-N1N2 construct purification by amylose column affinity chromatography

To isolate recombinant MBP-N1N2 (MW 70 kDa) domain construct, sonicated cell lysates from bacteria culture were diluted in column buffer and passed over an amylose column, which was washed (12x volume) and eluted with 10 mM maltose. Fractions were collected, pooled, and concentrated. Absorbance readings at 280 nm measured using a NanoDrop™ spectrophotometer were used to calculate protein concentrations. SDS-PAGE gels were stained with Coomassie blue for 1 h and de-stained with MilliQ water overnight. Samples from two individual expression and purification preparations (1^{st} and 2^{nd}) are loaded. MW, molecular weight; MBP, maltose-binding protein; N1N2, N-terminal domain; FT, flow through; PE, post-elution.

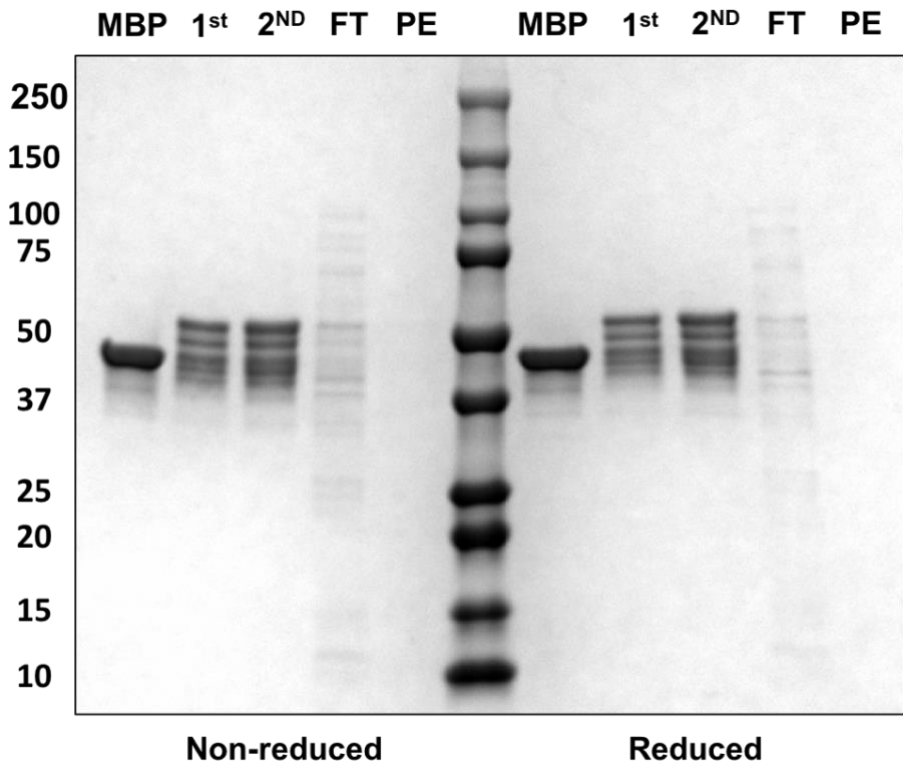
MBP
1st
2ND
FT
PE
MBP
1st
2ND
FT
PE
250
150
100
75
50
37
25
20
15
10
Non-reduced
Reduced

Figure 26: SDS-PAGE analysis of MBP-PRR1 construct purification by amylose column affinity chromatography

To isolate recombinant MBP-PRR1 (MW 50 kDa) domain construct, sonicated cell lysates from bacteria culture were diluted in column buffer and passed over an amylose column, which was washed (12x volume) and eluted with 10 mM maltose. Fractions were collected, pooled, and concentrated. Absorbance readings at 280 nm measured using a NanoDrop™ spectrophotometer were used to calculate protein concentrations. SDS-PAGE gels were stained with Coomassie blue for 1 h and de-stained with MilliQ water overnight. Samples from two individual expression and purification preparations (1^{st} and 2^{nd}) are loaded. MW, molecular weight; MBP, maltose-binding protein; PRR1, proline-rich region 1 domain; FT, flow through; PE, post-elution.

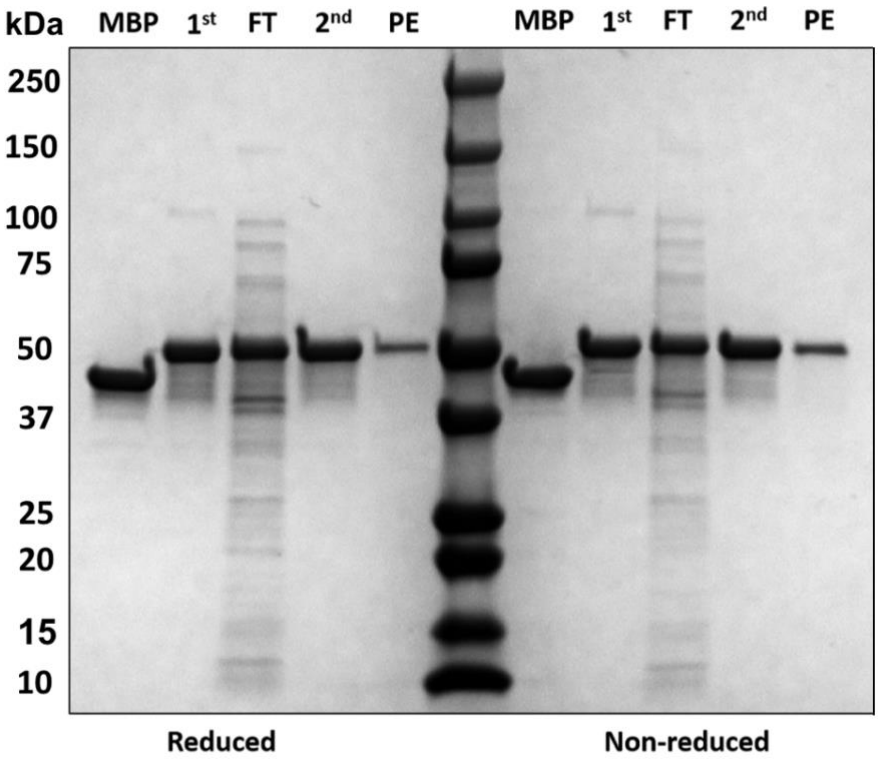
kDa
MBP
1st
FT
2nd
PE
MBP
1st
FT
2nd
PE
250
150
100
75
50
37
25
20
15
10
Reduced
Non-reduced

Figure 27: SDS-PAGE analysis of MBP-HRR construct purification by amylose column affinity chromatography

To isolate recombinant MBP-HRR (MW 50 kDa) domain construct, sonicated cell lysates from bacteria culture were diluted in column buffer and passed over an amylose column, which was washed (12x volume) and eluted with 10 mM maltose. Fractions were collected, pooled, and concentrated. Absorbance readings at 280 nm measured using a NanoDrop™ spectrophotometer were used to calculate protein concentrations. SDS-PAGE gels were stained with Coomassie blue for 1 h and de-stained with MilliQ water overnight. Samples from two individual expression and purification preparations (1^{st} and 2^{nd}) are loaded. MW, molecular weight; MBP, maltose-binding protein; HRR, histidine-rich region; FT, flow through; PE, post-elution.

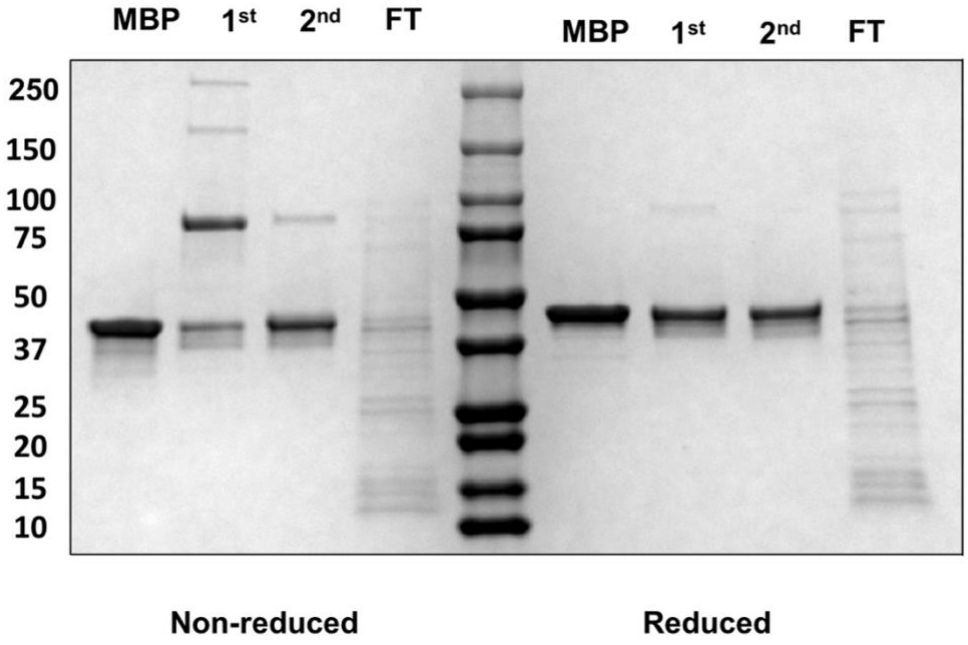
MBP
1st
2nd
FT
MBP
1st
2nd
FT
250
150
100
75
50
37
25
20
15
10
Non-reduced
Reduced

Figure 28: SDS-PAGE analysis of MBP-PRR2 construct purification by amylose column affinity chromatography

To isolate recombinant MBP-PRR2 (MW 46 kDa) domain construct, sonicated cell lysates from bacteria culture were diluted in column buffer and passed over an amylose column, which was washed (12x volume) and eluted with 10 mM maltose. Fractions were collected, pooled, and concentrated. Absorbance readings at 280 nm measured using a NanoDrop™ spectrophotometer were used to calculate protein concentrations. SDS-PAGE gels were stained with Coomassie blue for 1 h and de-stained with MilliQ water overnight. Samples from two individual expression and purification preparations (1^{st} and 2^{nd}) are loaded. MW, molecular weight; MBP, maltose-binding protein; PRR2, proline-rich region 2 domain; FT, flow through; PE, post-elution.

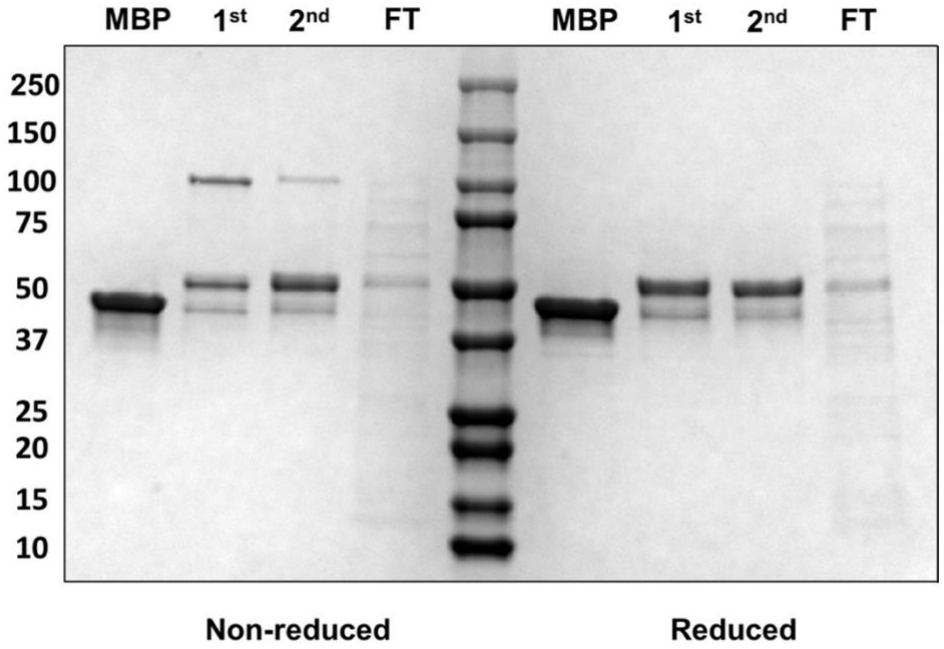
MBP
1st
2nd
FT
MBP
1st
2nd
FT
250
150
100
75
50
37
25
20
15
10
Non-reduced
Reduced

Figure 29. SDS-PAGE analysis of MBP-COOH construct purification by amylose column affinity chromatography

To isolate recombinant MBP-COOH (MW 51 kDa) domain construct, sonicated cell lysates from bacteria culture were diluted in column buffer and passed over an amylose column, which was washed (12x volume) and eluted with 10 mM maltose. Fractions were collected, pooled, and concentrated. Absorbance readings at 280 nm measured using a NanoDrop™ spectrophotometer were used to calculate protein concentrations. SDS-PAGE gels were stained with Coomassie blue for 1 h and de-stained with MilliQ water overnight. Samples from two individual expression and purification preparations (1^{st} and 2^{nd}) are loaded. MW, molecular weight; MBP, maltose-binding protein; COOH, carboxyl terminal domain; FT, flow through; PE, post-elution.

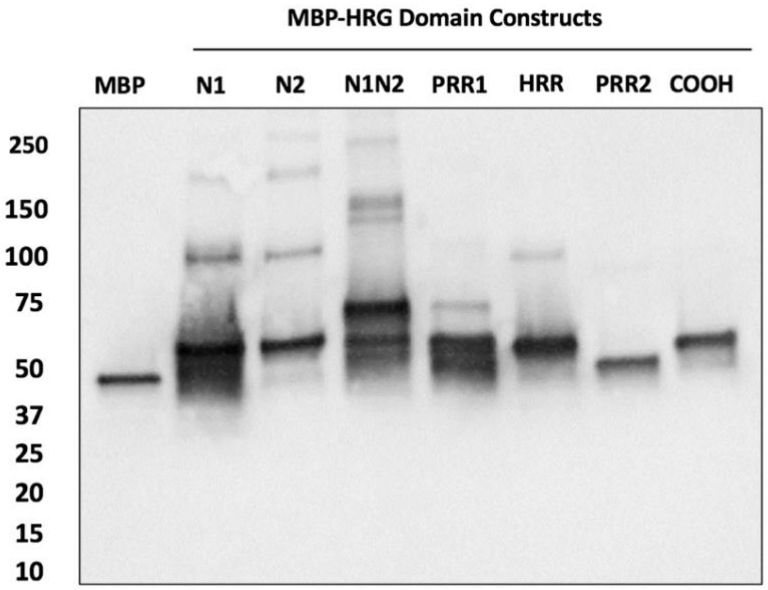

MBP-HRG Construct	MW
MBP	40
MBP-N1	56
MBP-N2	56
MBP-N1N2	70
MBP-PRR1	50
MBP-HRR	50
MBP-PRR2	46
MBP-COOH	51

Figure 30: Western blot analysis of MBP-HRG domain recombinants using anti-MBP antibody

Recombinant MBP-HRG domain constructs and control MBP were subjected to SDS-PAGE analysis on 4-15% polyacrylamide gels in the presence of 0.1% sodium dodecyl sulfate (SDS) and 0.14 M β-mercaptoethanol. Separated proteins were transferred onto a nitrocellulose membrane. The membrane was probed with affinity-purified polyclonal rabbit anti-MBP primary antibody (0.1 µg/ml) and sheep anti-rabbit HRP secondary antibody (0.2 µg/ml). To detect the presence of HRG and HRG domain constructs, the blot was incubated with the detection reagent and chemiluminescence was measured using a Chemi-Doc gel imager. Molecular weight (kDa) of MBP-HRG domain constructs are provided in legend. MBP, maltose-binding protein; HRG, histidine-rich glycoprotein; N1/N2; N-terminal domains; PRR1/PRR2, proline-rich regions; HRR, histidine-rich region; COOH, carboxyl terminal domain

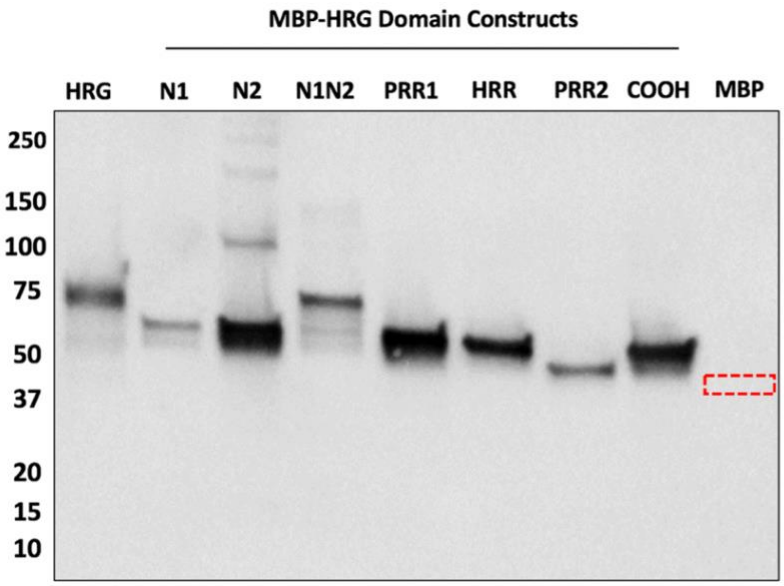

MBP-HRG Construct	MW
HRG	75
MBP-N1	56
MBP-N2	56
MBP-N1N2	70
MBP-PRR1	50
MBP-HRR	50
MBP-PRR2	46
MBP-COOH	51
MBP	40

Figure 31: Western blot analysis of MBP-HRG domain constructs using anti-HRG antibody

MBP-HRR recombinant protein and control plasma HRG samples were subjected to SDS-PAGE analysis on 4-15% polyacrylamide gels (Bio-Rad) in the presence of 0.1% sodium dodecyl sulfate (SDS) and 0.14 M β-mercaptoethanol. Separated proteins were transferred onto a nitrocellulose membrane (Bio-Rad) overnight. The membrane was probed with affinity-purified polyclonal sheep HRP-labelled anti-human IgG-HRG antibody (0.2 µg/ml). To detect the presence of HRG, the blot was incubated with the detection reagent and chemiluminescence was measured using a Chemi-Doc gel imager. Molecular weights (kDa) of HRG and MBP-HRG domain constructs are provided in legend. MBP, maltose-binding protein; HRG, histidine-rich glycoprotein; N1/N2; N-terminal domains; PRR1/PRR2, proline-rich regions; HRR, histidine-rich region; COOH, carboxyl terminal domain. Red box indicates no binding of anti-HRG antibody to MBP control as expected.

6.3 Effect of MBP-HRG domain constructs on FXII autoactivation mediated by polyphosphate

To examine the functional integrity of the HRG domain constructs, the inhibitory effect of MBP-HRG domain constructs on short chain polyphosphate-induced FXII autoactivation was examined and compared with that of plasma-derived HRG. HRG fully inhibits polyphosphate mediated FXII autoactivation in a dose-dependent and saturable manner (Figure 32) with an IC_{50} of 275 ± 10 nM. Complete inhibition (>95%) occurs with concentrations between 4 to 5 μM. This is consistent with the inhibitory effect of HRG when FXII autoactivation is initiated by dextran sulfate (IC_{50} ~200 nM) (see Figure 11). These findings show the inhibitory effect of HRG to downregulate the procoagulant activity of platelet-size polyphosphate (70-100 phosphate units) in FXII autoactivation.

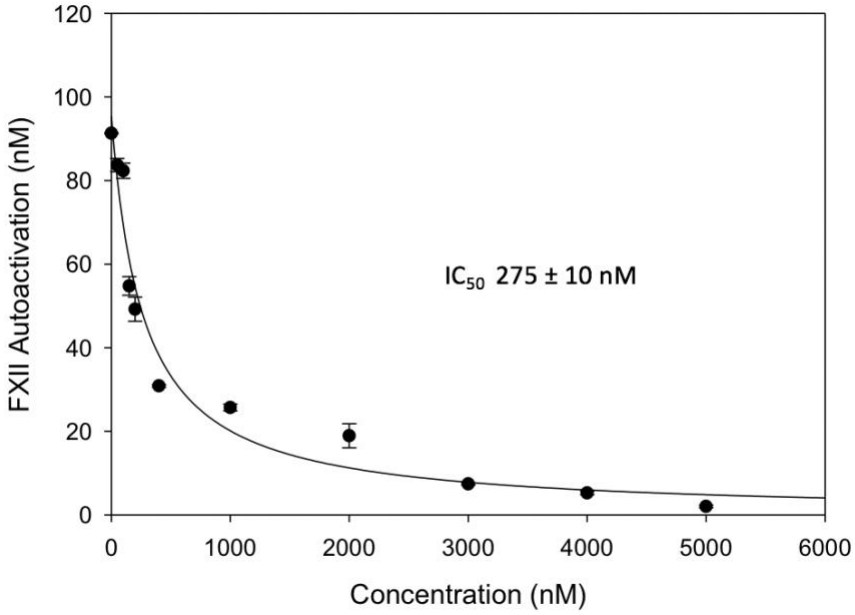
120
100
80
60
40
20
0
FXII Autoactivation (nM)
IC50 275 ± 10 nM
0
1000
2000
3000
4000
5000
6000
Concentration (nM)

Figure 32: Effect of HRG on FXII autoactivation mediated by short chain polyphosphate

Autoactivation was assessed by incubating 100 nM FXII in buffer containing 6 µM $ZnCl_2$ in the absence or presence of HRG (0-5000 nM). Autoactivation was stimulated with 1.5 µg/mL short chain polyphosphate. FXIIa activity was monitored by measuring the hydrolysis of FXIIa-directed chromogenic substrate (S-2302) at A405 in a continuous assay. FXIIa generation was quantified by comparison with a standard curve of FXIIa activity and was plotted against HRG concentration. Data represent the mean of three experiments each done in duplicate. Symbols represent the mean, whereas bars reflect the standard deviation. Non-linear regression analysis was performed to determine IC_{50} value (fitted line) by rectangular hyperbola analysis (TableCurve 2D).

Like HRG, MBP-HRG domain constructs significantly inhibit FXII autoactivation in a dose-dependent and saturable manner compared with MBP control ($P < 0.001$) (Figure 33A). The inhibitory capacity varied among MBP-HRG domain constructs. Comparable to plasma HRG (IC_{50} 275 ± 10 nM), MBP-HRR inhibits FXII autoactivation by over 85% with an IC_{50} value of 509 ± 59 nM ($P = 0.545$) (Figure 33B). Similarly, MBP-PRR2 has an IC_{50} value of 652 ± 56 nM ($P = 0.202$). The remaining domains had significantly lower potencies compared with HRG ($IC_{50} > 800$ nM; $P < 0.05$). At concentrations of up to 8 μM, all MBP-HRG domain constructs, except MBP-N2, inhibit FXII autoactivation by >80%. MBP-N1N2 domain construct (IC_{50} 809 ± 59 nM) was significantly more potent than MBP-N1 and MBP-N2 (IC_{50} 3189 ± 275 and 1476 ± 420 nM, respectively; $P < 0.001$ and 0.008). MBP-N2 was shown to inhibit FXII autoactivation by up to 58% (IC_{50} 1476 ± 420 nM). MBP-PRR1 and MBP-COOH have IC_{50} values of 3840 ± 309 and 1519 ± 140 nM, respectively. Together, these findings suggest that the HRR and PRR2 are the predominant domains of HRG responsible for inhibition of FXII autoactivation mediated by short chain polyphosphate.

A.

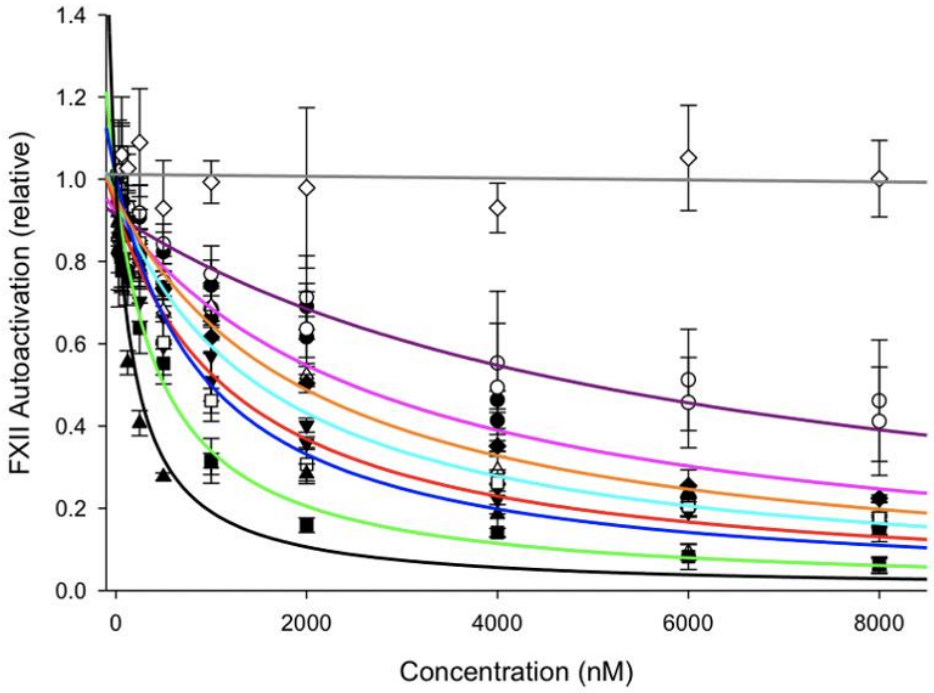
FXII Autoactivation (relative)
1.4
1.2
1.0
0.8
0.6
0.4
0.2
0.0
0
2000
4000
6000
8000
Concentration (nM)

B.

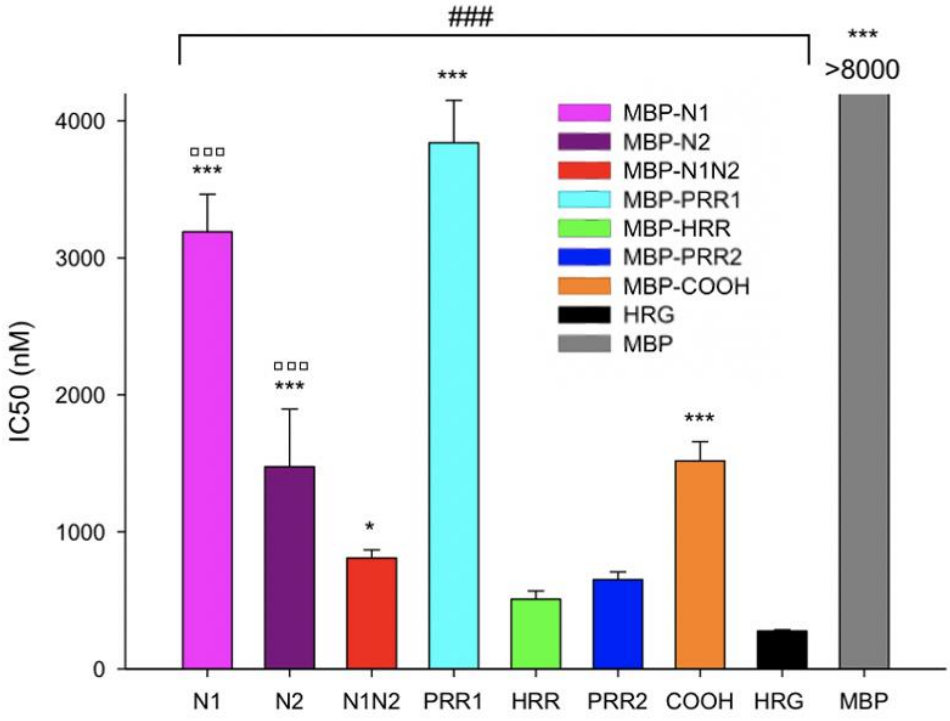
###
***
>8000
***
***
***
***
***
IC50 (nM)
4000
3000
2000
1000
0
MBP-N1
MBP-N2
MBP-N1N2
MBP-PRR1
MBP-HRR
MBP-PRR2
MBP-COOH
HRG
MBP
N1
N2
N1N2
PRR1
HRR
PRR2
COOH
HRG
MBP

Figure 33: Effect of recombinant MBP-HRG domain constructs on FXII autoactivation mediated by short chain polyphosphate

FXII autoactivation was assessed by incubating 100 nM FXII in buffer containing 6 µM $ZnCl_2$ in the absence or presence of HRG or MBP-HRG domain constructs at the concentrations shown (A). Autoactivation was stimulated with 1.5 µg/mL short chain polyphosphate. Hydrolysis of chromogenic substrate S-2302 (200 µM) was monitored to quantify FXIIa generated by continuous assay. FXII autoactivation rates were normalised to that in the absence of HRG or MBP-HRG domain constructs and plotted vs. HRG or MBP-HRG domain construct concentration. Data represent the mean of three experiments each done in duplicate. Symbols represent the mean, whereas bars reflect the standard deviation. IC_{50} values were determined by non-linear regression analysis (n=3; duplicates) and plotted (B). Bars represent mean ± standard deviation. $^{###}P < 0.001$ compared with MBP control; $*P < 0.05$ and $***P < 0.001$ compared with HRG; ▫$P < 0.05$ and ▫▫▫$P < 0.001$ compared with MBP-N1N2 (ANOVA, Holm-Sidak method). MBP; maltose-binding protein, N1/N2; N-terminal domain, PRR1/2; proline-rich regions, HRR; histidine-rich region, COOH; carboxyl terminal domain, HRG; histidine-rich glycoprotein

6.4 Effect of MBP-HRG domain constructs on clotting in HRG-depleted human plasma

We have previously shown that HRG addition prolongs the activated partial thromboplastin time (aPTT) in HRG-depleted plasma in a FXIIa-dependent manner, but has only a minor effect on the prothrombin time (PT) (MacQuarrie et al., 2011). Thus, the effect of the recombinant MBP-HRG domain constructs on clotting in HRG-depleted human plasma was investigated. The majority of MBP-HRG domain constructs produced less than 1.2-fold prolongation of the PT in HRG-depleted plasma, which was comparable to control human plasma ($P < 0.067$) (Figure 34A). HRG and MBP-PRR1 prolonged the PT by 1.5- and 1.7-fold, respectively ($P < 0.001$). These findings show that like HRG, MBP-HRG domain constructs have a modest (< 2-fold, but statistically significant) to minor (< 2-fold and non-significant) effect on the PT. In the aPTT, HRG and MBP-HRR significantly prolonged clotting in HRG-depleted plasma by 8.8- and 7.2-fold ($P < 0.001$) (Figure 34B). MBP-PRR2 also prolonged the aPTT by 2.3-fold ($P = 0.014$). The remaining constructs (MBP-N1, MBP-N2, MBP-N1N2, MBP-PRR1, and MBP-COOH) had a minor effect on the aPTT (prolongation < 2-fold; $P > 0.3$). These results confirm that the effect of HRG is localized to the intrinsic pathway of coagulation, and that the anticoagulant properties of HRG are likely mediated through the HRR.

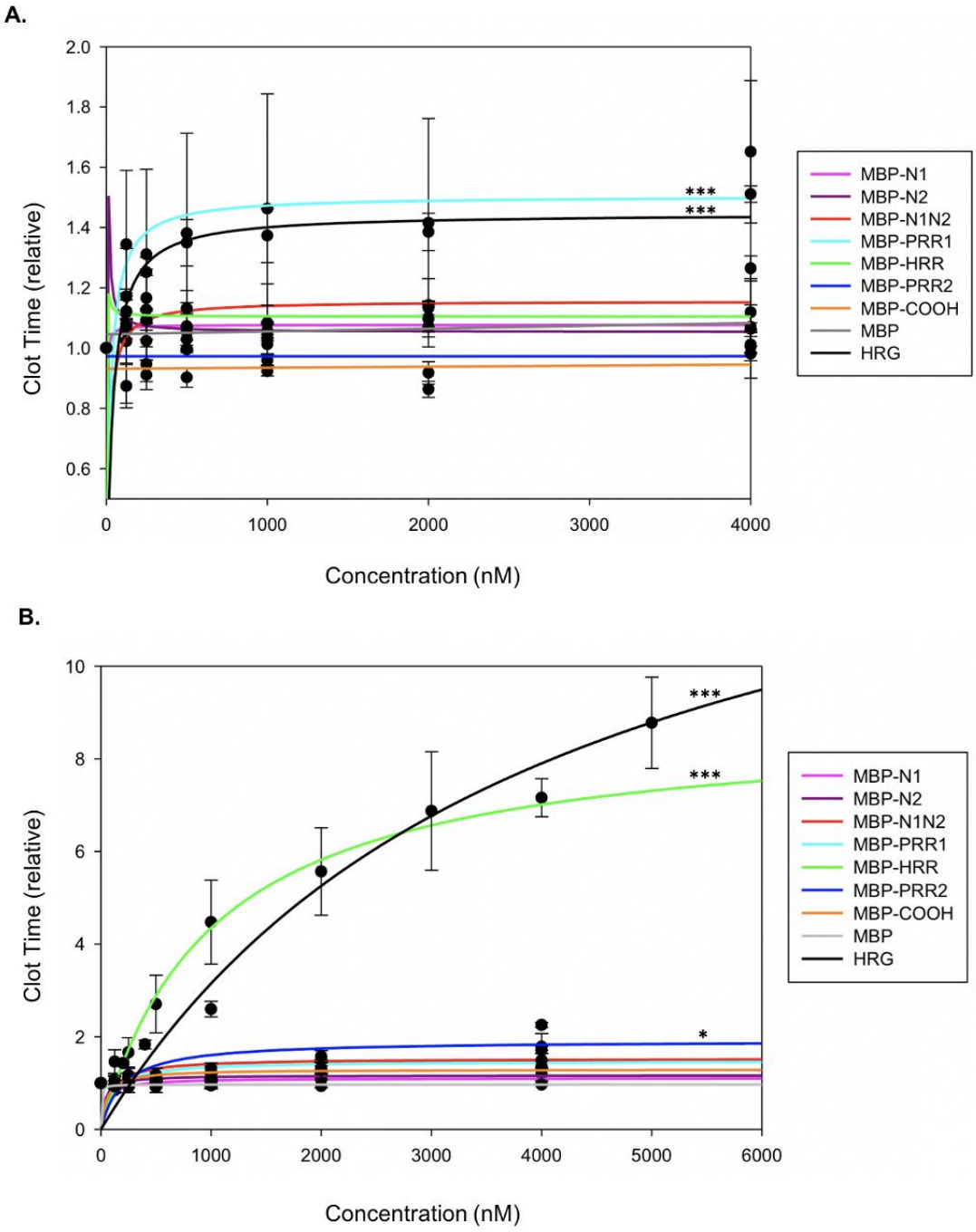
A.
Clot Time (relative)
Concentration (nM)
MBP-N1
MBP-N2
MBP-N1N2
MBP-PRR1
MBP-HRR
MBP-PRR2
MBP-COOH
MBP
HRG
***
***
B.
Clot Time (relative)
Concentration (nM)
MBP-N1
MBP-N2
MBP-N1N2
MBP-PRR1
MBP-HRR
MBP-PRR2
MBP-COOH
MBP
HRG
***
***
*

Figure 34: Effect of recombinant MBP-HRG domain constructs on clotting in HRG-depleted human plasma

HRG-depleted human plasma was incubated in the presence of HRG (0-5000 nM) or MBP-HRG domain constructs (0-4000 nM) with 1:100 RecombiPlasTin reagent (A) or 1:10 activated partial thromboplastin reagent (APTT-SP) (B) before clotting was initiated with 26 mM $CaCl_2$ at 37°C. The time to reach for half-maximal absorbance (clot time) was determined. Clot time was normalised to that in the absence of HRG or MBP-HRG domain constructs. Data represent three sets of experiments done in duplicate. Data was fitted using non-linear regression analysis (fitted lines). Bars represent mean ± standard deviation. *$P < 0.05$ and ***$P < 0.001$ compared with control HRG-depleted human plasma (ANOVA, Holm-Sidak method). MBP; maltose-binding protein, N1/N2; N-terminal domain, PRR1/2; proline-rich regions, HRR; histidine-rich region, COOH; carboxyl terminal domain, HRG; histidine-rich glycoprotein

7.0 CHAPTER 7: EFFECT OF SYNTHETIC HRR PEPTIDES ON CONTACT ACTIVATION, PLASMA CLOTTING, AND POLYPHOSPHATE-INDUCED THROMBIN GENERATION

7.1 Effect of synthetic HRR peptides on FXII autoactivation by various activators

Our current findings suggest that the HRG-FXIIa interaction is mediated by the HRR domain of HRG, which is its zinc binding domain. HRR is unique because of its unusually high content of histidine (13% of total amino acids) and the presence of tandem repeats of a consensus sequence (His-His-Pro-His-Gly). To examine the role of the HRR domain of HRG in contact pathway inhibition, we synthesized histidine-rich peptide analogues of the HRR consensus sequence and poly-histidine peptides and compared them with intact HRG in terms of their capacity to attenuate FXII autoactivation by various activators. Human HRG contains 4 repeats of the consensus sequence (Borza & Morgan, 1998; Doñate et al., 2004), thus we synthesized peptide analogs containing 1 to 4 repeats of the His-His-Pro-His-Gly consensus sequence, $(HHPHG)_{1-4}$ (Doñate et al., 2004), as well as a scrambled peptide, $Scr(HAHG)_5H$ containing five repeats of HAHG and poly-His peptides consisting of 6 or 12 residues (H-6 and H-12) (Table 2). Peptide mimicry of the HRR provides a complementary approach to the recombinant domain constructs of HRG. Moreover, synthetic peptides of the HRR provide a more direct investigation into the role of the consensus sequence, in addition to the importance of the histidine residues in domain function.

Consistent with previous findings, HRG inhibits FXII autoactivation induced by dextran sulfate in a dose-dependent manner with an IC_{50} of 248 ± 18 nM (Figure 35A,C). HRR-derived tetramer peptide, $(HHPHG)_4$, as well as Poly-His peptides (H-6 and H-12) inhibit FXII autoactivation with potencies similar to that of HRG (P = 0.107 to 0.764). The scrambled HRR peptide, $Scr(HAHG)_5H$ (IC_{50} 152 ± 26 nM) is significantly more potent than HRG (P = 0.004). The monomer peptide, $(HHPHG)_1$ however, does not affect FXII autoactivation. Silica was used as a control and an alternative non-physiological activator, because dextran sulfate has been shown to bind to HRG (MacQuarrie et al., 2011). The effect of HRG on the inhibition of FXII autoactivation is significantly greater when activation is induced with silica than with dextran sulfate (IC_{50} 27 ± 8 vs. 248 ± 18 nM, respectively; P < 0.001) (Figure 35C,D). The inhibitory effect of $(HHPHG)_4$ was also significantly more potent in silica induced FXII autoactivation (IC_{50} 117 ± 10 vs. 198 ± 25 nM, respectively; P = 0.018). Poly-His peptides (H-6 and H-12) inhibit FXII autoactivation to a similar extent regardless of the stimulant (IC_{50} ~230 nM; P= 0.445 and P= 0.201, respectively) (Figure 35C,D).

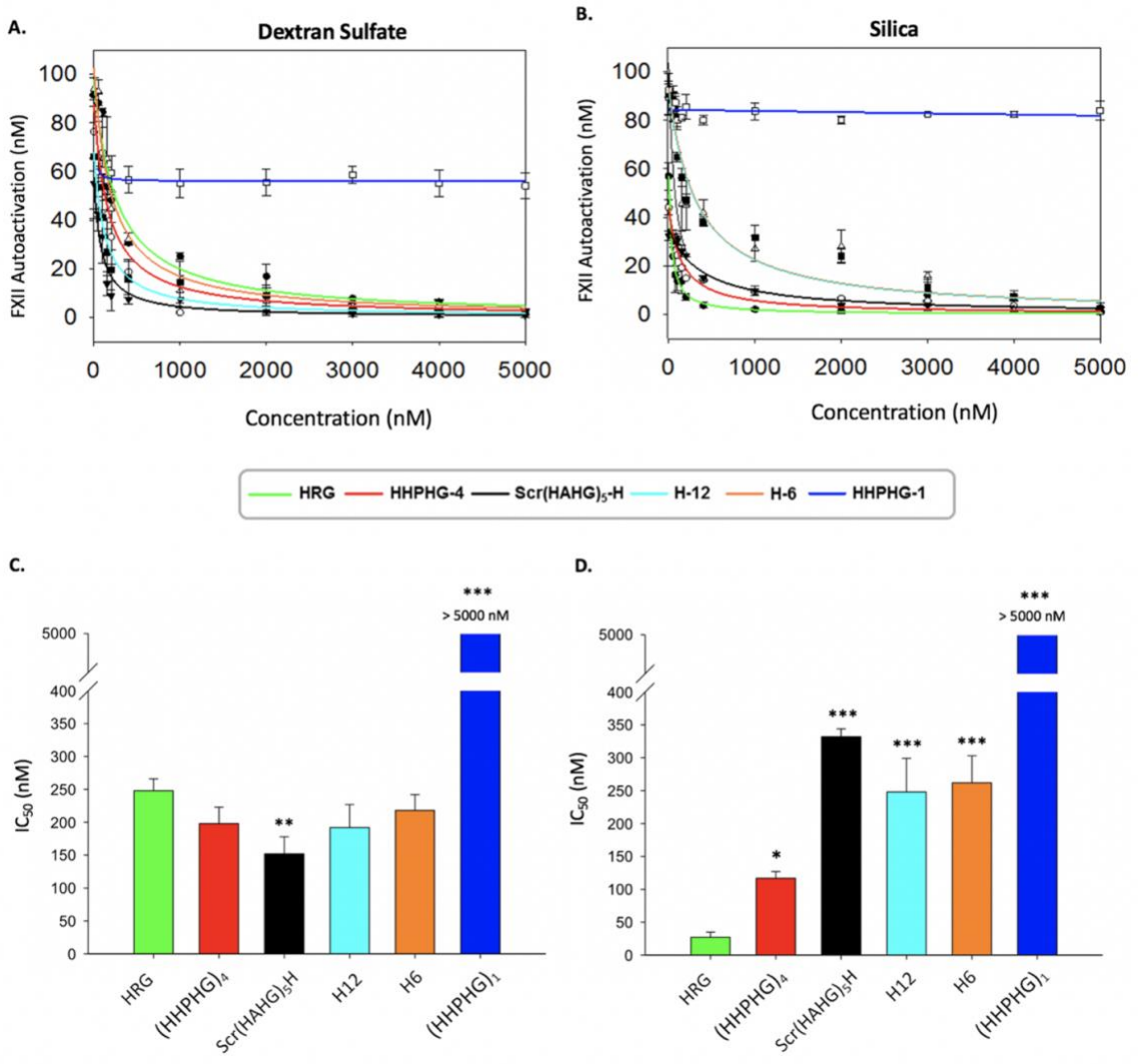
A.
Dextran Sulfate
FXII Autoactivation (nM)
Concentration (nM)
B.
Silica
FXII Autoactivation (nM)
Concentration (nM)
HRG
HHPHG-4
Scr(HAHG)5-H
H-12
H-6
HHPHG-1
C.
IC50 (nM)
> 5000 nM
HRG
(HHPHG)4
Scr(HAHG)5H
H12
H6
(HHPHG)1
D.
IC50 (nM)
> 5000 nM
HRG
(HHPHG)4
Scr(HAHG)5H
H12
H6
(HHPHG)1

Figure 35: Effect of HRG and HRR-derived peptides on FXII autoactivation

Autoactivation was assessed by incubating 100 nM FXII in buffer containing 6 µM $ZnCl_2$ in the absence or presence of HRG or HRR peptides at the concentrations shown. Autoactivation was induced with 1 µg/mL dextran sulfate (A) or 40 µg/mL silica (B). FXIIa generation was quantified by monitoring hydrolysis of 200 µM S-2302. FXIIa concentration was then plotted versus HRG or HRR peptide concentration. Data represent the mean of three experiments each done in duplicate. Symbols represent the mean, whereas bars reflect the standard deviation. IC_{50} values were determined by non-linear regression analysis (n=3; duplicates) and plotted (C, D). Bars represent mean ± standard deviation. *$P < 0.05$ and ***$P < 0.001$ compared with HRG (ANOVA, Holm-Sidak method).

To determine the minimal number of consensus repeats required for HRR to exert its inhibitory effect, we compared the effect of HRR peptides comprised of 1-4 repeats on silica induced FXII autoactivation. Peptides with 2, 3, or 4 repeats attenuate FXII autoactivation with similar IC_{50} values, whereas the peptide with only 1 consensus sequence has no effect (Figure 36). These findings suggest that more than one HHPHG repeat is required for inhibition of FXII autoactivation and that the number of His residues within the HRR may be an important determinant of its activity.

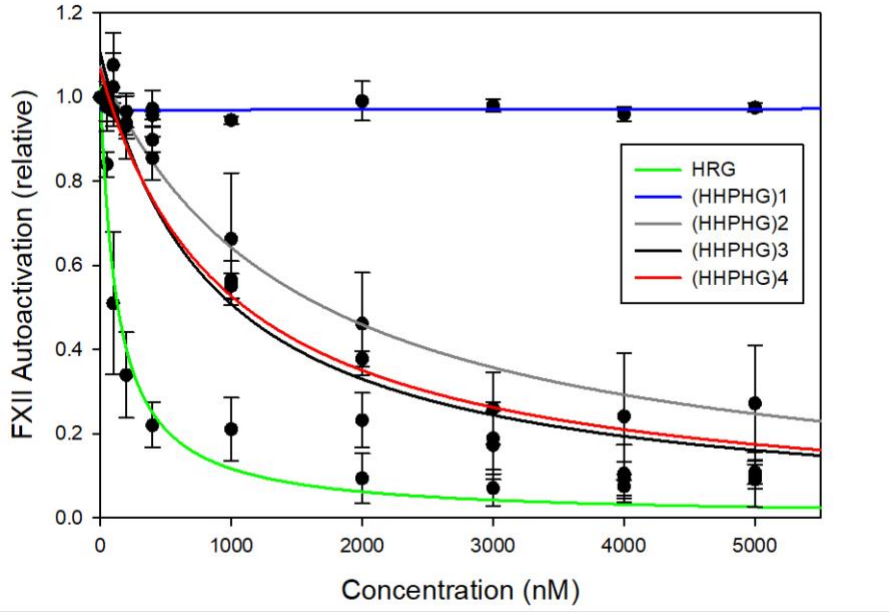
FXII Autoactivation (relative)
Concentration (nM)
HRG
(HHPHG)1
(HHPHG)2
(HHPHG)3
(HHPHG)4
0.0
0.2
0.4
0.6
0.8
1.0
1.2
0
1000
2000
3000
4000
5000

Figure 36: Effect of HRG and His peptides on silica induced FXII autoactivation

FXII (100 nM) was incubated with 50 µg/ml silica and 0-5 µM of HRG or His peptides [$(HHPHG)_1$ or $(HHPHG)_4$] in HBS-Tween (0.005%) containing 12.5 µM $ZnCl_2$ for 30 min at 37°C. FXIIa generation was quantified by monitoring the hydrolysis of 200 µM S-2302 d at 405 nm every 10 sec for 60 min. The amount of FXIIa generated was normalized relative to that measured in the absence of HRG or His peptides and was plotted versus HRG or HRR peptide concentration. Data represent the mean of three experiments each done in duplicate. Symbols represent the mean, whereas bars reflect the standard deviation. Rectangular hyperbola (non-linear regression) analysis was performed to determine IC_{50} values (fitted lines).

Short chain polyP (70-100 phosphate units) and long chain polyP (>1000 phosphate units) promote FXII autoactivation to a similar extent (Figure 37A-B). With either short or long chain polyphosphate, HRG attenuates FXII autoactivation with an IC_{50} of ~200 nM (Figure 37C). Similar findings are obtained when dextran sulfate is used to induce FXII autoactivation (Figure 35A). $(HHPHG)_4$ inhibits FXII autoactivation in the presence of short chain polyphosphate with significantly ($P < 0.001$) greater potency (IC_{50} 59 ± 18 nM) than the other HRR- peptides or intact HRG (IC_{50} ~200 nM) (Figure 37C). In the presence of long chain polyphosphate, HRR peptides attenuates FXII autoactivation with comparable IC_{50} of ~20 nM ($P = 0.7$ to 0.9). Consistent with previous findings, $(HHPHG)_1$ had no effect on FXII autoactivation induced by either short or long chain polyphosphate. HRR analogs inhibit FXII autoactivation with greater potency in the presence of short chain or long chain polyphosphate compared with HRG ($P < 0.001$) (Figure 37C,D). Interestingly, the inhibitory effect of HRG and HRR peptides were greater in the presence of long chain polyphosphate in comparison with short chain polyphosphate. Except $(HHPHG)_4$ ($P = 0.140$), HRG and HRR peptides were significantly more potent in long chain induced than short chain polyphosphate induced FXII autoactivation ($P < 0.001$). These findings suggest potential differences in how HRG and HRR analogs interact with the various activators, as well as their subsequent effect on FXII autoactivation.

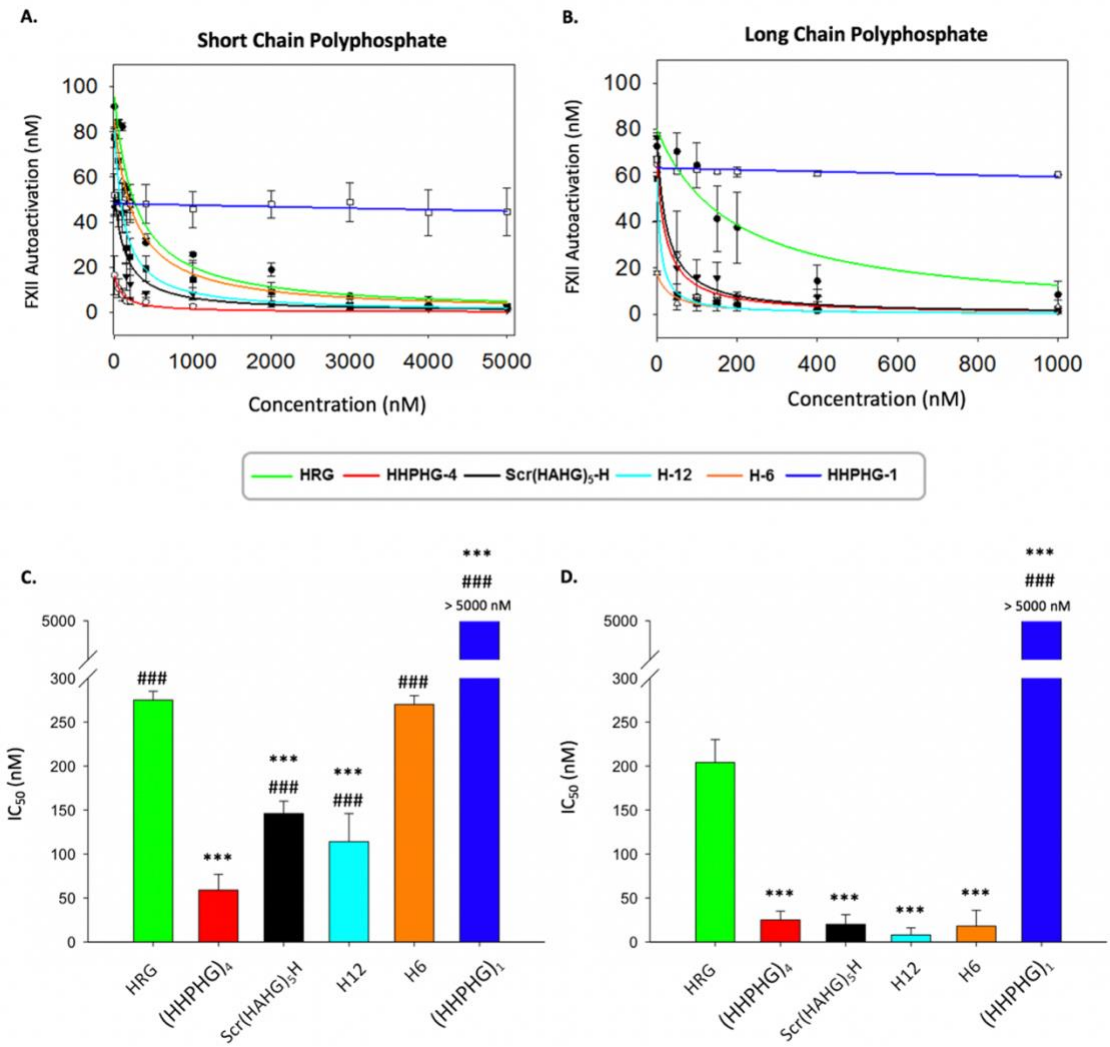
A.
Short Chain Polyphosphate
FXII Autoactivation (nM)
Concentration (nM)
B.
Long Chain Polyphosphate
FXII Autoactivation (nM)
Concentration (nM)
HRG
HHPHG-4
Scr(HAHG)5-H
H-12
H-6
HHPHG-1
C.
IC50 (nM)
> 5000 nM
HRG
(HHPHG)4
Scr(HAHG)5H
H12
H6
(HHPHG)1
D.
IC50 (nM)
> 5000 nM
HRG
(HHPHG)4
Scr(HAHG)5H
H12
H6
(HHPHG)1

Figure 37: Effect of HRG and HRR-derived peptides on FXII autoactivation

Autoactivation was assessed by incubating 100 nM FXII in buffer containing 6 µM $ZnCl_2$ in the absence or presence of HRG or HRR peptides at the concentrations shown. Autoactivation was induced with 8 µg/mL short chain polyP (A) or 8 µg/mL long chain polyP (B) and FXIIa generation was quantified by monitoring the hydrolysis of 200 µM S-2302 and the FXIIa concentrations were then plotted versus HRG or HRR peptide concentration. Data represent the mean of three experiments each done in duplicate. Symbols represent the mean, whereas bars reflect the standard deviation. IC_{50} values were determined by non-linear regression analysis (n=3; duplicates) and plotted (C, D). Bars represent mean ± standard deviation. $^{*}P < 0.05$ and $^{***}P < 0.001$ compared with HRG; $^{\#\#\#}P < 0.001$ compared with $(HHPHG)_4$ (ANOVA, Holm-Sidak method).

7.2 Effect of synthetic HRR peptides on FXIIa-mediated activation of FXI and prekallikrein

Additional intrinsic pathway reactions were examined to reveal whether the effect of HRR peptides were specific for FXII autoactivation. We have previously shown that HRG inhibits FXIIa-mediated FXI activation in the presence of Zn^{2+} by more than 95% with an IC_{50} of 287 nM in a dose-dependent manner (MacQuarrie et al., 2011). In the presence of HK, $ZnCl_2$, and dextran sulfate, FXI activation by FXIIa was assessed in the absence or presence of HRG or HRR peptides (Figure 38A). Like HRG, $Scr(HAHG)_5H$ and H-12 inhibit FXI activation by more than 90% in comparable manner ($P = 0.764$ and 0.081, respectively). However, $Scr(HAHG)_5H$ (IC_{50} 392 ± 18 nM) is significantly more potent than HRG and H-12 (IC_{50} 476 ± 14 and 781 ± 16 nM, respectively; $P < 0.001$) (Figure 38C). $(HHPHG)_4$ and H-6 inhibit FXI activation with similar capacity by 60%, although the tetramer peptide is significantly more potent (IC_{50} 225 ± 21 and 824 ± 24 nM, respectively; $P < 0.001$). Consistent with our findings in FXII autoactivation, $(HHPHG)_1$ had very little effect here as well (3.6% inhibition). These results show that HRG and HRR analogs significantly ($P < 0.001$) attenuate FXIIa-mediated activation of FXI in a dose-dependent and saturable manner.

Next, the effect of HRG or HRR peptides on FXIIa-mediated activation of prekallikrein was assessed in the presence of Zn^{2+} and short chain polyphosphate (Figure 38B). Like HRG, HRR peptides inhibit prekallikrein activation by ~30% to 60%. However, HRG is significantly more potent than the HRR peptides (IC_{50} 163 ± 25 nM; $P < 0.001$)

(Figure 38D). Scr(HAHG)$_5$H (IC_{50} 343 ± 21 nM significantly inhibits FXI activation by FXIIa compared with (HHPHG)$_4$, H-12, and H-6 (IC_{50} 512 ± 13, 797 ± 29, and 1677 ± 38 nM, respectively; $P < 0.001$). (HHPHG)$_1$ inhibits by only 18% with $IC_{50} > 5000$ nM. These findings suggest that HRR peptides have the ability to mimic the inhibitory effect of HRG on FXIIa-mediated activation of prekallikrein.

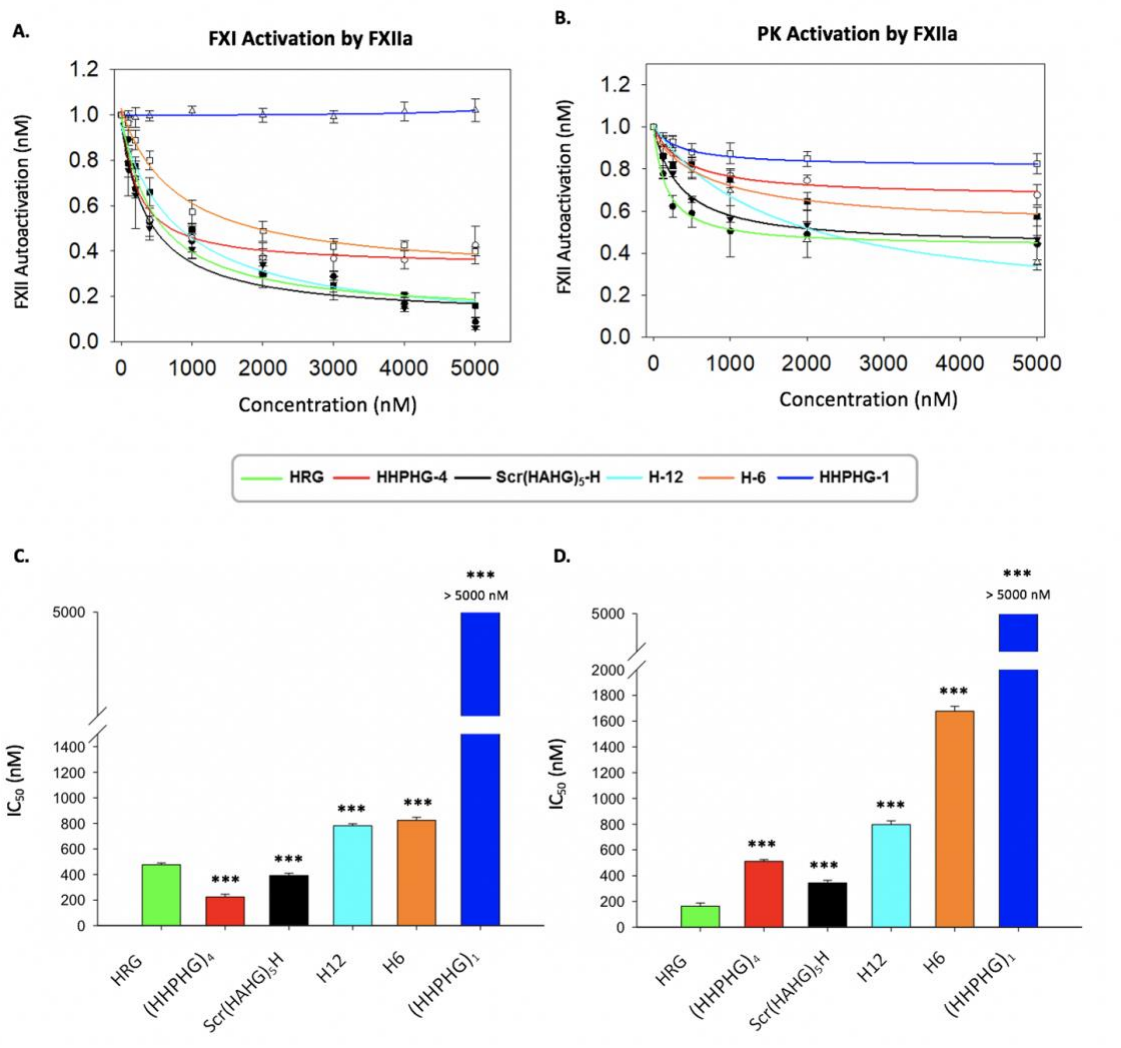
A.
FXI Activation by FXIIa
FXII Autoactivation (nM)
Concentration (nM)
B.
PK Activation by FXIIa
FXII Autoactivation (nM)
Concentration (nM)
HRG
HHPHG-4
Scr(HAHG)5-H
H-12
H-6
HHPHG-1
C.
IC50 (nM)
> 5000 nM
HRG
(HHPHG)4
Scr(HAHG)5H
H12
H6
(HHPHG)1
D.
IC50 (nM)
> 5000 nM
HRG
(HHPHG)4
Scr(HAHG)5H
H12
H6
(HHPHG)1

Figure 38: Effect of HRG and HRR-derived peptides on activation of FXI or PK by FXIIa

Effects of HRG or HRR peptides on FXIIa activation of (A) FXI or (B) prekallikrein (PK) were assessed by adding 0-5000 nM HRG or HRR peptides into well of a multi-well plate. Activation of 100 nM FXI activation by 10 nM FXIIa was assessed in the presence of 0.2 µg/ml dextran sulfate, 12.5 µM $ZnCl_2$ and 100 nM high molecular weight kininogen (HK), by monitoring the hydrolysis of S-2366 after addition of 30 nM corn trypsin inhibitor (CTI) to inhibit FXIIa activity. Activation of 120 nM PK by 2 nM FXIIa in the presence of 5 µg/ml short chain polyphosphate and 6 µM $ZnCl_2$ was determined by monitoring the hydrolysis of S-2302 after addition of 1 µM CTI. The concentrations of FXIa or kallikrein generated were normalized relative to those measured in the absence of HRG and HRR peptides. Data represent the mean of three experiments each done in duplicate. Symbols represent the mean, whereas bars reflect the standard deviation. IC_{50} values were determined by non-linear regression analysis (n=3; duplicates) and plotted (C, D). Bars represent mean ± standard deviation. ***$P < 0.001$ compared with HRG (ANOVA, Holm-Sidak method).

7.3 Effect of synthetic HRR peptides on clotting in human plasma

We have previously shown that HRG prolongs the activated partial thromboplastin time (aPTT) in HRG-depleted plasma in a FXIIa-dependent manner, but has no effect on the prothrombin time (PT) (MacQuarrie et al., 2011). Thus, the effect of the HRR-derived peptides on clotting in control and HRG-depleted human plasma was investigated. Like HRG, HRR peptides had little to no effect on the PT in control plasma (<1.5-fold prolongation) (Figure 39B). In contrast, the HRR-derived peptides significantly ($P < 0.001$) prolonged the aPTT with potency similar or greater than that of HRG (Figure 39A). Comparable with HRG (3.1-fold prolongation), $(HHPHG)_4$ and H-12 prolonged the aPTT by 3.4-fold ($P = 0.555$) and 4-fold ($P = 0.184$), respectively. Conversely, H-6 peptide and the monomer peptide $(HHPHG)_1$ prolonged the aPTT comparable to control human plasma (1.9-fold and 1.4-fold, respectively; $P = 0.158$ and 0.575). Lastly, the scrambled peptide, $Scr(HAHG)_5H$ significantly prolonged the aPTT in comparison with HRG (5.2-fold prolongation; $P = 0.005$). Thus, HRR peptides with higher histidine content (>11 His residues) delayed clotting with a similar or greater effectiveness as HRG.

In HRG-depleted plasma, HRG and HRR-peptides significantly prolonged the aPTT compared to control ($P < 0.001$). HRG significantly prolonged the aPTT by 10.5-fold in comparison with $(HHPHG)_4$ and $Scr(HAHG)_5H$ (3.8-fold and 3.4-fold, respectively; $P < 0.001$) (Figure 39C). Poly-His peptides, H-6 and H-12 prolonged the aPTT by ~2-fold, which was comparable to the monomer peptide (1.7-fold) ($P = 0.132$ and 0.113, respectively). HRG and HRR peptides had little to no effect on the PT (<1.3-fold prolongation) (Figure 39D). The findings using a silica-based aPTT reagent (APTT-SP)

reflect the inhibitory effects of HRG on FXII autoactivation mediated by silica in comparison with the HRR peptides (IC_{50} values of 27 nM vs >117 nM; $P < 0.001$). Further studies examining short chain polyphosphate mediated clotting in HRG-depleted plasma would determine whether the tetramer would be more potent than HRG, as it was in the purified system (IC_{50} 59 nM vs 275 nM, respectively; $P < 0.001$) as previously mentioned above. Together, these results confirm that the effect of HRG is localized to the intrinsic pathway of coagulation and the important role of the HRR domain in modulating the anticoagulant properties of HRG.

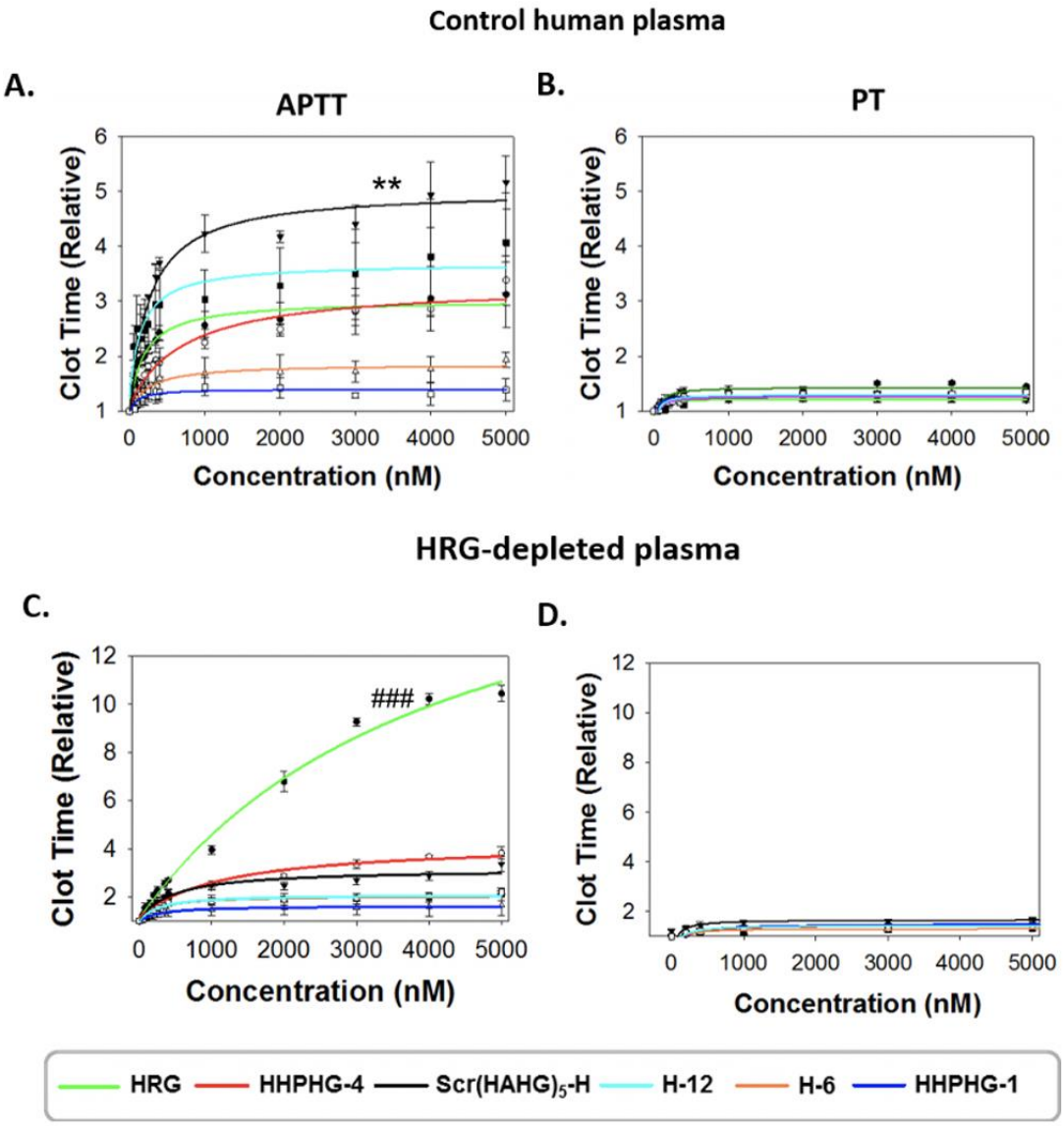
Control human plasma
A.
APTT
B.
PT
Clot Time (Relative)
Concentration (nM)
**
HRG-depleted plasma
C.
D.
###
HRG
HHPHG-4
Scr(HAHG)5-H
H-12
H-6
HHPHG-1

Figure 39: Effect of HRG and HRR-derived peptides on clotting in control and HRG-depleted human plasma

(A-B) Control or (C-D) HRG-depleted human plasma containing 0-5000 nM HRG or HRR peptides was incubated for 10 min at 37°C with 1:10 activated partial thromboplastin reagent (APTT-SP) (A and C) or 1:100 RecombiPlasTin reagent (B and D) before clotting was initiated with 26 mM $CaCl_2$. The time to reach half-maximal absorbance (clot time) was determined and normalized relative to that measured in the absence of HRG or HRR peptides. Data represent the mean of three experiments each done in duplicate. Symbols represent the mean, whereas bars reflect the standard deviation. The fitted lines reflect the results of non-linear regression analysis. $^{**}P < 0.005$ compared with HRG; $^{\#\#\#}P < 0.001$ compared with all (ANOVA, Holm-Sidak method).

7.4 Effect of synthetic HRR peptides on polyphosphate induced thrombin generation

Finally, the effect of HRG and HRR-derived peptides on thrombin generation induced by short chain polyphosphate was examined in HRG-depleted human plasma. HRG and HRR peptides significantly ($P < 0.001$) prolonged the time to peak thrombin and decreased peak thrombin in a dose-dependent manner (Figure 40A-D). In comparison with control, HRG and Scr$(HAHG)_5$H prolonged the time to peak thrombin by 2.5-fold and 2-fold, respectively (Figure 40C). $(HHPHG)_4$ and H-12 prolonged the peak thrombin time by 3.1-fold and 3.4-fold, respectively. Further, HRG and HRR peptides decreased peak thrombin up to ~2.5-fold in a dose-dependent and saturable manner (Figure 40D). $(HHPHG)_1$ had little effect on thrombin generation. These findings suggest that like HRG, HRR peptides have the capacity to down regulate the procoagulant effect of polyphosphate in human plasma.

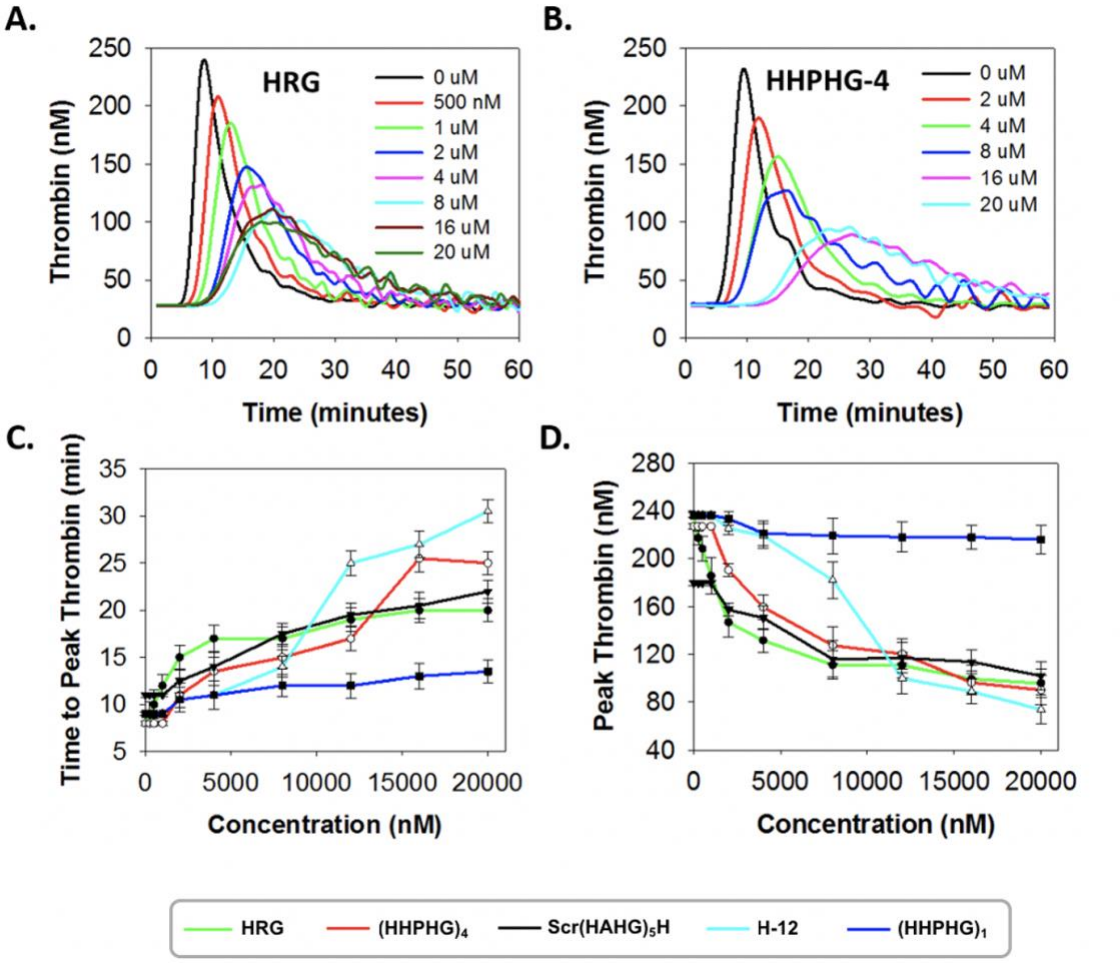
A.
HRG
0 uM
500 nM
1 uM
2 uM
4 uM
8 uM
16 uM
20 uM
Thrombin (nM)
Time (minutes)
B.
HHPHG-4
0 uM
2 uM
4 uM
8 uM
16 uM
20 uM
Thrombin (nM)
Time (minutes)
C.
Time to Peak Thrombin (min)
Concentration (nM)
D.
Peak Thrombin (nM)
Concentration (nM)
HRG
(HHPHG)4
Scr(HAHG)5H
H-12
(HHPHG)1

Figure 40: Effect of HRG and HRR-derived peptides on polyphosphate-induced thrombin generation in HRG-depleted human plasma

Thrombin generation in HRG-depleted human plasma was triggered by short chain polyphosphate (40 μg/ml) in the presence of 0-20 μM (A) HRG or (B) $(HHPHG)_4$. After the addition of 15 mM $CaCl_2$, hydrolysis of Z-Gly-Gly-Arg-AMC substrate was monitored. Thrombin generation profiles (A-B) were analyzed using Technothrombin TGA software. Thrombin generation parameters time to peak (C) and peak thrombin concentration (D) are plotted for HRG and all peptides. Data representative of three sets of experiments done in duplicate. Lines represent mean (points) ± standard deviation (bars).

8.0 CHAPTER 8: BINDING INTERACTIONS BETWEEN HRG, FXIIA, AND POLYPHOSPHATE

8.1 SPR analysis of the interaction of MBP-HRG domain constructs with FXIIa, FXII, β-FXIIa

We have previously shown that HRG binds to FXIIa, but not FXII or β-FXIIa in the presence of Zn^{2+} with high affinity (MacQuarrie et al., 2011). The affinities of MBP-HRG domain constructs for FXIIa, β-FXIIa, and FXII were determined by surface plasmon resonance (SPR) and compared with the affinity of plasma derived HRG. Biotinylated FXIIa, β-FXIIa, or amine coupled FXII were immobilized on streptavidin-coated flow cells and flow cell with streptavidin alone was used as a control. In the presence of 13 μM $ZnCl_2$, increasing concentrations of analyte, either 0-500 nM HRG or MBP-HRG domain constructs were injected into all four flow cells, followed by running buffer alone. Flow cells were regenerated with 250 mM NaCl, 62.5 mM imidazole and 5 mM EDTA.

MBP-HRG domain constructs bind to FXIIa with varying affinities (Figure 41), but do not bind to FXII or β-FXIIa (data not shown). Like HRG, MBP-HRR binds to FXIIa with high affinity (K_d of 123 ± 7 nM; P = 0.319) (Figure 42B). Moreover, SPR analysis showed that MBP-HRR binds to FXIIa with similar binding kinetics as HRG, whereby there is a high on rate and slow off rate. MBP-N1 and MBP-N1N2 (Figure 42C,E) have similar (P = 0.944) affinity for FXIIa that is comparable with HRG (K_d values of 151 ± 16 and 155 ± 26 nM, respectively; P = 0.168 and 0.163). Although, the affinity is comparable with MBP-HRR, MBP-N1 and MBP-N1N2 have high off rates, suggesting relatively weak

interaction with FXIIa. In contrast, the remaining domains (MBP-N2, MBP-PRR1/2, MBP-COOH) bind significantly less than HRG to FXIIa ($P < 0.001$). MBP-N2 binds to FXIIa with a K_d value of 1037 ± 38 nM (Figure 42D). MBP-PRR2 (Figure 42G) binds FXIIa with higher affinity than MBP-PRR1 (Figure 42F) (K_d values 307 ± 110 nM and 4009 ± 164 nM, respectively; $P < 0.001$). MBP-COOH binds to FXIIa with a K_d value of 739 ± 33 nM. Both MBP-PRR1 and MBP-COOH have high off rates like the N-terminal domain constructs. MBP control does not bind to FXIIa, FXII, or β-FXIIa. HRG and HRG domain constructs bind to FXIIa significantly more than MBP control ($P < 0.001$). Together, these findings suggest that the interaction of HRG with FXIIa involves multiple domains, whereby the HRR and N1 are the predominant domains binding FXIIa.

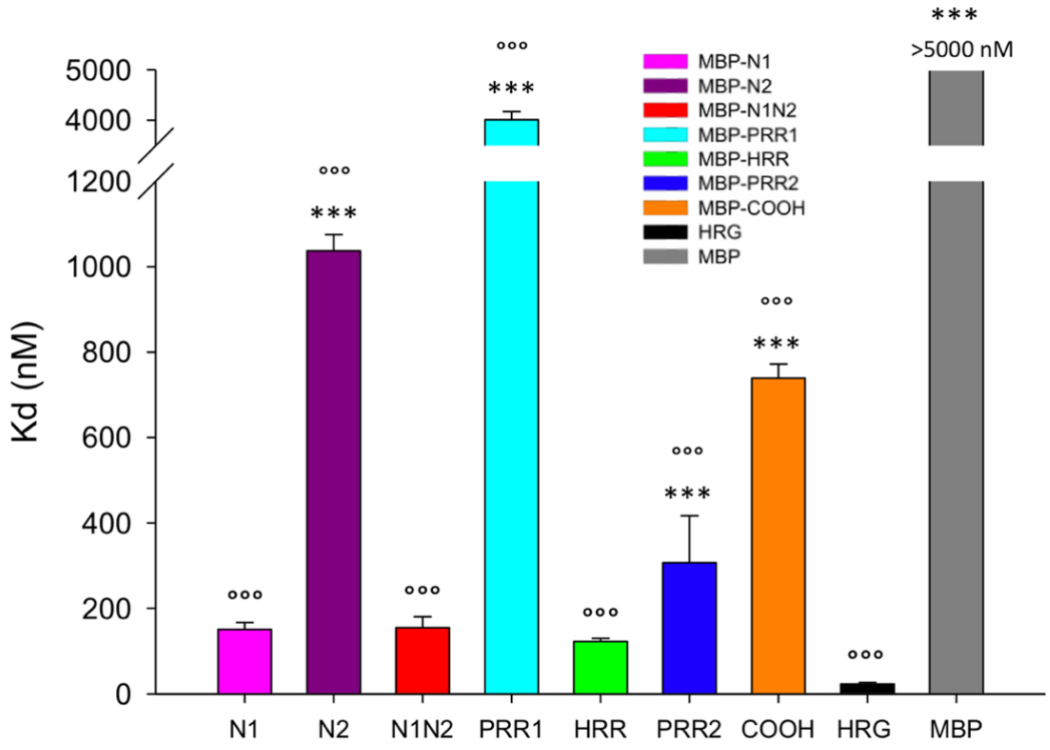
Kd (nM)
5000
4000
1200
1000
800
600
400
200
0
MBP-N1
MBP-N2
MBP-N1N2
MBP-PRR1
MBP-HRR
MBP-PRR2
MBP-COOH
HRG
MBP
***
>5000 nM
°°°
***
N1
N2
N1N2
PRR1
HRR
PRR2
COOH
HRG
MBP

Figure 41: Binding affinity of MBP-HRG domain constructs for FXIIa

Binding of recombinant MBP-tagged constructs expressing individual domains of HRG (N1, N2, N1N2, PRR1, HRR, PRR2, COOH) to immobilized FXIIa was quantified using surface plasmon resonance (SPR). Dissociation constant (K_d) values were determined from equilibrium values by the BIAcore T200 evaluation software. ***$P < 0.005$ compared with HRG; °°°$P < 0.001$ compared with MBP control (ANOVA, Holm-Sidak method). MBP, maltose-binding protein; N1/N2, N-terminal domains; PRR1/PRR2, proline-rich regions; HRR, histidine-rich region; COOH, carboxyl terminal domain; HRG, histidine-rich glycoprotein

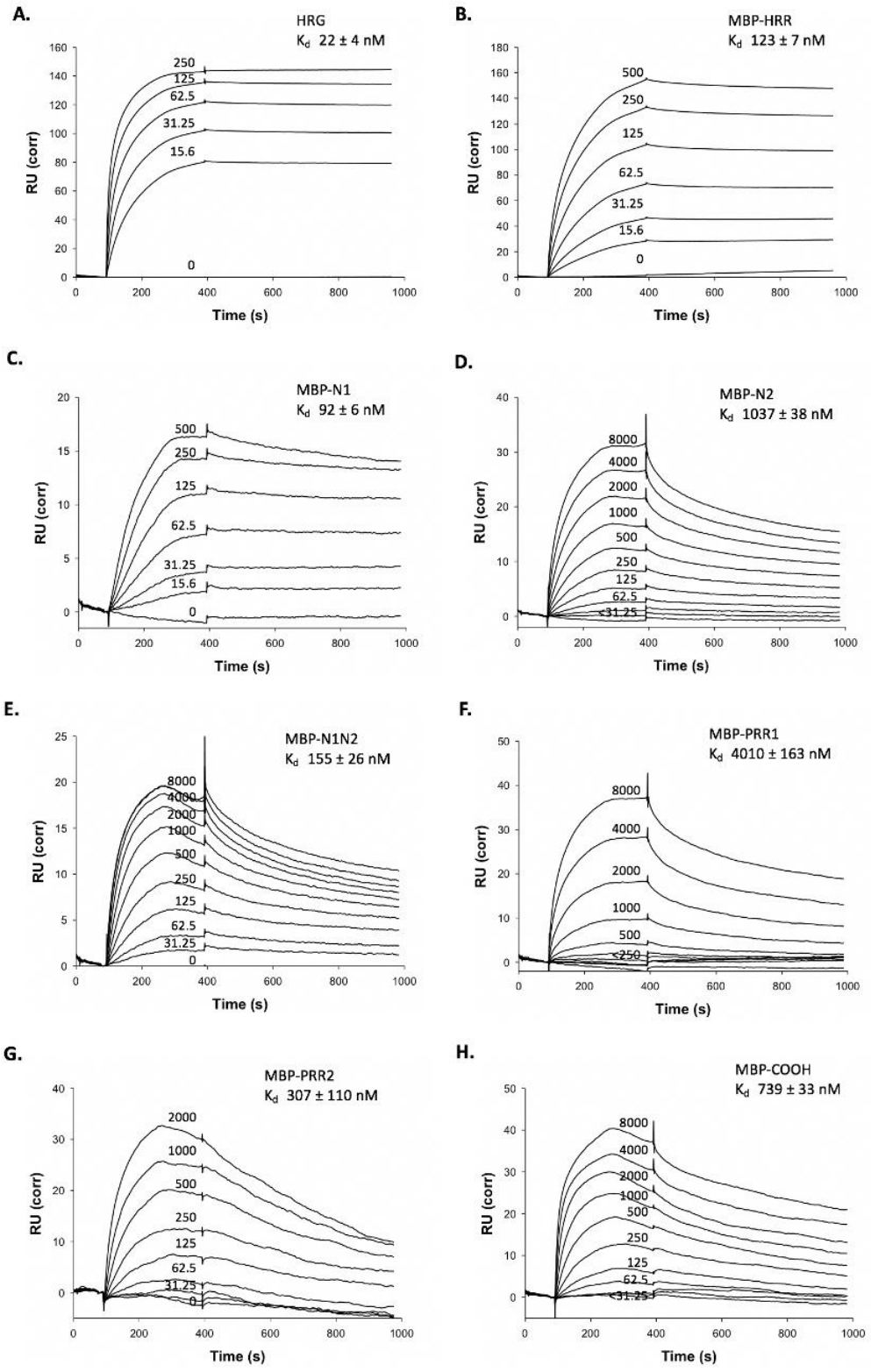
A.
HRG
K_d 22 ± 4 nM
250
125
62.5
31.25
15.6
0
RU (corr)
Time (s)
B.
MBP-HRR
K_d 123 ± 7 nM
500
250
125
62.5
31.25
15.6
0
RU (corr)
Time (s)
C.
MBP-N1
K_d 92 ± 6 nM
500
250
125
62.5
31.25
15.6
0
RU (corr)
Time (s)
D.
MBP-N2
K_d 1037 ± 38 nM
8000
4000
2000
1000
500
250
125
62.5
<31.25
RU (corr)
Time (s)
E.
MBP-N1N2
K_d 155 ± 26 nM
8000
4000
2000
1000
500
250
125
62.5
31.25
0
RU (corr)
Time (s)
F.
MBP-PRR1
K_d 4010 ± 163 nM
8000
4000
2000
1000
500
<250
RU (corr)
Time (s)
G.
MBP-PRR2
K_d 307 ± 110 nM
2000
1000
500
250
125
62.5
31.25
0
RU (corr)
Time (s)
H.
MBP-COOH
K_d 739 ± 33 nM
8000
4000
2000
1000
500
250
125
62.5
<31.25
RU (corr)
Time (s)

Figure 42: SPR analysis of MBP-HRG domain constructs binding to FXIIa

Binding affinity was determined on a BIAcore T200 using immobilized b-FPR-FXIIa adsorbed onto a streptavidin-coated (SA) CM4 sensor chip to 500 RU. Increasing concentrations of A) HRG, B) MBP-HRR, C) MBP-N1N2, or D) MBP-PRR2 were passed over the flow cell in the presence of 13 µM $ZnCl_2$ for 300 sec at a flow rate of 50 µl/min, followed by running buffer alone (900 sec). RU values were corrected with SA control flow cell alone (RU (corr)) and plotted vs. time. Panels are representative sensorgrams for MBP-HRG domain constructs with high affinity for FXIIa. Sensorgrams for remaining constructs are not shown. Dissociation constant (K_d) values were determined as previously described.

8.2 SPR analysis of the affinities of synthetic HRR peptides for FXIIa, FXII, and β-FXIIa

The affinities of HRR peptides for FXIIa, β-FXIIa, and FXII were determined by SPR and compared with the affinity of plasma derived HRG. Increasing concentrations of analyte, either 0-500 nM HRG or 0-1000 nM HRR-derived peptides, were injected into all four flow cells, followed by running buffer alone. Flow cells were regenerated with 250 mM NaCl, 62.5 mM imidazole, and 5 mM EDTA. In the presence of 13 μM Zn^{2+}, HRG and $(HHPHG)_4$ bind to immobilized biotinylated FXIIa (b-FXIIa) with K_d values of 12 ± 0.03 nM and 222 ± 20 nM, respectively (Figure 43A-B), whereas $Scr(HAHG)_5H$ binds b-FXIIa with a K_d value of 443 ± 0.9 nM (Figure 43C). The slow off rate observed for both $(HHPHG)_4$ and $Scr(HAHG)_5$-H is comparable to that with HRG, suggesting strong interaction with FXIIa. As expected, the monomer peptide, $(HHPHG)_1$ does not bind to FXIIa. Binding of HRG and HRR peptides to FXIIa is reversible as the interaction is abrogated with imidazole, suggesting the interaction to FXIIa is predominately mediated by His residues. Interestingly, the H-6 and H-12 peptides do not bind to FXIIa (Figure 43D). Thus, His residues alone do not appear to provide the necessary conformation required for FXIIa binding. HRR peptides do not bind FXIIa in the absence of Zn^{2+}. Neither HRG nor HRR peptides bind to immobilized β-FXIIa or FXII in the absence or presence of Zn^{2+}. This supports our hypothesis that the binding of HRG is specific for FXIIa and localized to its heavy chain, and not its catalytic domain.

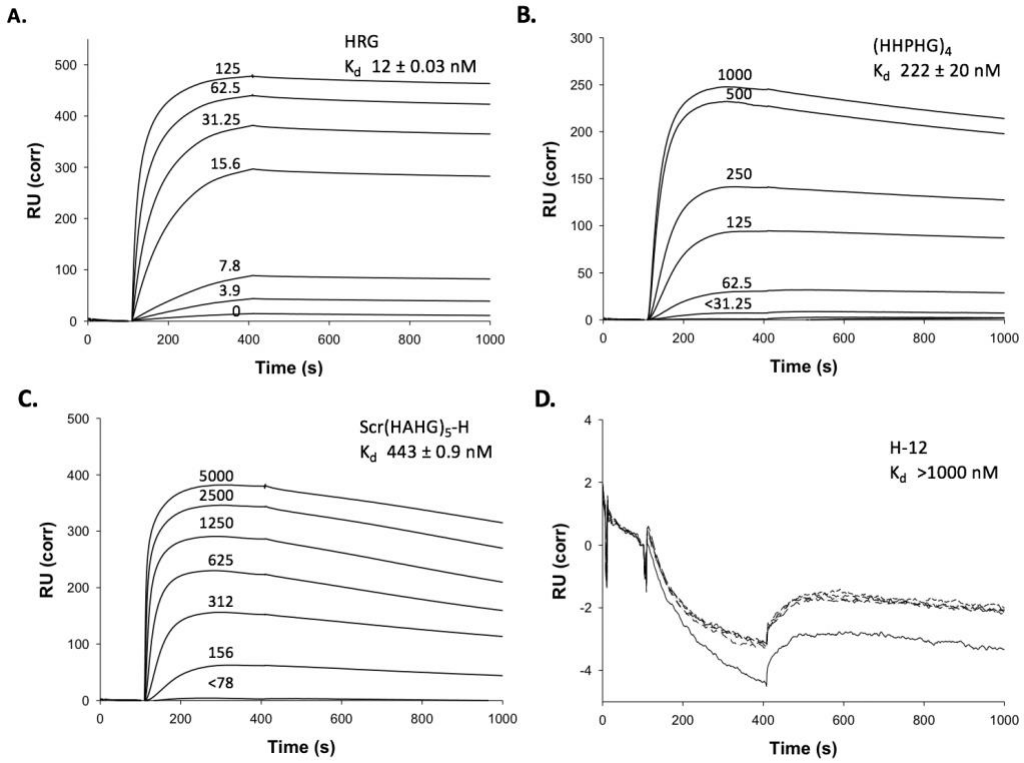
A.
HRG
K_d 12 ± 0.03 nM
125
62.5
31.25
15.6
7.8
3.9
0
RU (corr)
Time (s)
B.
$(HHPHG)_4$
K_d 222 ± 20 nM
1000
500
250
125
62.5
<31.25
RU (corr)
Time (s)
C.
$Scr(HAHG)_5$-H
K_d 443 ± 0.9 nM
5000
2500
1250
625
312
156
<78
RU (corr)
Time (s)
D.
H-12
K_d >1000 nM
RU (corr)
Time (s)

Figure 43: SPR analysis of synthetic HRR peptides binding to FXIIa

Binding affinity was determined on a BIAcore T200 using immobilized b-FPR-FXIIa adsorbed onto a streptavidin-coated (SA) CM4 sensor chip to 500 RU. Increasing concentrations of A) HRG, B) $(HHPHG)_4$, C) $Scr(HAHG)_5H$, or D) H-12 were passed over the flow cell in the presence of 13 µM $ZnCl_2$ for 300 sec at a flow rate of 50 µl/min, followed by running buffer alone (900 sec). RU values were corrected with SA control flow cell alone (RU (corr)) and plotted vs. time. Dissociation constant (K_d) values were determined from equilibrium values by the BIAcore T200 evaluation software.

8.3 SPR analysis of FXII fragments binding to HRG

We have previously shown that HRG does not bind to zymogen FXII or β-FXIIa, which localizes the binding site to the non-catalytic heavy chain of FXIIa (MacQuarrie et al., 2011). To further understand the interaction between HRG and FXIIa, the affinity of HRG for recombinant full length heavy chain of FXII (HC-FXII) or the N-terminal domains (NH_2-fibronectin (FN) type II domain and epidermal growth factor (EGF)-like domain 1) of FXII (NFE-FXII) was determined by SPR analysis. FXII fragments were generous gifts from Dr. Jonas Emsley (University of Nottingham, UK). As expected, SDS-PAGE analysis of NFE fragment of FXII compared with FXII and FXIIa show one single band under reducing and non-reducing conditions at ~15 kDa (Figure 44).

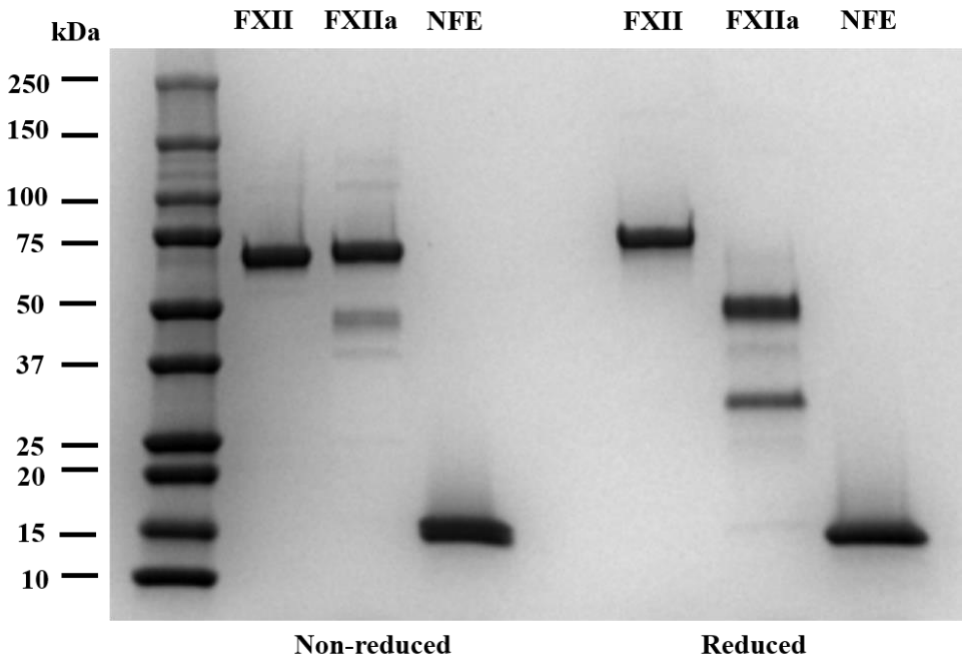
kDa
250
150
100
75
50
37
25
20
15
10
FXII
FXIIa
NFE
FXII
FXIIa
NFE
Non-reduced
Reduced

Figure 44: SDS-Page gel analysis of FXII fragments compared to FXII and FXIIa

SDS-Page gel analysis of FXII, FXIIa, and recombinant NH_2-FNII-EGF1 (NFE) fragment of FXII. Samples were run on SDS-PAGE gel under non-reduced and reduced conditions. Approximately, 3 μg of protein were loaded onto a 4-15% polyacrylamide gradient gel and electrophoresed in the presence of SDS. Gels were stained with Bio-Safe Coomassie G-250 blue stain and imaged using Image Lab Software on the Gel/ChemiDoc MP Imager System. Molecular weight marker is indicated on the left lane.

The affinity of HRG for FXII fragments containing either HC-FXII or NFE-FXII was determined by SPR and compared with that of FXIIa. Immobilized HRG was titrated with increasing concentrations (0 to 1000 nM) of FXIIa or FXII fragments in the presence of 13 µM $ZnCl_2$. FXIIa binds HRG with a K_d value of 67 ± 0.9 nM (Figure 45A). As expected, the heavy chain fragment of FXII binds to HRG with high affinity (K_d value of 19 ± 1.9 nM) (Figure 45B). This confirms the interaction of HRG with the non-catalytic region of FXIIa and supports the notion that the binding site is encrypted and only exposed when FXII is activated to FXIIa. To further localize the binding site of HRG on FXIIa, we show that the NFE domain of FXII binds HRG with a K_d value of 74 nM ± 0.7 nM, a value similar to that of full-length FXIIa (Figure 45C). Retention of the high-affinity interaction in the reverse binding experiment verifies the initial observation of high-affinity of FXIIa to HRG in the presence of Zn^{2+}. These findings suggest binding of HRG is localized within the FNII or EGF1 domains of FXII and that FXII fragments of the heavy chain allowed for direct binding of HRG and FXII.

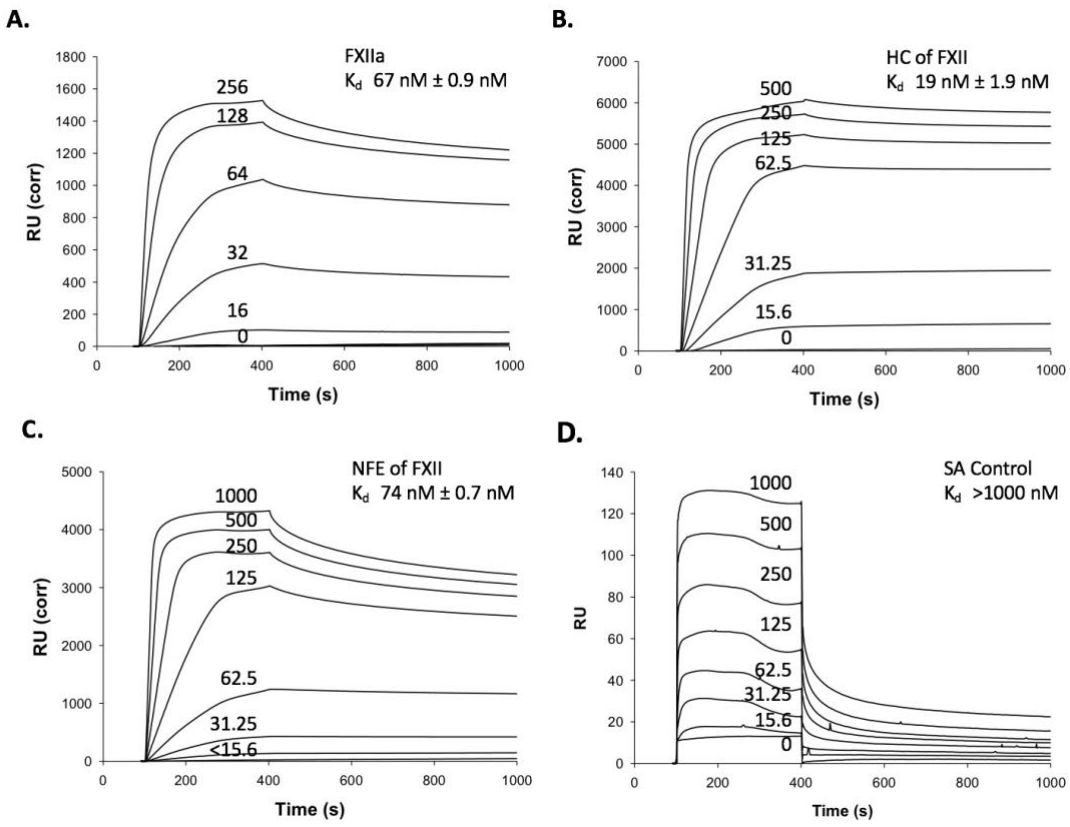
A.
FXIIa
K_d 67 nM ± 0.9 nM
256
128
64
32
16
0
RU (corr)
Time (s)
B.
HC of FXII
K_d 19 nM ± 1.9 nM
500
250
125
62.5
31.25
15.6
0
RU (corr)
Time (s)
C.
NFE of FXII
K_d 74 nM ± 0.7 nM
1000
500
250
125
62.5
31.25
<15.6
RU (corr)
Time (s)
D.
SA Control
K_d >1000 nM
1000
500
250
125
62.5
31.25
15.6
0
RU
Time (s)

Figure 45: SPR analysis of FXII fragments binding to HRG

The affinity of HRG for FXII fragments containing either the full-length heavy chain (HC) of FXII (A) or the N-terminal domains (Fibronectin Type II domain and EGF-like domain 1) (NFE) of FXII (B) was determined by SPR analysis. Immobilized b-HRG was titrated with increasing concentrations (0 to 1000 nM) of FXII fragments, HC-FXII or NFE-FXII in the presence of 13 μM $ZnCl_2$. RU values were determined and plotted vs. time. Concentrations of FXII fragments are indicated. Sensorgrams were analyzed with BIAcore T200 evaluation software Version 1.0 (BIAcore). RU values were corrected (RU (corr)) with SA control flow cell alone (D) and plotted vs. time. Dissociation constant (K_d) values were determined from equilibrium values by the BIAcore T200 evaluation software.

8.4 SPR analysis of HRG binding to short chain polyphosphate

We have previously shown that HRG binds to nucleic acids, RNA and DNA with high affinity and attenuates their capacity to activate the intrinsic pathway of coagulation (Vu et al., 2016). The affinity of plasma derived HRG for short chain polyP in the presence or absence of Zn^{2+} was determined by SPR analysis. Biotinylated polyP (100 phosphate units) was absorbed to bound streptavidin coated flow cells to ~100-180 RU. Binding experiments were performed similarly to experiments mentioned above. In the presence of 13 μM $ZnCl_2$, HRG binds to immobilized short chain polyP with high affinity (K_d value of 110 ± 16 nM) (Figure 46). In the absence of Zn^{2+}, HRG binds to polyphosphate with similar affinity (K_d value of 110 ± 0.9 nM), however, there is a 5.3-fold reduction in the capacity of HRG to bind polyP (from 800 RU to 150 RU).

A.

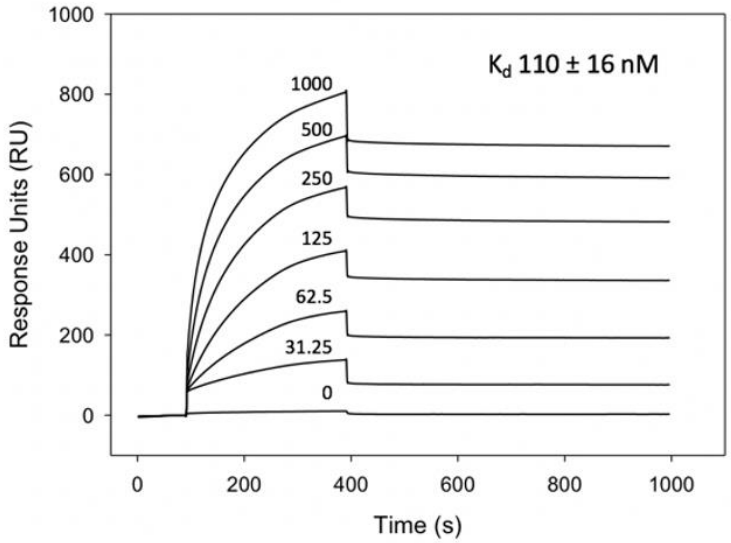
K_d 110 ± 16 nM
1000
500
250
125
62.5
31.25
0
Response Units (RU)
Time (s)
0
200
400
600
800
1000

B.

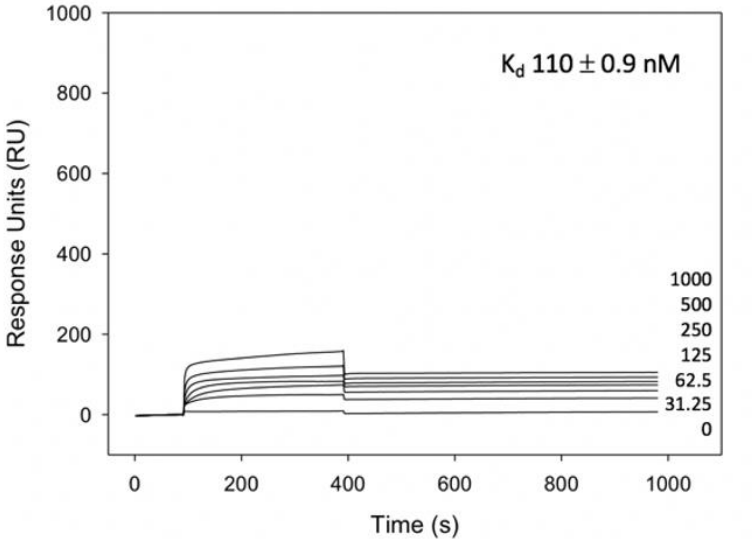
K_d 110 ± 0.9 nM
1000
500
250
125
62.5
31.25
0
Response Units (RU)
Time (s)
0
200
400
600
800
1000

Figure 46: SPR analysis of HRG binding short chain polyphosphate

The affinity of HRG for short chain polyphosphate in the presence (A) or absence (B) of 13 μM $ZnCl_2$ was determined by SPR analysis. Immobilized biotinylated polyP (100 phosphate units) adsorbed onto a streptavidin-coated (SA) CM4 sensor chip to 50-100 RU was titrated with increasing concentrations (0 to 1000 nM) of plasma-derived HRG. RU values were determined and plotted vs. time. Concentrations of HRG are indicated. Sensorgrams were analyzed with BIAcore T200 evaluation software Version 1.0 (BIAcore). RU values were obtained from the instrument software. Dissociation constant (K_d) values were determined from equilibrium values by the BIAcore T200 evaluation software.

8.5 Immunoassay analysis of MBP-HRG domain constructs binding to polyphosphate

Next, the affinities of MBP-HRG domain constructs for short chain polyP were determined by enzyme-linked immunosorbent assay (ELISA). Streptavidin-coated 96-well plates were incubated with biotinylated short chain polyP (70-mer, BK Giulini). Increasing concentrations of MBP-HRG domain constructs (0-500 nM) were added to wells, then incubated with primary polyclonal rabbit antibody against MBP and secondary goat anti-rabbit HRP-conjugated antibody. Binding was detected with substrate solution containing o-phenylenediamine dihydrochloride (OPD). Reaction was stopped with 2.5 M sulfuric acid and absorbance was measured by endpoint read at 490 nm.

Histidine-proline rich domains of HRG bind immobilized biotinylated short chain polyP with high affinity (Figure 47). MBP-HRR has the highest affinity for short chain polyP with a K_d value of 12 nM. MBP-PRR2 and MBP-COOH have similar affinity for polyP (K_d values 26 nM and 30 nM, respectively). The remaining domains of HRG also bind to polyP, but with lower affinity. MBP-N1N2 and MBP-N2 have K_d values of 87 nM and 114 nM, respectively. MBP-N1 and MBP-PRR1 has the lowest affinity to polyP (K_d values of 557 nM and 671 nM, respectively). MBP does not bind to short chain polyP. These findings suggest that histidine-proline rich domains of HRG predominately mediates HRG binding to short chain polyP, whereas the remaining domains assist in the interaction to a lesser degree.

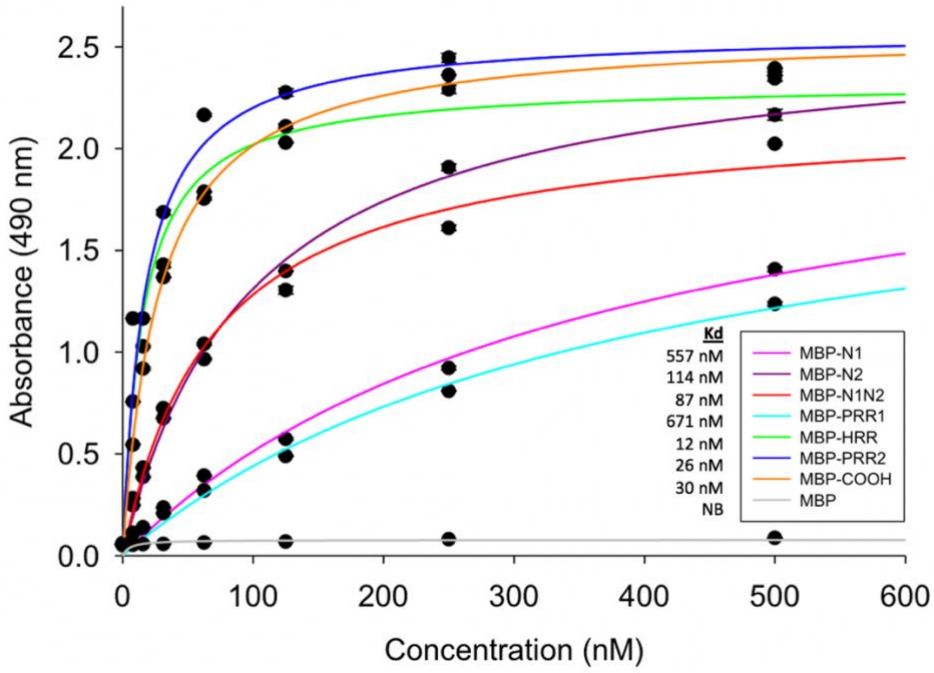
Absorbance (490 nm)
2.5
2.0
1.5
1.0
0.5
0.0
0
100
200
300
400
500
600
Concentration (nM)
Kd
557 nM
114 nM
87 nM
671 nM
12 nM
26 nM
30 nM
NB
MBP-N1
MBP-N2
MBP-N1N2
MBP-PRR1
MBP-HRR
MBP-PRR2
MBP-COOH
MBP

Figure 47: Binding affinity of MBP-HRG domain constructs to polyphosphate by ELISA

Streptavidin-coated 96-well plates were incubated with biotinylated short chain polyphosphate (polyP) (70-mer, BK Giulini). Increasing concentrations of MBP-HRG domain constructs (0-500 nM) were added to wells, then incubated with primary polyclonal rabbit antibody against MBP and secondary goat anti-rabbit HRP-conjugated antibody. Binding was detected with substrate solution containing o-phenylenediamine dihydrochloride (OPD). Reaction was stopped with 2.5 M sulfuric acid. Absorbance was measured by endpoint read at 490 nm and plotted vs MBP-HRG domain construct concentration. Data were analyzed using TableCurve 2D and rectangular hyperbola (non-linear regression) analysis (fitted lines) to determine dissociation constant (K_d) values. MBP, maltose-binding protein; N1/2, N-terminal domains; PRR1/2, proline-rich regions; HRR, histidine-rich region; COOH, carboxyl terminal region; NB, no binding observed

8.6 SPR analysis of synthetic HRR peptides binding to polyphosphate

The affinity of synthetic HRR peptides for short chain polyphosphate was determined by SPR analysis. Consistent with data shown above, plasma derived HRG binds to immobilized short chain polyP (70-100 phosphate units) with a K_d value of 193 ± 11 nM in the presence of 13 μM $ZnCl_2$. $(HHPHG)_4$ binds to polyP with significantly ($P < .001$) lower affinity than HRG (K_d value of 526 ± 4 nM) (Figure 48). Although binding was observed, the 2.7-fold reduction in affinity suggests that synthetic peptides of HRR do not have the same capacity to interact with polyphosphate as HRG or the full-length domain of HRR (as shown above in Figure 46 and Figure 47, respectively). Moreover, $(HHPHG)_1$ does not bind to short chain polyphosphate. These findings suggest that the HRR binds to polyphosphate in the presence of Zn^{2+}. Binding of HRR to polyphosphate requires more than one repeat of the histidine-rich consensus sequence (HHPHG) and approximately 12 His residues.

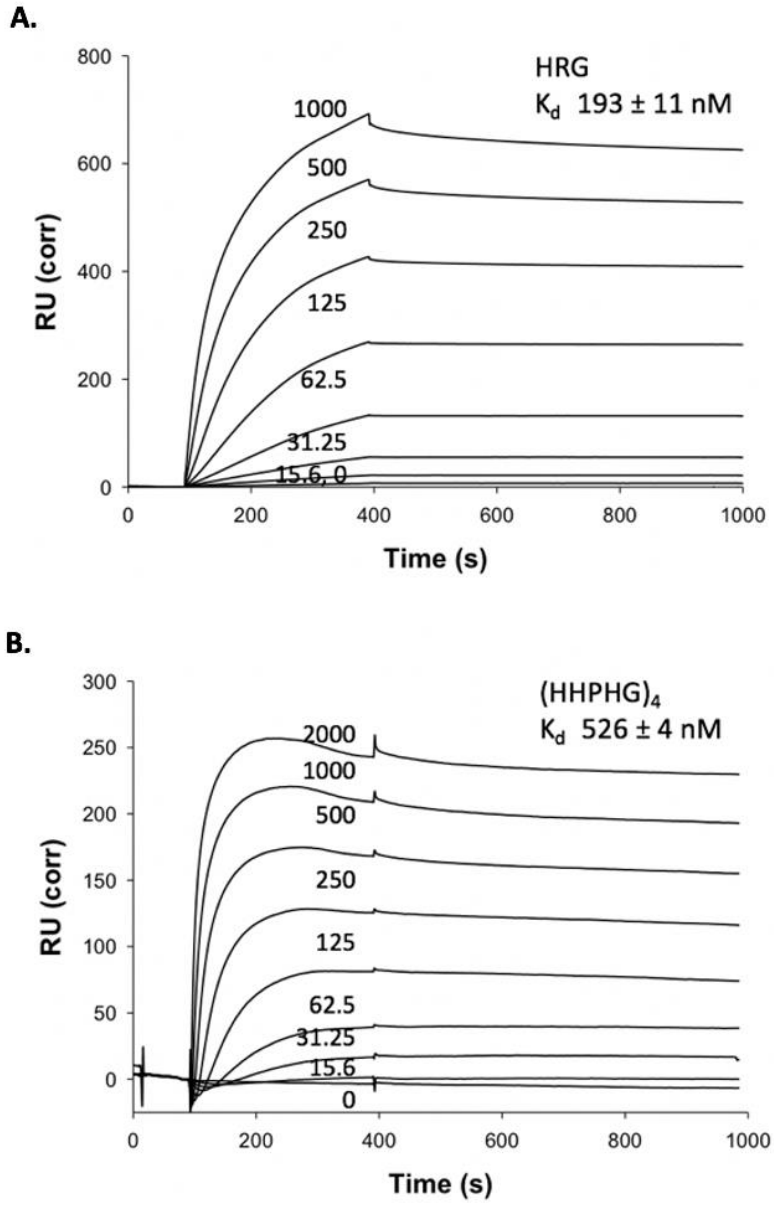
A.
HRG
K_d 193 ± 11 nM
1000
500
250
125
62.5
31.25
15.6, 0
RU (corr)
Time (s)
B.
$(HHPHG)_4$
K_d 526 ± 4 nM
2000
1000
500
250
125
62.5
31.25
15.6
0
RU (corr)
Time (s)

Figure 48: SPR analysis of HRG and $(HHPHG)_4$ binding to polyphosphate

The affinity of HRG (A) and $(HHPHG)_4$ (B) for short chain polyphosphate (70-100 phosphate units) in the presence of 13 μM $ZnCl_2$ was determined by SPR analysis. Immobilized b-polyphosphate adsorbed onto a streptavidin-coated (SA) CM4 sensor chip to 50-100 RU was titrated with increasing concentrations (0-1000 nM) of plasma-derived HRG or (0-2000 nM) of $(HHPHG)_4$. RU values were determined and plotted vs. time. Concentrations of HRG are indicated. Sensorgrams were analyzed with BIAcore T200 evaluation software Version 1.0 (BIAcore). RU values were corrected with SA control flow cell alone (RU (corr)) and plotted vs. time. Dissociation constant (K_d) values were determined from equilibrium values by the BIAcore T200 evaluation software.

8.7 SPR analysis of the FXII and FXIIa interaction with short chain polyphosphate

Given the important role of polyphosphate in triggering FXII autoactivation, as well as other FXIIa-mediated reactions, the affinity of FXIIa for short chain polyP was determined by SPR analysis. In the presence of 13 μM $ZnCl_2$, FXIIa binds to immobilized short chain polyP (100 phosphate units) with high affinity (K_d value of 202 nM) (Figure 49). The zymogen, FXII also binds to polyP with similar affinity (K_d value of 262 nM). Interestingly, polyP exhibited little or no binding to β-FXIIa (K_d value >500 nM). These data suggest that the polyP binding site on FXIIa resides within the non-catalytic heavy chain, which is consistent with recent findings that the EGF1 domain is important for binding to kaolin and polyP (Clark et al., 2020).

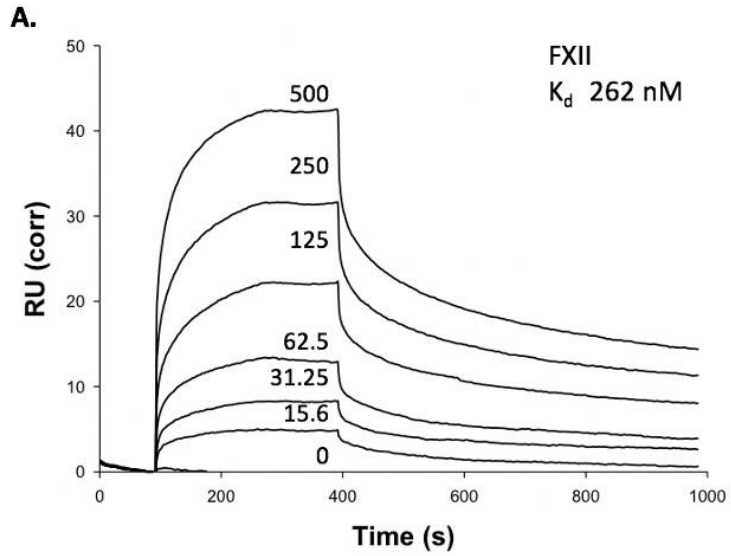
A.
FXII
K_d 262 nM
500
250
125
62.5
31.25
15.6
0
RU (corr)
Time (s)
0
10
20
30
40
50
0
200
400
600
800
1000

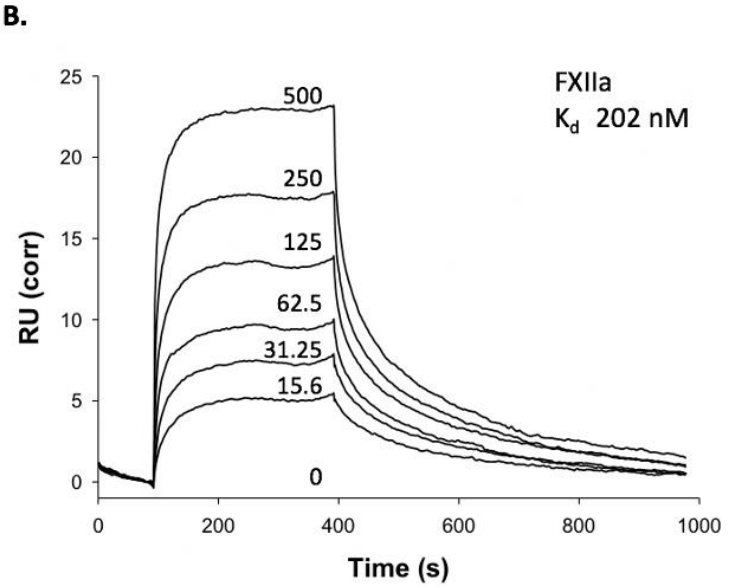
B.
FXIIa
K_d 202 nM
500
250
125
62.5
31.25
15.6
0
RU (corr)
Time (s)
0
5
10
15
20
25
0
200
400
600
800
1000

Figure 49: SPR analysis of FXII and FXIIa binding short chain polyphosphate

The affinity of FXII (A) and FXIIa (B) for short chain polyphosphate in the presence of 13 μM $ZnCl_2$ was determined by SPR analysis. Immobilized b-polyphosphate (polyP) (70-100 phosphate units) adsorbed onto a streptavidin-coated (SA) CM4 sensor chip to 50-100 RU was titrated with increasing concentrations (0 to 500 nM) of FXII or FXIIa. RU values were determined and plotted vs. time. Concentrations of FXII and FXIIa are indicated. Sensorgrams were analyzed with BIAcore T200 evaluation software Version 1.0 (BIAcore). RU values were corrected with SA control flow cell alone (RU (corr)) and plotted vs. time. Dissociation constant (K_d) values were determined from equilibrium values by the BIAcore T200 evaluation software.

9.0 CHAPTER 9: DISCUSSION

Recent interest has focused on components of the contact pathway, particularly FXI and FXII, as potential targets for the development of safer anticoagulants given the bleeding risk that still occurs with DOACs (Weitz, 2016). Indeed, the main objective in anticoagulation therapy is to attenuate thrombosis without affecting hemostasis (Fredenburgh et al., 2017; Weitz, 2016). The identification of physiological activators (ie. DNA, RNA, polyP) of the intrinsic pathway suggests that complementary mechanisms must exist to down regulate this process. However, it remains unclear how this pathway is regulated to prevent uncontrolled clotting. C1-INH is proposed to be the main physiological regulator of FXIIa, through active site inhibition of the protease (Schmaier, 2008; Wagenaar-Bos & Hack, 2006). However, the non-specific and slow rate of FXIIa inhibition by C1-INH suggests that other regulators of FXIIa exist (Agostoni et al., 2004; Cugno et al., 1997; Olson & Gettins, 2011; Wagenaar-Bos & Hack, 2006). FXIIa is protected from inactivation by C1-INH when it is bound to nucleic acids or endothelial cells (Kolyadko et al., 2014; Pixley et al., 1985, 1987; Schousboe, 2003). Interestingly, although patients with either hereditary or acquired C1-INH deficiency demonstrate activation of the coagulation and kallikrein-kinin systems during angioedema attacks, no bleeding diathesis or thrombosis-related complications are described (Cugno et al., 1997; Davis, 2005; Nzeako et al., 2001). Therefore, C1-INH is most likely not the primary inhibitor when it comes to physiological activation of FXIIa, which suggests that other regulators of FXIIa exist.

We have previously shown that HRG regulates the contact pathway by binding FXIIa with high affinity and inhibiting FXII autoactivation and FXIIa-mediated FXI activation (MacQuarrie et al., 2011). In addition, HRG also binds nucleic acids (DNA and RNA) and attenuates their capacity to activate the contact pathway (Vu et al., 2016). This thesis aimed to identify the complementary binding domains of HRG and FXIIa to further elucidate the underlying mechanism of the anticoagulant properties of HRG on the contact pathway. HRG has been proposed to regulate coagulation through its interaction with the activated form of FXII (FXIIa), as HRG does not bind to the zymogen FXII, or to FXI or FIX (MacQuarrie et al., 2011). The binding interaction between HRG and FXIIa is the highest described affinity for any HRG ligand, higher than its affinity for heparin or fibrinogen (Priebatsch, Kvansakul, et al., 2017). The specific and high affinity of HRG for FXIIa, as well as the inhibitory effects of HRG on FXIIa-mediated contact activation imply a potentially significant physiological anticoagulant role for this interaction. However, the mechanism of HRG inhibition of FXIIa is not fully understood and necessitates further investigation. We took several approaches to identify the domain of HRG responsible for FXIIa-mediated contact pathway inhibition including, 1) fragmentation of HRG by limited proteolysis (Chapter 5), 2) generation of recombinant HRG domain constructs (Chapter 6), and 3) synthesis of HRR-derived peptides (Chapter 7). Each experimental approach allowed for the subsequent localization of the inhibitory domain of HRG required for FXIIa-mediated contact activation.

9.1 Fragmentation of HRG domains by limited proteolysis

HRG has a modular structure consisting of two NH_2-terminal cystatin-like domains (N1 and N2), a central histidine-rich region (HRR) flanked by two proline-rich regions (PRR1 and PRR2), and a COOH-terminal domain (COOH) (Jones et al., 2005; Poon et al., 2011). We have previously demonstrated that the affinity of HRG for FXIIa increases 1000-fold in the presence of zinc and that the HRG-FXIIa interaction is abrogated with imidazole, a histidine analogue (MacQuarrie et al., 2011). Based on these findings we hypothesized that the HRG-FXIIa interaction is mediated by the HRR domain of HRG, which is its zinc binding domain. Previous studies have shown that limited proteolysis of HRG by trypsin or plasmin results in the generation of HRG fragments (~30 kDa) and the release of the HRR/PRR domain (Kassaar et al., 2014). Poon *et al*. showed that proteolytic cleavage of HRG by plasmin inhibits the ability of HRG to function as a pH and Zn^{2+} sensor in response to tissue injury (Poon et al., 2009). Indeed, protease cleavage of HRG may provide an additional level of regulation that directs HRG activity (Poon et al., 2009; Thulin et al., 2009).

We show that proteolytically cleaved fragments of HRG (MW ~30-40 kDa) retained inhibitory function. However, prolonged proteolysis resulted in loss of a 37 kDa tryptic HRG fragment, which corresponded with a significant decrease in the inhibitory effect on FXII autoactivation by HRG (Chapter 6). Thus, limited proteolysis of HRG resulted in a loss of function for HRG to inhibit FXIIa. The tryptic band of interest was shown to interact with FXIIa, which suggests that the FXIIa-binding domain of HRG may

be localized within the 37 kDa tryptic fragment. Mass spectrometry data suggest that trypsin digestion of HRG results in cleavage of the HRR/PRR2 and COOH domains, while the N-terminal domains and PRR1 remain intact and resistant to further trypsin digestion. However, due to the challenges of limited proteolysis and limited information provided by mass spectrometry, we were unable to identify the FXIIa binding fragment of HRG using this approach. Accordingly, to further examine the role of the histidine-rich region (HRR), as well as the potential role of other HRG domains in FXII-mediated contact activation, we used recombinant DNA technology to express and purify individual HRG domain constructs in *E coli*.

9.2 Role of HRG domains in FXIIa-mediated contact pathway inhibition

PolyP triggers the contact pathway by providing a surface that binds FXII and HK and induces FXII autoactivation and promotes K activation of FXII (Smith et al., 2006, 2010; van der Vaart & Pretorius, 2008). Here, we show that HRG downregulates the procoagulant activity of platelet-size polyP (70-100 phosphate units) in FXII autoactivation in a dose-dependent and saturable manner (Chapter 7). Like intact HRG, recombinant HRG domain constructs expressing the HRR and PRR2 domains inhibit FXII autoactivation, whereas the remaining domains had significantly lower potencies compared with HRG. These findings suggest that the HRR and PRR2 are the predominant domains of HRG responsible for inhibition of FXII autoactivation mediated by short chain polyP. We have previously shown that HRG addition prolongs the aPTT in HRG-depleted plasma in a FXIIa-dependent manner, but has little effect on the PT (MacQuarrie et al., 2011). Our data

show that like HRG, MBP-HRG domain constructs have at most, a modest effect on the PT, whereas in the aPTT, HRG and MBP-HRR significantly prolonged clotting in HRG-depleted plasma by 8.8- and 7.2-fold, respectively. MBP-PRR2 also prolonged the aPTT by 2.3-fold. These results confirm that the regulatory effect of HRG is localized to the intrinsic pathway of coagulation, and that the anticoagulant properties of HRG are likely mediated through the HRR.

9.3 Inhibition of FXII autoactivation by HRR

Given that the interaction between HRG and FXIIa is zinc-dependent and inhibited by imidazole (a histidine analogue) (MacQuarrie et al., 2011), we hypothesized that histidine-containing HRR analogs would exhibit anticoagulant properties similar to those of HRG. The HRR of HRG contains distinctive tandem repeats of the consensus sequence His-His-Pro-His-Gly (HHPHG) (Jones et al., 2005). To test this hypothesis, we examined the effect synthetic peptides derived from the HRR consensus sequence in various *in vitro* functional assays in both purified and plasma systems (Chapter 8). Previous studies have shown that the antiangiogenic activity of HRG is localized to its histidine-proline-rich domain and that HRR-derived peptides can mimic the antiangiogenic effects of HRG (Doñate et al., 2004). These findings suggest that peptides which correspond to particular sections of the HRR mimic some of the molecular properties associated with HRG or its large proteolytic fragment. Here, we show that HRG inhibits contact activation and exerts its anticoagulant properties at least in part through its HRR domain.

HRG attenuates the capacity of FXIIa to propagate coagulation through autoactivation and subsequent activation of FXI (MacQuarrie et al., 2011). We show that not only does intact HRG inhibit polyP-mediated FXII autoactivation in a dose-dependent and saturable manner (IC_{50} ~200 nM), but HRR-derived peptides are able to do so with greater potency ($1C_{50}$ <25 nM). These findings suggest that the interaction of HRG with polyP and FXIIa is mediated through the HRR, as the peptides had similar inhibitory effects compared with HRG when using various synthetic activators of FXII autoactivation. With dextran sulfate-induced FXII autoactivation, HRR-derived tetramer peptide, $(HHPHG)_4$, as well as poly-His peptides (H-6 and H-12) inhibit FXII autoactivation with potencies similar to that of HRG, whereas the scrambled peptide, $Scr(HAHG)_5H$ was significantly more potent than HRG. In contrast, the effects of HRG and $(HHPHG)_4$ on the inhibition of FXII autoactivation are significantly greater when activation is induced with silica than with dextran sulfate. Moreover, we show that more than one HHPHG repeat is required for inhibition of FXII autoactivation and that the number of His residues within the HRR may be an important determinant of its activity. With either short or long chain polyP, which are physiological activators of FXII, HRG attenuates FXII autoactivation with an IC_{50} of ~200 nM. $(HHPHG)_4$ inhibits FXII autoactivation in the presence of short chain polyP with significantly greater potency than intact HRG or the other HRR peptides. Indeed, HRR analogues inhibit FXII autoactivation with greater potency in the presence of short chain or long chain polyP than intact HRG. Interestingly, the inhibitory effect of HRG and HRR peptides are greater in the presence of long chain polyP than with short chain polyP. These

findings suggest potential differences in how HRG and HRR analogs interact with the various activators, as well as their subsequent effect on FXII autoactivation.

Histidine contains an α-amino group, a carboxylic acid group, and an imidazole side chain, classifying it as a positively charged amino acid at physiological pH. The imidazole side chains of the His residues allow the HRR to bind Zn^{2+} (Priebatsch, Kvansakul, et al., 2017), in addition to promoting binding to negatively charged polyanions, such as nucleic acids and polyP (Vu et al., 2016). With respect to His composition, H-6 and $(HHPHG)_2$ contain 6 His residues. H-12 and $(HHPHG)_4$ contain 12 His residues, whereas the scrambled peptide, $Scr(HAHG)_5H$ contains 11 His residues. The monomer peptide, $(HHPHG)_1$, contains only 3 His residues. The inhibitory effects of the scrambled peptide (11 His residues) and Poly-His peptides (H-6 and H-12) lead us to believe that between 6 to 12 His residues are necessary for HRG to exert its effects on FXIIa-mediated contact activation. Interestingly, when HRR-derived peptides of varying repeats of the HHPHG consensus sequence were examined, there was no significant difference between 2, 3, or 4 repeats, suggesting that the number of His residues is a more important determinant of the inhibitory effect of the domain than the consensus sequence. This is consistent with previous studies studying the antiangiogenic effects of HRR-derived peptides (Doñate et al., 2004; Thulin et al., 2009; Vanwildemeersch et al., 2006). Together, these findings may allow for a greater understanding of the underlying mechanism of how the HRR may be exerting its anticoagulant effects on FXII autoactivation.

9.4 Inhibition of FXIIa-mediated reactions by HRR

We have previously shown that HRG inhibits FXIIa-mediated FXI activation in the presence of Zn^{2+} by more than 95% with an IC_{50} of 287 nM (MacQuarrie et al., 2011). Like HRG, Scr$(HAHG)_5$H and H-12 inhibit FXI activation by more than 90% (Chapter 8). However, Scr$(HAHG)_5$H is significantly more potent than HRG and the remaining HRR-derived peptides. $(HHPHG)_4$ and H-6 inhibit FXI activation by 60%, although the tetramer peptide is significantly more potent. These results show that HRG and HRR analogs significantly attenuate FXIIa-mediated activation of FXI in a dose-dependent and saturable manner. To speculate on the potential mechanism of inhibition by HRG, we look to the binding site of FXI on FXII. The FXI interaction site on FXII is believed to reside within the N-terminal fibronectin type II domain of the FXII heavy chain (amino acids residues 3-19) (Baglia et al., 1993; Citarella et al., 1998), which is presumably exposed when FXII assumes an extended confirmation upon activation by negatively charged surfaces (de Maat & Maas, 2016). The N-terminal domains of FXII also contains binding sites for zinc and endothelial cell interaction (de Maat & Maas, 2016; Stavrou & Schmaier, 2010). Together, these findings suggest that once HRG binds to FXIIa, this interaction not only inhibits FXII autoactivation but prevents activation of FXI by blocking the interaction site on FXIIa.

Given that FXII and prekallikrein comprise an activation feedback loop, the effect of HRG and HRR-derived peptides on FXIIa-mediated activation of prekallikrein was also assessed (Chapter 8). Prekallikrein has two binding sites on FXII, one within the catalytic domain at $Arg_{353}Val_{354,}$ responsible for kallikrein cleavage and the other within the kringle

domain of the heavy chain, which enhances the susceptibility to cleavage by kallikrein (Jukema et al., 2016; Maas et al., 2011; Stavrou & Schmaier, 2010). High molecular weight kininogen acts as an important co-factor for PK activation as well as FXI activation given that HK circulates in complex with FXI (Schmaier, 2016; Thompson et al., 1979). HK and HRG share homology because HK also contain histidine- and glycine-rich regions in the light chain of its protein structure. The $D5_H$ region of HK has been identified as HK's artificial surface binding region, whereby it is able to bind to anionic surfaces, zinc, and heparin (Colman & Schmaier, 1997; Kawasaki et al., 2003). Moreover, the $D6_H$ region of HK allows for PK/FXI binding (Colman & Schmaier, 1997). Interestingly, like HRG, HRR-derived peptides moderately inhibit FXIIa-mediated activation of prekallikrein in a dose-dependent manner by 30% to 60% (Chapter 8). These findings are consistent with previous results from our laboratory where in the absence of HK, HRG was shown to inhibit PK activation by 75% with an IC_{50} of 160 nM. We show that HRG inhibits PK activation in a similar manner by ~50% with the same magnitude of inhibition. Indeed, HRG is significantly more potent than the HRR peptides. These findings suggest that HRR peptides have the ability to mimic the inhibitory effect of HRG on FXIIa-mediated activation of prekallikrein but suggest additional involvement of other domains or the requirement of an intact protein.

The differences in the inhibitory effect of HRG on FXIIa-mediated FXI and PK activation suggest that HRG plays a greater role in regulating the intrinsic pathway of coagulation than the contact pathway/kallikrein-kinin system. These inhibitory differences may provide further insight into the mechanism by which HRG binds to FXIIa and

subsequently exerts its downstream effects on the contact pathway. Moreover, these differences may be due to the differential binding sites on FXIIa for its substrates. Kallikrein and FXIIa cleave FXII at the Arg_{343}-Val_{354} peptide bond within the catalytic domain, thereby generating α-FXIIa, whereas the FXI binding site is proposed to reside within the FNII domain of FXII (de Maat & Maas, 2016; Pathak et al., 2015). Both reactions examined here are greatly enhanced by polyanionic surfaces, such as polyP and dextran sulfate (Gajsiewicz et al., 2017). By binding to FXIIa, HRG may be competing with polyP to inhibit both FXI activation and PK activation by FXIIa. We have previously shown that HRG binds to nucleic acids, and attenuates their procoagulant properties (Vu et al., 2016). HRG may be interacting with both FXIIa and polyP to down-regulate FXIIa-mediated reactions. These differences suggest that HRG preferentially exerts its inhibitory effects on FXIIa-mediated FXI activation, while moderately influencing PK activation by FXIIa. These findings also implicate down-regulation of FXIIa-mediated FXI activation through the inhibition of HRG as a potentially useful antithrombotic approach.

9.5 Anticoagulant properties of HRR in plasma systems

Driven by our initial observations that addition of HRG to plasma prolongs the aPTT but has no effect on the PT, we have since demonstrated that thrombosis is accelerated in HRG-deficient mice and that reconstitution of HRG protects these mice from thrombosis triggered by FXII and nucleic acids (Vu et al., 2015). Here, we show that like HRG, HRR-derived peptides prolong the aPTT, but not the PT in control and HRG-depleted human plasma further supporting the role of the HRR in FXIIa-mediated contact

activation (Chapter 8). The effect of HRG is specific to FXIIa-mediated contact activation and the intrinsic pathway, with no effect in the extrinsic pathway. Furthermore, we show that in HRG-depleted human plasma, HRR-derived peptides prolong and decrease polyP-induced thrombin generation comparably to HRG.

Like HRG, HRR peptides had little to no effect on the PT in control plasma. In contrast, the HRR-derived peptides significantly prolonged the aPTT with potency similar to or greater than that of HRG. $(HHPHG)_4$ and H-12 prolonged the aPTT to a similar extent as HRG. Thus, HRR peptides with higher histidine content (>11 His residues) delayed clotting with a similar or greater extent than HRG. In HRG-depleted plasma, HRG significantly prolonged the aPTT by 10.5-fold whereas $(HHPHG)_4$ and $Scr(HAHG)_5H$ produced a 3.8-fold and 3.4-fold prolongation, respectively. Together, these results confirm that the effect of HRG is localized to the intrinsic pathway of coagulation and they highlight the important role of the HRR domain in modulating the anticoagulant properties of HRG.

Our findings suggest that like HRG, HRR peptides have the capacity to down regulate the procoagulant effect of polyP in human plasma. HRG and HRR peptides significantly prolonged the time to peak thrombin and decreased peak thrombin in a dose-dependent manner. $(HHPHG)_4$ and $Scr(HAHG)_5H$ prolonged the peak thrombin time by 3.1-fold and 3.4-fold, respectively. Further, HRG and HRR peptides decreased peak thrombin up to 2.5-fold in a dose-dependent and saturable manner. These findings are consistent with the anticoagulant effects observed in polyP induced FXII autoactivation with HRG and HRR peptides. Therefore, HRG may be interacting with both FXIIa and polyP to downregulate coagulation.

9.6 Binding of FXIIa and polyphosphate to HRG

In the presence of Zn^{2+}, the affinity of FXIIa for HRG increases by 1000-fold (K_d value of 9 pM) (MacQuarrie et al., 2011; Priebatsch, Kvansakul, et al., 2017). HRG is speculated to bind FXIIa more avidly at sites of vascular injury where there is a localized increase in Zn^{2+}concentration due to its release from the dense granules of activated platelets (MacQuarrie et al., 2011; Renné, 2012). However, this interaction is not Zn^{2+}-dependent, because HRG can still bind FXIIa and modulate clotting even in the absence of Zn^{2+} (K_d value of 1.6 nM at physiological pH) (MacQuarrie et al., 2011; Priebatsch, Kvansakul, et al., 2017; Priebatsch, Poon, et al., 2017). MBP-HRG domain constructs bind to FXIIa with varying affinities, but do not bind to FXII or β-FXIIa (Chapter 9). Like HRG, MBP-HRR binds FXIIa with high affinity. Like MBP-HRR, MBP-N1 and MBP-N1N2 have high affinity for FXIIa, but have high off rates, suggesting relatively weak interaction with FXIIa. In contrast, the remaining domains (MBP-N2, MBP-PRR1/2, MBP-COOH) bind with lower affinity in comparison with HRG to FXIIa. These findings suggest that the interaction of HRG with FXIIa involves multiple domains, whereby the HRR and N1 are the predominant domains binding FXIIa.

Interestingly, HRG-specific and non-specific His-containing peptides inhibit FXII autoactivation to a similar extent as HRG (Chapter 7). These findings suggest that HRG exerts its inhibitory activities on FXIIa through the His residues of the HRR. Binding of HRG to some of its ligands, such as heparin (Borza & Morgan, 1998; Vanwildemeersch et al., 2006) and tropomysin (Doñate et al., 2004; Guan et al., 2004), is believed to be

mediated by the HRR in an interaction that has been proposed to be influenced by the concentration of divalent ions, particularly Zn^{2+} (Borza & Morgan, 1998; Jones et al., 2005). The imidazole side chains of the His residues are thought to extend outward, which allows for multiple Zn^{2+}-binding sites throughout the HRR and PRR domains (Jones et al., 2005; Kassaar et al., 2014). These interactions have been well-documented to have important antiangiogenic, anti-tumour, antibacterial, and antifungal activities mediated by the His-Pro rich domain of HRG (Doñate et al., 2004; Guan et al., 2004; Priebatsch, Kvansakul, et al., 2017; Rydengård et al., 2007, 2008). Binding of HRG and HRR peptides to FXIIa is reversible as the interaction is abrogated with imidazole, suggesting that the interaction with FXIIa is predominately mediated by His residues (Chapter 8). Interestingly, the H-6 and H-12 peptides do not bind to FXIIa. Thus, His residues alone do not appear to provide the necessary conformation required for FXIIa binding. In the absence of Zn^{2+}, HRR peptides do not bind FXIIa, whereas intact HRG still binds, most likely through its N1 domain to a weaker extent.

Although HRG still binds FXIIa in the absence of Zn^{2+}, the role of the divalent metal ion in this setting may provide an essential regulatory link for the anticoagulant activity of HRG on FXIIa activity. As previously mentioned, the Zn^{2+}-dependent interaction between HRG and heparan sulfate is mediated by its NH_2-terminal cystatin domains (Jones et al., 2005; Priebatsch, Kvansakul, et al., 2017). Given that the binding site for Zn^{2+} on HRG is within the HRR domain, this suggests that binding of Zn^{2+} to the HRR has the capacity to modulate other HRG domains. HRG has the ability to exert both pro- and anticoagulant activities by its interaction with its inorganic cofactor Zn^{2+} (Vu et

al., 2013). Transition metals, such as Zn^{2+}, Ni^{2+}, and Cu^{2+}, are regulated by the imidazole side chains of the HRR (Fu & Horn, 2002). Binding of Zn^{2+} to the HRR induces a conformational change in the molecule, increasing the affinity of HRG for a number of molecules, including heparin, fibrinogen, and FXIIa (Kassaar et al., 2015; Vu et al., 2013). HRG binds to the heparin with high affinity (K_d value of 2 nM) in the presence of Zn^{2+} and inhibits the formation of the heparin-AT complex (Barnett et al., 2013; MacQuarrie et al., 2011). Zn^{2+}, serving as a cofactor, interacts with HRG to stimulate HRG-heparin complex formation (Kassaar et al., 2015). The NH_2-terminal cystatin domains of HRG, and not its HRR domain, mediate the Zn^{2+}-dependent interaction with heparan sulfate. This suggests that binding of Zn^{2+} to the HRR domain has the capacity to modulate other domains in HRG. Binding of HRG to heparin neutralizes its anticoagulant activity in both purified and plasma systems, therefore endowing the HRG-heparin interaction with a pro-coagulant effect (Barnett et al., 2013; Fu & Horn, 2002). Here, we see that the Zn^{2+}-mediated interaction between FXIIa and HRG occurs predominately through the HRR domain of HRG with the involvement of the NH_2-terminal cystatin (N1) domain. Heparin interacts with HRG at lower Zn^{2+} concentrations (< 1 µM), whereas higher concentrations of Zn^{2+} (<5 µM) promote binding of HRG to FXIIa (Priebatsch, Kvansakul, et al., 2017). Thus, Zn^{2+} acts as an important regulator of coagulation by mediating the pro- and anticoagulant effects of HRG with heparin and FXIIa, respectively.

Naturally occurring polyphosphates (short chain polyP from activated platelets, 70-100 units; long chain polyP released from bacteria, >1000 units) have been identified as potent activators of the contact pathway. However, their mechanism of interaction with

components of the contact pathway remain elusive. Previous studies have shown that HRG binds to nucleic acids with high affinity (K_d value of 1 nM) most likely through the phosphate head group of phosphatidic acid of DNA and RNA and attenuates their procoagulant activity by competing with contact factors, such as FXII and FXI, for binding to nucleic acids (Priebatsch, Kvansakul, et al., 2017; Vu et al., 2016). Here we show that in the presence of Zn^{2+}, HRG binds to immobilized short chain polyP with high affinity (Chapter 8). In the absence of zinc, HRG binds to polyP with similar affinity, however, there is a 5.3-fold reduction in the capacity of HRG to bind polyP. The histidine-proline rich domains of HRG bind immobilized biotin-polyP (100 phosphate units) with high affinity. MBP-HRR has the highest affinity for short chain polyP with a Kd value of 12 nM. MBP-PRR2 and MBP-COOH have similar affinity for polyP (K_d values 26 nM and 30 nM, respectively). The remaining domains of HRG also bind to polyP, but with lower affinity. Our findings suggest that the histidine-proline rich domains of HRG predominately mediate HRG binding to short chain polyP, whereas the remaining domains assist in the interaction to a lesser extent. In addition, we show that like HRG, HRR-derived peptides bind to short chain polyP with high affinity in a Zn^{2+}-dependent manner. The observed interaction of HRG with polyP suggests that HRG may be attenuating the procoagulant effect by binding to polyP, further supporting a secondary mechanism for the inhibitory effect of HRG on contact activation.

9.7 Binding of HRG and polyphosphate to FXIIa

Neither HRG nor HRR peptides binds to immobilized β-FXIIa or FXII in the absence or presence of Zn^{2+} (Chapter 8). These findings suggest that binding of HRG through the HRR is localized within the non-catalytic heavy chain domain of FXIIa. Consistent with our previous findings, we show that FXIIa binds HRG with a K_d value of 67 ± 0.9 nM. As expected, the heavy chain fragment of FXII binds to HRG with high affinity (K_d value of 19 ± 1.9 nM). This confirms the interaction of HRG with the non-catalytic region of FXIIa and supports the notion that the binding site is encrypted and only exposed when FXII is activated to FXIIa. To further localize the binding site of HRG on FXIIa, we show that the NFE domain of FXII binds HRG with a K_d value of 74 nM ± 0.7 nM, a value similar to that of full-length FXIIa. Retention of the high-affinity interaction in the reverse binding experiment verifies the initial observation of the high-affinity interaction of FXIIa with HRG in the presence of Zn^{2+}. Together, these findings suggest that binding of HRG is localized within the FNII or EGF1 domains of FXII and that FXII fragments of the heavy chain allow for direct binding of HRG to FXII.

The FNII domain serves as a critical negative regulator of FXII activation by shielding the activation loop (catalytic site). The FNII domain also contains the binding site for FXI (Hofman et al., 2020). Our data suggest that the polyP binding site on FXIIa resides within the non-catalytic heavy chain, which is consistent with recent findings that the EGF1 domain is important for FXII binding to kaolin and polyP (Clark et al., 2020). Zn^{2+} binds to FXII through the histidine residues within the FNII-EGF1 and EGF2 domains (Røjkaer

& Schousboe, 1997; Stavrou & Schmaier, 2010). In the presence of $ZnCl_2$, FXIIa binds to immobilized short chain polyP (100 phosphate units) with high affinity. The zymogen FXII also binds to polyP with similar affinity. Interestingly, polyP exhibited little or no binding to β-FXIIa. Thus, these results provide evidence for direct protein interaction between FXII(a) and platelet-size polyP, which is a potent activator of the contact pathway and has been shown to induce thrombosis in murine models (Baker et al., 2018; Renné, 2012; Smith et al., 2012). In addition, the comparable affinity of short chain polyP for both FXII and FXIIa suggests a dynamic role of polyP in not only triggering contact pathway, but potentially modulating downstream events involved in FXII regulation.

9.8 Mechanism of HRG contact pathway inhibition

Here we provide evidence for two potential mechanisms through which HRG modulates the contact pathway. These include by 1) inhibiting FXIIa activity and 2) attenuating the procoagulant effect of polyanions, such as polyP on FXIIa-mediated reactions (Figure 50). Our data show that HRG binds to FXIIa with high affinity in the presence of Zn^{2+}, as well as to short chain polyP. Given that the binding site for Zn^{2+} on HRG is within the HRR domain, this suggests that binding of Zn^{2+} to the HRR has the capacity to modulate other domains in HRG (Priebatsch, Kvansakul, et al., 2017). When zinc or hydrogen ions bind to the PRR-HRR region of HRG they induce local conformational changes that are transmitted throughout the molecule. Such changes are believed to indirectly modulate the binding of the N1N2 and COOH domains to their ligands (Borza et al., 1996; Jones et al., 2005; Priebatsch, Kvansakul, et al., 2017). We

show that the interaction of HRG with FXIIa involves multiple domains, whereby the HRR and N1 are the predominant domains responsible for binding to FXIIa. HRG suppresses the contact pathway by blocking FXII autoactivation, and subsequent FXIIa activation of FXI and PK (Figure 50). It is still unknown whether autoactivation occurs by a) basal amounts of FXIIa activating FXII bound to polyanions or b) through "self-cleavage" of FXII upon induction of a conformational change by its interaction with polyanions (i.e., intra- or inter-molecular). HRG only binds FXIIa and not the zymogen, suggesting that HRG either inhibits inter-molecular FXII autoactivation or possibly binds to an intermediate form of cleaved FXII and prevents it from undergoing complete activation. Thus, the precise mechanism of FXII autoactivation remains elusive and requires further study.

We have previously shown that HRG binds to FXIIa, but not to zymogen FXII or β-FXIIa (MacQuarrie et al., 2011). Here we show that HRG and HRR analogs bind to the heavy chain of FXII, more specifically the NH_2-FNII-EGF1 (NFE) domains of FXII. These findings localize HRG binding within the domains of FXII outside its catalytic domain that are important for contact pathway activation, such as FXI (FNII), polyanions (EGF1) and Zn^{2+} (FNII-EGF1 and EGF2) (Røjkaer & Schousboe, 1997; Stavrou & Schmaier, 2010). In this setting, Zn^{2+} may serve as an additional control element or cofactor for HRG to locally regulate FXIIa activation on the fibrin clot or the removal of FXIIa from the thrombus (Priebatsch, Kvansakul, et al., 2017; Ranieri-Raggi et al., 2014; Vu et al., 2013). In the absence of vascular injury, HRG is unlikely to play a role in hemostasis, as free Zn^{2+} levels in plasma are less than 1 μM, far below the range (6-12 μM) that allows for HRG binding to FXIIa (Priebatsch, Kvansakul, et al., 2017; Vu et al., 2013). However, when FXII is

activated at sites of injury and local levels of Zn^{2+} are elevated in response to platelet activation, HRG can bind to FXIIa with higher affinity (MacQuarrie et al., 2011). Therefore, HRG may serve as an effector of coagulation and be an important regulator of thrombogenesis (MacQuarrie et al., 2011).

Activated platelets release short chain polyP (70-100 phosphate units) from their dense granules and result in the potent activation of the contact pathway through activation of FXII, as well as potentiating the activation of FXI by thrombin (Baker et al., 2018; Fredenburgh et al., 2017). Both HRG and FXII(a) bind to short chain polyP, suggesting a dynamic complex whereby HRG has the capacity to downregulate the procoagulant activity of polyP-induced contact pathway activation. Maas and colleagues recently reported that the EGF1 domain of FXII mediates surface binding as it contains the binding site for kaolin and polyanions (Clark et al., 2020). Interestingly, short chain polyP binds to both FXII and FXIIa with similar affinity, potentially modulating downstream events involved in FXII regulation such as binding to HRG. Our findings suggest that histidine-proline rich domains of HRG predominately mediate HRG binding to short chain polyP. Previous studies have shown that HRG binds to nucleic acids with high affinity (K_d value of 1 nM) most likely through the phosphate head group of phosphatidic acid of DNA and RNA and attenuates their procoagulant activity by competing with contact factors, such as FXII and FXI, for binding to nucleic acids (Priebatsch, Kvansakul, et al., 2017; Vu et al., 2016). The observed interaction of HRG with polyP suggests that HRG may be attenuating the procoagulant effect by binding to polyP, further supporting a secondary mechanism to the inhibitory effect of HRG on contact activation (Figure 50).

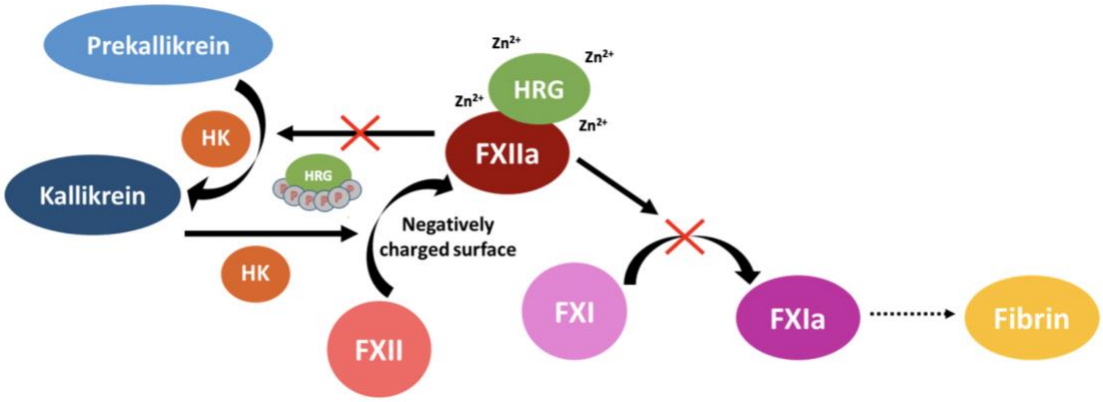
Prekallikrein
HK
Kallikrein
HRG
HK
FXII
Negatively
charged surface
Zn2+
Zn2+
Zn2+
Zn2+
HRG
FXIIa
FXI
FXIa
Fibrin

Figure 50: Mechanism of inhibition of FXIIa-mediated contact activation by HRG

Upon contact with a negatively charged surface, FXII autoactivates to its two-chain activated form, FXIIa. HRG (green) binds to FXIIa (red) with high affinity in the presence of Zn^{2+}, as well as to short chain polyP (grey). HRG down regulates the contact pathway by two potential mechanisms including 1) inhibiting FXIIa activity and 2) attenuating the procoagulant effect of polyanions, such as polyP on FXIIa-mediated reactions. The anticoagulant effects of HRG are predominately mediated by its Zn^{2+}-binding HRR domain, which binds to the heavy chain of FXIIa and to short chain polyP. Inhibition of FXIIa by HRG subsequently attenuates FXIIa-mediated activation of FXI (intrinsic pathway) and prekallikrein (kallikrein-kinin system). HRG, histidine-rich glycoprotein; FXII/a, factor XII/a; FXI/a, factor XI/a; HK, high molecular weight kininogen; Zn^{2+}, zinc

9.9 CONCLUSION

In summary, these findings build on the proposed mechanism of how HRG exerts its anticoagulant properties, whereby HRG modulates the contact pathway by inhibiting FXIIa activity (MacQuarrie et al., 2011), as well as attenuating the procoagulant effect of polyanions, such as polyP (Vu et al., 2016). We have identified the complementary binding domains of HRG and FXIIa to be localized within the HRR domain of HRG and NFE domains of FXIIa. Moreover, we show that the HRR binds to short chain polyP with high affinity, suggesting a dynamic complex between HRG, FXIIa, and polyP on activated platelets. The interaction between HRG and FXIIa provides the basis of a novel physiological anticoagulant mechanism that is not fully understood and necessitates further elucidation. An emerging frontier of anticoagulant therapy involves the contact pathway, particularly FXII and FXI, as potential targets in the development of safer anticoagulants (Bickmann et al., 2017; Fredenburgh et al., 2017; Gailani et al., 2015; Müller, Gailani, & Renne, 2011; Weitz, 2016; Weitz & Fredenburgh, 2017a). Our data support the emerging data that HRG has an important regulatory role as a physiological modulator of FXIIa in thrombogenesis, as well as other processes such as angiogenesis, inflammation, and immunity (Poon et al., 2011; Priebatsch, Kvansakul, et al., 2017). Exploiting the importance of the interaction between HRG and FXIIa may allow us to develop novel therapeutic strategies to treat thrombotic disorders. Indeed, we show that synthetic HRR peptides have the capacity to recapitulate the anticoagulant effects of HRG by down regulating the contact pathway. Future studies that reveal the important binding sites for FXIIa and polyanions, such as polyP and nucleic acids on HRG may provide attractive targets for therapeutic intervention. For

example, developing small molecule inhibitors of FXIIa targeting the HRG-FXIIa binding sites may serve to be as or more effective as intact HRG. Therefore, further examination of the role of the HRR will serve to provide greater insight into the antithrombotic potential of HRR analogs in attenuating thrombosis without disrupting hemostasis.

10.0 CHAPTER 10: FUTURE DIRECTIONS

Although we have demonstrated that HRG serves as a potent inhibitor of the contact pathway through its interaction with FXIIa and polyP, there are several avenues of research that would broaden our understanding of its physiological functions, clinical relevance and therapeutic potential. This section proposes 3 such projects aimed at increasing our understanding of: (i) the interaction of the histidine-rich region (HRR) with FXIIa, to further localize the complementary binding sites; (ii) the role of Zn^{2+} in the regulation of the antithrombotic function of HRG; and (iii) the effect of HRR analogs in a polyP-induced murine model of thrombosis to complement our *in vitro* studies.

10.1 Project #1: Structural characterization of the binding sites on the histidine-rich region of HRG and heavy chain of FXIIa

10.1.1 Rationale:

Structural studies of HRG domains have been limited due to the intrinsically disordered, heavily glycosylated and insoluble nature of HRG. To date, only the N2 domain of HRG has been crystallized by Kassaar *et al*. using serum-purified rabbit HRG (Kassaar et al., 2014). The authors confirm that the N2, along with the N1 domain, possesses a cystatin-like fold composed of 5-stranded antiparallel β-sheets wrapped around a 5-turn α-helix (Kassaar et al., 2014). The histidine- and proline-rich regions are predicted to be intrinsically disordered but N1, N2, and the COOH domains are likely to have ordered structures (Poon et al., 2011). The secondary structure of the HRR domain is predicted to

have a helical and elongated core with protruding imidazole side chains that form metal binding sites, for metal ions such as Zn^{2+} and Ca^{2+} (Poon et al., 2009). As mentioned previously, the HRR (53% histidine residues) is similar to the His-rich region of HK and contain very few hydrophobic and basic amino acids (Borza et al., 1996). In contrast, structural studies have been performed to determine the crystal structures for the FXII protease domain, fibronectin type I and II domains (FNI, FNII), and epidermal growth factor-like domains (EGF) (Dementiev et al., 2018; Kaira et al., 2020; Pathak et al., 2015, 2019). We have shown that HRR analogs bind to the heavy chain of FXIIa with high affinity (Chapter 8), localizing the binding sites to the HRR domain of HRG and the N-terminal FNII-EGF1 domains (NFE) on the heavy chain (HC) of FXIIa. Thus, to further localize the binding sites on the HRR of HRG and HC of FXIIa, protein crystallization and structural analysis will be necessary.

10.1.2 Aim 1: Protein crystallization and structural analysis of HRG-FXIIa interacting domains (HRR-FXIIa interaction)

To further examine the HRG-FXIIa protein-protein interaction, co-crystallization experiments will be performed using either recombinant HRR domain or synthetic HRR-derived peptide, $(HHPHG)_4$ with recombinant FXII fragments of the heavy chain (NFE, FEK, full-length HC) in the absence or presence of Zn^{2+} (6-12µM). Our data suggest the involvement of the N-terminal cystatin-like domains in the FXIIa interaction. Thus, recombinant domains of N1, N2, and N1N2 of HRG will also be investigated by protein crystallization by co-localization with fragments of the heavy chain of FXIIa. Experiments

will be performed in collaboration with Dr. Jonas Emsley (University of Nottingham, UK) as similarly described (Kaira et al., 2020). Briefly, purified samples will be first dialyzed into Tris-buffered saline. Crystallization experiments will be performed using sparse matrix screens (Qiagen) in sitting drop plates. Crystals will be observed in conditions of 0.1M HEPES (pH 7.5), 1.6M $(NH_4)_2SO_4$, and 2% (w/v) poly(ethylene glycol) 1000 as previously described (Pathak et al., 2015). Single crystals will be transferred to a reservoir solution containing 25% glycerol, and flash cooled in liquid nitrogen. Diffraction data will be collected at DIAMOND beamline I04 and structures will be determined by molecular replacement (PHASER) with coordinates from the Protein Data Bank. Models will be built with map-fitting software program, COOT (Emsley & Cowtan, 2004) and refined with REFMAC (Pathak et al., 2015). Some limitations in this study may arise due to the low solubility and intrinsically disordered nature of the HRR, which may result in fragile crystals that are difficult to handle or diffract to low resolution and suffer from radiation damage during the diffraction experiment (Carpenter et al., 2008). To overcome potential challenges, co-crystallization studies will be conducted with smaller fragments of the interacting protein-protein domains of interest, rather than intact protein to allow for greater crystallization yield and experimental results. Based on our current findings, we expect that the binding sites for the HRR-HC interaction will involve approximately 10-12 histidine residues of the HRR of HRG and be localized within the zinc- and FXI-binding FNII domain of FXIIa.

10.2 Project #2: Role of Zn^{2+} in the regulation of the antithrombotic function of HRG

10.2.1 Rationale:

The surrounding environment plays an important role in controlling the function of HRG through changes in pH levels and Zn^{2+} coordination, which subsequently regulate ligand recognition (Priebatsch, Kvansakul, et al., 2017). As such, HRG is commonly defined as a pH and Zn^{2+}-sensing adaptor molecule (Borza & Morgan, 1998; Priebatsch, Poon, et al., 2017). Zn^{2+} has the capacity to serve as both a cofactor for FXII activation and an inhibitor of FXIIa, suggesting that Zn^{2+} provides a regulatory switch for control of the contact pathway (Kassaar et al., 2015; Vu et al., 2013). Our data show that HRG and HRR analogs bind with high affinity to FXIIa in the presence of Zn^{2+} (Chapter 7). HRG binds to Zn^{2+} with a Kd ranging between 4 µM to 12 µM, with a suggestive stoichiometry of 10 (MacQuarrie et al., 2011; Priebatsch, Poon, et al., 2017), which coincides with plasma Zn^{2+} concentration upon release from dense granules of activated platelets (Henderson et al., unpublished data). Given that the binding site for Zn^{2+} on HRG is within the HRR domain, this suggests that binding of Zn^{2+} to the HRR has the capacity to modulate other domains in HRG (Priebatsch, Kvansakul, et al., 2017). When zinc or hydrogen ions bind to the PRR-HRR region of HRG, they induce local conformational changes that are transmitted throughout the molecule. Such changes are believed to indirectly modulate the binding of the N1N2 and COOH domains to their ligands (Borza et al., 1996; Jones et al., 2005; Priebatsch, Kvansakul, et al., 2017). Thus, further investigation of the regulatory role of

Zn^{2+} will allow for better understanding of the underlying mechanism of the HRG-FXIIa interaction in contact pathway inhibition.

10.2.2 Aim 1: Characterization of Zn^{2+}-binding domains on HRG and FXIIa

Using a fluorescent Zn^{2+}-binding probe (FluoZin^{TM}-1, ThermoFisher Scientific), binding affinities of individual domains of HRG and FXIIa for Zn^{2+} will be determined. Recombinant HRG domains constructs (MBP-N1, MBP-N2, MBP-N1N2, MBP-PRR1, MBP-HRR, MBP-PRR2, MBP-COOH), as well as synthetic HRR-derived peptides $(HHPHG)_1$, $(HHPHG)_4$, Scr$(HAHG)_5$H, and poly-His peptides (H-6, H-12) will be examined to determine the Zn^{2+}-binding domain(s) of HRG. Experiments will be performed in tricine-buffered saline, as tricine serves as a Zn^{2+} buffering system by maintaining the free Zn^{2+}-concentration at a constant level in the presence of Zn^{2+}-binding proteins (Low et al., 2000). Fluorescence monitoring of FluoZin-1 will be performed using a LS 50B fluorescence spectrometer as previously described (Henderson et al., 2015). Based on our current findings, we expect that HRR analogs will have similar or greater affinity for Zn^{2+} in comparison with intact HRG. Given the involvement of the N1 domain in our in vitro studies, it would be expected that this domain would also interact with Zn^{2+}, but with lower affinity, whereas the remaining domains do not bind to Zn^{2+}.

There are four Zn^{2+} binding sites on FXII, whereby one binding site is lost when FXII is converted to α-FXIIa, and further conversion to β-FXIIa results in the complete loss of Zn^{2+} binding (Kaira et al., 2020). The Zn^{2+} binding sites are suggested to reside within the FNII domain (residues 40-44 and 78-82), and residues 94-131 in EGF1 domain

and residues 174-176 in EGF2 domain (Kaira et al., 2020; Stavrou & Schmaier, 2010). These findings suggest that Zn^{2+} interacts predominantly with the heavy chain of FXII, and not the catalytic domain of FXII. Thus, parallel experiments will be performed to determine the affinity of individual FXII heavy chain domains (FNII, EGF1, FNI, EGF2, PR) for Zn^{2+}. Controls will include β-FXIIa, which contains only the catalytic light chain of FXII and the heavy chain remnant. Based on our current understanding of the potential Zn^{2+}-binding domains of FXII, we expect that the FNII domain of FXIIa will have the greatest affinity for Zn^{2+}, as well as the EGF1/2 domains, but with lower affinity. These findings will provide further understanding of the role of Zn^{2+} in not only surface binding and activation of FXII, but its role in regulating FXIIa inhibition by HRG.

10.3 Project #3: Characterization of HRR analogs in polyphosphate induced murine thrombosis model

10.3.1 Rationale:

HRG is a potent inhibitor of polyP induced FXII autoactivation in the presence of elevated Zn^{2+} levels due to local platelet activation. HRG and HRR analogs binds to platelet-size polyP (70-100 phosphate units) with high affinity (Chapter 8) and prolong the peak thrombin time in and decreased the peak thrombin generation by 2.5-fold in polyP induced thrombin generation in HRG-depleted human plasma (Chapter 7). Thus, like HRG, HRR peptides have the capacity to down regulate the procoagulant effect of polyP in human plasma. Recent findings from our laboratory (Malik et al., 2020; manuscript in progress) show that intraperitoneal injection of polyP enhances peak thrombin generation, increases

thrombin-antithrombin complexes (TAT) levels, reduces lung perfusion, and promotes pulmonary fibrin deposition to a greater extent in HRG knockout ($HRG^{-/-}$) mice compared with wildtype (WT) mice. Moreover, these prothrombotic effects were shown to be FXII-dependent as these effects were attenuated by FXII-specific antisense oligonucleotide (ASO) knockdown prior to polyP injection. Thus, HRG binds polyP via the HRR and attenuates its prothrombotic activity in a FXII dependent manner. Further examination of the antithrombotic role of the HRR in polyP-driven contact activation would provide greater understanding of the secondary mechanism via which HRG modulates the intrinsic pathway of coagulation and attenuates thrombosis.

10.3.2 Aim 1: Characterization of HRR-derived peptides in polyphosphate induced $HRG^{-/-}$ mice thrombosis model

The antithrombotic effects of HRR analogs will be investigated in $HRG^{-/-}$ mice to determine whether like intact HRG, synthetic HRR-derived peptides have the capacity to rescue the prothrombotic phenotype in the polyP-induced thrombosis model. This study will enable us to compare the potencies of the synthetic HRR-derived tetramer peptide, $(HHPHG)_4$ to that of intact HRG. A pilot study will first be conducted to determine optimal dosing of synthetic peptides, whereby $(HHPHG)_4$ or $(HHPHG)_1$ will be injected intravenously at concentrations between 0 and 15 µM (anticipated plasma level). Blood samples will be collected from the inferior vena cava (IVC) to measure levels of the synthetic peptides and to determine optimal concentration for study. We have previously determined the optimal dose of purified HRG at 5.8 mg/kg body weight, which is within

physiological plasma concentration (1-3 μM) (Vu et al., 2015). Once optimal dosing has been determined for synthetic peptides, $HRG^{-/-}$ mice will be given intravenous injection of either purified HRG, or synthetic $(HHPHG)_4$ or $(HHPHG)_1$ peptides 5 min prior to intraperitoneal (IP) polyP (100 mg/kg) or an equivalent volume of saline. Wildtype (WT; C57BL/6) mice will be used as control to compare HRG plasma levels. Blood samples will be collected at various time intervals (15, 30, 60 min) to determine thrombin generation and TAT levels. After 60 min, lung tissue will be fixed in 10% formalin and embedded in paraffin. Fibrin deposition will be assessed by immunohistochemistry. As a control, we will also assess the effect of these fragments on bleeding in a tail amputation model. Although we have determined the optimal route of polyP injection into $HRG^{-/-}$ mice, one limitation would be the variable concentration of circulating polyP plasma levels due to IP injection. To measure polyP plasma levels, blood samples will be collected and thrombin generation of plasma samples from IP-injected polyP-induced $HRG^{-/-}$ mice will be performed to ensure sufficient levels of polyP are obtained. Based on our current findings, HRG and HRR-derived peptides will decrease thrombus formation and fibrin deposition in polyP-induced $HRG^{-/-}$ mice thrombosis model. This study will provide *in vivo* evidence of the capacity of HRG and HRR analogs to downregulate FXIIa-mediated contact activation and polyP-induced thrombosis.

LIST OF REFERENCES

Abildgaard, U. (1969). Binding of thrombin to antithrombin III. *Scandinavian Journal of Clinical and Laboratory Investigation*, *24*(1), 23–27. https://doi.org/10.3109/00365516909080127

Agostoni, A., Aygören-Pürsün, E., Binkley, K. E., Blanch, A., Bork, K., Bouillet, L., Bucher, C., Castaldo, A. J., Cicardi, M., Davis, A. E., De Carolis, C., Drouet, C., Duponchel, C., Farkas, H., Fáy, K., Fekete, B., Fischer, B., Fontana, L., Füst, G., … Zingale, L. (2004). Hereditary and acquired angioedema: Problems and progress: Proceedings of the third C1 esterase inhibitor deficiency workshop and beyond. *Journal of Allergy and Clinical Immunology*, *114*(3 Suppl.), 51–131. https://doi.org/10.1016/j.jaci.2004.06.047

Amphlett, G. W., Kisiel, W., & Castellino, F. J. (1981). Interaction of Calcium with Bovine Plasma Protein C. *Biochemistry*, *20*(8), 2156–2161. https://doi.org/10.1021/bi00511a013

Bäck, J., Lang, M. H., Elgue, G., Kalbitz, M., Sanchez, J., Nilsson Ekdahl, K., & Nilsson, B. (2009). Distinctive regulation of contact activation by antithrombin and C1-inhibitor on activated platelets and material surfaces. *Biomaterials*, *30*(34), 6573–6580. https://doi.org/10.1016/j.biomaterials.2009.07.052

Badimon, L., Padró, T., & Vilahur, G. (2012). Atherosclerosis, platelets and thrombosis in acute ischaemic heart disease. *European Heart Journal: Acute Cardiovascular Care*, *1*(1), 60–74. https://doi.org/10.1177/2048872612441582

Baglia, F. A., Jameson, B. A., & Walsh, P. N. (1993). Identification and characterization of a binding site for factor XIIa in the Apple 4 domain of coagulation factor XI. *The Journal of Biological Chemistry*, *268*(6), 3838–3844. http://www.ncbi.nlm.nih.gov/pubmed/8440679

Baker, C. J., Smith, S. A., & Morrissey, J. H. (2018). Polyphosphate in thrombosis, hemostasis, and inflammation. *Research and Practice in Thrombosis and Haemostasis*, *3*(1), 18–25. https://doi.org/10.1002/rth2.12162

Barnett, J. P., Blindauer, C. A., Kassaar, O., Khazaipoul, S., Martin, E. M., Sadler, P. J., & Stewart, A. J. (2013). Allosteric modulation of zinc speciation by fatty acids. *Biochimica et Biophysica Acta (BBA) - General Subjects*, *1830*(12), 5456–5464. https://doi.org/10.1016/J.BBAGEN.2013.05.028

Beckman, M. G., Hooper, W. C., Critchley, S. E., & Ortel, T. L. (2010). Venous Thromboembolism. A Public Health Concern. *American Journal of Preventive Medicine*, *38*(4 Suppl). https://doi.org/10.1016/j.amepre.2009.12.017

Bentzon, J. F., Otsuka, F., Virmani, R., & Falk, E. (2014). Mechanisms of Plaque Formation and Rupture. *Circulation Research*, *114*(12), 1852–1866. https://doi.org/10.1161/CIRCRESAHA.114.302721

Bergqvist, D. (2006). Review of fondaparinux sodium injection for the prevention of venous thromboembolism in patients undergoing surgery. *Vascular Health and Risk Management*, *2*(4), 365–370. https://doi.org/10.2147/vhrm.2006.2.4.365

Bernardo, M. M., Day, D. E., Olson, S. T., & Shore, J. D. (1993). Surface-independent acceleration of factor XII activation by zinc ions. *Journal of Biological Chemistry*, *268*(17), 12468–12476.

Bickmann, J. K., Baglin, T., Meijers, J. C. M., & Renné, T. (2017). Novel targets for anticoagulants lacking bleeding risk. *Current Opinion in Hematology*, *24*(5), 419–426. https://doi.org/10.1097/MOH.0000000000000367

Blajchman, M. A. (1994). An overview of the mechanism of action of antithrombin and its inherited deficiency states. *Blood Coagulation and Fibrinolysis*, *5*(Suppl 1). https://doi.org/10.1097/00001721-199401000-00002

Bloom, J. W., Nesheim, M. E., & Mann, K. G. (1979). Phospholipid-Binding Properties of Bovine Factor V and Factor Va. *Biochemistry*, *18*(20), 4419–4425. https://doi.org/10.1021/bi00587a023

Bolin, M., Akerud, P., Hansson, A., & Akerud, H. (2011). Histidine-Rich Glycoprotein as an Early Biomarker of Preeclampsia. *American Journal of Hypertension*, *24*(4), 496–501. https://doi.org/10.1038/ajh.2010.264

Borza, D. B., & Morgan, W. T. (1998). Histidine-proline-rich glycoprotein as a plasma pH sensor: Modulation of its interaction with glycosaminoglycans by pH and metals. *Journal of Biological Chemistry*, *273*(10), 5493–5499. https://doi.org/10.1074/jbc.273.10.5493

Borza, D. B., Shipulina, N. V., & Morgan, W. T. (2004). Effects of histidine-proline-rich glycoprotein on plasminogen activation in solution and on surfaces. *Blood Coagulation and Fibrinolysis*, *15*(8), 663–672. https://doi.org/10.1097/00001721-200412000-00006

Borza, D. B., Tatum, F. M., & Morgan, W. T. (1996). Domain structure and conformation of histidine-proline-rich glycoprotein. *Biochemistry*, *35*(6), 1925–1934. https://doi.org/10.1021/bi952061t

Brill, A., Fuchs, T. A., Savchenko, A. S., Thomas, G. M., Martinod, K., De Meyer, S. F., Bhandari, A. A., & Wagner, D. D. (2012). Neutrophil extracellular traps promote deep vein thrombosis in mice. *Journal of Thrombosis and Haemostasis : JTH*, *10*(1), 136–144. https://doi.org/10.1111/j.1538-7836.2011.04544.x

Bussey, H., Francis, J. L., & Consensus Group, T. H. (2004). Heparin Overview and Issues. *Pharmacotherapy*, *24*(8 Part 2), 103S-107S. https://doi.org/10.1592/phco.24.12.103S.36109

Cade, W. T. (2008). Diabetes-related microvascular and macrovascular diseases in the physical therapy setting. *Physical Therapy*, *88*(11), 1322–1335. https://doi.org/10.2522/ptj.20080008

Carpenter, E. P., Beis, K., Cameron, A. D., & Iwata, S. (2008). Overcoming the

challenges of membrane protein crystallography. *Current Opinion in Structural Biology*, *18*(5), 581–586. https://doi.org/10.1016/j.sbi.2008.07.001

Carpenter, S. L., & Mathew, P. (2008). α2-antiplasmin and its deficiency: Fibrinolysis out of balance. *Haemophilia*, *14*(6), 1250–1254. https://doi.org/10.1111/j.1365-2516.2008.01766.x

Chandra, T., Stackhouse, R., Kidd, V. J., & Woo, S. L. C. (1983). Isolation and sequence characterization of a cDNA clone of human antithrombin III. *Proceedings of the National Academy of Sciences of the United States of America*, *80*(7 I), 1845–1848. https://doi.org/10.1073/pnas.80.7.1845

Choi, S. H., Smith, S. A., & Morrissey, J. H. (2011). Polyphosphate is a cofactor for the activation of factor XI by thrombin. *Blood*, *118*(26), 6963–6970. https://doi.org/10.1182/blood-2011-07-368811

Chu, A. J. (2010). Blood coagulation as an intrinsic pathway for proinflammation: a mini review. *Inflammation & Allergy Drug Targets*, *9*(1), 32–44. https://doi.org/10.2174/187152810791292890

Citarella, F., Fedele, G., Roem, D., Fantoni, A., & Hack, C. E. (1998). The second exon-encoded factor XII region is involved in the interaction of factor XII with factor XI and does not contribute to the binding site for negatively charged surfaces. *Blood*, *92*(11), 4198–4206.

Clark, C. C., Hofman, Z. L. M., Sanrattana, W., den Braven, L., de Maat, S., & Maas, C. (2020). The Fibronectin Type II Domain of Factor XII Ensures Zymogen Quiescence. *Thromb Haemost*, *120*(3), 400–411.

Colman, R. W. (2006). Are hemostasis and thrombosis two sides of the same coin? *Journal of Experimental Medicine*, *203*(3), 493–495. https://doi.org/10.1084/jem.20060217

Colman, R. W., & Schmaier, A. H. (1997). Contact system: a vascular biology modulator with anticoagulant, profibrinolytic, antiadhesive, and proinflammatory attributes. *Blood*, *90*(10), 3819–3843. http://www.bloodjournal.org/content/90/10/3819.abstract

Comin, J., & Kallmes, D. F. (2012). Dabigatran (Pradaxa). *American Journal of Neuroradiology*, *33*(3), 426–428. https://doi.org/10.3174/ajnr.A3000

Conners, M. S., & Money, S. R. (2002). The new heparins. *Ochsner Journal*, *4*(1), 41–47. https://doi.org/10.1097/00019501-199802000-00002

Costa, S., Almeida, A., Castro, A., & Domingues, L. (2014). Fusion tags for protein solubility, purification, and immunogenicity in Escherichia coli: The novel Fh8 system. *Frontiers in Microbiology*, *5*(63), 1–20. https://doi.org/10.3389/fmicb.2014.00063

Crosby, J. R., Marzec, U., Revenko, A. S., Zhao, C., Gao, D., Matafonov, A., Gailani, D., MacLeod, A. R., Tucker, E. I., Gruber, A., Hanson, S. R., & Monia, B. P. (2013). Antithrombotic effect of antisense factor XI oligonucleotide treatment in primates. *Arteriosclerosis, Thrombosis, and Vascular Biology*, *33*(7), 1670–1678.

https://doi.org/10.1161/ATVBAHA.113.301282

Cugno, M., Cicardi, M., Bottasso, B., Coppola, R., Paonessa, R., Mannucci, P. M., & Agostoni, A. (1997). Activation of the coagulation cascade in C1-inhibitor deficiencies. *Blood*, *89*(9), 3213–3218. http://www.bloodjournal.org/content/89/9/3213.abstract

Dahlbäck, B., Guo, L. J., Livaja-Koshiar, R., & Tran, S. (2018). Factor V-short and protein S as synergistic tissue factor pathway inhibitor (TFPIα) cofactors. *Research and Practice in Thrombosis and Haemostasis*, *2*(1), 114–124. https://doi.org/10.1002/rth2.12057

Dahlbäck, B., & Villoutreix, B. O. (2005). The anticoagulant protein C pathway. In *FEBS Letters* (Vol. 579, Issue 15, pp. 3310–3316). https://doi.org/10.1016/j.febslet.2005.03.001

Davis, A. E. (2005). The pathophysiology of hereditary angioedema. *Clinical Immunology*, *114*(1), 3–9. https://doi.org/10.1016/j.clim.2004.05.007

de Agostini, A., Lijnen, H. R., Pixley, R. A., Colman, R. W., & Schapira, M. (1984). Inactivation of factor XII active fragment in normal plasma. Predominant role of C1-inhibitor. *Journal of Clinical Investigation*, *73*(6), 1542–1549. https://doi.org/10.1172/JCI111360

De Caterina, R., Husted, S., Wallentin, L., Andreotti, F., Arnesen, H., Bachmann, F., Baigent, C., Huber, K., Jespersen, J., Kristensen, S. D., Lip, G. Y. H., Morais, J., Rasmussen, L. H., Siegbahn, A., Verheugt, F. W. A., & Weitz, J. I. (2013). Vitamin K antagonists in heart disease: Current status and perspectives (Section III): Position paper of the ESC working group on thrombosis - Task force on anticoagulants in heart disease. *Thrombosis and Haemostasis*, *110*(6), 1087–1107. https://doi.org/10.1160/TH13-06-0443

de Maat, S., & Maas, C. (2016). Factor XII: form determines function. *Journal of Thrombosis and Haemostasis*, *14*(8), 1498–1506. https://doi.org/10.1111/jth.13383

Deloughery, E. P., Olson, S. R., Puy, C., McCarty, O. J. T., & Shatzel, J. J. (2019). The Safety and Efficacy of Novel Agents Targeting Factors XI and XII in Early Phase Human Trials. *Seminars in Thrombosis and Hemostasis*, *45*(5), 502–508. https://doi.org/10.1055/s-0039-1692439

Dementiev, A., Silva, A., Yee, C., Li, Z., Flavin, M. T., Sham, H., & Partridge, J. R. (2018). Structures of human plasma β-factor XIIa cocrystallized with potent inhibitors. *Blood Advances*, *2*(5), 549–558. https://doi.org/10.1182/bloodadvances.2018016337

Desai, U. R. (2004). New Antithrombin-Based Anticoagulants. *Med Res Rev*, *24*(2), 151–181. https://doi.org/10.1002/med.10058

Dickneite, G., & Mescheder, A. (2000). Antithrombin III and Tissue Factor Pathway Inhibitor: Two Physiologic Protease Inhibitors of the Coagulation System. *Multiple Organ Failure*, 505–513. https://doi.org/10.1007/978-1-4612-1222-5_50

Doñate, F., Juarez, J. C., Guan, X., Shipulina, N. V, Plunkett, M. L., Tel-Tsur, Z., Shaw, D. E., Morgan, W. T., & Mazar, A. P. (2004). Peptides Derived from the Histidine-Proline Domain of the Histidine-Proline-Rich Glycoprotein Bind to Tropomyosin and Have Antiangiogenic and Antitumor Activities. *Cancer Research*, *64*, 5812–5817. https://doi.org/0.1158/0008-5472.CAN-04-0440

Drasin, T., & Sahud, M. (1996). Blood-type and age affect human plasma levels of histidine-rich glycoprotein in a large population. *Thrombosis Research*, *84*(3), 179–188. https://doi.org/10.1016/0049-3848(96)00174-0

Eitzman, D. T., Westrick, R. J., Bi, X., Manning, S. L., Wilkinson, J. E., Broze, G. J., & Ginsburg, D. (2002). Lethal perinatal thrombosis in mice resulting from the interaction of tissue factor pathway inhibitor deficiency and factor V Leiden. *Circulation*, *105*(18), 2139–2142. https://doi.org/10.1161/01.CIR.0000017361.39256.82

Emsley, P., & Cowtan, K. (2004). Coot: Model-building tools for molecular graphics. *Acta Crystallographica Section D: Biological Crystallography*, *60*, 2126–2132. https://doi.org/10.1107/S0907444904019158

Eriksson, B. I., Quinlan, D. J., & Weitz, J. I. (2009). Comparative Pharmacodynamics and Pharmacokinetics of Oral Direct Thrombin and Factor Xa Inhibitors in Development. In *Clin Pharmacokinet* (Vol. 48, Issue 1).

Esmon, C. T. (2000). Regulation of blood coagulation. *Biochimica et Biophysica Acta - Protein Structure and Molecular Enzymology*, *1477*(1–2), 349–360. https://doi.org/10.1016/S0167-4838(99)00266-6

Esmon, C. T. (2004). Crosstalk between inflammation and thrombosis. *Maturitas*, *47*(4), 305–314. https://doi.org/10.1016/j.maturitas.2003.10.015

Esmon, C. T., & Esmon, N. L. (2011). The Link Between Vascular Features and Thrombosis. *Annual Review of Physiology*, *73*(1), 503–514. https://doi.org/10.1146/annurev-physiol-012110-142300

Fang, J., Ruiz, F. A., Docampo, M., Luo, S., Rodrigues, J. C. F., Motta, L. S., Rohloff, P., & Docampo, R. (2007). Overexpression of a Zn2+-sensitive soluble exopolyphosphatase from Trypanosoma cruzi depletes polyphosphate and affects osmoregulation. *Journal of Biological Chemistry*, *282*(44), 32501–32510. https://doi.org/10.1074/jbc.M704841200

Fredenburgh, J. C., Gross, P. L., & Weitz, J. I. (2017). Emerging anticoagulant strategies. *Blood*, *129*(2), 147–154. https://doi.org/10.1182/blood-2016-09-692996

Fredenburgh, J. C., & Weitz, J. I. (2018). Overview of Hemostasis and Thrombosis. In *Hematology (Seventh Edition)* (pp. 1831–1842). Elsevier Inc.

Fu, C. L., & Horn, M. K. (2002). Histidine-rich glycoprotein plus zinc to neutralize heparin. *Journal of Laboratory and Clinical Medicine*, *139*(4), 211–217. https://doi.org/10.1067/mlc.2002.121854

Fujikawa, K., & McMullen, B. (1983). Amino Acid Sequence of Human β-Factor XIIa.

Journal of Biological Chemistry, *258*(18), 10924–10933.

Gailani, D., Bane, C. E., & Gruber, A. (2015). Factor XI and contact activation as targets for antithrombotic therapy. *Journal of Thrombosis and Haemostasis : JTH*, *13*(8), 1383–1395. https://doi.org/10.1111/jth.13005

Gailani, D., & Renné, T. (2007a). Intrinsic Pathway of Coagulation and Arterial Thrombosis. *Arteriosclerosis, Thrombosis, and Vascular Biology*, *27*(12), 2507–2513. https://doi.org/10.1161/ATVBAHA.107.155952

Gailani, D., & Renné, T. (2007b). The intrinsic pathway of coagulation: A target for treating thromboembolic disease? *Journal of Thrombosis and Haemostasis*, *5*, 1106–1112. https://doi.org/10.1111/j.1538-7836.2007.02446.x

Gajsiewicz, J. M., Smith, S. A., & Morrissey, J. H. (2017). Polyphosphate and RNA differentially modulate the contact pathway of blood clotting. *Journal of Biological Chemistry*, *292*(5), 1808–1814. https://doi.org/10.1074/jbc.M116.754325

Garcia, D. A., Baglin, T. P., Weitz, J. I., & Samama, M. M. (2012). Parenteral anticoagulants - Antithrombotic therapy and prevention of thrombosis, 9th ed: American College of Chest Physicians evidence-based clinical practice guidelines. *Chest*, *141*(2 Suppl), e24S-e43S. https://doi.org/10.1378/chest.11-2291

Geddings, J., & Mackman, N. (2014). New players in haemostasis and thrombosis. *Thrombosis and Haemostasis*, *111*(04), 570–574. https://doi.org/10.1160/TH13-10-0812

Geng, Y. J., & Libby, P. (2002). Progression of atheroma: A struggle between death and procreation. *Arteriosclerosis, Thrombosis, and Vascular Biology*, *22*(9), 1370–1380. https://doi.org/10.1161/01.ATV.0000031341.84618.A4

Ghosh, S., Shukla, D., Suman, K., Jyothi Lakshmi, B., Manorama, R., Kumar, S., & Bhandari, R. (2013). Inositol hexakisphosphate kinase 1 maintains hemostasis in mice by regulating platelet polyphosphate levels. *Blood*, *122*(8), 1478–1486. https://doi.org/10.1182/blood-2013-01-481549

Griffin, J. H., Fernández, J. A., Gale, A. J., & Mosnier, L. O. (2007). Activated protein C. *Journal of Thrombosis and Haemostasis*, *5*(SUPPL. 1), 73–80. https://doi.org/10.1111/j.1538-7836.2007.02491.x

Gross, P., Murray, R., & Rand, M. (2012). Hemostasis & Thrombosis. In R. Murray, D. Benner, K. Botham, P. Kennelly, V. Rodwell, & A. Well (Eds.), *Harper's Illustrated Biochemistry, Twenty-Ninth Edition* (pp. 2–11). McGraw-Hill Companies, Inc.

Grover, S. P., & Mackman, N. (2018). Tissue Factor: An Essential Mediator of Hemostasis and Trigger of Thrombosis. *Arteriosclerosis, Thrombosis, and Vascular Biology*, *38*(4), 709–725. https://doi.org/10.1161/ATVBAHA.117.309846

Grover, S. P., & Mackman, N. (2019). Intrinsic Pathway of Coagulation and Thrombosis. *Arteriosclerosis, Thrombosis, and Vascular Biology*, *39*(3), 331–338. https://doi.org/10.1161/ATVBAHA.118.312130

Gruber, A. (2014). The Role of the Contact Pathway in Thrombus Propagation. *Thrombosis Research*, *133*, S45–S47. https://doi.org/10.1016/j.thromres.2014.03.019

Guan, X., Juarez, J., Qi, X., Shipulina, N., Shaw, D., Morgan, W., McCrae, K., Mazar, A., & Doñate, F. (2004). Histidine-Proline Rich Glycoprotein (HPRG) binds and transduces anti-angiogenic signals through cell surface tropomyosin on endothelial cells. *Thrombosis and Haemostasis*, *92*(08), 403–412. https://doi.org/10.1160/TH04-02-0073

Halvorsen, S., Ghanima, W., Tvete, I. F., Hoxmark, C., Falck, P., Solli, O., & Jonasson, C. (2017). A nationwide registry study to compare bleeding rates in patients with atrial fibrillation being prescribed oral anticoagulants. *European Heart Journal — Cardiovascular Pharmacotherapy*, *3*(1), 28. https://doi.org/10.1093/EHJCVP/PVW031

Heimburger, N., Haupt, H., Kranz, T., & Baudner, S. (1972). Human serum proteins with high affinity for carboxymethylcellulose. II. Physico-chemical and immunological characterization of a histidine 3, 8S2-glycoprotein (CM-Protein I) (in German). *Hoppe Seyler Z. Physiol. Chem.*, *353*(7), 1133–1140. https://doi.org/10.1515/bchm2.1972.353.2.1125

Henderson, S. J., Stafford, A. R., Leslie, B. A., Kim, P. Y., Vaezzadeh, N., Ni, R., Fredenburgh, J. C., & Weitz, J. I. (2015). Zinc delays clot lysis by attenuating plasminogen activation and plasmin-mediated fibrin degradation. *Thrombosis and Haemostasis*, *113*(06), 1278–1288. https://doi.org/10.1160/TH14-09-0771

Hirsh, J. (1998). Low-Molecular-Weight Heparin A Review of the Results of Recent Studies of the Treatment of Venous Thromboembolism and Unstable Angina. *Circulation*, *98*, 1575–1582. http://ahajournals.org

Hirsh, J., & Raschke, R. (2004). Heparin and low-molecular-weight heparin: The Seventh ACCP Conference on Antithrombotic and Thrombolytic Therapy. *Chest*, *126*(3 Suppl), 188S-203S. https://doi.org/10.1378/chest.126.3_suppl.188S

Hirsh, J., Raschke, R., Warkentin, T. E., Dalen, J. E., Deykin, D., & Poller, L. (1995). Heparin: Mechanism of action, pharmacokinetics, dosing considerations, monitoring, efficacy, and safety. *Chest*, *108*(4 Suppl), 258S-275S. https://doi.org/10.1378/chest.108.4_Supplement.258S

Hoffman, M. (2003). Remodeling the blood coagulation cascade. *Journal of Thrombosis and Thrombolysis*, *16*(1–2), 17–20. https://doi.org/10.1023/B:THRO.0000014588.95061.28

Hoffman, M., & Monroe, D. M. (2001). A cell-based model of hemostasis. *Thromb Haemost*, *85*(6), 958–965. https://doi.org/10.1055/s-0037-1615947

Hoffman, M., & Monroe, D. M. (2007). Coagulation 2006: A Modern View of Hemostasis. *Hematology/Oncology Clinics of North America*, *21*(1), 1–11. https://doi.org/10.1016/j.hoc.2006.11.004

Hofman, Z. L. M., Clark, C. C., Sanrattana, W., Nosairi, A., Parr, N. M. J., Živkovic, M.,

Krause, K., Mahnke, N. A., Scheffel, J., Erik Hack, C., Maurer, M., de Maat, S., & Coen Maas, X. (2020). A mutation in the kringle domain of human factor XII that causes autoinflammation, disturbs zymogen quiescence, and accelerates activation. *Journal of Biological Chemistry*, *295*(2), 363–374. https://doi.org/10.1074/jbc.RA119.009788

Hsu, E., & Moosavi, L. (2019). Biochemistry, Antithrombin III. In *StatPearls*. StatPearls Publishing. http://www.ncbi.nlm.nih.gov/pubmed/31424879

Jaffer, I. H., & Weitz, J. I. (2018). Antithrombotic Drugs. In *Hematology: Basic Principles and Practice* (pp. 2168–2188). Elsevier Inc. https://doi.org/10.1016/B978-0-323-35762-3.00149-9

Jain, S., Pitoc, G. A., Holl, E. K., Zhang, Y., Borst, L., Leong, K. W., Lee, J., & Sullenger, B. A. (2012). Nucleic acid scavengers inhibit thrombosis without increasing bleeding. *Proceedings of the National Academy of Sciences of the United States of America*, *109*(32), 12938–12943. https://doi.org/10.1073/pnas.1204928109

Jespersen, J., Petersen, K. R., & Skouby, S. O. (1990). Effects of newer oral contraceptives on the inhibition of coagulation and fibrinolysis in relation to dosage and type of steroid. *American Journal of Obstetrics and Gynecology*, *163*(1 PART 2), 396–403. https://doi.org/10.1016/0002-9378(90)90590-4

Jones, A. L., Hulett, M. D., & Parish, C. R. (2005). Histidine-rich glycoprotein: A novel adaptor protein in plasma that modulates the immune, vascular and coagulation systems. *Immunology and Cell Biology*, *83*(2), 106–118. https://doi.org/10.1111/j.1440-1711.2005.01320.x

Jukema, B. N., de Maat, S., & Maas, C. (2016). Processing of Factor XII during Inflammatory Reactions. *Frontiers in Medicine*, *3*(52), 1–7. https://doi.org/10.3389/FMED.2016.00052

Kaira, B. G., Slater, A., McCrae, K. R., Dreveny, I., Sumya, U., Mutch, N. J., Searle, M., & Emsley, J. (2020). Factor XII and kininogen asymmetric assembly with gC1qR/C1QBP/P32 is governed by allostery. *Blood*, *136*(14), 1685–1697. https://doi.org/10.1182/blood.2020004818

Kalaska, B., Sokolowska, E., Kaminski, K., Szczubialka, K., Kramkowski, K., Mogielnicki, A., Nowakowska, M., & Buczko, W. (2012). Cationic derivative of dextran reverses anticoagulant activity of unfractionated heparin in animal models of arterial and venous thrombosis. *European Journal of Pharmacology*, *686*(1–3), 81–89. https://doi.org/10.1016/j.ejphar.2012.04.037

Kannemeier, C., Shibamiya, A., Nakazawa, F., Trusheim, H., Ruppert, C., Markart, P., Song, Y., Tzima, E., Kennerknecht, E., Niepmann, M., von Bruehl, M., Sedding, D., Massberg, S., Günther, A., Engelmann, B., & Preissner, K. T. (2007). Extracellular RNA constitutes a natural procoagulant cofactor in blood coagulation. *Proceedings of the National Academy of Sciences of the United States of America*, *104*(15), 6388–6393. https://doi.org/10.1073/pnas.0608647104

Kassaar, O., McMahon, S. A., Thompson, R., Botting, C. H., Naismith, J. H., & Stewart, A. J. (2014). Crystal structure of histidine-rich glycoprotein N2 domain reveals redox activity at an interdomain disulfide bridge: Implications for angiogenic regulation. *Blood*, *123*(12), 1948–1955. https://doi.org/10.1182/blood-2013-11-535963

Kassaar, O., Schwarz-Linek, U., Blindauer, C. A., & Stewart, A. J. (2015). Plasma free fatty acid levels influence Zn2+-dependent histidine-rich glycoprotein-heparin interactions via an allosteric switch on serum albumin. *Journal of Thrombosis and Haemostasis*, *13*(1), 101–110. https://doi.org/10.1111/jth.12771

Kawasaki, M., Maeda, T., Hanasawa, K., Ohkubo, I., & Tani, T. (2003). Effect of His-Gly-Lys motif derived from domain 5 of high molecular weight kininogen on suppression of cancer metastasis both in vitro and in vivo. *The Journal of Biological Chemistry*, *278*(49), 49301–49307. https://doi.org/10.1074/jbc.M308790200

Kenne, E., & Renné, T. (2014). Factor XII: a drug target for safe interference with thrombosis and inflammation. *Drug Discovery Today*, *19*(9), 1459–1464. https://doi.org/10.1016/j.drudis.2014.06.024

Kleinschnitz, C. (2006). Targeting coagulation factor XII provides protection from pathological thrombosis in cerebral ischemia without interfering with hemostasis. *Journal of Experimental Medicine*, *203*(3), 513–518. https://doi.org/10.1084/jem.20052458

Kolyadko, V. N., Korneeva, V. A., Ataullakhanov, F. I., & Panteleev, M. A. (2014). Molecular mechanisms of thrombosis. Fundamental and applied aspects of the contact activation. *Biochemistry (Moscow) Supplement Series A: Membrane and Cell Biology*, *8*(4), 279–289. https://doi.org/10.1134/S1990747814040059

Konings, J., Govers-Riemslag, J. W. P., Philippou, H., Mutch, N. J., Borissoff, J. I., Allan, P., Mohan, S., Tans, G., Ten Cate, H., & Ariëns, R. A. S. (2011). Factor XIIa regulates the structure of the fibrin clot independently of thrombin generation through direct interaction with fibrin. *Blood*, *118*(14), 3942–3951. https://doi.org/10.1182/blood-2011-03-339572

Kretz, C., Cuddy, K., Stafford, A., Fredenburgh, J., Roberts, R., & Weitz, J. (2010). HD1, a thrombin- and prothrombin-binding DNA aptamer, inhibits thrombin generation by attenuating prothrombin activation and thrombin feedback reactions. *Thrombosis and Haemostasis*, *103*(01), 83–96. https://doi.org/10.1160/TH09-04-0237

Kurachi, K., Fujikawa, K., Schmer, G., & Davie, E. W. (1976). Inhibition of Bovine Factor IXa and Factor Xaβ by Antithrombin III. *Biochemistry*, *15*(2), 373–377. https://doi.org/10.1021/bi00647a021

Larsson, M., Rayzman, V., Nolte, M. W., Nickel, K. F., Björkqvist, J., Jämsä, A., Hardy, M. P., Fries, M., Schmidbauer, S., Hedenqvist, P., Broomé, M., Pragst, I., Dickneite, G., Wilson, M. J., Nash, A. D., Panousis, C., & Renné, T. (2014). A factor XIIa inhibitory antibody provides thromboprotection in extracorporeal circulation without increasing bleeding risk. *Science Translational Medicine*, *6*(222), 1–13.

https://doi.org/10.1126/scitranslmed.3006804

Laslett, L. J., Alagona, P., Clark, B. A., Drozda, J. P., Saldivar, F., Wilson, S. R., Poe, C., & Hart, M. (2012). The Worldwide Environment of Cardiovascular Disease: Prevalence, Diagnosis, Therapy, and Policy Issues. *Journal of the American College of Cardiology*, *60*(25), S1–S49. https://doi.org/10.1016/j.jacc.2012.11.002

Lee, C. J., & Ansell, J. E. (2011). Direct thrombin inhibitors. *British Journal of Clinical Pharmacology*, *72*(4), 581–592. https://doi.org/10.1111/j.1365-2125.2011.03916.x

Leung, L. L. K., Harpel, P. C., Nachman, R. L., & Rabellino, E. M. (1983). Histidine-Rich Glycoprotein is Present in Human Platelets and is Released Following Thrombin Stimulation. *Blood*, *62*(5), 1016–1021. www.bloodjournal.org

Lindahl, U., Backstrom, G., Hook, M., Thunberg, L., Fransson, L. A., & Linker, A. (1979). Structure of the antithrombin binding site in heparin. *Proceedings of the National Academy of Sciences of the United States of America*, *76*(7), 3198–3202. https://doi.org/10.1073/pnas.76.7.3198

López-López, J. A., Sterne, J. A. C., Thom, H. H. Z., Higgins, J. P. T., Hingorani, A. D., Okoli, G. N., Davies, P. A., Bodalia, P. N., Bryden, P. A., Welton, N. J., Hollingworth, W., Caldwell, D. M., Savovic, J., Dias, S., Salisbury, C., Eaton, D., Stephens-Boal, A., & Sofat, R. (2017). Oral anticoagulants for prevention of stroke in atrial fibrillation: Systematic review, network meta-Analysis, and cost effectiveness analysis. *BMJ*, *359*, 1–13. https://doi.org/10.1136/bmj.j5058

Low, C., Lyuboslavsky, P., & Traynelis, S. F. (2000). Molecular determinants of coordinated proton and zinc inhibition of N-methyl-D-aspartate NR1/NR2A receptors. *Proceedings of the National Academy of Sciences of the United States of America*, *97*(20), 11062–11067. https://doi.org/10.1073/pnas.180307497

Luo, J., Zhang, W., Zeng, Q., Zhou, W., Cao, Q., & Zhou, W. (2018). Familial early-onset deep venous thrombosis associated with a novel HRG mutation. *European Journal of Medical Genetics*, *61*(2), 68–71. https://doi.org/10.1016/j.ejmg.2017.10.019

Maas, C., Oschatz, C., & Renné, T. (2011). The Plasma Contact System 2.0. *Seminars in Thrombosis and Hemostasis*, *37*(04), 375–381. https://doi.org/10.1055/s-0031-1276586

Maas, C., Renné, T., & Renné, R. (2018). Coagulation factor XII in thrombosis and inflammation. *Blood*, *131*(17), 1903–1909. www.bloodjournal.org

Mackman, N. (2004). Role of Tissue Factor in Hemostasis, Thrombosis, and Vascular Development. *Arteriosclerosis, Thrombosis, and Vascular Biology*, *24*(6), 1015–1022. https://doi.org/10.1161/01.ATV.0000130465.23430.74

Mackman, N. (2006). Role of tissue factor in hemostasis and thrombosis. *Blood Cells, Molecules, and Diseases*, *36*(2), 104–107. https://doi.org/10.1016/j.bcmd.2005.12.008

Mackman, N. (2008). Triggers, targets and treatments for thrombosis. *Nature*, *451*(7181),

914–918. https://doi.org/10.1038/nature06797

Mackman, N., & Becker, R. C. (2010). DVT: a new era in anticoagulant therapy. *Arteriosclerosis, Thrombosis, and Vascular Biology*, *30*(3), 369–371. https://doi.org/10.1161/ATVBAHA.110.203497

Mackman, N., Tilley, R. E., & Key, N. S. (2007). Role of the Extrinsic Pathway of Blood Coagulation in Hemostasis and Thrombosis. *Arteriosclerosis, Thrombosis, and Vascular Biology*, *27*(8), 1687–1693. https://doi.org/10.1161/ATVBAHA.107.141911

MacQuarrie, J. L., Stafford, A. R., Yau, J. W., Leslie, B. a., Vu, T. T., Fredenburgh, J. C., & Weitz, J. I. (2011). Histidine-rich glycoprotein binds factor XIIa with high affinity and inhibits contact-initiated coagulation. *Blood*, *117*(15), 4134–4141. https://doi.org/10.1182/blood-2010-07-290551

Manco-Johnson, M. J., Bomgaars, L., Palascak, J., Shapiro, A., Geil, J., Fritsch, S., Pavlova, B. G., & Gelmont, D. (2016). Efficacy and safety of protein C concentrate to treat purpura fulminans and thromboembolic events in severe congenital protein C deficiency. *Thrombosis and Haemostasis*, *116*(1), 58–68. https://doi.org/10.1160/TH15-10-0786

Mann, K. G. (1999). Biochemistry and physiology of blood coagulation. *Thrombosis and Haemostasis*, *82*(2), 165–174. https://doi.org/10.1055/s-0037-1615780

Marx, G., Korner, G., Mou, X., & Gorodetsky, R. (1993). Packaging zinc, fibrinogen, and factor XIII in platelet alpha-granules. *Journal of Cellular Physiology*, *156*(3), 437–442. https://doi.org/10.1002/jcp.1041560302

Masliah-Planchon, J., Darnige, L., & Bellucci, S. (2013). Molecular determinants of platelet delta storage pool deficiencies: an update. *British Journal of Haematology*, *160*(1), 5–11. https://doi.org/10.1111/bjh.12064

Mast, A. E. (2016). Tissue Factor Pathway Inhibitor: Multiple Anticoagulant Activities for a Single Protein. *Arteriosclerosis, Thrombosis, and Vascular Biology*, *36*(1), 9–14. https://doi.org/10.1161/ATVBAHA.115.305996

Matafonov, A., Leung, P. Y., Gailani, A. E., Grach, S. L., Puy, C., Cheng, Q., Sun, M. F., McCarty, O. J. T., Tucker, E. I., Kataoka, H., Renné, T., Morrissey, J. H., Gruber, A., & Gailani, D. (2014). Factor XII inhibition reduces thrombus formation in a primate thrombosis model. *Blood*, *123*(11), 1739–1746. https://doi.org/10.1182/blood-2013-04-499111

Mehta, S. R., Boden, W. E., Eikelboom, J. W., Flather, M., Steg, P. G., Avezum, A., Afzal, R., Piegas, L. S., Faxon, D. P., Widimsky, P., Budaj, A., Chrolavicius, S., Rupprecht, H. J., Jolly, S., Granger, C. B., Fox, K. A. A., Bassand, J. P., & Yusuf, S. (2008). Antithrombotic therapy with fondaparinux in relation to interventional management strategy in patients with ST-and non-ST-segment elevation acute coronary syndromes an individual patient-level combined analysis of the fifth and sixth organization to assess strategies in ischemic syndromes (OASIS 5 and 6)

randomized trials. *Circulation*, *118*(20), 2038–2046. https://doi.org/10.1161/CIRCULATIONAHA.108.789479

Mekaj, Y. H., Mekaj, A. Y., Duci, S. B., & Miftari, E. I. (2015). New oral anticoagulants: Their advantages and disadvantages compared with vitamin K antagonists in the prevention and treatment of patients with thromboembolic events. *Therapeutics and Clinical Risk Management*, *11*, 967–977. https://doi.org/10.2147/TCRM.S84210

Melnikova, I. (2009). The anticoagulants market Irena Melnikova. *Nature Reviews Drug Discovery*, *8*(5), 353–354. https://doi.org/10.1038/nrd2851

Merkulov, S., Zhang, W.-M., Komar, A. A., Schmaier, A. H., Barnes, E., Zhou, Y., Lu, X., Iwaki, T., Castellino, F. J., Luo, G., & McCrae, K. R. (2008). Deletion of murine kininogen gene 1 (mKng1) causes loss of plasma kininogen and delays thrombosis. *Blood*, *111*(3), 1274–1281. https://doi.org/10.1182/blood-2007-06-092338

Monroe, D. M., & Hoffman, M. (2006). What Does It Take to Make the Perfect Clot? *Arteriosclerosis, Thrombosis, and Vascular Biology*, *26*(1), 41–48. https://doi.org/10.1161/01.ATV.0000193624.28251.83

Mordillo, C., Martinez-Marchán, E., Fontcuberta, J., & Soria, J. M. (2007). Molecular analysis of multiple genetic variants in Spanish FXII-deficient families. *Haematologica*, *92*(11), 1569–1572. https://doi.org/10.3324/haematol.11388

Moreno-Sanchez, D., Hernandez-Ruiz, L., Ruiz, F. A., & Docampo, R. (2012). Polyphosphate is a novel pro-inflammatory regulator of mast cells and is located in acidocalcisomes. *Journal of Biological Chemistry*, *287*(34), 28435–28444. https://doi.org/10.1074/jbc.M112.385823

Morrissey, J. H., Choi, S. H., & Smith, S. A. (2012). Polyphosphate: an ancient molecule that links platelets, coagulation, and inflammation. *Blood*, *119*(25), 5972–5979. https://doi.org/10.1182/blood-2012-03-306605

Müller, F., Gailani, D., & Renne, T. (2011). Factor XI and XII as antithrombotic targets. *Current Opinion in Hematology*, *18*(5), 349–355. https://doi.org/10.1097/MOH.0b013e3283497e61.Factor

Müller, F., Gailani, D., & Renné, T. (2011). Factor XI and XII as antithrombotic targets. *Current Opinion in Hematology*, *18*(5), 349–355. https://doi.org/10.1097/MOH.0b013e3283497e61

Müller, F., Mutch, N. J., Schenk, W. A., Smith, S. A., Esterl, L., Spronk, H. M., Schmidbauer, S., Gahl, W. A., Morrissey, J. H., & Renné, T. (2009). Platelet polyphosphates are proinflammatory and procoagulant mediators in vivo. *Cell*, *139*(6), 1143–1156. https://doi.org/10.1016/j.cell.2009.11.001

Mulloy, B., Hogwood, J., Gray, E., Lever, R., & Page, C. P. (2015). Pharmacology of Heparin and Related Drugs. *Pharmacological Reviews*, *68*(1), 76–141. https://doi.org/10.1124/pr.115.011247

Nzeako, U. C., Frigas, E., & Tremaine, W. J. (2001). Hereditary angioedema: a broad review for clinicians. *Archives of Internal Medicine*, *161*(20), 2417–2429.

http://www.ncbi.nlm.nih.gov/pubmed/11700154

Olson, S. T., & Gettins, P. G. W. (2011). Regulation of Proteases by Protein Inhibitors of the Serpin Superfamily. *Progress in Molecular Biology and Translational Science*, *99*, 185–240. https://doi.org/10.1016/B978-0-12-385504-6.00005-1

Owens, A. P. I., & Mackman, N. (2010). Tissue factor and thrombosis: The clot starts here. *Thrombosis and Haemostasis*, *104*(3), 432–439. https://doi.org/10.1160/TH09-11-0771

Owens, A. P. I. & Mackman, N. (2011). Microparticles in Hemostasis and Thrombosis. *Circ Res.*, *108*(10), 1284–1297. https://doi.org/10.1161/CIRCRESAHA.110.233056.Microparticles

Patel, K., Kumar, A., & Durani, S. (2007). Analysis of the structural consensus of the zinc coordination centers of metalloprotein structures. *Biochimica et Biophysica Acta - Proteins and Proteomics*, *1774*(10), 1247–1253. https://doi.org/10.1016/j.bbapap.2007.07.010

Pathak, M., Manna, R., Li, C., Kaira, B. G., Hamad, B. K., Belviso, B. D., Bonturi, C. R., Dreveny, I., Fischer, P. M., Dekker, L. V., Oliva, M. L. V., & Emsley, J. (2019). Crystal structures of the recombinant β-factor XIIa protease with bound Thr-Arg and Pro-Arg substrate mimetics. *Acta Crystallographica Section D Structural Biology*, *75*(6), 578–591. https://doi.org/10.1107/S2059798319006910

Pathak, M., Wilmann, P., Awford, J., Li, C., Hamad, B. K., Fischer, P. M., Dreveny, I., Dekker, L. V., & Emsley, J. (2015). Coagulation factor XII protease domain crystal structure. *Journal of Thrombosis and Haemostasis*, *13*(4), 580–591. https://doi.org/10.1111/jth.12849

Perry, D. J. (1994). Antithrombin and its inherited deficiencies. *Blood Reviews*, *8*(1), 37–55. https://doi.org/10.1016/0268-960X(94)90006-X

Perzborn, E., Roehrig, S., Straub, A., Kubitza, D., Mueck, W., & Laux, V. (2010). Rivaroxaban: A new oral factor xa inhibitor. In *Arteriosclerosis, Thrombosis, and Vascular Biology* (Vol. 30, Issue 3, pp. 376–381). https://doi.org/10.1161/ATVBAHA.110.202978

Perzborn, E., Tersteegen, A., Harwardt, M., & Lange, U. (2009). Different Characteristics of Direct Factor Xa Inhibitors: In Vitro Comparative Studies of Rivaroxaban and Apixaban. *Blood*, *114*(22), 4170–4170. https://doi.org/10.1182/blood.v114.22.4170.4170

Peterson, L. C., Valentin, S., & Hedner, U. (1995). Regulation of the Extrinsic Pathway System in Health and Disease: The Role of Factor VIIa and Tissue Factor Pathway Inhibitor. *Thrombosis Research*, *79*(1), 1–47.

Pham, M., Stoll, G., Nieswandt, B., Bendszus, M., & Kleinschnitz, C. (2012). Blood coagulation factor XII—a neglected player in stroke pathophysiology. *Journal of Molecular Medicine*, *90*(2), 119–126. https://doi.org/10.1007/s00109-011-0812-9

Pixley, R. A., Schapira, M., & Colman, R. W. (1985). The regulation of human factor

XIIa by plasma proteinase inhibitors. *The Journal of Biological Chemistry*, *260*(3), 1723–1729. http://www.ncbi.nlm.nih.gov/pubmed/2578463

Pixley, R. A., Schmaier, A., & Colman, R. W. (1987). Effect of negatively charged activating compounds on inactivation of factor XIIa by Cl- inhibitor. *Archives of Biochemistry and Biophysics*, *256*(2), 490–498. https://doi.org/10.1016/0003-9861(87)90606-0

Poon, I. K. H., Olsson, A., Hulett, M. D., & Parish, C. R. (2009). Regulation of histidine-rich glycoprotein (HRG) function via plasmin-mediated proteolytic cleavage. *The Biochemical Journal*, *424*(1), 27–37. https://doi.org/10.1042/BJ20090794

Poon, I. K. H., Patel, K. K., Davis, D. S., Parish, C. R., & Hulett, M. D. (2011). Histidine-rich glycoprotein: The Swiss Army knife of mammalian plasma. *Blood*, *117*(7), 2093–2101. https://doi.org/10.1182/blood-2010-09-303842

Priebatsch, K. M., Kvansakul, M., Poon, I. K. H., & Hulett, M. D. (2017). Functional regulation of the plasma protein histidine-rich glycoprotein by Zn2+ in settings of tissue injury. *Biomolecules*, *7*(1). https://doi.org/10.3390/biom7010022

Priebatsch, K. M., Poon, I. K. H., Patel, K. K., Kvansakul, M., & Hulett, M. D. (2017). Divalent metal binding by histidine-rich glycoprotein differentially regulates higher order oligomerisation and proteolytic processing. *FEBS Letters*, *591*(1), 164–176. https://doi.org/10.1002/1873-3468.12520

Puy, C., Tucker, E. I., Wong, Z. C., Gailani, D., Smith, S. A., Choi, S. H., Morrissey, J. H., Gruber, A., & McCarty, O. J. T. (2013). Factor XII promotes blood coagulation independent of factor XI in the presence of long-chain polyphosphates. *Journal of Thrombosis and Haemostasis : JTH*, *11*(7), 1341–1352. https://doi.org/10.1111/jth.12295

Rana, K., & Neeves, K. B. (2016). Blood flow and mass transfer regulation of coagulation. *Blood Reviews*, *30*(5), 357–368. https://doi.org/10.1016/j.blre.2016.04.004

Ranieri-Raggi, M., Moir, A., & Raggi, A. (2014). The Role of Histidine-Proline-Rich Glycoprotein as Zinc Chaperone for Skeletal Muscle AMP Deaminase. *Biomolecules*, *4*(4), 474–497. https://doi.org/10.3390/biom4020474

Raskob, G. E., Angchaisuksiri, P., Blanco, A. N., Buller, H., Gallus, A., Hunt, B. J., Hylek, E. M., Kakkar, A., Konstantinides, S. V., McCumber, M., Ozaki, Y., Wendelboe, A., & Weitz, J. I. (2014). Thrombosis: a major contributor to global disease burden. *Thrombosis Research*, *134*(5), 931–938. https://doi.org/10.1016/j.thromres.2014.08.014

Renné, T. (2012). The procoagulant and proinflammatory plasma contact system. *Seminars in Immunopathology*, *34*(1), 31–41. https://doi.org/10.1007/s00281-011-0288-2

Renné, T., & Gailani, D. (2007). Role of Factor XII in hemostasis and thrombosis: clinical implications. *Expert Rev. Cardiovasc. Ther*, *5*(4), 733–741.

https://doi.org/10.1586/14779072.5.4.733

Renné, T., Nieswandt, B., & Gailani, D. (2006). The intrinsic pathway of coagulation is essential for thrombus stability in mice. *Blood Cells, Molecules, and Diseases*, *36*(2), 148–151. https://doi.org/10.1016/j.bcmd.2005.12.014

Renné, T., Pozgajová, M., Grüner, S., Schuh, K., Pauer, H.-U., Burfeind, P., Gailani, D., & Nieswandt, B. (2005). Defective thrombus formation in mice lacking coagulation factor XII. *The Journal of Experimental Medicine*, *202*(2), 271–281. https://doi.org/10.1084/jem.20050664

Renné, T., Schmaier, A. H., Nickel, K. F., Blombäck, M., & Maas, C. (2012). In vivo roles of factor XII. *Blood*, *120*(22), 4296–4303. https://doi.org/10.1182/blood-2012-07-292094

Revenko, A. S., Gao, D., Crosby, J. R., Bhattacharjee, G., Zhao, C., May, C., Gailani, D., Monia, B. P., & MacLeod, a. R. (2011). Selective depletion of plasma prekallikrein or coagulation factor XII inhibits thrombosis in mice without increased risk of bleeding. *Blood*, *118*(19), 5302–5311. https://doi.org/10.1182/blood-2011-05-355248

Reynolds, N. A., Perry, C. M., & Scott, L. J. (2004). Fondaparinux sodium: A review of its use in the prevention of venous thromboembolism following major orthopaedic surgery. *Drugs*, *64*(14), 1575–1596. https://doi.org/10.2165/00003495-200464140-00005

Røjkaer, R., & Schousboe, I. (1997). Partial identification of the Zn2+-binding sites in factor XII and its activation derivatives. *European Journal of Biochemistry / FEBS*, *247*(2), 491–496. http://www.ncbi.nlm.nih.gov/pubmed/9266689

Ronca, F., & Raggi, A. (2015). Structure-function relationships in mammalian histidine-proline-rich glycoprotein. *Biochimie*, *118*, 207–220. https://doi.org/10.1016/j.biochi.2015.09.024

Rosano, G. L., & Ceccarelli, E. A. (2014). Recombinant protein expression in Escherichia coli: Advances and challenges. *Frontiers in Microbiology*, *5*(172), 1–17. https://doi.org/10.3389/fmicb.2014.00172

Rydengård, V., Olsson, A., Mörgelin, M., & Schmidtchen, A. (2007). Histidine-rich glycoprotein exerts antibacterial activity. *FEBS Journal*, *274*(2), 377–389. https://doi.org/10.1111/j.1742-4658.2006.05586.x

Rydengård, V., Shannon, O., Lundqvist, K., Kacprzyk, L., Chalupka, A., Olsson, A., Mörgelin, M., Jahnen-Dechent, W., Malmsten, M., & Schmidtchen, A. (2008). Histidine-Rich Glycoprotein Protects from Systemic Candida Infection. *PLoS Pathogens*, *4*(8), e1000116. https://doi.org/10.1371/journal.ppat.1000116

Sabbatini, A. R. M., Mattii, L., Battolla, B., Polizzi, E., Martini, D., Ranieri-Raggi, M., Moir, A. J. G., & Raggi, A. (2011). Evidence that muscle cells do not express the histidine-rich glycoprotein associated with AMP deaminase but can internalise the plasma protein. *European Journal of Histochemistry*, *55*(1), 33–38.

https://doi.org/10.4081/ejh.2011.e6

Saigo, K., Yoshida, A., Ryo, R., Yamaguchi, N., & Leung, L. L. K. (1990). Histidine-rich glycoprotein as a negative acute phase reactant. *American Journal of Hematology*, *34*(2), 149–150. https://doi.org/10.1002/ajh.2830340212

Salomon, O., Steinberg, D. M., Koren-Morag, N., Tanne, D., & Seligsohn, U. (2008). Reduced incidence of ischemic stroke in patients with severe factor XI deficiency. *Blood*, *111*(8), 4113–4117. https://doi.org/10.1182/blood-2007-10-120139

Salomon, O., Zivelin, A., Livnat, T., Dardik, R., Loewenthal, R., Avishai, O., Steinberg, D. M., Rosove, M. H., O'Connell, N., Lee, C. A., & Seligsohn, U. (2003). Prevalence, causes, and characterization of factor XI inhibitors in patients with inherited factor XI deficiency. *Blood*, *101*(12), 4783–4788. https://doi.org/10.1182/blood-2002-09-2794

Schmaier, A. H. (2008). The elusive physiologic role of Factor XII. *Journal of Clinical Investigation*, *118*(9), 3006–3009. https://doi.org/10.1172/JCI36617

Schmaier, A. H. (2016). The Contact Activation and Kallikrein/Kinin Systems: Pathophysiologic and Physiologic Activities. *Journal of Thrombosis and Haemostasis*, *1*(14), 28–39. https://doi.org/10.1111/jth.13194

Schousboe, I. (2003). Binding of activated Factor XII to endothelial cells affects its inactivation by the C1-esterase inhibitor. *Eur.J.Biochem.*, *270*, 111–118. https://doi.org/10.1046/j.1432-1033.2003.03367.x

Shigekiyo, T., Yoshida, H., Kanagawa, Y., Satoh, K., Wakabayashi, S., Matsumoto, T., & Koide, T. (2000). Histidine-rich glycoprotein (HRG) Tokushima 2: Novel HRG deficiency, molecular and cellular characterization. *Thrombosis and Haemostasis*, *84*(4), 675–679. https://doi.org/10.1055/s-0037-1614086

Shigekiyo, T., Yoshida, H., Matsumoto, K., Azuma, H., Wakabayashi, S., Saito, S., Fujikawa, K., & Koide, T. (1998). *HRG Tokushima: Molecular and Cellular Characterization of Histidine-Rich Glycoprotein (HRG) Deficiency*. *91*(1), 128–133.

Shimada, K., Kobayashi, M., Kimura, S., Nishinaga, M., Takeuchi, K., Ozawa, T., Shimada, K., Kobayashi, M., Kimura, S., Nishinaga, M., Takeuchi, K., & Ozawa, T. (1991). Anticoagulant Heparin-like Glycosaminoglycans on Endothelial Cell Surface. *Japanese Circulation Journal*, *55*(10), 1016–1021. https://doi.org/10.1253/jcj.55.1016

Siddiqui, F., Hoppensteadt, D., Jeske, W., Iqbal, O., Tafur, A., & Fareed, J. (2019). Factor Xa Inhibitory Profile of Apixaban, Betrixaban, Edoxaban, and Rivaroxaban Does Not Fully Reflect Their Biologic Spectrum. *Clinical and Applied Thrombosis/Hemostasis*, *25*. https://doi.org/10.1177/1076029619847524

Sinhadri, B. C. S., Jin, D. Y., Stafford, D. W., & Tie, J. K. (2017). Vitamin K epoxide reductase and its paralogous enzyme have different structures and functions. *Scientific Reports*, *7*(1), 1–12. https://doi.org/10.1038/s41598-017-18008-3

Smith, A., Nuiry, I., & Morgan, W. T. (1985). Proteolysis of histidine-rich glycoprotein

in plasma and in patients undergoing thrombolytic therapy. *Thrombosis Research*, *40*(5), 653–661. https://doi.org/10.1016/0049-3848(85)90303-2

Smith, S. A., Choi, S. H., Collins, J. N. R., Travers, R. J., Cooley, B. C., & Morrissey, J. H. (2012). Inhibition of polyphosphate as a novel strategy for preventing thrombosis and inflammation. *Blood*, *120*(26), 5103–5110. https://doi.org/10.1182/blood-2012-07-444935

Smith, S. A., Choi, S. H., Davis-Harrison, R., Huyck, J., Boettcher, J., Rienstra, C. M., Reinstra, C. M., & Morrissey, J. H. (2010). Polyphosphate exerts differential effects on blood clotting, depending on polymer size. *Blood*, *116*(20), 4353–4359. https://doi.org/10.1182/blood-2010-01-266791

Smith, S. A., Mutch, N. J., Baskar, D., Rohloff, P., Docampo, R., & Morrissey, J. H. (2006). Polyphosphate modulates blood coagulation and fibrinolysis. *Proceedings of the National Academy of Sciences of the United States of America*, *103*(4), 903–908. https://doi.org/10.1073/pnas.0507195103

Stachowicz, A., Zabczyk, M., Natorska, J., Suski, M., Olszanecki, R., Korbut, R., Wiśniewski, J. R., & Undas, A. (2018). Differences in plasma fibrin clot composition in patients with thrombotic antiphospholipid syndrome compared with venous thromboembolism. *Scientific Reports*, *8*(1). https://doi.org/10.1038/s41598-018-35034-x

Stavrou, E., & Schmaier, A. H. (2010). Factor XII: What does it contribute to our understanding of the physiology and pathophysiology of hemostasis & thrombosis. *Thrombosis Research*, *125*(3), 210–215. https://doi.org/10.1016/j.thromres.2009.11.028

Stone, J., Hangge, P., Albadawi, H., Wallace, A., Shamoun, F., Knuttien, M. G., Naidu, S., & Oklu, R. (2017). Deep vein thrombosis: pathogenesis, diagnosis, and medical management. *Cardiovascular Diagnosis and Therapy*, *7*(Suppl 3), S276–S284. https://doi.org/10.21037/cdt.2017.09.01

Thompson, R. E., Mandle, R., & Kaplan, A. P. (1979). Studies of binding of prekallikrein and Factor XI to high molecular weight kininogen and its light chain. *Proceedings of the National Academy of Sciences of the United States of America*, *76*(10), 4862–4866. https://doi.org/10.1073/PNAS.76.10.4862

Thulin, Å., Ringvall, M., Dimberg, A., Kårehed, K., Väisänen, T., Väisänen, M. R., Hamad, O., Wang, J., Bjerkvig, R., Nilsson, B., Pihlajaniemi, T., Åkerud, H., Pietras, K., Jahnen-Dechent, W., Siegbahn, A., & Olsson, A. K. (2009). Activated platelets provide a functional microenvironment for the antiangiogenic fragment of histidine-rich glycoprotein. *Molecular Cancer Research*, *7*(11), 1792–1802. https://doi.org/10.1158/1541-7786.MCR-09-0094

Tie, J. K., Carneiro, J. D. A., Jin, D. Y., Martinhago, C. D., Vermeer, C., & Stafford, D. W. (2016). Characterization of vitamin K-dependent carboxylase mutations that cause bleeding and nonbleeding disorders. *Blood*, *127*(15), 1847–1855. https://doi.org/10.1182/blood-2015-10-677633

Tie, J. K., & Stafford, D. W. (2016). Structural and functional insights into enzymes of the vitamin K cycle. In *Journal of Thrombosis and Haemostasis* (Vol. 14, Issue 2, pp. 236–247). Blackwell Publishing Ltd. https://doi.org/10.1111/jth.13217

Tsuchida-Straeten, N., Ensslen, S., Schäfer, C., Wöltje, M., Denecke, B., Moser, M., Gräber, S., Wakabayashi, S., Koide, T., & Jahnen-Dechent, W. (2005). Enhanced blood coagulation and fibrinolysis in mice lacking histidine-rich glycoprotein (HRG). *Journal of Thrombosis and Haemostasis*, *3*(5), 865–872. https://doi.org/10.1111/j.1538-7836.2005.01238.x

University of Virginia Medical School. (2020). *Protein Analysis by Mass Spectrometry | Biomolecular Analysis Facility*. https://med.virginia.edu/biomolecular-analysis-facility/services/mass-spectrometry/protein-analysis-by-mass-spectrometry/

van der Vaart, M., & Pretorius, P. J. (2008). Circulating DNA. It's origin and fluctuation. *Annals of the New York Academy of Sciences*, *1137*, 18–26. https://doi.org/10.1196/annals.1448.022

Vanwildemeersch, M., Olsson, A., Gottfridsson, E., Claesson-Welsh, L., Lindahl, U., & Spillmann, D. (2006). The anti-angiogenic His/Pro-rich fragment of histidine-rich glycoprotein binds to endothelial cell heparan sulfate in a Zn2+-dependent manner. *The Journal of Biological Chemistry*, *281*(15), 10298–10304. https://doi.org/10.1074/jbc.M508483200

Versteeg, H. H., Heemskerk, J. W. M., Levi, M., & Reitsma, P. H. (2013). New Fundamentals in Hemostasis. *Physiological Reviews*, *93*(1), 327–358. https://doi.org/10.1152/physrev.00016.2011

von Brühl, M., Stark, K., Steinhart, A., Chandraratne, S., Konrad, I., Lorenz, M., Khandoga, A., Tirniceriu, A., Coletti, R., Köllnberger, M., Byrne, R. A., Laitinen, I., Walch, A., Brill, A., Pfeiler, S., Manukyan, D., Braun, S., Lange, P., Riegger, J., … Massberg, S. (2012). Monocytes, neutrophils, and platelets cooperate to initiate and propagate venous thrombosis in mice in vivo. *The Journal of Experimental Medicine*, *209*(4), 819–835. https://doi.org/10.1084/jem.20112322

Vu, T. T., Fredenburgh, J. C., & Weitz, J. I. (2013). Zinc: an important cofactor in haemostasis and thrombosis. *Thrombosis and Haemostasis*, *109*(3), 421–430. https://doi.org/10.1160/TH12-07-0465

Vu, T. T., Leslie, B. A., Stafford, A. R., Zhou, J., Fredenburgh, J. C., & Weitz, J. I. (2016). Histidine-rich glycoprotein binds DNA and RNA and attenuates their capacity to activate the intrinsic coagulation pathway. *Thrombosis and Haemostasis*, *115*, 89–98.

Vu, T. T., Zhou, J., Leslie, B. A., Stafford, A. R., Fredenburgh, J. C., Ni, R., Qiao, S., Vaezzadeh, N., Jahnen-Dechent, W., Monia, B. P., Gross, P. L., & Weitz, J. I. (2015). Arterial thrombosis is accelerated in mice deficient in histidine-rich glycoprotein. *Blood*, *125*(17), 2712–2719. https://doi.org/10.1182/blood-2014-11-611319

Wagenaar-Bos, I. G. A., & Hack, C. E. (2006). Structure and Function of C1-Inhibitor. *Immunology and Allergy Clinics of North America*, *26*(4), 615–632. https://doi.org/10.1016/j.iac.2006.08.004

Wang, X., Smith, P. L., Hsu, M. Y., Gailani, D., Schumacher, W. A., Ogletree, M. L., & Seiffert, D. A. (2006). Effects of factor XI deficiency on ferric chloride-induced vena cava thrombosis in mice. *Journal of Thrombosis and Haemostasis*, *4*(9), 1982–1988. https://doi.org/10.1111/j.1538-7836.2006.02093.x

Weitz, J. I. (2003). Heparan sulfate: Antithrombotic or not? *Journal of Clinical Investigation*, *111*(7), 952–954. https://doi.org/10.1172/JCI200318234

Weitz, J. I. (2012). Overview of Hemostasis and Thrombosis. In *Hematology: Basic Principles and Practice Elsevier Saunders Edition 6)* (Sixth Edit). Elsevier Inc. https://doi.org/10.1016/B978-1-4377-2928-3.00124-6

Weitz, J. I. (2016). Factor XI and factor XII as targets for new anticoagulants. *Thrombosis Research*, *141*, S40–S45. https://doi.org/10.1016/S0049-3848(16)30363-2

Weitz, J. I., & Chan, N. C. (2018). Advances in Antithrombotic Therapy . *Ateriocler Thromb Vasc Biol*, 7–12. https://doi.org/10.1161/ATVBAHA.118.310960

Weitz, J. I., & Fredenburgh, J. C. (2017a). Factors XI and XII as Targets for New Anticoagulants. *Frontiers in Medicine*, *4*, 19. https://doi.org/10.3389/fmed.2017.00019

Weitz, J. I., & Fredenburgh, J. C. (2017b). Platelet polyphosphate: the long and the short of it. *Blood*, *129*(12), 1574–1575. https://doi.org/10.1182/blood-2017-01-761593

Wendelboe, A. M., & Raskob, G. E. (2016). Global Burden of Thrombosis: Epidemiologic Aspects. *Circulation Research*, *118*(9), 1340–1347. https://doi.org/10.1161/CIRCRESAHA.115.306841

Wildgoose, P., & Kisiel, W. (1989). Activation of Human Factor VII by Factors IXa and Xa on Human Bladder Carcinoma Cells. *Blood*, *73*(7), 1888–1895. https://ashpublications.org/blood/article-pdf/73/7/1888/600270/1888.pdf

Wood, J. P., Ellery, P. E. R., Maroney, S. A., & Mast, A. E. (2014). Biology of tissue factor pathway inhibitor. *Blood*, *123*(19), 2934–2943. https://doi.org/10.1182/blood-2013

Wu, Y. (2015). Contact pathway of coagulation and inflammation. *Thrombosis Journal*, *13*(1), 17. https://doi.org/10.1186/s12959-015-0048-y

Yau, J. W., Liao, P., Fredenburgh, J. C., Stafford, A. R., Revenko, A. S., Monia, B. P., & Weitz, J. I. (2014). Selective depletion of factor XI or factor XII with antisense oligonucleotides attenuates catheter thrombosis in rabbits. *Blood*, *123*(13), 2102–2107. https://doi.org/10.1182/blood-2013-12-540872

Yau, J. W., Stafford, A. R., Liao, P., Fredenburgh, J. C., Roberts, R., Brash, J. L., & Weitz, J. I. (2012). Corn trypsin inhibitor coating attenuates the prothrombotic

properties of catheters in vitro and in vivo. *Acta Biomaterialia*, *8*(11), 4092–4100. https://doi.org/10.1016/j.actbio.2012.07.019

Younis, H. S., Crosby, J., Huh, J., Lee, H. S., Rime, S., Monia, B., & Henry, S. P. (2012). Antisense inhibition of coagulation factor XI prolongs APTT without increased bleeding risk in cynomolgus monkeys. *Blood*, *119*(10), 2401–2408. https://doi.org/10.1182/blood-2011-10-387134

Zhang, H., Löwenberg, E. C., Crosby, J. R., MacLeod, A. R., Zhao, C., Gao, D., Black, C., Revenko, A. S., Meijers, J. C. M., Stroes, E. S., Levi, M., & Monia, B. P. (2010). Inhibition of the Intrinsic Coagulation Pathway Factor XI by Antisense Oligonucleotides: A Novel Antithrombotic Strategy with Lowered Bleeding Risk. *Blood*, *116*(22), 4684–4692. https://doi.org/10.1182/blood-2010-04-277798

Zhu, S., Travers, R. J., Morrissey, J. H., & Diamond, S. L. (2015). FXIa and platelet polyphosphate as therapeutic targets during human blood clotting on collagen/tissue factor surfaces under flow. *Blood*, *126*(12), 1494–1503. https://doi.org/10.1182/blood-2015-04-641472

Zirlik, A., & Bode, C. (2017). Vitamin K antagonists: relative strengths and weaknesses vs. direct oral anticoagulants for stroke prevention in patients with atrial fibrillation. *Journal of Thrombosis and Thrombolysis*, *43*(3), 365–379. https://doi.org/10.1007/s11239-016-1446-0